July 2016

INNOVATIVE AND CONVENTIONAL APPROACHES TO DETRITAL ZIRCON PROVENANCE ANALYSIS: LOOKING TO THE PAST, PRESENT, AND FUTURE

Gregory Karl Wissink
Syracuse University

General Abstract

Detrital provenance analysis is an important tool in our understanding paleo-fluvial drainages, erosion of landscapes, paleogeographic reconstructions, and regional geologic and tectonic histories. Here, we examine the utility of multiple provenance analysis techniques through their application to paleo, modern, and synthetic detrital datasets. Zircon is a common accessory mineral found in most detrital sediments, primarily due to its refractory nature. During formation, zircon preferentially incorporates the element U and Th into its crystal lattice while excluding Pb, making it ideal for radiometric dating. Inexpensive and time-efficient U/Pb age acquisition techniques make zircon the mineral of choice for a majority of provenance studies.

The sedimentary basins between the Yangtze River and Red River have long been used to argue for a Mississippi River-scale paleo-drainage. We examine the U/Pb zircon ages of Cenozoic deposits ranging from Eocene to Pliocene age from basins surrounding the first bend of the Yangtze River and upper reaches of the Red River. We combine this data with a comprehensive suite of zircon grain-ages from contemporaneous deposits, modern fluvial sediments, and bedrock source units from previously published literature. Using the new technique developed here, of combining age spectra deconvolution and age component interpolation maps, it becomes clear that Cenozoic deposits of the Southeastern margin of the Tibetan Plateau do not share provenance with offshore sediments associated with the Paleo Red River in the Yinggehai Song-Hong Basin. This, coupled with detailed stratigraphic measurements and interpretations, as well as paleoflow measurements strongly suggests that at least since the Eocene, there was no connectivity between the Yangtze and Red Rivers.

In a modern setting, examination of provenance of fluvial sediments collected throughout

a known catchment can provide insight into regional erosional patterns. The modern Yangtze River, the largest river in Eurasia, provides a perfect setting to apply detrital zircon provenance analysis. We use a previously published zircon U/Pb age distribution dataset of fifteen trunk stream samples and ten samples of the largest tributaries feeding the Yangtze. We apply a series of age-distribution analysis techniques to examine both downstream changes in provenance of trunk stream samples as well as identify the key bedrock and tributary sources of sediment to the trunk stream samples throughout the Yangtze's reach. The original work using this dataset argued that increasing anthropogenic influences, primarily agricultural, lead to a greater than expected influence of the Han, Yuan, and Xiang Rivers, whose confluence with the Yangtze occur in the middle-to lower reaches. The quantitative analysis developed here, however, shows a consistent distribution of U/Pb ages for Yangtze River trunk stream sediments is established in the upper reaches of the Yangtze after the first bend and is maintained some 3000km downstream. The signal is most likely derived from the erosion of the geologic terranes of the Songpan Ganze Terrane and the Longmenshan range, which are sourced primarily by the Yalong, Min, and Dadu rivers. These sources of sediment are consistent with known areas of greater stream power due to higher slopes, exhumation rates, and tectonic activity.

One technique that has recently been applied to detrital zircon datasets is multidimensional scaling, or MDS. MDS transforms pairwise dissimilarity measurements of sample U/Pb age distributions into Euclidian distances and then some optimal configuration, where greater distances between sample points represents greater dissimilarity between their respective age distributions. While MDS is not new, its application to detrital zircon datasets has never been rigorously tested. We examine several important issues in the application of MDS to detrital zircon research, including how intra-sample variation is represented as well as how

dissimilarities are calculated; how random sampling associated with dating a limited number of zircon grain ages can and does affect the resulting MDS configuration; and how MDS differentiation is affected by samples containing either varying degrees of overlapping, shared, or unique age components. In application of MDS to both synthetic and real-world datasets, we illustrate the usefulness of the approach in the interpretation of detrital zircon age data; which suggests that thoughtful application of MDS mapping to detrital zircon data can afford significant advantages in the geologic interpretation of zircon grain ages.

INNOVATIVE AND CONVENTIONAL APPROACHES TO DETRITAL ZIRCON PROVENANCE ANALYSIS: LOOKING TO THE PAST, PRESENT, AND FUTURE.

by

Gregory Karl Wissink

B.A. Boston University, 2011

DISSERTATION

Submitted in partial fulfillment of the requirements for the degree of
Doctor of Philosophy in Earth Sciences

Syracuse University

July 2016

Acknowledgements

This PhD would not have been possible without the help, support, and patience of a considerable number of people, and although I only specifically name a few here, I thank all those who were part of my time at Syracuse University. First I must acknowledge my PhD advisor, Dr. Gregory Hoke, who guided and mentored me throughout all phases of my PhD, through the good times and the bad. I must also thank Dr. Bruce Wilkinson, whose tough but always supportive hand and perspective helped shape much of the work below. I thank my remaining committee members, Dr. Paul Fitzgerald, Dr. Robert Moucha, and Dr. Carmala Garzione for their thoughts, advice, and commitment to my success. I also thank all the field assistants and drivers who helped me conduct my work in China, with particular thanks to Vicky Wang and Lao Li. Mariana Bonich deserves particular acknowledgment for the countless hours of research discussions, the endless support, and being my unwavering rock through this PhD. Thanks of course to my family, especially my parents, David and Jennifer Wissink, for all the support they have given me both here at Syracuse and throughout my life leading to this point. Thanks to my research group, particularly Pedro Val, for his thoughts, discussions, and help. I'd like to thank my many friends, both still in Syracuse and those who have moved on, for providing much needed respites from the stress of graduate school. I must acknowledge the staff of Syracuse University, in particular Julie Neri, Bonnie Andrews, and Jolene Fitch for all their help. And lastly, I must acknowledge the institutions that provided me financial support to conduct this research, including Syracuse University and the National Science Foundation.

Table of Contents

Table of Illustrative Materials

Appendix I

Figures

Tables

Appendix II

Figures

Tables

Appendix III

Figures

Chapter 1. Temporal and spatial patterns of sediment routing across the southeast margin of the

Tibetan Plateau: insights from detrital zircon

Submitted as:

Wissink, G.K., Hoke, G.D., Garzione, C.N., Liu-Zeng, J. (2016). Temporal and spatial patterns

of sediment routing across the southeast margin of the Tibetan Plateau: insights from

detrital zircon. Tectonics (in review)

Abstract

The Cenozoic deposits of the Tibetan Plateau's southeastern margin are often cited as part of a continental-scale river system connecting the paleo-Yangtze River with the Paleo-Red River. Confirming the purported connection and any subsequent drainage reorganization, has garnered significant attention and varied proposed ages for reorganization. This study presents detrital zircon U/Pb ages and paleocurrents in Eocene to Pleistocene sedimentary basin deposits distributed over a broad area of the southeast Plateau margin within the area of proposed paleo-river connectivity. When combined with previously published studies, our U/Pb ages allow examination of the temporal and spatial distribution of provenance throughout the Cenozoic. We identify six key age components of the detrital U/Pb age distributions and use these to examine the patterns of sediment provenance for different Cenozoic Epochs. Detailed analysis of these components shows provenance for both on- and offshore deposits is best described by local bedrock sources and provides little to no evidence of regional changes in provenance. This suggests that a stable fluvial system similar to the modern drainage network has existed since the Eocene with no evidence for major provenance-altering river capture. Paleoflow measurements taken throughout the SE margin further corroborate the results of detrital zircon provenance. The combination of U/Pb age components and paleocurrent directions suggests no Cenozoic connection between the Paleo-Yangtze and Paleo-Red Rivers.

Introduction

Today, many of the great rivers of Asia have their headwaters in the Tibetan Plateau. The history and development of the rivers of the SE margin of the Plateau has captured the attention of geologists for decades (Koons, 1995; Clark et al., 2004; Hallet and Molnar, 2001; Clift, Blusztajn, et al., 2006; Lee, 1934; Gregory and Gregory, 1936; George and George, 1936; Abendanon, 1908; van Hoang et al., 2009; Wei et al., 2015; Zheng et al., 2013; Kong et al., 2012). Their temporal and spatial evolution is believed to hold important clues to the topographic evolution of the Tibetan Plateau. The southeast margin of the Plateau, with its overall gentle topographic gradient (Clark and Royden, 2000) yet large number of strike-slip fault systems with tens to hundreds of kilometers of displacement (Wang et al., 2000; Tapponnier et al., 1986), hosts several of these rivers (Figure 1.1). Clark et al., (2004) presented a comprehensive attempt to reconstruct the river networks of the southeastern margin. Their reconstruction advocates for an initially integrated, Mississippi-scale drainage basin that combined the upper reaches of today's large Southeast Asian rivers, principally with the connected Yangtze River and Red River forming the trunk stream (Figure 1.2). The integrated drainage was subsequently fragmented throughout the Cenozoic via a series of river captures and flow reversals that evolved into today's drainage basins (e.g. Clark et al., 2004; Clift et al., 2006a; Kong et al., 2012; Yan et al., 2012). The disconnection of the upper Yangtze and Red Rivers, often viewed as the key change in the network's evolution, is envisioned to have occurred at or near the Yangtze's "first bend" (Figure 1.2) and to have coincided with the capture of the upper Yangtze by the middle Yangtze, though the timing of this has been contested (e.g. Clark et al., 2004; Clift and Sun, 2006; Kong et al., 2012; van Hoang et al., 2009).

Since fluvial systems theoretically respond rapidly to tectonic perturbations (e.g. Whipple

and Tucker, 1999), an increase in incision rates may reflect a tectonic driver of river reorganization. Based on low temperature thermochronology data, Clark et al. (2005, 2004) and Ouimet et al. (2010) favored a middle to late Miocene regional surface uplift which may have driven the breakup of the SE margin fluvial system to coincide with passive surface uplift induced by lower crustal flow from the central Tibetan Plateau towards its SE Margin. However, recent stable isotope paleoaltimetry estimates from the SE margin suggests similar to modern day elevations since at least the Eocene (Hoke et al., 2014; Li, Currie, et al., 2015), complicating the link to late Miocene lower crustal flow (Hoke et al., 2014). Furthermore, recent work has also indicated that river capture in this area and the formation of elevated low relief surfaces may be driven by subtle differences in local relief and base level changes starving catchments not obviously linked to discrete episodes of tectonic activity, such as lower crustal flow (Yang et al., 2015).

Detrital zircon U/Pb age-distributions are commonly applied as a provenance tool to constrain the routing of sediment through time, and therefore may be used to reveal otherwise elusive changes in paleo-flow patterns of drainage networks. The underlying assumption of this technique is that major changes in measured zircon age distributions reflect coeval changes in the contributing bedrock source areas. A previous Yangtze-Red River connection should be manifested by a continuity of U/Pb ages in deposits of the SE margin, located between the modern Yangtze and the Red Rivers, and offshore deposits of the Red River, indicating connection along the hypothetical integrated catchment (Figure 1.1 and 1.2). Shared provenance of these deposits, hypothetically, would also cease in subsequent deposits postdating the capture of the upper Yangtze by its modern middle-lower reach. This assumes that the provenance of deposits derived from the upper Yangtze differ from those of the Red River catchment. Lastly,

further evidence of a hypothetical paleo-Red-Yangtze system could come from paleo-flow directions of sediments from large river deposits. These predictions have yet to be rigorously tested, because prior work in this region has typically been spatially or temporally limited to areas either near to or far downstream of proposed capture points (Kong et al., 2012, 2009; Wei et al., 2015; Yan et al., 2012; Clift and Sun, 2006; van Hoang et al., 2009; Zheng et al., 2013).

To overcome some of these limitations, we sampled Cenozoic strata within a 250,000km^2 area along the SE margin surrounding the First Bend of the Yangtze and the upper reaches of the Red River (Figure 1.1 and 1.2). This study combines 33 new detrital zircon U/Pb age samples and combines them with 27 previously published samples to create a synoptic spatial overview of zircon U/Pb age-distributions from the Eocene to the Pliocene; a dataset that spans over 600,000km^2. The previously published data include offshore sediment samples of the Yinggehai-Song Hong Basin of Oligocene to Quaternary in age (Yan et al., 2011; Zhao et al., 2015). In addition, we compiled a suite of 37 U/Pb zircon age distributions of modern fluvial samples from the Red (Clift, Carter, et al., 2006; van Hoang et al., 2009), Yangtze (He et al., 2013; Clift, Blusztajn, et al., 2006), and Lancang Rivers (Chen et al., 2014; Clift, Carter, et al., 2006) (Appendix I.; Figure I.1). Finally, we assemble a comprehensive compilation of 97 bedrock U/Pb distributions throughout and immediately surrounding the study area to help identify the bedrock provenance of the detrital samples (Figure 1.1 and Appendix I. Figure I.2). It is important to note, the modern samples from Hainan Island, the Nanpan River, and Ou River are used as both bedrock and modern samples as they represent integrated bedrock samples in areas where we have poor U/Pb age coverage and minimal shared catchment area with the Cenozoic sediments examined here. Lastly, we pair the detrital zircon data with paleoflow measurements of Cenozoic strata to better understand regional transport patterns. Our analysis shows a lack of evidence for a

connection between the Paleo-Yangtze and Paleo-Red Rivers since at least Eocene time.

Regional Geomorphic Background

The Tibetan Plateau is characterized by steep, high relief margins with the exception of the SE Plateau margin (Figure 1.1) (Clark and Royden, 2000). Here, the topography is characterized by high-elevation, low-relief surfaces commonly interpreted as remnants of a relict landscape passively uplifted by ductile lower crustal flow (Royden et al., 1997; Clark and Royden, 2000; Clark et al., 2005; Schoenbohm et al., 2006; Cook and Royden, 2008). The low relief landscape of the southeast margin is often treated as relict paleotopography and used as a datum (Clark et al., 2004, 2005; Ouimet et al., 2010; Clift and Sun, 2006). Paleoaltimetry data suggests that the southeastern edge of the plateau attained its modern elevations by at least Eocene time (Hoke et al., 2014; Li, Currie, et al., 2015). Recent work, however, strongly suggests that what is commonly described as the relict landscape of the southeast plateau margin may instead be the product of an autogenic river capture process (Yang et al., 2015). This process, driven by differences in local base levels in adjacent basins, does not necessitate a continuous, uplifted relict topography as envisioned by Clark et al. (2004).

The Modern Yangtze, Lancang, and Salween Rivers all have their headwaters on the Tibetan Plateau and drain parallel to the curvature of the eastern syntaxis (Figure 1.1; Hallet and Molnar, 2001). The rivers have incised ~2 km deep, parallel canyons, separated by narrow mountain ranges along their southward flow paths off the plateau. The Yangtze River, however, makes a sharp turn at the First Bend and begins flowing eastward (Figure 1.1 and 1.2), eventually draining into the East China Sea. In contrast to these main rivers, the Red River's headwaters are not on the plateau and its course is largely controlled by the Ailao Shan-Red

River fault system (Allen et al., 1984; Leloup et al., 1993, 2006) before draining into the

Yinggehai-Song Hong Basin (YSHB) in the northwest corner of the South China Sea.

Previous Work

Geochemical, thermochronologic, and geochronologic data have been used in various

attempts to constrain the Cenozoic history of drainage (Clift and Sun, 2006; Clift, Blusztajn, et

al., 2006; Kong et al., 2009; Robinson et al., 2014; van Hoang et al., 2009; Yan et al., 2012;

Zheng et al., 2013), with timings of fluvial changes ranging from Eocene to Plio-Pleistocene.

Using (U-Th)/He and fission track ages of bedrock apatites, Richardson et al. (2010) noted an

Eocene change in fluvial incision rates from the middle Yangtze River. This was interpreted to

be possible evidence for the capture of the upper Yangtze by the lower and its possible

disconnect from the Red River. Changes in Nd isotopic data, seismic analysis, and sediment

budgets of deposits of the YSHB and Hanoi Basin by Clift and Sun (2006) and Clift et al. (2006)

were interpreted as significant changes in the Red River drainage occurring between the middle

Miocene to late Oligocene. Sediment budget estimates from Clift et al. (2006) may be under

represented as they estimate the total mass lost below the 'stable' paleosurfaces of the SE margin

proposed by Clark et al. (2004). Using a modern average erosion rate of 90m/Ma of these

purported paleosurfaces calculated near the Yangtze First Bend by McPhillips et al. (2016), and

applying it to the modern Red River catchment, one arrives much closer to the estimated offshore

volumes. Clift et al.'s (2006) sediment budgets do not consider inputs from Vietnam and Hainan

Island, making the loss of Red River drainage unnecessary to close the sediment budget gap

(Zhao et al., 2015). Interpreted changes in provenance in the late Oligocene are not unique to the

YSHB, as evidenced by a study correlating zircon ages with sequence stratigraphic relations in

the Jianchuan Basin, considered to be the most likely location of a Red River–Yangtze

connection (Yan et al., 2012). Oligocene provenance changes were interpreted as a drainage response to regional strike-slip deformation along the Ailao-Shan Fault Zone (Yan et al., 2012).

The Pliocene to Pleistocene reorganization proposed by Kong et al. (2012) is linked to large-scale deformation associated with clockwise rotation of the Eastern Himalayan syntaxis. The middle to late Miocene incision reported by McPhillips et al., (2016) below the wind gap of purported paleoflow, all but precludes the timing of Kong's et al. (2016). Overall stability of the Red River drainage (van Hoang et al., 2009) and the lower Yangtze River Drainage (Zheng et al., 2013) since at least the late Miocene and Oligocene, respectively, have been interpreted from lack of local temporal variation in zircon distributions.

A series of recent studies calls into question the previously assumed connection of the Yangtze and Red River. Analysis of sediment cores and stratigraphy of the southern Jianchuan Basin found no evidence of a southward flowing fluvial system in the basin in Eocene and younger deposits (Wei et al., 2015). This is supported by recent river incision data at the first bend, documented from cosmogenic nuclide dating of cave deposits, which precludes late Miocene or younger capture (McPhillips et al., 2016). Study of the offshore YSHB finds no geochemical evidence of capture in Oligocene and younger deposits, favoring instead consistent flux of sediment from Hainan Island and Central Vietnam since the late Oligocene (Zhao et al., 2015). Despite extensive study, no conclusive consensus has been reached for the evolution of the modern drainages along the southeastern plateau, though most lean towards Miocene or earlier capture. Our study attempts to better constrain when or if connectivity of the Yangtze and Red River existed using a much greater spatial and temporal detrital zircon record than previously published.

Methodology

Sampling strategy

For this study, we collected samples from basins near several hypothesized capture points as well as other exposures of Cenozoic deposits. These basins include the Jianchuan, Yanyuan, and Jinggu basins, as well as exposures near the cities of Lühe, Dali, Lanping, Lijiang, Midu, and Jianshui (Figure 1.1 and 1.2).

The samples collected in the Jianchuan Basin, as well as those from near Lijiang, Lanping, and Dali fall within the area of hypothesized connectivity, south of the modern Yangtze to the northern headwaters of the Red River (Figure 1.2). A connected fluvial system passing through these basins would be reflected as a continuous and relatively uniform distribution of U/Pb ages from the SE margin deposits to along the course of the hypothesized river and the offshore deposits in the YSHB. The sedimentary facies throughout the SE margin include axial river, alluvial fan, large fluvial, lacustrine, and eolian deposits. Fluvial facies on the scale of paleo Yangtze-Red River are restricted generally to the Paleogene of the Jianchuan and Jinggu basins, while other sedimentary deposits reflect axial rivers or alluvial fans associated with transverse drainage systems. The U/Pb age signal from the upper Yangtze and the basins between the first bend and headwaters of the Red River would be transmitted downstream by a connected Yangtze-Red River. This signal would therefore be imparted to any YSHB and paleo Red River deposits.

The Jianchuan Basin (Figure 1.2) is a ~100km long and ~30km wide basin and is the largest exposure of Cenozoic deposits within the SE Tibet margin. The center of the basin lies ~30km to the west of the First Bend and is the best-sampled basin of the SE Plateau margin. Two Eocene

samples were collected in the Baoxiangsi formation. The lower, middle, and upper Baoxiangsi

formation consist of massive clast supported conglomerates with interbedded massive poorly

sorted sandstones (Wei et al., 2015); thickly bedded and well-sorted mature cross bedded

sandstones in the north and channel fills of braided rivers in the south; and red fluvial sandstones

siltstones and mudstones a well developed floodplains, respectively. Detrital samples were

collected from the middle and upper Baoxiangsi Formation. One Oligocene sample was collected

in the northern Jianchuan Basin from the massive well-sorted sandstones intercalated with

conglomerates and mudstones of the Jinsichang formation (Figure 1.2). Two additional Eocene

samples were collected in central Jianchuan Basin near the city of Shigu from transverse fluvial

deposits, and three Miocene samples were collected in the southern basin from medium-thickly

bedded trough and planer cross-bedded sandstones, which were interbedded with mudstones. In

addition, four previously published samples from the southern Jianchuan Basin (Yan et al.,

2012), one from each Epoch from the Eocene to Pliocene, were included in our dataset. Poor

depositional age constraints place the well-sorted, medium to thickly bedded fluvial deposits

collected near Midu, located within the modern catchment of the Red River, as very late Eocene

age (given a significant proportion of Priabonian age zircon) or Oligocene age. An Eocene

sample from lenticular sandstone lenses intercalated with imbricated conglomerates was

collected in the deposits near Lijiang ~40km east of the First Bend (Figure 1.2). Additional

Pliocene samples were collected just south of the Jianchuan Basin near Dali from medium-

thickly bedded sandstones overlying massive conglomerates (one sample) and ~100 km west of

the Jianchuan Basin near Lanping in the Shuanghe Formation, consisting primarily of grey to red

interbedded mudstone, siltstones, and sandstones and marl deposits (three samples) (Figure 1.2).

The Cenozoic sedimentary rocks of the Jinggu basin collected ~60km east of the Lancang

River and ~125km west of the Red River, fall completely within the modern drainage of the Lancang, and borders the drainage divide of these two rivers. The Jinggu Basin may represent the path of the Paleo-Lancang River and possibly a point of connection where the Lancang River drained into the Red River (Figure 1.1 and 2). The Paleogene sample collected from the fluvial red-beds of the basin is poorly constrained as either Eocene or Oligocene age. The five Neogene samples were collected from periodic massive sandstones beds within the primarily lacustrine deposits of the Miocene Shanhaogou and Huihuan Formations. By examining the provenance of these units, we will be able to better constrain the existence of the modern Lancang–Red River divide in the late Paleogene-Miocene.

The Yanyuan Basin lies to the northeast of the First Bend ~40km west of the Yalong River, a major tributary of the Yangtze River often included in the Paleo Yangtze-Red River reconstructions. Eocene samples of the Yanyuan Basin are from the northern and southern extremes of the basin in sand lenses within conglomerates and alluvial fan deposits, respectively, and should provide insight into the U/Pb age signal of deposits derived from bedrock sources in the NE. The basin's proximity to the modern Yalong River, a major tributary of the upper Yangtze, allows for the reasonable expectation of shared provenance between modern and paleo deposits in the event of Yalong-Yangtze-Red River connectivity. With high exhumation on the Longmenshan documented to be as early as Eocene (Wang, Kirby, et al., 2012), it would likely impart the Yalong's unique U/Pb age character on the Yanyuan Basin to the on- and offshore deposits of the Yangtze-Red River system. The four Pliocene samples were collected from point bar and active channel deposits from Yanyuan and may help establish any major changes in provenance between the Eocene and Pliocene.

Samples collected near the city of Jianshui are Pliocene deposits, which vary from imbricated

pebble-cobble conglomerates to finely laminated mudstones. We collected three Pliocene samples within the western border of the Nanpan River Catchment and 45km from the modern Red River. The location of these samples helps establish the position of the drainage divide between the Nanpan and the Red River in the late Neogene.

The late Miocene sample collected in the Lühe coalmine is from the Huanggang formation consisting of primarily interbedded brown medium to coarse tuffaceous sandstone with trough cross beds and black organic rich grey-black coal deposits. It lies within the Red River catchment ~100 km to the west of Midu, just south of the modern Yangtze-Red River divide and may help define the drainage divide in the Miocene.

In addition to these SE margin deposits, we use six Miocene samples from fluvial deposits analyzed by van Hoang et al. (2009), five from along the modern Red River and the sixth from the Nanpan River catchment (Figure 1.1B). These data are grouped with our Miocene samples. Miocene connectivity would give rise to matching provenance of these deposits to those of the northern basins associated with the upper and middle Yangtze River.

We compiled U/Pb data of offshore deposits of the Red River in the YSHB. Two Oligocene, nine Miocene, and five Pliocene samples from the previously published works of Yan et al. (2011) and Zhao et al. (2015) are also included in our detrital dataset. The modern fluvial deposits (Appendix I. Figure I.1) include 23 detrital samples from the modern Yangtze sediment (He et al., 2013), three samples from the Lancang River (Chen et al., 2014; Clift, Carter, et al., 2006), and two from the Red River (van Hoang et al., 2009). Lastly, a literature review produced a dataset containing 31,276 zircon ages from 97 potential contributing bedrock source distributions spanning much of East Asia (Figure 1.1, Appendix I. Figure I.2). Ages for compiled

data were primarily measured using LA-ICP-MS analysis; however, sensitive high-resolution ion microprobe (SHRIMP) and thermal ionization mass spectrometry (TIMS) ages are included in the bedrock data when no LA-ICP-MS data were available, despite the lower analytical uncertainties of the aforementioned methods, as we do not make direct analytical comparisons of distributions measured using varying methodologies.

Sample Processing

All samples were collected from medium to very coarse-grained sandstones. Zircon grains were collected between the size fraction of 60-250 μm. Zircon was separated using standard magnetic and heavy-liquid separation techniques and handpicked at random under a binocular microscope avoiding grains with obvious fractures or large inclusions. Grains were mounted in epoxy and imaged using an electron microprobe, acquiring cathodoluminescence images. U and Pb isotope ratios were measured via laser ablation ICP-MS at the University of Arizona LaserChron Center using a Micromass Isoprobe multicollector equipped with a DUV 193 laser ablation system following the procedures outlined in Gehrels et al., (2008). $^{206}Pb/^{238}U$ ages were used for ages <900Ma and $^{206}Pb/^{207}Pb$ ages for those >900Ma. Ages exceeding 20% discordance or 5% reverse discordance were excluded from the dataset. Ages with uncertainties exceeding 10% of the determined age were also excluded. All uncertainties are reported to 1σ (See Appendix I. Material). In total, we measured 2,614 ages for 33 detrital samples. Zircon grains were imaged using cathodoluminescence to identify and avoid areas of strong zonation.

Component Analysis and Spatial Interpolation

Zircon U/Pb distributions for a given sample can be thought as the summation of one or more discrete age components. We define a 'component' as a discrete suite of zircon ages centered on a mean value. Each age component theoretically represents some zircon-forming event that

exhibits age variance about a mean value. A detrital sample U/Pb age frequency distribution consists of one or more of these components. Probability distribution functions (PDF), used here, or kernel density estimations (KDE) are typically employed to represent the distribution of ages within a sample (Figure 1.2 and 1.3).

In addition to a distribution for each sample, we created a distribution representing the overall variance within the 60 Eocene-Pliocene detrital samples (this study and compiled) by summing the PDFs of each sample into a single distribution that was renormalized to unity. Equal weight is given to each distribution in the aggregate, regardless of the number of zircon grains dated within each sample, creating a representative average frequency distribution of the dataset (Figure 1.3a; Black Line). By giving equal weight to each sample, the data is not biased towards samples with more measured ages. Summation of PDFs or KDEs yields similar curves (Figure 1.3a); however, we choose to work with PDFs, because KDEs require the use of a bandwidth to define the size of the kernels, much like a bin-width of a histogram. Optimal bandwidth algorithms exist (e.g. Botev et al., 2010) but the bandwidth is strongly dependent on the number and distribution of ages, which vary from sample to sample. KDE bandwidths can be predefined to reduce data heterogeneities; however, doing so can result in an overly smoothed or noisy probability function. In contrast, PDFs sum the Gaussian representation of the measured analytical ages and uncertainties, which are consistently computed for the samples of the aggregate summation.

To identify key components in our summed distribution, we use a deconvolution algorithm, which fits a Gaussian curve to each component while minimizing the mean square error for each (Figure 1.3a). This defines a mean and standard deviation for each identified component. The components are calculated as the mean ±2 standard deviations. The algorithm

runs until ≥90% of the variance of our summed distribution is described.

Identification of these discrete components in the aggregate, denoted henceforth as "master" components, allows for calculation of the approximate proportions of each master component present in all individual samples. The proportion of a given master component is approximated by integrating the PDF for a sample over the master's age range (x-values; Figure 1.3c). This proportion is applied as the vertical axis of a 3D plot, where X and Y values are the longitude and latitude of the sampling location. After each master component proportion is determined for all samples for a given time slice map (Figure 1.3), a Kriging interpolation is applied to the X, Y, Z coordinates to calculate the spatial distribution of a master component for all samples plotted. We use an X, Y grid resolution of 0.1° (Figure 1.3d). The node value at a point X, Y (Z_{xy}) is calculated using the equation:

$$Z_{xy} = \sum_{i=1}^{n} W_i Z_i \ (1)$$

where Z_i is the value of a sample location with the given weight W_i. One major advantage of using a Kriging function is that all weights will sum to unity, which serves to remove biases related to multiple-sample sections. Kriging also allows for empty sections of the grid to be calculated creating a smooth, continuous surface (Sunila and Kollo, 2007). For each master component, we create six interpolation maps (Figures 1.5-1.10). These six maps include modern fluvial detrital samples (Figures 1.5-1.10a), detrital results of four Epochs of the Cenozoic (Pliocene-Eocene; Figure 1.5-1.10b-e), and possible contributing bedrock source samples (Figures 1.5-1.10f). We assume, for the sake of simplicity, that the position of samples relative to one another is approximately fixed from Eocene time to present. The Jinggu and Lanping

localities are potential exceptions to this assumption because they lie west of Red-River Ailao Shan Shear Zone of strike-slip motion and its northern extension.

Paleoflow Measurements

Paleoflow measurements were collected in measured sections and scattered Cenozoic outcrops throughout the SE margin. This provides a second set of observations that complements the detrital zircon data. Paleoflow data was collected at 45 separate sites with the majority from conglomerate clast imbrications, as these were the most abundant paleoflow indicators regionally. For these, at least 10 orientation measurements of imbricated clasts were taken at each location to determine paleoflow. Within the northern Jianchuan basin, large scale, trough cross-beds were measured in eolian dune deposits. For these measurements, left and right limbs were measured to calculate paleoflows. Paleoflow direction was determined from the trend and plunge of the axis of the trough as determined from the two populations of fold limb measurements. All paleoflows are adjusted for regional tilting and were calculated and plotted using Stereonet software (Allmendinger et al., 2013; Cardozo and Allmendinger, 2013). We supplement our paleoflow dataset with additional measurements from seven sites reported by Wei et al. (2015) (Figure 1.4). While paleoflows measured from conglomerate imbrications likely represent flow directions of transverse river systems, and thus not necessarily a large axial river, they do provide information on the local character of the drainage basins where transverse rivers may have fed into axial through-going rivers.

Results

Spatial Interpolation

In our aggregate dataset, seven age components describe >90% of the total variance of the summed population. These components, defined by $\mu \pm 2\sigma$ (given as $\mu\text{-}2\sigma\text{-}\mu\text{+}2\sigma$) are: 32-40 Ma; 89-125 Ma; 203-239 Ma; 216-288 Ma; 377-495 Ma; 695-895 Ma; and 1816-1926 Ma (Figure 1.3). Due to overlapping components, we reduce the Permo-Triassic component to 239-288 so it falls outside of the late Triassic component. This is necessary because of the bimodal ages and geographically distinct locations of Mesozoic (primarily Triassic) volcanism in the headwaters of the Yangtze and Hainan Island (Figure 1.7 and Figure 1.8). We group samples from the Jinggu Basin and Midu Basins as Paleogene because of depositional constraint uncertainties and thus include them in both Paleogene Epoch maps. The proportions of each master component above are calculated for all samples, creating the spatially interpolated maps of Figures 1.5-1.10. For consistency we divide the proportions or concentrations of master components into categories of absent, very low (1-5%), low (6-10%), moderate (11-20%), high (21-30%), and very high (> 30%) (Figures 1.5-1.10). The 377-495 Ma component has no strong spatial patterns and is included in the Appendix I. material. The remaining six master components, and their potential utility in recognizing linkages the paleodrainage development, are described below.

Paleogene component (32-40 Ma)

Paleogene age zircon, between 32-40Ma, are present in Late Eocene to Pliocene deposits within the SE margin and in the YSHB (Figure 1.5). High concentrations are localized in the area between the First Bend and the upper reaches of the Red River Catchment near the city of Dali. Three of five Miocene samples adjacent to the Red River contain Cenozoic zircon of very low

and moderate proportions, with a moderate peak that quickly reduces in samples to the north or south. Proportions of this component are very low in Oligocene-Pliocene deposits of the YSHB, consistent with the 1% concentrations of modern Red River sediment (Clift, Carter, et al., 2006). High concentrations are centered near the first bend where the ~2000 km Ailao Shan-Jinshajiang potassic igneous belt occurs (Chung et al., 1998) (Figure 1.5f).

Cretaceous component (89-125 Ma)

The mid-Cretaceous component (89-125 Ma) has consistently higher concentrations in Oligocene to Pliocene deposits of the YSHB with concentrations reaching >60% for several samples from Miocene deposits and >20% for an Oligocene sample (Figure 1.6). Very low concentrations are found within the deposits of the SE margin, regardless of depositional age. The mid-Cretaceous zircon component reaches its highest (5-10%) in the Jinggu Basin, Yanyuan Basin, and near Midu and Lanping. There is a notable absence of Cretaceous zircon south-southeast and east of the first bend near Dali, Jianshui, and Lijiang as well as in the Jianchuan Basin. Miocene deposits from within the present-day Red River catchment have absent to low concentrations of mid-Cretaceous zircon. This component is also notably absent in modern river deposits of the Yangtze River near the first bend, the Lancang River west of our study area and the modern Red River deposits. Modern fluvial sediment from Hainan Island within the S. China Sea has the highest concentrations, reaching moderate levels comparable to Cenozoic sediments of the YSHB.

Late Triassic component (203-239 Ma)

Late Triassic zircon ages are found in multiple regions throughout the study area and are related to Indosinian post-collision magmatism following the closure of the Paleo-Tethyan Ocean (Dong et al., 2013; Peng et al., 2014a, 2014b; Figure 1.7). There are several potential

sources for zircon of this age (see Figure 1.7f), including: the arc volcanics of the Eastern Yidun

block (YA) (Reid et al., 2007; Peng et al., 2014b); Lincang granitic intrusions (LG) (Dong et al.,

2013), and Qiangtang Block volcanics (QV) (Peng et al., 2014a). Recycling of Mesozoic strata is

another potential source of Late Triassic zircon. Moderate-high concentrations are found within

the Eocene deposits of the Yanyuan Basin, while low-moderate concentrations are more

common for deposits west and south of the First Bend (Figure 1.7a). Concentrations increase

from moderate in the Eocene to very high in Oligocene deposits of northern Jianchuan Basin,

while moderate concentrations are found throughout the remaining SE margin. The Oligocene

deposits of the YSHB display moderate-high concentrations. However, a closer inspection

reveals that the modal zircon ages within these deposits fall primarily in the Permo-Triassic

component (see below) and not in the Late Triassic. In Miocene deposits of the SE margin, the

Jinggu Basin's Late Triassic zircon concentrations are moderate-very high. The remaining

onshore Miocene sediments throughout the SE margin, including those along the Red River have

low late Triassic zircon concentrations. Miocene samples of the YSHB have low concentrations

in northern samples and moderate concentrations in southern samples. In the Pliocene,

concentrations are highest near Lanping (moderate-high), while elsewhere, concentrations

remain low including in the YSHB. In modern rivers, moderate concentrations are found in

Lancang River deposits (Figure 1.7a) as it flows west of the Qiangtang Volcanics and in

tributaries of the Yangtze downstream of the first bend. The Red River has low concentrations of

late Triassic zircon.

Permo-Triassic component (239-288 Ma)

The Permo-Triassic component, spanning 216-288 Ma (Figure 1.8), and adjusted to 239-

288Ma, with a mean of 254Ma, is related to the emplacement of basaltic Emeishan LIP (Figure

1.8; EIP) (Shellnutt, 2014); Jomda-Weixi arc volcanics (Figure 1.8; WV) (Yang, Ding, et al., 2014); western Yidun arc (Figure 1.8; YA) (Reid et al., 2005; Peng et al., 2014b; Reid et al., 2007); early emplacement of the southern Lincang complex (Figure 1.8; LG) (Dong et al., 2013) and Hainan Island volcanics (Figure 1.8; HI) (Xu, Sun, Yi, et al., 2014; Wang, Liang, et al., 2015). Concentrations in Eocene sandstones from the Jianchuan basin are very high in the north, moderate-high just west of the first bend and low-moderate in the southern basin. Northeast (Yanyuan Basin) and southeast (Jinggu) samples have low concentrations. Oligocene samples found in southern Jianchuan and the YSHB both contain very high proportions of Permo-Triassic zircon in Oligocene deposits, with apparently strong gradients away from these locations. Miocene deposits show the highest concentrations of this age component in the southernmost YSHB, with a marked decrease towards moderate concentrations similar to that of onshore Miocene deposits found within the Red River catchment. Within the suite of Miocene deposits of the SE margin, concentrations are very low to low in the Jinggu Basin and Jianchuan basin, the latter being dominated by Cenozoic volcanics. Modern samples from the Red River, Yangtze and Lancang Rivers have moderate concentrations and Hainan Island deposits are moderate-high.

Neoproterozoic component (695-895 Ma)

The Neoproterozoic age component (Figure 1.9) is primarily related to a series of Neoproterozoic volcanic terranes of both continental arc and back arc extensional regimes associated with the subduction and convergence of North and South China Blocks (Druschke et al., 2014). Today, Neoproterozoic bedrock exposures are found in the Longmen and Qingling Mountains (LM in Figure 1.9f) (Pei et al., 2009), the Yanbian Terrane east of our study area (YT) (Zhou et al., 2006) and the related Luliang Formation (Zhuo et al., 2013). In Paleogene and Neogene detrital samples, a longitudinal and latitudinal decreasing gradient in the concentration

of Neoproterozoic zircon moving away from the Yanyuan Basin is apparent. Notably, concentrations are low for most samples collected along the SE margin of the Plateau (Figure 1.9b-e). One Miocene sample from the southern Jianchuan Basin with strikingly high Neoproterozoic zircon concentrations is an exception (Yan et al., 2012). Neoproterozoic age zircon are absent in Oligocene YSHB deposits. Miocene YSHB samples, however, have a clear latitudinal gradient offshore, with increasing concentrations toward the northern margin. The highest offshore concentrations in the Miocene match the moderate-high values found in onshore Miocene deposits of the Red River catchment. Miocene, Pliocene, and modern samples collected along the Red River all show similar trends of high-very high concentrations in northern samples to moderate concentrations approaching the coast of Vietnam. The Neoproterozoic age component constitutes a major proportion of zircon components in modern Yangtze River sediment downstream of the first bend (He et al., 2013, 2014). Following the incorporation of the Yalongjiang, which contains 63% Neoproterozoic ages, concentrations exceed 15% in modern Yangtze trunk stream samples east of this juncture.

Paleoproterozoic component (1,816 to 1,926 Ma)

The 1,816-1,926 Ma Paleoproterozoic zircon age component (Figure 1.10) is associated with extensive granitic plutons throughout the Western Yangtze Block (Figure 1.10; YB) (Sun et al., 2009), and, to a lesser extent, the North China Craton and Eastern Cathaysian Block. The Paleoproterozoic component is an important component of zircon in the Mesozoic deposits of the Sichuan Basin (SB) and is common in contemporaneous deposits throughout the region (She et al., 2012; Weislogel and Robinson, 2010; Fei et al., 2013). Within the SE margin, Eocene samples of the Jianchuan and Yanyuan Basin contain moderate-high concentrations, while other onshore Eocene samples have low concentrations. Within the Oligocene, Miocene, and Pliocene

similar patterns emerge with low concentrations found throughout most of the SE margin and slightly higher concentrations in the Jianchuan Yanyuan and Jinggu Basins. In the Pliocene, the samples from Jianshui also show moderate concentrations. Paleoproterozoic zircon in Oligocene to Miocene deposits of the YSHB never exceeds low concentrations, similar to the onshore Miocene deposits along the Red River. Within modern deposits, Neoproterozoic concentrations are low in the Yangtze and Lancang Rivers despite the high concentrations found in bedrock of their headwaters. Samples from the modern Red River show similarly low concentrations to those of the Miocene deposits and the northern YSHB basin.

Paleoflow Results

Individual paleoflow measurements were compiled into regional and temporal trends (Figure 1.4). Eocene paleoflows in both Northern and Southern Jianchuan Basin indicate flow in all non-southward directions. The Eocene in the Jianchuan Basin is part of the Baoxiangsi formation; the lower is composed of breccias and clast supported conglomerates. Here, the lower Baoxiangsi of the northern Jianchuan Basin reveals paleoflows towards the north, consistent with similar measurements of Wei et al. (2015). Southern Jianchuan Basin Eocene deposits indicate westward flow. The middle Baoxiangsi formation in the northern Jianchuan Basin, interpreted as eolian dune deposits (Cui 2013), have cross-beds with measured flow directions consistently eastward. Wei et al., 2015 found similar cross-bed flow directions of northeast to north in fluvial derived cross-beds of the southern Jianchuan Basin. Eocene deposits near Jianshui (Figure 1.4) indicate northeastward flow. Aside from Eocene deposits in the southern Jianchuan basin that show westward flow, all Eocene paleoflow directions in the Jianchuan basin show northward to eastward paleoflow directions.

Imbricated conglomerate flow directions of Oligocene deposits of the Jianchuan Basin change from westward to eastward flow moving up section, the latter consistent with the results and interpretations of Wei et al. (2015) (Figure 1.4). Near Lijiang, Oligocene conglomerates reveal southwestward flow (Figure 1.4). Neogene deposits throughout the SE margin are characterized by lower depositional energy regimes yielding fewer paleoflow indicators. Two Miocene paleoflow measurements were taken from imbricated conglomerates near Jianchuan and Jianshui (Figure 1.4). Westward flow is indicated in imbricated conglomerates near Jianchuan while imbrications near Jianshui indicate flows to the northwest, consistent with tributary flows of the modern Nanpan River. Near Yanyuan, eastern and western flanking Pliocene deposits indicate eastward flow while the central deposits show southward flow. The southward flow parallels the modern drainage pattern of the Yanyuan Basin.

Discussion

A connection between the Yangtze and Red River should be recorded in the detrital zircon record as a spatially consistent stretch of age components ranging from the SE margin of the Tibetan Plateau towards the contemporaneous deposits in the YSHB (Figures 1.5-1.11). While we recognize that the majority of sampled deposits along the southeast Plateau margin do not represent large fluvial deposits, the characteristic ages of northern derived zircons from actively eroding areas should comprise important components of any integrated paleodrainage. As sediment is routed into progressively larger parts of the river networks, and given the areal extent of the Jianchuan, Jinggu and Yanyuan Basins (Figure 1.2), they must have been important sources of sediment for a connected Yangtze-Red River. Similarly, if the middle Yangtze once flowed southwest (current eastward) as a segment of the Red River, U/Pb age distributions offshore of the YSHB and any onshore fluvial deposits, should carry a middle Yangtze signature.

A connection between any portion of the Yangtze, SE margin basins, and YSHB would require a commensurate change in U/Pb distributions following any reversal or capture of the middle and upper Yangtze.

The use of distinct Gaussian age components determined from the summation of zircon age frequencies from Cenozoic deposits spanning a wide area of the SE margin provides constraints on the temporal and spatial evolution of the river networks. Conventional comparison techniques, which serve to reveal similarities and differentiate components, such as likeness (Satkoski et al., 2013), probability density crossplots (Saylor et al., 2013), and Kolmogorov-Smirnov tests (Wilk and Gnanadesikan, 1968) which are common in detrital zircon work, often become difficult to apply as datasets grow. This is, in part, because they provide a quantitative metric of dissimilarity, but cannot describe the root of the similarities or discrepancies.

Deposits in the basins of the SE margin and YSHB have zircon components that are largely consistent with local bedrock. Notably, detrital zircon distributions containing moderate to very high concentrations of a particular Gaussian component, are consistent with local bedrock sources with similarly high concentrations of the same component (Figures 1.5-1.10). For example, high concentrations of Paleogene zircon in the southeast margin are localized, lacking spatial continuity and occur near igneous bodies related to the Ailao Shan-Jinshajiang potassic igneous belt (e.g. Wang et al., 2001; Yan et al., 2012). Both Cretaceous and Permo-Triassic components, found in higher proportions within the YSHB basin, are explained by the associated high concentrations found in Hainan Island and bedrock within the modern Red River Catchment (Xu, Sun, Cai, et al., 2014). Similarly, the deposits of the southeast margin outside the Red River Catchment have low concentrations of these components, rejecting a correlation between the basins of the SE margin and the YSHB. Offshore YSHB deposits are dominated by

the Permo-Triassic age volcanics attributed to deposits from Western Hainan Island and Vietnam (Cao et al., 2015). This is further supported by the work of Yan et al. (2011), who documented euhedral zircon grains of the YSHB as evidence of a local source for the YSHB. In contrast, the majority southeast margin sediments show a much stronger affinity for late Triassic zircons. The clear consistent offshore gradients of the YSHB basin, with samples proximal to the Red River closely resembling on-shore Miocene deposits and more distal samples more closely matching Hainan Island distributions, indicates little to no provenance change since at least the Oligocene (Zhao et al., 2015; Wang, Liang, et al., 2014). Higher concentrations of Late Triassic zircon in the Eocene deposits of Yanyuan (Figure 1.7e) and Miocene of Jinggu (Figure 1.7c) are easily linked to the nearby Yidun Arc Volcanics (Reid et al., 2007) (Figure 1.7f; YA) and Lincang Granites (Figure 1.7f; LG), respectively. High concentrations of the late Triassic component in Miocene deposits of the southern Jinggu Basin are most likely derived from the nearby Lincang Volcanic Complex (Dong et al., 2013).

We assert that a large integrated network would show a certain degree of continuity following the incorporation of a bedrock or zircon source units into its catchment. Instead, within the entire Cenozoic sedimentary record examined here, we only observe "hot spots" in certain Gaussian components that are best explained by local sources. Temporary sediment storage along the trunk stream and major tributaries has the potential to mask provenance signals. In one case, deposition, storage and remobilization in a river system with an anomaolous U-shaped map pattern, results in significant sediment remobilization downstream (Nie et al., 2015). Yet, in other environments, with typical trunk stream geometry, there is little evidence for storage impacting sediment delivery downstream (e.g. Dobson et al., 2001; He et al., 2013; Reiners, 2005). While we cannot necessarily rule out sediment storage as a possibility, a major reduction

in the upstream signal would require a large fraction of river transported sediment be sequestered in partial sediment storage.

A critical component for demonstrating connectivity of the upper Yangtze and basins of the SE margin with the paleo-Red River are late Triassic zircon ages between 203-239 Ma. Modern deposits collected from the Yangtze, Lancang, and Red River show that the source of modal components are indicative of sources north and west of the Yangtze at the first bend. The late Triassic zircon components are absent to low from sandstones collected within the Red River catchment. However, the abundance of late Triassic zircon ages in samples from the adjacent Lancang River are approximately three times that of the Red River; the Yangtze at the first bend has approximately double. Only 3% of the zircon from the Red River fall within the late Triassic component and do not define a clear age mode. Higher late Triassic zircon concentrations found in the Paleogene, Neogene, and modern deposits of the southeast Margin, while minimal concentrations are found in the modern and ancient deposits within the current Red River Catchment and YSHB, suggesting no connectivity between the Red River and the upper Yangtze River over much of the Cenozoic.

Neoproterozoic age zircon is an important age component of the middle Yangtze River, ancient and modern Red River deposits, and the YSHB. Therefore, the presence of this component in offshore sediments does not preclude connectivity between the two rivers. The Red River catchment encompasses exposures of Neoproterozoic rift related volcanics (Zhuo et al., 2013), providing a clear source for zircon of this age, while not requiring connectivity. With respect to the southeast margin, there is a significant decrease in concentrations of Neoproterozoic zircon moving from east to west throughout the basins of the SE margin. Neoproterozoic ages are found within these sedimentary basins, but in concentrations far lower

than those of modern fluvial deposits of the middle Yangtze where concentrations often exceed 15% (He et al., 2013, 2014). This conspicuous lack of Neoproterozoic, and therefore middle Yangtze signal, suggests the paleo- middle Yangtze was not flowing westward through the SE margin in our Eocene-Pliocene deposits.

Consistent similarities between zircon U/Pb age components of northern deposits of the YSHB, the Miocene deposits along the Red River, and modern Red River fluvial deposits are indicative of little change in catchment area in the Cenozoic record, consistent with the findings previous studies (van Hoang et al., 2009; Jiang et al., 2015; Cao et al., 2015). There is a clear increase in Hainan Island component in deposits further south and east in the YSHB as Indosinian and Cretaceous age zircon concentrations rise.

Offshore detrital zircon U/Pb records only extend to the Oligocene. Therefore, any inferences we make predating the Oligocene must be based paleoflows, stratigraphic interpretations, and zircon distributions of the SE margin. Paleocene deposits of the southern Jianchuan Basin are primarily mudstone and siltstone with interbedded lacustrine limestone deposits (Wei et al., 2015) that are not indicative of a large fluvial network. Eocene sedimentation within the Jianchuan Basin is primarily alluvial (Wei et al., 2015) with paleoflows indicating both northward and westward flow, depositional facies suggesting axial fluvial systems, while Eocene proximal alluvial fan deposits in Yanyuan do not have paleoflow indicators. Though not inconsistent with a large southward draining large fluvial system, the lack of regionally contemporaneous fluvial deposits does not support such a hypothesis. The late Eocene deposits of the Baoxiangsi formation are eolian deposits in the northern Jianchuan Basin and fluvial in the southern basin. Even assuming all late Eocene trough cross-bed deposits of the Jianchuan Basin represent fluvial deposits from a large through-going river, cross-bed

paleoflows in the northern and southern basin indicate eastward and northward flow, and not a southward flowing fluvial system.

The northeastward Eocene flows of the Jianshui Basin suggest that the divide between the Nanpan and Red River catchments existed in the Eocene. Oligocene imbricated deposits of the SE margin do indicate southward flow, although there are a limited number and geographic distribution of sites and little other evidence for southward flow, particularly on cross-bedded strata. Miocene paleoflows measure no discrepancies between paleo-directions and modern fluvial drainages.

Most studies calling for connectivity between the Red and Yangtze Rivers, suggest a major change in catchment area. However, a telling and consistent feature of our spatial interpolation maps is the temporal consistency in offshore deposits of the Yinggehai-Song Hong Basin and their effective discontinuity with the basins of the southeast plateau margin. Oligocene to Pliocene detrital zircon age spectra of samples from the YSHB exhibit no major changes, which points towards a consistent sediment source. The dramatic loss of area associated with the capture of the Upper Yangtze River should be apparent in the detrital record, but is not observed. Conservatively, integrating only the catchment of the Yangtze upstream of the first bend (the commonly purported capture point) would increase the total catchment area of the Red River from ~158,000km^2 to ~466,000 km^2. Assuming the integrated network included the first major tributary of the Yangtze, the Yalong River, would add an additional ~180,000 km^2 the total catchment area of the Red River. The > 400% larger catchment area and distinct set of zircon age components in both the upper and middle Yangtze make it unlikely that the zircon age signature would not be imparted to the detrital zircon record deposits downstream on the connection point in a once integrated network. However, we find no evidence for zircon provenance outside of the

modern drainage areas feeding the Yinggehai Song Hong Basin throughout the history of deposition of this basin.

We recognize the variability in lithologic types represented in the bedrock interpolation maps is inconsistent with the character of solely detrital sample maps; however, the purpose of the bedrock plots remains the same, to spatially represent approximate zircon age concentrations. Unlike the detrital samples, bedrock units are of variable age and lithology. Because we do not necessarily know which lithologic units were eroding during the deposition of sediments, we need a spatially averaged representation of all bedrock distributions. A geologic bedrock map where proportion boundaries are divided by lithologies may provide greater clarity, but problems arise; particularly for paleo-sediments, which can and do vary in provenance by stratigraphic age, changing vertically (within the column) but not spatially. Therefore, for consistency and simplicity, bedrock interpolation maps contain points for all included distributions regardless of age or lithology.

Multi-dimensional scaling (MDS) plots potentially aid in the visualization of detrital zircon age datasets (Vermeesch, 2013). For MDS plots of detrital zircon, a matrix of dissimilarities for each sample is transformed into N-dimensional coordinates (often two or three), where the distances between points represents the dissimilarities between samples (Vermeesch, 2013). In an MDS plot, each sample, with its own unique distribution of zircon ages, is represented as a point in space; greater distances between two points indicate greater differences between the two sample U/Pb age distributions. Here, we calculated likeness dissimilarities (Satkoski et al., 2013) of pairwise PDF comparisons for detrital samples of the southeast margin of Tibet; Cenozoic samples from the YSHB; Miocene onshore Red River deposits (van Hoang et al., 2009); modern fluvial samples of the Yangtze, Red, and Mekong

River; and of idealized distributions of the six Gaussian components above. Using the table of likeness values, we apply metric MDS to plot the measures of dissimilarity as a function of distance in 3-dimensions (Figure 1.11). Note, in Figure 1.11, circles are scaled in size for relative distance into the page as calculated from their X and Y coordinates for clarity in their configuration and the axes are unitless. Several interesting patterns emerge in MDS space. Samples from the onshore SE margin and the offshore YSHB are clearly distinguishable based on their relative clustering (Figure 1.11; blue and red circles). Sediment from the modern Yangtze and Lancang Rivers are clearly associated with the sources related to the SE margin, while ancient deposits from the YSHB form two distinct groupings, one around the Red River and the other around Hainan Island. We note that the samples most associated with Hainan Island are greater distances from the mouth of the Red River, suggesting an increase in contributions from Hainan Island further offshore. The clustering near the Red River and Hainan Island of the Cenozoic YSHB deposits does strongly indicate similar or shared provenance of both paleo and modern sediment. Onshore Miocene samples of the Red River catchment also show a stronger affinity than samples collected to the north to the Red River rather than to the Yangtze and Lancang River. The clear separation of the Cenozoic deposits of SE margin and their affinity for sediments associated with the modern Lancang and Yangtze River further supports our claim of little to no shared provenance, nor change in sediment source for the sediments of the Paleo-Red River. Lastly, we observe here that the Paleogene, late Triassic and Neoproterozoic Gaussian age components are indicative of northern sources and thus onshore basins of the SE margin, while the Cretaceous and Permo-Triassic components more closely reflect provenance from the area sourcing the deposits of the YSHB, consistent with the spatial interpolation maps above.

Interpolation maps based on component age present within a detrital dataset provide a novel approach to visualizing detrital age data (Figures 1.5-1.10). This approach could be used to characterize detrital distributions for any period of deposition over any appropriate spatial scale. What it uniquely provides compared to the majority of distribution comparison measures is a geographic relationship of components between detrital samples. Limitations of this method include its dependence on component proportions, its potential to be skewed by components with high concentrations, dependence on the distribution of samples collected in space, and on defining the time slices and components to plot. Random sampling biases do have the potential to skew the apparent age distributions of samples, which will vary the interpolation map output. However, multiple samples from specific regions have the potential to average random sampling errors closer to the mean. Additionally, by using ranges of proportions rather than exact values, random sampling uncertainties become less impactful. By capping the proportions at >30%, the focus of the map sharpens on components containing less unimodal abundances while also establishing regions of clear, high proportions. The dependence of the overall spatial distribution of collected samples relies primarily on rock exposure and sample number. We provide a quantitative approach to major component identification; eliminating potential user biases in age bracket selection as well as establishing a clear set of components that describe the dataset. Our paired method of component identification and spatial interpolation of U/Pb age distributions is a potentially powerful tool in the detrital geochronologist's tool belt as it provides a much-needed method of viewing and comparing U/Pb age distributions in geographic space.

Conclusions

Despite the numerous studies identifying purported large-scale river captures and reorganizations in the Cenozoic along the SE margin of the Tibetan plateau, the detrital zircon

record does not support an integrated Yangtze-Red River in the Cenozoic. We combined bedrock sources, onshore Cenozoic and modern sediment samples, and samples of the YSHB to monitor changing sediment flux by way of changing zircon U/Pb age patterns. Detrital zircon age analysis shows that most age components associated with Paleogene and Neogene detrital samples of the SE Tibetan margin can be attributed to local sources, which are not present in the offshore record of the Yinggehai-Song Hong Basin. Stratigraphic analysis of deposits along the margin does not suggest a large integrated fluvial system, but rather that alluvial and lacustrine systems dominated sedimentary basins of SE Tibet throughout the Cenozoic. The preserved stratigraphy is not indicative of a fluvial system on the order of 500,000 km^2 in a portion of the Cenozoic sedimentary record we examined. It is therefore likely that they Yangtze and Red River were not part of a single river network since at least Eocene time and possibly throughout the entire Cenozoic.

Acknowledgements
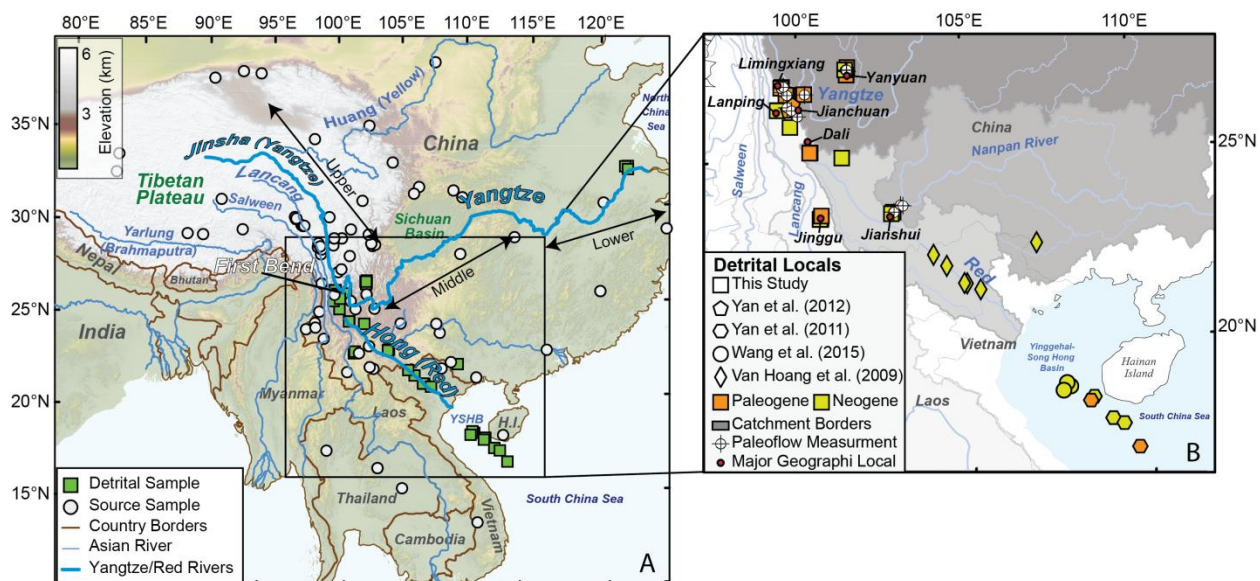
Figures

Figure 1.1. Maps of study area A: DEM of Southeast Asia. Detrital samples are indicated by green squares. Potential contributing bedrock sources are indicated by grey circles. B: Zoom in on detrital zircon data. Squares denote samples from this study. Other shapes indicate data from the literature. Areas in shades of gray mark the modern catchments of SE Asia. Crosshairs indicate paleoflow measurement locations.
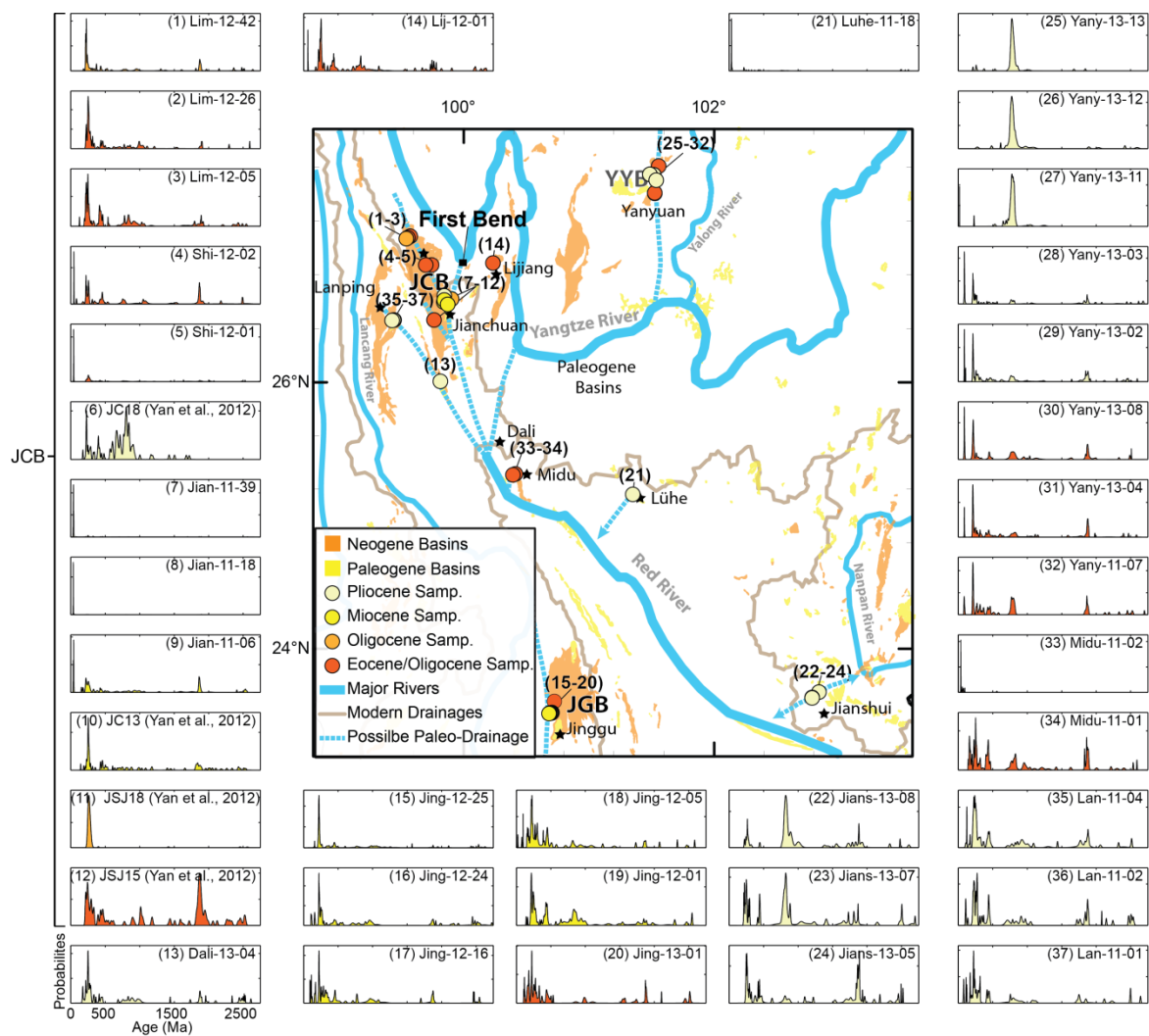
Figure 1.2. Sample locations, probability density plots and possible paleo drainages.
Probability Density Functions (PDF) of U/Pb ages of detrital zircon collected along the SE margin. Included are four samples from the Jianchuan Basin collected by Yan et al., 2012. Each curve represents zircon age-distributions between 0-2750 Ma. The locations of samples collected are numbered by PDF and colored by depositional age. Dashed lines indicate possible flow paths for paleo-drainage history of the SE margin. JCB = Jianchuan Basin; JGB = Jinggu Basin; YYB = Yanyuan Basin.
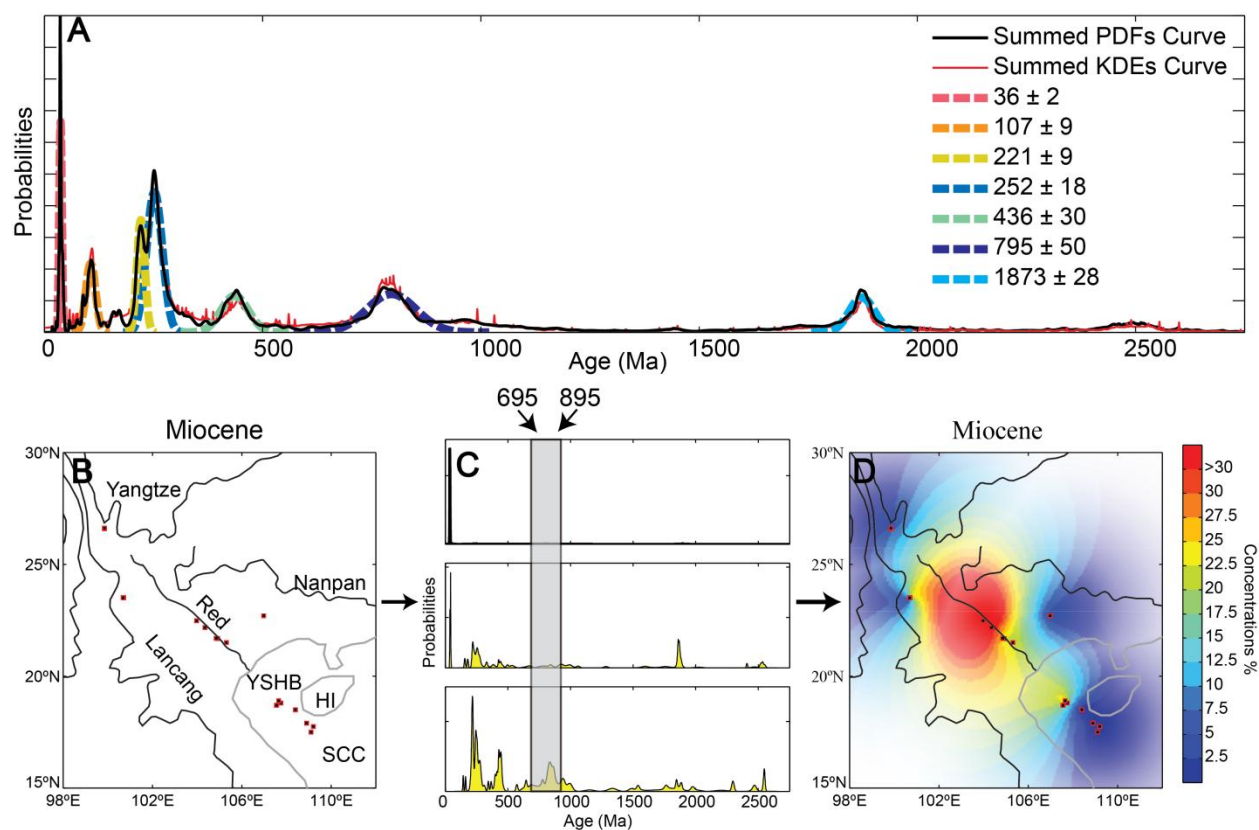
Figure 1.3. Visual representation of method. A: The black and thin red curves represent the summed probability curves for all Cenozoic detrital zircon samples. The Gaussian Components identified are given as dashed colored lines. B: Plot showing the sampling locations for Miocene detrital zircon samples, HI = Hainan Island, SCS = South China Sea, YSHB = Yinggehai-Song Hong Basin. C: 3-representative probability curves of Miocene age. The grey bar represents one of the Gaussian components. Values are integrated between the grey bars and applied as Z values for interpolation maps. D: The full interpolation map of 695-895Ma age zircon in Miocene deposits throughout our study area. Interpolation map is contoured by proportion: higher proportion means greater probability of finding zircon of this age range.
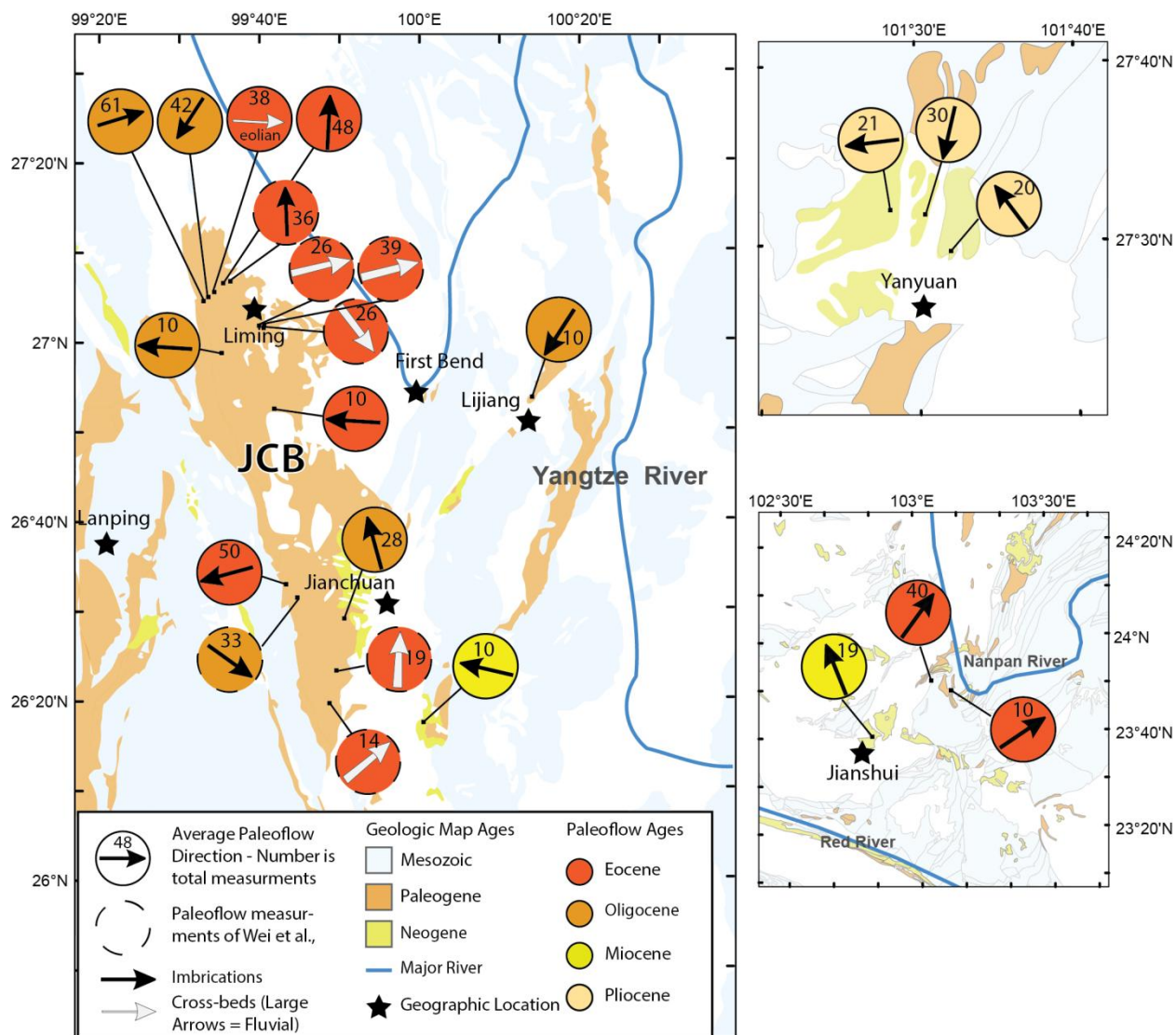
Figure 1.4. Paleoflow measurements taken throughout the southeastern Margin.

Paleoflow measurements taken throughout the southeastern Margin. Colors of circles represent depositional age of sediment and arrows indicate flow direction. Black arrows are for imbrications measurements and white arrows are for cross-bed flow measurements. Note that only in the Oligocene to flows indicate southward flow.
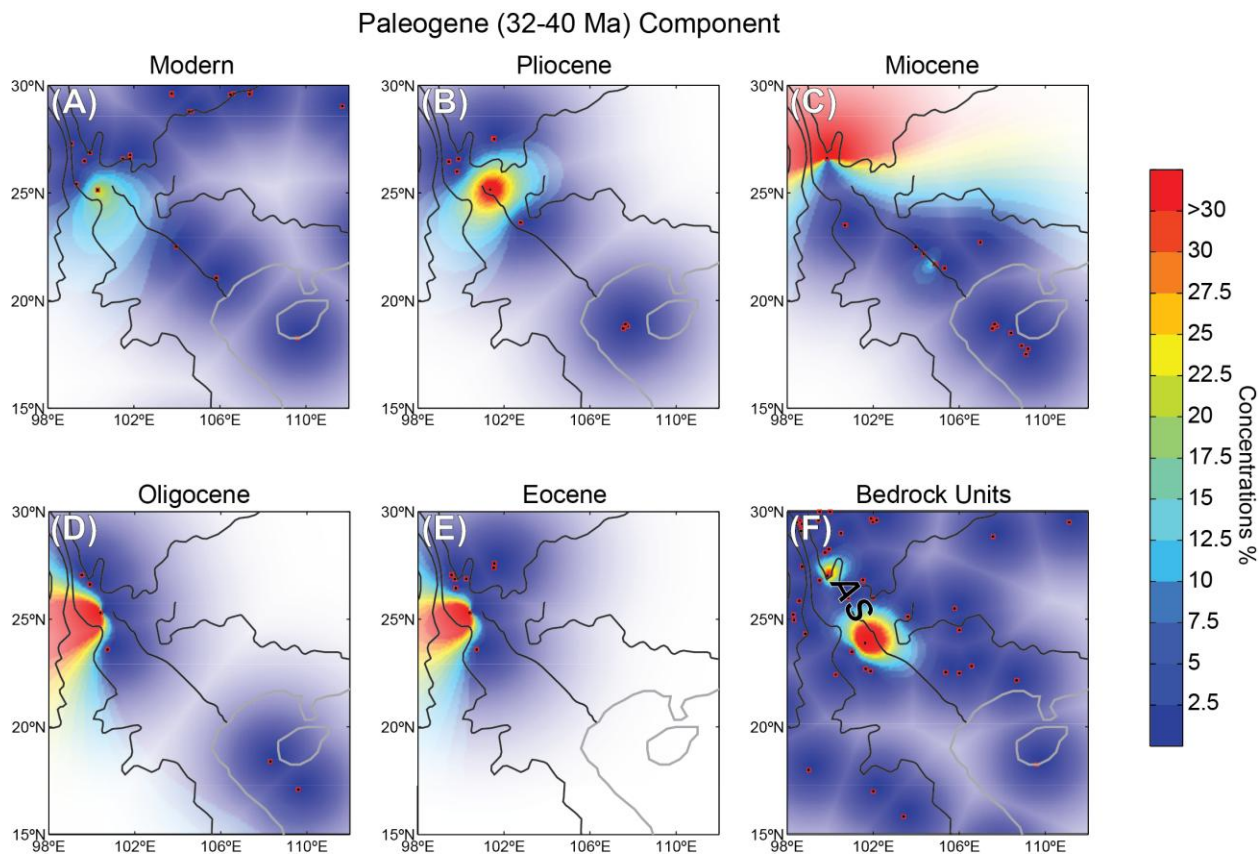
Figure 1.5. Paleogene Component (32-40Ma). Each map represents a different sampling suite with **(a) – (e)** are interpolation maps based on depositional ages and **(f)** of bedrock units of depositional or emplacement age of Eocene or older. Interpolation points are indicated by small red dots. Colors are scaled to interpolated concentrations of zircon of Paleogene age for each depositional time slice. Component concentrations are in percents. Opacity of interpolation map decreases with cubic distance from nearest sampling location. ASJ in **(f)** is for the Ailao Shan-Jinshajiang potassic igneous belt.
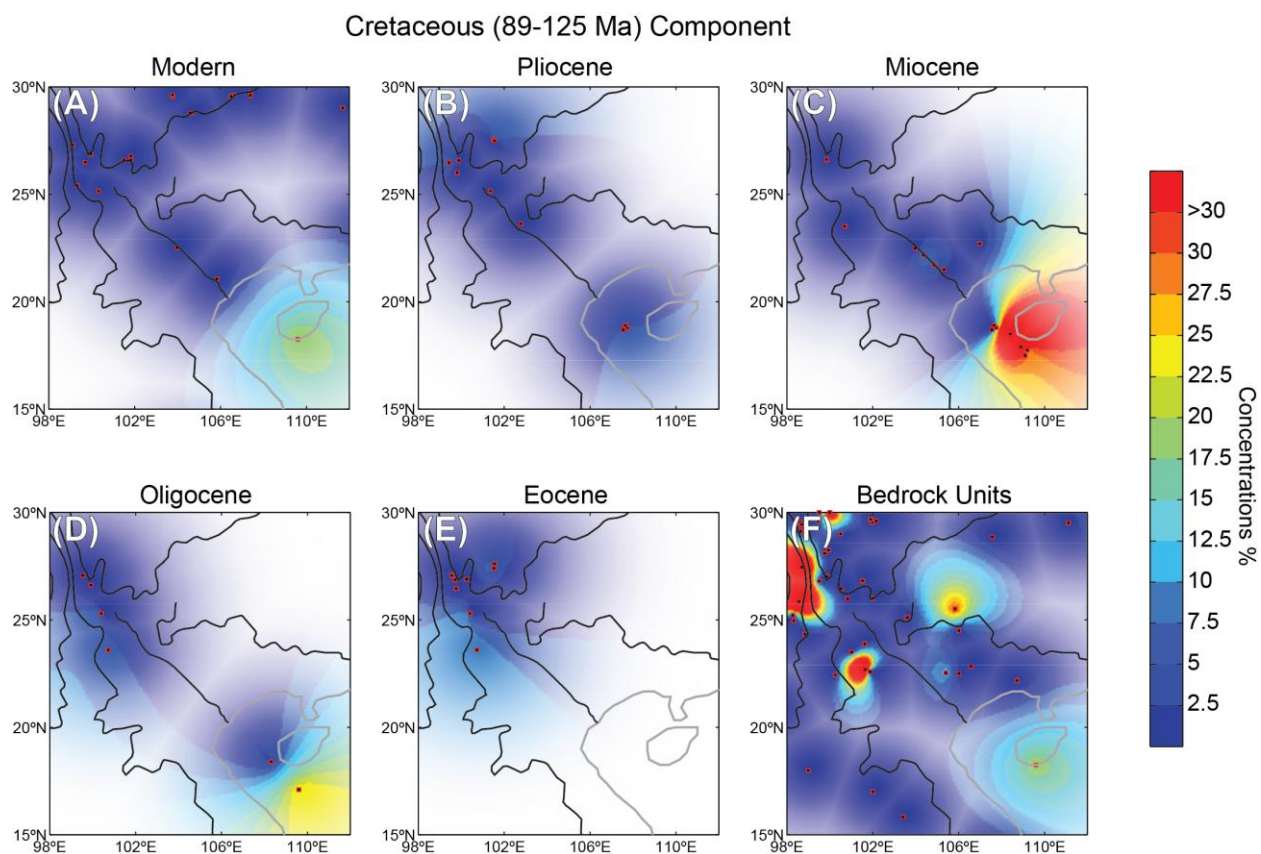
Figure 1.6. Cretaceous Component (89-125Ma). Each map represents a different sampling suite with **(a) – (e)** are interpolation maps based on depositional ages and **(f)** of bedrock units of depositional or emplacement age greater than the Eocene. Interpolation points are indicated by small red dots. Colors are scaled to interpolated concentrations of zircon of Paleogene age for each depositional time slice. Component concentrations are in percents. Opacity of interpolation map decreases with cubic distance from nearest sampling location.
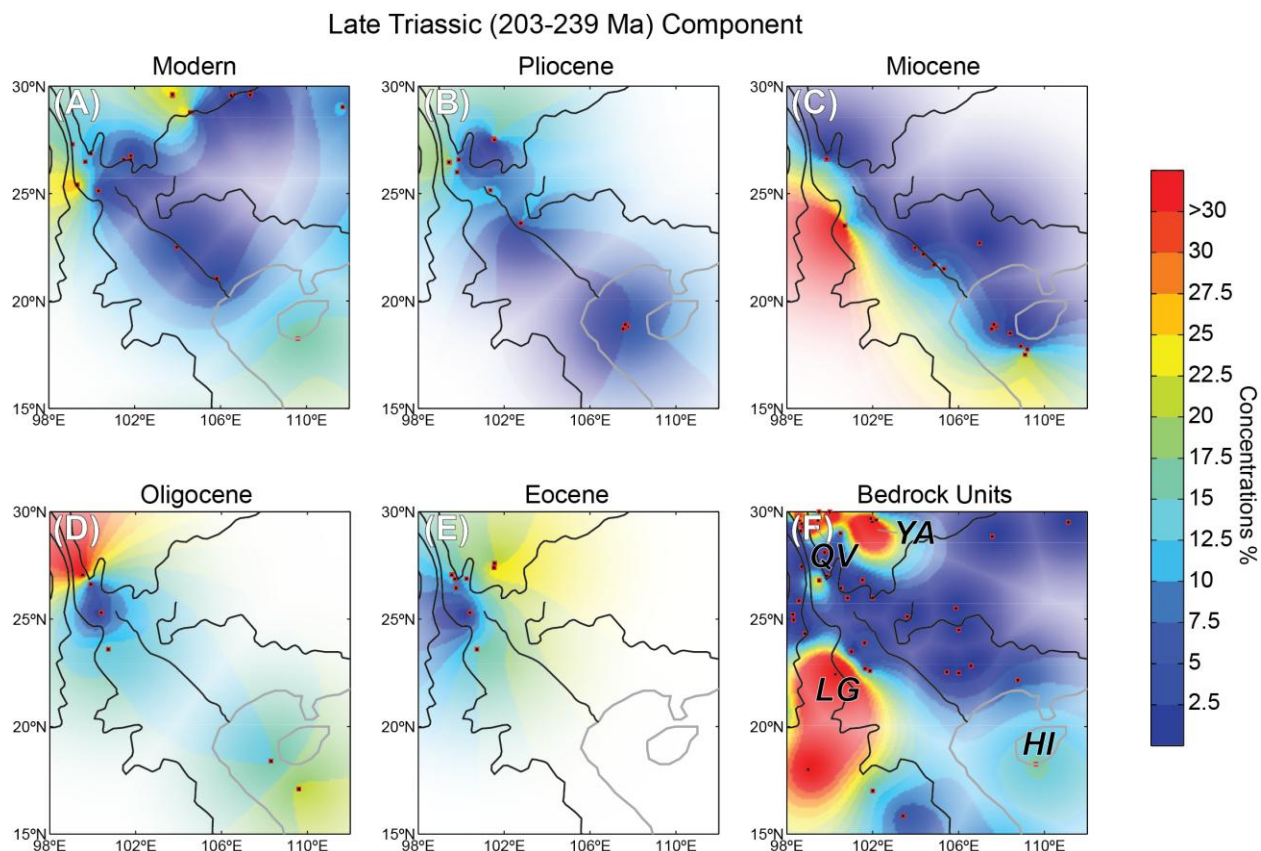
Figure 1.7. Late Triassic Component 203-239Ma. Each map represents a different sampling suite with **(a) – (e)** are interpolation maps based on depositional ages and **(f)** of bedrock units of depositional or emplacement age greater than the Eocene. Interpolation points are indicated by small red dots. Colors are scaled to interpolated concentrations of zircon of Paleogene age for each depositional time slice. Component concentrations are in percents. Opacity of interpolation map decreases with cubic distance from nearest sampling location. In **(f)** QV = Qiangtang Volcanics; LG = Lincang Granitic Complex; YA = Yidun Arc Volcanics; HI = Hainan Island.
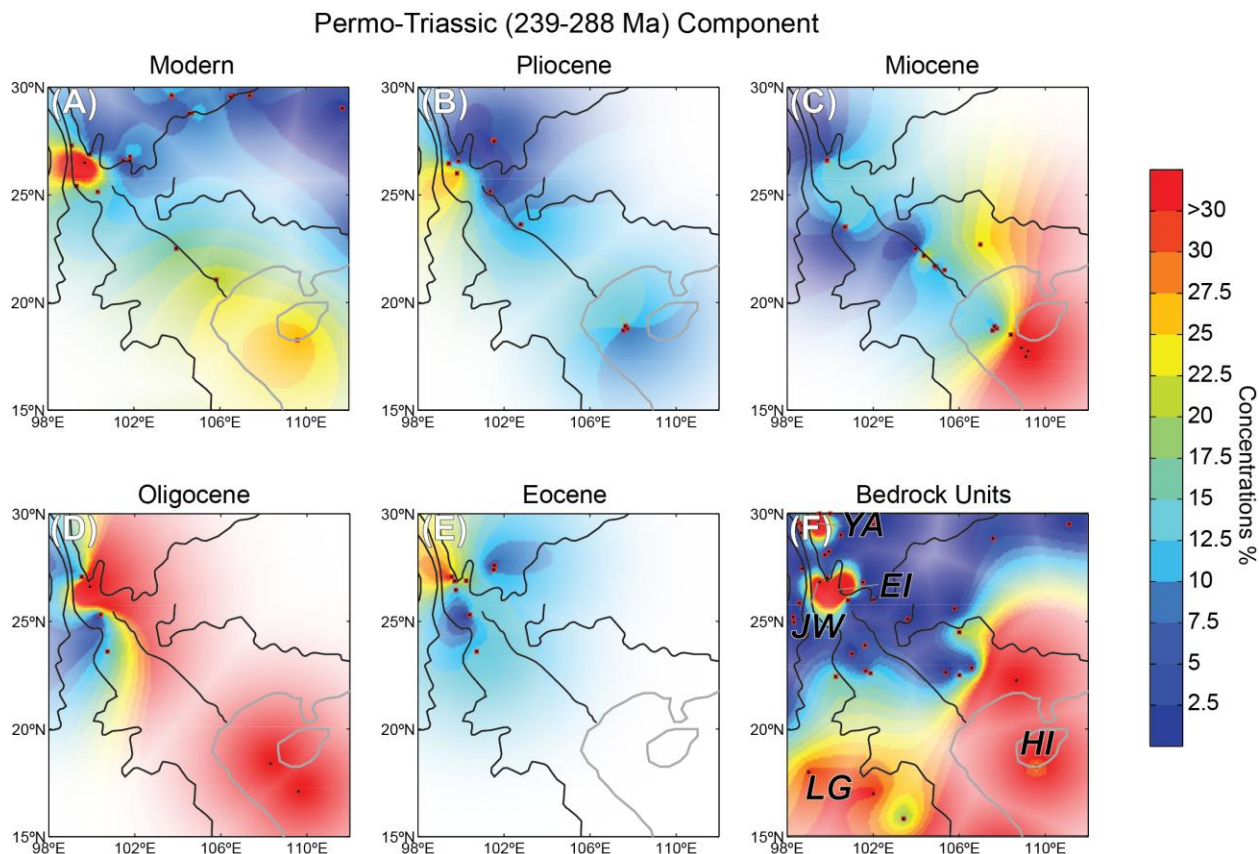
Figure 1.8. Permo-Triassic Component 239-288Ma. Each map represents a different sampling suite with **(a) – (e)** are interpolation maps based on depositional ages and **(f)** of bedrock units of depositional or emplacement age greater than the Eocene. Interpolation points are indicated by small red dots. Colors are scaled to interpolated concentrations of zircon of Paleogene age for each depositional time slice. Component concentrations are in percents. Opacity of interpolation map decreases with cubic distance from nearest sampling location. In **(f)** JW = Jomda-Weixi Arc Volcanics; LG = Lincang Granitic Complex; YA = Yidun Arc Volcanics; HI = Hainan Island; EIP = Emeishan Flood Basalts.
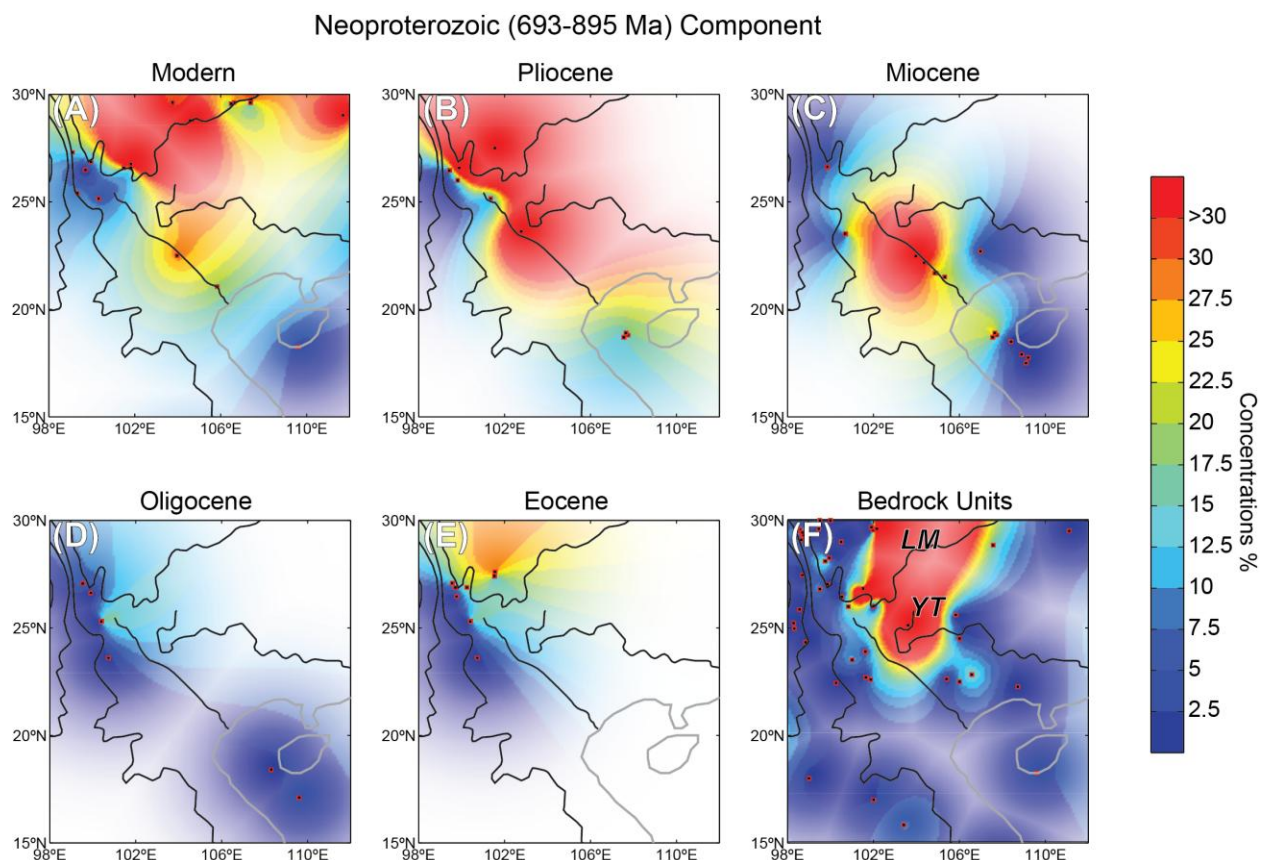
Figure 1.9. Neoproterozoic Component 695-895Ma. Each map represents a different sampling suite with **(a) – (e)** are interpolation maps based on depositional ages and **(f)** of bedrock units of depositional or emplacement age greater than the Eocene. Interpolation points are indicated by small red dots. Colors are scaled to interpolated concentrations of zircon of Paleogene age for each depositional time slice. Component concentrations are in percents. Opacity of interpolation map decreases with cubic distance from nearest sampling location. In **(f)** LM = Longmenshan Mountains; YT = Yanbian Terrane.
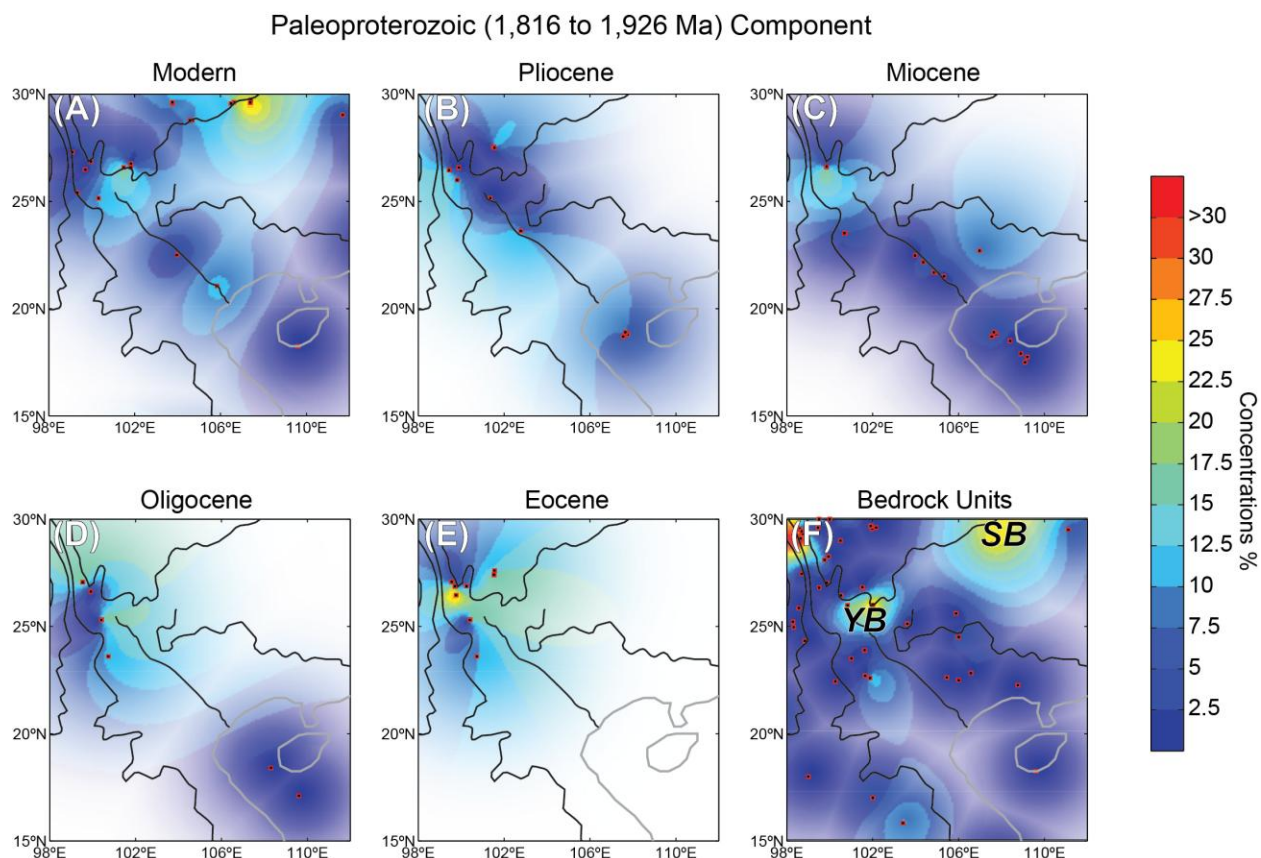
Figure 1.10. Paleoproterozoic Component 1816-1926Ma. Each map represents a different sampling suite with **(a) – (e)** are interpolation maps based on depositional ages and **(f)** of bedrock units of depositional or emplacement age greater than the Eocene. Interpolation points are indicated by small red dots. Colors are scaled to interpolated concentrations of zircon of Paleogene age for each depositional time slice. Component concentrations are in percents. Opacity of interpolation map decreases with cubic distance from nearest sampling location. In **(f)** YB = Yangtze Block; SB = Sichuan Basin.
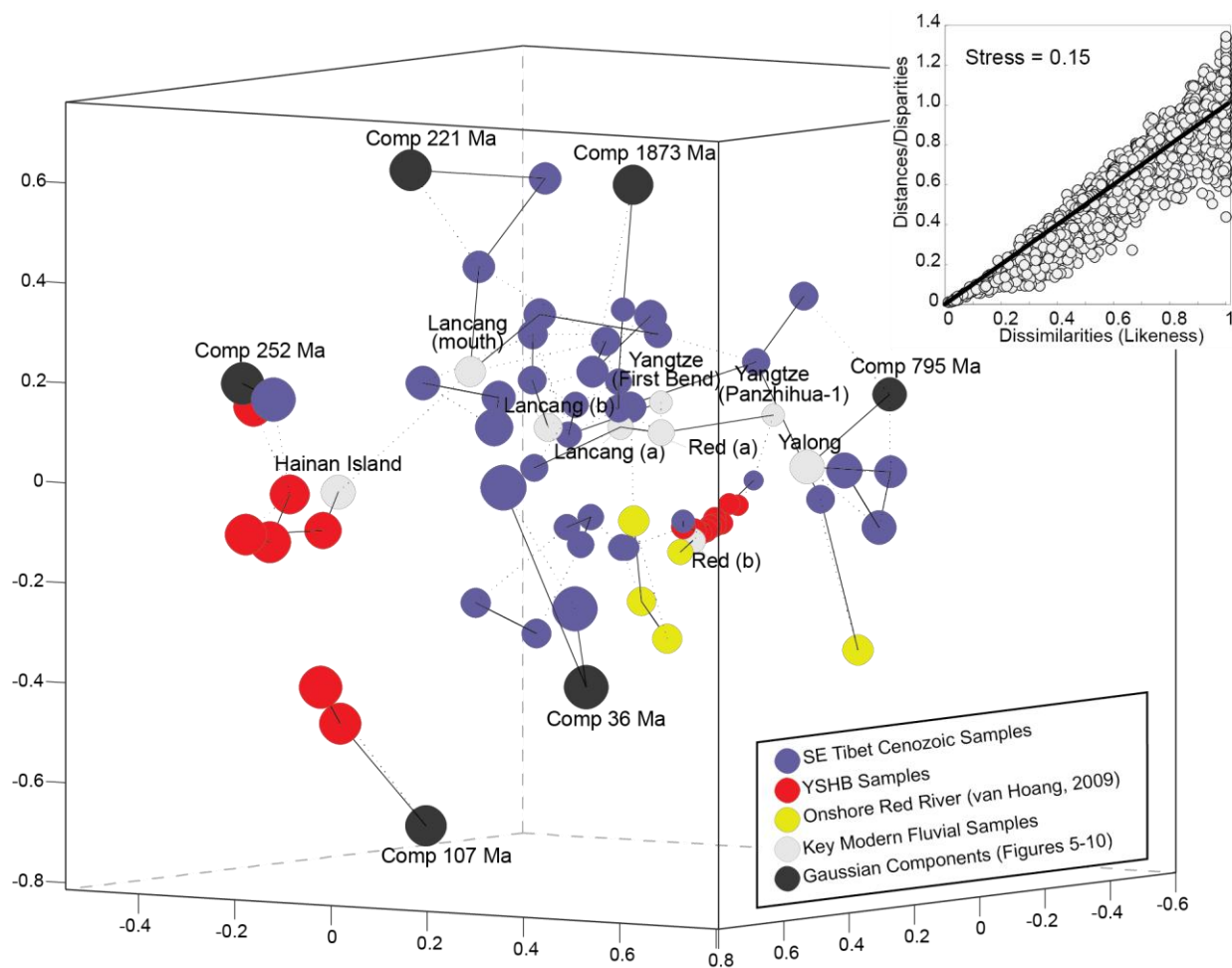
Figure 1.11. MDS plot of detrital deposits. Metric Multidimensional scaling plot of Cenozoic deposits in three dimensions. Greater distances represent greater degrees of dissimilarity as measured using likeness. Circle sizes are scaled for distance into page. Colors represent location deposits were derived. Blue circles are deposits collected in the area surrounding the Yangtze First Bend and upper reaches of the Red River catchments that are between Eocene and Pliocene in depositional age. Yellow circles are the Miocene deposits collected by van Hoang et al., 2009 along the trace of the modern Red River. Red circles are samples collected offshore in the deposits of the YSHB of Oligocene to Pliocene in age. Grey circles are modern fluvial detrital samples and black circles are the six Gaussian components

discussed. Solid and dashed lines between sample points are nearest and second nearest neighbor lines with respect to measured likeness values. Note the obvious divide between samples of the SE margin (blue) and samples of the YSHB (red). The YSHB basin shows two clear groupings, samples resembling modern Red River sediments and samples resembling modern Hainan Island sediments. The similarities of the SE margin deposits are closely associated with deposits of the Lancang and Yangtze River.

Chapter 2. Eastern margin of Tibet supplies most sediment to the Yangtze River

Submitted as:

Wissink, G.K., Hoke, G.D. (2016). Eastern margin of Tibet supplies most sediment to the

Yangtze River. Lithosphere (in review)

Abstract

Zircon provenance studies of modern and ancient fluvial systems help reveal the relative contributions and importance of upstream sediment sources. A previous study by He et al. (2014) of detrital zircon U/Pb age distributions from the Yangtze River and its tributaries proposed a strong anthropogenic control on sediment flux. Their data, along with other data from the region, is reanalyzed using multiple detrital zircon U/Pb age-distribution comparison techniques and a distribution-mixing model to construct an improved and quantitative view of provenance. The variability in the Yangtze River trunk stream U/Pb age-distributions is evaluated with respect to trunk-to-trunk stream comparisons, trunk-to-tributary comparisons, as well as in mixture models that consider contributions purely from the tributaries and trunk stream samples themselves. In addition to the modern river sands, contributions from a comprehensive compilation of bedrock source terranes across China are also evaluated. Uniformity in the zircon age distribution of the Yangtze's trunk is established in the upper reaches of the Yangtze and maintained to its outlet based on inter-trunk comparisons of detrital zircon distributions. Whether considering the bedrock source terranes or only the modern Yangtze sediments, the major source of sediments contributing to Yangtze is clearly the eastern edge of the Tibetan Plateau (e.g. Songpan Ganze Terrane, Longmenshan Range) were rock uplift rates are high. The purported increase in anthropogenic impact on sediment yield in the lowlands, at least as viewed through detrital zircon age distributions, is insignificant.

Introduction

With its headwaters in the Tibetan Plateau, the Yangtze River is the longest river in Asia. The Yangtze traverses the eastern two thirds of China and integrates multiple large tributaries draining crustal terranes with characteristic detrital zircon U-Pb age signatures. Zircon U-Pb ages may help fingerprint the dominant sediment sources to the trunk stream of the Yangtze River and thus the spatial pattern of erosion across the catchment. Accurate constraints on the zircon contribution from different catchments enhance our understanding of the catchment wide erosional patterns and may help frame future studies on how the river's course has evolved over time.

The expeditious and inexpensive acquisition of data made possible by laser ablation – inductively coupled mass spectrometry (LA-ICPMS) (e.g. Gehrels et al. 2008) has made zircon the mineral of choice for many modern and ancient provenance studies. In ancient settings, detrital zircon ages are routinely used to deduce drainage network reorganization and the timing of local and regional tectonic events (e.g., Gehrels et al. 2003; Darby & Gehrels 2006; van Hoang et al. 2009; Gehrels et al. 2011; Yan et al. 2012; Wang et al. 2013; He et al. 2013; Wang et al. 2014). At its simplest, erosion and rock uplift control the zircon contributions of progressively unroofed rock to fluvial sediments; thus, measured zircon ages should be traceable to a unique source. Studies have shown that variable zircon concentrations in source areas (Malusà et al., 2015, 2013; Moecher and Samson, 2006) can affect downstream age distributions, and that U/Pb age distributions of detritus may differ significantly from its source over very short distances (Bonich et al., in review). The interpretation of U-Pb ages from larger river systems may be further complicated by spatial variability in erosion due to climate change, or large but

irregular influxes of sediment, for example from coseismic landslides (Gallen et al., 2015).

However, despite some limitations, detrital zircon U/Pb ages have proven a valuable provenance

tool in studies of basin evolution (Yan et al., 2012; Zheng et al., 2013; Wang, Liang, et al.,

2014), crustal evolution (e.g. Xu et al. 2014; Wang et al. 2010), tectonics and erosional histories

(e.g. Weislogel et al. 2010; Lang et al. 2013).

Much of the landscape traversed by the Yangtze is tectonically inactive with the

exception of the eastern and southeastern margin of the Tibetan Plateau. Punctuated episodes of

rapid river incision into the eastern and southeastern margins of the Plateau reached localized

rates of >300m/Ma (Ouimet et al., 2010; Clark et al., 2005), with an abrupt decrease at ~ 7 Ma

(McPhillips et al., 2016). The Yangtze catchment, like much of China, is subject to moderate to

intense agricultural activity (He et al., 2014). At values of 30 m/Ma, ^{10}Be-derived erosion rates in

the main course of the upper Yangtze (Jinsha River) are remarkably low, yet some small modern

tributaries are rapidly eroding at 500 m/Ma (Henck et al., 2011). Immediately following large

earthquakes, such as the 2008 Wenchuan earthquake, the mountain rivers of the eastern plateau

margin become choked with material shed off the failed hillslopes (Parker et al., 2011). Active

rock uplift decreases dramatically east of the plateau margin (Richardson et al., 2008), and

variations in anthropogenic activity, principally from agriculture, likely become important agents

of erosion (Wilkinson and McElroy, 2007). Indeed, previous work examining detrital zircon

U/Pb age distributions from the Yangtze and its tributaries concluded that a major portion of the

zircons are derived from tributaries characterized by high agricultural land use (He et al., 2014).

We revisit this data through a more detailed analysis of the modern U/Pb age-distributions, and

include an extensive compilation of bedrock zircon data across the Yangtze catchment. Our

attempt to resolve the provenance of zircon in the Yangtze includes multiple visual

representations of qualitative and quantitative zircon U-Pb age distribution comparisons and two

mixing models that consider 1) the modern fluvial distributions and 2) potential bedrock sources

within the modern drainage area to determine their relative contributions of zircon to the Yangtze

River sedimentary budget. By combining multiple approaches to describe the provenance of the

Yangtze River, we are able to better characterize the age distributions of the Yangtze River and,

as a result, reinterpret their implications for spatial variability in erosional throughout its

catchment.

Datasets

We reanalyze the modern Yangtze River dataset comprising of 25 sand samples spanning

nearly the entire length of the river and its major tributaries first reported by He et al.

(2013)(Figure 2.1). As part of He et al.'s 2013 study, samples were collected in 2008 and 2009

from channel deposits (mid-channel, lateral, and point bars) exposed at low river levels. They

collected riverbed sand in multiple locations around each sampling site to sample a

representative mixture at each local (He et al., 2013).

The detrital zircon age data (Figure 2.3) is coupled with the zircon age distributions of 35

potential bedrock sources compiled from the literature (Figure 2.1). The major geologic

provinces encompassed by the Yangtze catchment and described by these 35 bedrock units

include the Songpan Ganze Terrane, the eastern Qiangtang Terrane, the Yidun Terrane, the

Sichuan Basin, the Yangtze Craton, the Longmenshan, the Qinling-Dabieshan fold belt, the

South China Fold Belt, and several smaller geologic provinces that also may contribute zircons

(Figure 2.1 and Figure 2.2). The majority of the 35 bedrock U/Pb age-distributions represent the

combined zircon ages of multiple genetically related samples. For example, sandstone samples

with similar geographic extent, sedimentary facies, depositional age, and age distributions were combined to generate an average distribution for a particular suite of samples, simplifying the dataset. Unimodal bedrock units, particularly plutonic outcrops, were only combined when age distributions were statistically indistinguishable.

Zircon distributions are represented as probability density functions (PDFs; e.g. Hurford et al., 1984), which represent the summed probabilities of U/Pb ages as measured by the Gaussian representation of U/Pb ages and their associated analytical uncertainties.

Methods

We apply multiple conventional and new approaches of detrital zircon data analysis in our re-examination of the spatial distribution of provenance changes for the modern Yangtze River.

Kolmogorov-Smirnov Test, Likeness, and Crossplot R^2 values

The two-sample Kolmogorov-Smirnov Test (K-S test) is one of the most widely utilized non-parametric statistical tests in detrital zircon geochronology (e.g. Press et al. 1987; Guynn & Gehrels 2010). The null hypothesis of the K-S test is that the two sample distributions are derived from the initial same distribution, thus a rejection implies they are drawn from distinct distributions. The results of the K-S test are contingent on the K-S statistic, or sample effect size (KS_{SE}), which is the maximum difference between the empirical cumulative distribution functions for each sample. The KS_{SE} is used to calculate the K-S Test's *p*-value to evaluate the null hypothesis. The K-S test provides a binary representation of whether any pair of distributions are statistically unique from one another (Table 2.1). The goal of this approach is to

statistically test if downstream samples are in fact derived from the same or different

distributions than their upstream counterparts.

As the K-S test is both binary and weighted towards the center of age distributions, other

comparison metrics are better suited to highlight differences between zircon age distributions.

Likeness (Satkoski et al., 2013) and probability function crossplot R^2 (CPR) values (Saylor et al.,

2013) have been proposed as alternative quantitative metric of comparison. The value of CPR

and likeness is their sensitivity to both shapes of components within the distributions and the

presence and absences of components. Likeness (Satkoski et al., 2013), or its inverse, percent

area mismatch (Amidon et al., 2005a), is a measure of the absolute difference between two

probability curves. Likeness varies from 0 to 1, with a value of 1 representing two identical

distributions (Figure 2.4). Probability function crossplots are generated by plotting the

probabilities of two distributions against each other over a given range of ages (Saylor et al.,

2013). The coefficient of determination (R^2 value), calculated from a linear fit to the plot,

provides the CPR value. Similar to likeness, values range from 0 to 1 with, 1 reflecting identical

distributions.

Multidimensional Scaling

Multidimensional scaling (MDS) is a technique common in statistical analysis of datasets

(e.g. Hayward and Smale, 1992; Carroll and Arabie, 1980; Smosna et al., 1999), however is

relatively new in its application to detrital zircon U/Pb age datasets (Vermeesch, 2013; Spencer

and Kirkland, 2015; Vermeesch and Garzanti, 2015). MDS in detrital zircon geochronology,

attempts to translate pairwise dissimilarities measured between sample age-distributions (e.g.

Likeness, CPR, or KS-Statistic) into Euclidian distances, generally into 2-dimensional

configurations (Vermeesch, 2013). In this construct, greater Euclidean distances between two samples, represented as points in MDS configurations, indicate increasing degrees of dissimilarity. MDS attempts to find the optimal spatial distribution of the sample points for the matrix of distances (e.g. translated dissimilarities). There are multiple evaluative loss functions for MDS, but the most common is stress (S) (Kruskal, 1964a). Lower stress values, generally below 0.10 indicating a good fit of the translated dissimilarity configuration while $S > 0.2$ generally indicates a poor fit. MDS can be applied to detrital data using either metric or nonmetric MDS. Metric MDS uses the absolute measures of the dissimilarities to solve for the configuration and stress value simultaneously (Vermeesch, 2013). Nonmetric MDS ranks the dissimilarities (i.e. ordinal data) and numerically (e.g. isotonic regression) finds the optimal configuration by minimizing the loss function (Vermeesch, 2013). Along with the stress value, a Shepard plot is a good tool for MDS evaluation; here, the measured dissimilarities are plotted against the translated distances, and a better fit to either a linear (metric MDS) or some nonparametric monotonically increasing function (nonmetric MDS) indicates a better configuration.

For this study, we follow a similar approach to that outlined in (Wissink et al., in review) 2016), where dissimilarities are a measure of the likeness, rather than KS_{SE} as originally applied by Vermeesch (2013). Here, we use nonmetric MDS as it yields lower stress values. MDS will highlight any differences in the Yangtze's trunk stream samples and identify which tributaries appear to the most similar to trunk stream samples (Figure 2.5), if any. For example, if several tributaries account for the majority zircon in the trunk streams, these tributaries should surround and possibly be clustered within the trunk stream samples from which they are derived, while the remaining, low zircon source tributaries should fall at greater distance from the trunk samples

around the periphery. Assuming a dramatic shift in provenance following the incorporation of a specific tributary, we would also expect an obvious downstream and upstream clustering of trunk stream samples, with the downstream samples closer in MDS space to the major contributing tributary. Should an upstream catchment dominate zircon supply, there would be little to no differentiation between up- and downstream trunk samples.

Gaussian Component Breakdown

He et al. (2014) broke the Yangtze dataset down into 6 age brackets. Their age intervals were 0-65 Ma, 100-300 Ma, 300-600 Ma, 600-1000 Ma, 1700-2000 Ma, and 2000-2700 Ma. However, closer inspection of both their detrital dataset and bedrock source data, suggests these age brackets do not adequately represent distinct geologic emplacement events within the Yangtze Catchment. Instead, we break the dataset down into individual Gaussian components that more effectively describe the trunk stream distributions. Here, a component is, at its simplest represent, a normally distributed suite of ages around some mean that represent some discrete geologic zircon producing event. Since our goal is to identify the variation in the Yangtze's trunk stream samples in relation to its tributaries and associated bedrock sources, we isolate the major components associated with the trunk stream distributions. We follow the approach outlined in Wissink (2016), where the probability density curves of all trunk stream samples are summed and normalized to unity. Following the summation, unique age components are identified using a deconvolution algorithm that fits a Gaussian curve to each of the largest, (in integrated area) age modes, minimizing the mean square error for each (Figure 2.6A). The mean and two standard deviations of each curve define an age component. The sum of the individual Gaussian functions approximates the original dataset. Similarly to He et al. (2014) we calculate the proportions of zircons within the Yangtze River sediments for each defined component. This is achieved by

integrating the PDFs for each sample between the endpoints defined by each component. Using this approach, we identify the major components and their overall variance within trunk stream samples, which we can use to make more robust inferences on provenance.

Mixing Models

We apply a simple mixing model modified from Lang et al. (2013) to assess whether changes in sediment source explain age-distribution variations observed in the Yangtze trunk stream detrital zircon dataset. Lang et al.'s (2013) mixing model determines the optimal mixing proportions of potential contributing sources with no a priori knowledge of which sources to include. Source distributions, here represented by probability functions, are mixed at varying proportions over a range of possible combinations, with the resulting mixture compared against the detrital sample. Mixtures are generated by multiplying the PDFs of each 'source' distribution by their respective percent contribution to that mixture and summing each, creating the mixed PDF. An optimal mixing of sources corresponds to that with the highest comparison metric (e.g. likeness, CPR, and KS-Statistic) of mixture to sample comparisons. We use Likeness (Satkoski et al., 2013) as it best represents the overall shape of the distributions (i.e. height and width of component). Here, we separately apply the mixing model to the detrital sediments of the Yangtze using two different constructs of source – bedrock and tributary rivers.

For the first model, sources are defined as any possible contributing lithologic unit, ranging from large sedimentary sequences to localized plutons. The contribution of a bedrock unit to a trunk stream sample is contingent on its inclusion within the drainage area upstream of a sample collection location. The compilation of lithologic units are presented in Figure 2.1, with either the exact geographic coordinate given for single representative sample, or approximate

locations for aggregates of related samples.

In the second approach, we assume that the sources of the Yangtze River trunk stream sediments are described by the U/Pb age-distributions of the main stem tributaries. Ideally, the model would exclusively use tributary distribution to represent the fluvial system. However, the 10 major tributaries sampled by He et al., (2013 & 2014) represent at most only 58% and as little as 25% of upstream areal catchment at any trunk stream sampling location collected downstream of the Yalongjiang (Figure 2.1, 2.2, 2.7B). Thus, only considering the tributaries means potentially ignoring ~50% of possible contributing area. To mitigate this, we include all upstream tributary and trunk sample distributions as possible source contributors for the mixing model. This model is predicated on each fluvial sample adequately and accurately representing the integrated U/Pb distributions of their upstream catchments.

In practice, it is difficult to identify more than 10 unique sources with confidence due to the small percentages of each source and random sampling uncertainties associated with 100 age draws as well as large computational times. For the bedrock-source scenario, there are over 30 possible contributing sources for trunk samples collected in the lower Yangtze reaches. Therefore, we modify how the mixing algorithm is applied depending on the number of potential contributing sources. When less than seven sources are identified as possible contributors, the mixing algorithm uses all combinations of source PDF's at 5% incremental changes. At eight to 12 possible sources, the incremental changes in mixing proportions are increased to 10% for computational efficiency. If the total number of possible contributing sources exceeds 12, we use a grid search technique that prioritizes those sources with the highest initial similarity metric values of source to sample comparisons (see Appendix II) to determine the optimal mixture for

each detrital sample.

Results

Results of K-S Test; Likeness; and Crossplot R^2 Values

The K-S test was used for each pairwise coupling of the Yangtze River trunk and tributary samples. The results are summarized in Table 2.1, where an **F** indicates a failure to reject the null hypothesis and therefore the samples cannot statistically be said to have derived from different distributions. Two-thirds of all Yangtze trunk-to-trunk sample comparisons fail to reject the null hypothesis, with no obvious differentiation between the upper and lower reaches of trunk stream samples. The trunk samples that appear to have the strongest differentiation, i.e. reject the null hypothesis most frequently, are at the first bend of the Yangtze (Shigu), and at Yibin (Figure 2.1; B, Figure 2.2 and 2.3; Table 2.1). In contrast to the trunk-to-trunk comparisons, only 18% of trunk-to-tributary comparisons fail to reject the null hypothesis, indicating far greater variance within the tributary age-distributions compared to the trunk. The shaded portion of Table 2.1 indicates the tributaries that are upstream of the trunk samples of the same row (also those falling below the bolded black line). The tributaries most closely resembling trunk samples using the K-S test are from the Xiangjiang, one of the tributaries identified by He et al. (2014) as a principle sediment contributor, and Yuanjiang. This is despite the merger of these tributaries with the Yangtze River occurring in the lower quarter of the catchment (Figure 2.1; Table 2.1). The tributaries associated with the upper and middle reaches of the Yangtze River (the Yalongjiang, Daduhe, and Minjiang) exhibit seemingly unique characteristics; failing to reject the null hypothesis for most trunk stream comparisons. Of the tributary-to-tributary comparison, only three pairs of tributaries fail to reject the null-hypothesis:

the Daduhe – Minjiang, the Xiangjiang – Ganjiang samples, and the Hanjiang – Ganjiang samples. The trunk-to-tributary and tributary-to-tributary comparisons suggest far greater differentiation amongst tributary samples, possibly making more focused and less binary characterization possible. It is important to note, that although a trunk stream sample may reject the null hypothesis in trunk-to-tributary comparison, this does not preclude the possibility of the tributary contributing to the trunk stream's sediment budget. All it suggests is the trunk stream sample is not exclusively derived from a given tributary.

Likeness and CPR values, which are more sensitive to the overall similarities and differences in the detrital U/Pb age distributions, are similar to the K-S test results (Figure 2.4). Likenesses of trunk-to-trunk comparisons vary between 37-63%, with an average of 52±6% (Figure 2.4A). Despite the wide range of ages in the Yangtze samples, the mean value for trunk-to-trunk sample comparisons is relatively close to the lower threshold of maximum likeness value of 72±6% established by sampling a *single*, multimodal parent distribution for multiple 100-age samples (Satkoski et al., 2013). Tributary-to-trunk comparisons yield lower likenesses from 23-61% with an average of 46±7% (Figure 2.4B). Inter-tributary comparisons yield the lowest values of 42±10% (Figure 2.4C). CPR values follow a similar pattern to Likeness (Figure 2.4D-F), though exhibiting more scatter and lower average values with an average of trunk-to-trunk CPR values of 0.26±0.13. The tributaries with the highest CPR and likeness values in trunk-to-tributary comparisons are the Dadu, Min, Yuan and Han tributaries, with no relationship between downstream incorporation and high values (see Appendix I; Table I.1. and I.2.). Assuming a significant single shift in provenance, one would expect a certain bimodality in likeness values of the inter-trunk comparisons. Samples downstream of such a shift would exhibit a positive increase in comparative likeness and decrease compared to the upstream

samples. It is clear there is no such step function present in the measures of similarity of down

vs. upstream samples. Trunk samples exhibit strong overall similarities, particularly at the

confluence of the Yalong River at Panzhihua.

Results of Multidimensional Scaling

The variability in the Yangtze dataset using Multidimensional Scaling is summarized in

Figure 2.5. The MDS configuration results in a strong clustering of trunk stream samples (filled

circles) in the center of the MDS Map, highlighting their overall similarity while also lending no

evidence of significant changes in provenance further downstream. This is not unexpected given

the results of the likeness test. The four trunk samples, nearest the mouth of the Yangtze (Hukou,

Datong, Nanjing, and Changxing Island), show no significant differentiation in MDS with

samples collect from the upper vs. lower reaches. The trunk samples furthest from the center

include Tuotuohe, Shigu, Yueyang-2 and Yibin, though even this differentiation is not

particularly robust. Tuotuohe and Shigu represent the upper reaches of the Yangtze and thus

possibly differing provenance or limited contributions to the river downstream of Panzhihua.

Yibin and Yueyang are both more closely linked to the Yalongjiang and Xiangjiang tributaries,

respectively; both tributaries represent the immediately preceding large tributary for each of the

respective trunk stream samples. The tributaries themselves (unfilled circles) fall to the outer rim

of MDS map (Figure 2.5), ringing the trunk samples. While this configuration may suggest all

tributaries are contributors in some fashion, the clustering of trunk stream samples demonstrates

a lack of downstream differentiation. Of the 10 Yangtze tributaries, those closest to the trunk

sample cluster are the Minjiang, Daduhe, and Jialingjiang tributaries; all of which occupy the

northwestern portion of the Yangtze Catchment.

Results of Gaussian Component Analysis

We identify 15 prominent components, which define ~80% of the overall variance within the Yangtze River trunk stream distributions (Figure 2.6; A). However, just six describe 75% of the total variance and, in decreasing order of proportional contribution and given as μ-2σ:μ+2σ, are 675-904 Ma, 1,734-1,974 Ma, 389-481 Ma, 199-225 Ma, 2,417-2,605 Ma, and 2,342-2,492 Ma. These ranges represent substantial revisions to those previously described by He et al. (2014). Using the Gaussian components defined above, we calculate the proportions of each in every Yangtze sediment sample, uniquely, and the average proportion of each component for the trunk sediment samples. This average allows us to examine the deviation of each sample age distribution from the trunk stream mean value for each component (Figure 2.6B). The mean value for each component is normalized to zero, and the deviation for each sample is given as a percentage point difference between the mean value and the proportion within that sample. For example, if component one has a mean value of 20% and sample one's age distribution is 25% component one, it would be given as a +5 percentage point (pp) deviation from the normalized 0 mean value. In Figure 2.6B, we plot the deviations of the six components described above as well as the Cenozoic component of 34-48Ma to more similarly match the components of He et al. (2014). The deviations for the remaining components can be seen in Appendix II. A striking feature revealed in Figure 2.6B, is the low deviation from the mean value for nearly all components for trunk stream distributions, generally falling within ±5 pp, throughout most of the fluvial system. The same cannot be said for the tributary component proportions, which differ widely, deviating 10-20 pp from the mean trunk values for the same components.

The establishment of the mean component values for the trunk stream appears to occur in the

upper Yangtze between Shigu, where component deviations are high (10-20 pp), and Panzhihua, where trunk stream proportions settle around the mean (Figure 2.6B). Following Panzhihua, trunk stream proportions rarely deviate significantly from mean proportions. There are clear spikes of certain components at trunk stream sites near Yibin (676-904 Ma) and Yueyang (389-481 Ma). Both increases occur after the incorporation of tributaries containing higher than average proportions of those specific age components (see tributaries Minjiang and Daduhe, and Xiangjiang, respectively). Nonetheless, they immediately return to proportions closer to the mean value by the next downstream trunk sample. The trunk samples with the greatest distance downstream from the incorporation of any major tributary are Yichang, Nanjing, and Changxing Island, and are likely the most homogenized. These samples show roughly equal proportions to those established at Panzhihua. The low deviation in values around mean of the trunk samples (Figure 2.6B) and the relatively high deviation for tributary samples (Figure 2.6C) match well with the results of the K-S test, and calculated dissimilarity values. The high deviations in values of tributary samples, and thus the uniqueness of these age distributions, also suggests that any major flux of sediments from one or more tributaries, should appear and persist downstream of its incorporation.

We construct a simple model for comparison with Figure 2.6B. Here, an essentially infinite age-distribution comprised of seven unique components with proportions equal to the seven mean values of the components of Figure 2.6B (legend), is randomly drawn from 15 100-age samples. The results of a single model run are given in Figure 2.6C. The results of this model yield nearly indistinguishable curves from the majority of trunk stream samples found downstream of the First Bend of the Yangtze. In multiple model runs, components with of a mean value between 1-4% yield standard deviations generally of ±1.5-2.5pp (1σ), 5-10%

components have standard deviations of approximately ±2-3 pp, and components with >10%

yield standard deviations of ±2.5-5.5 pp (Figure 2.6C). Therefore, the possible deviations of a

single random sampling can be >±10pp, particularly for larger components, but < ±10 pp

deviations are difficult to distinguish from random draws. Samples from Yibin and Yueyang-2,

which show the largest and likely not randomly derived, deviations, are easily associated with

immediately upstream tributaries. The remaining trunk samples at and downstream of Panzhihua

exhibit striking resemblance to the simple model, suggesting shared provenance.

Results of Yangtze River Mixture Models

The results of the mixture model applied to the Yangtze River dataset are described here and

illustrated in Figure 2.7. The optimal mixtures of bedrock sources achieved likeness values of

ranging from 57-75% when comparing the mixed distributions to the original sample

distributions. Of these bedrock mixtures, the Yangtze trunk samples, with the exception of

Tuotuohe in the headwaters, yielded maximum average likenesses of $67 \pm 4\%$, within the

maximum achievable resampled likeness of 72±6% described by Satkoski et al. (2013).

Tributaries also return similar averages of $67 \pm 5.5\%$ (See Appendix II. for tables). The bedrock

source distribution dataset consisted of a maximum of 35 possible source units. The results of the

optimal mixtures excluded nine from any of the sample optimal mixtures. For geographic and

geologic simplification, we can further reduce the number of geologically distinct bedrock units

to 17 units that contribute in one or more optimal mixtures. The full 26-source mixture model

can be found in Appendix II.

The units of the Songpan Ganze Terrane (SGT), the Triassic flysch deposits found near the

headwaters and left-bank tributaries of the upper-Yangtze (Figure 2.1; XVI, XVII, XVIII, XIX;

Figure 7A) show a clear dominance in zircon supply to modern trunk stream sediments. Deposits related the southern depocenter of the SGT (Weislogel et al., 2010) make up the majority of contributing sediments from this Terrane (Appendix II). Sediments from the Qamdo Basin, which shares a depositional history with the SGT (Shang et al., 2016), and the Jurassic Sediments of Yunnan Provence (Su et al., 2014), are included in two-thirds of trunk optimal mixtures. These units each have likeness values exceeding 45% with the SE depocenter of the SGT and thus may be difficult for the mixing model to differentiate, though all are present in the northwestern margin of the Yangtze catchment. By simply grouping sources derived from geologic terranes upstream of sample Panzihua-2, optimal trunk mixtures are 65-100% comprised of these bedrock units, averaging ~85% for the 15 trunk stream distributions. Together this grouping constitutes <20% of the overall area of the Yangtze catchment.

Two volcanic units associated with the Longmenshan Range and South China block both share Neoproterozoic emplacement ages and make clear contributions to the trunk stream samples. These units, in dark red and pink in Figure 2.7, respectively, are essentially unimodal and share a 33% likeness. While less likely to affect the final mixture output of <12 sources, these units may be difficult for the grid-search mixture model to differentiate. Following the incorporation of the Ganjiang and Yuanjiang Rivers, which both have very high South China components; we observe an increase in South China derived units at the apparent expense of Longmenshan units. Neoproterozoic ages account for ~5-25% of the overall composition of our mixtures. Other minor contributors include Cenozoic volcanics, the Laji and Dabieshan mountain ranges and sediments from the Sichuan basin.

The second mixture model using major tributaries and upstream trunk samples as sources for the downstream trunk distributions (Figure 2.7B), yields optimal mixtures with far stronger trunk stream contributions than tributary contributions. Twelve trunk stream samples contain at least one major tributary within their catchment; eight of which are best described by mixtures contain >70% trunk stream zircon (red outlined wedges of pie charts). These require minimal contributions from tributaries to push the mixing model toward higher optimal metric values. The remaining samples, those near Yibin, Fuliang, Yichang, and Wuhan range from 30-55% trunk stream contributions. Yibin, due to its high Neoproterozoic concentrations favors the incorporation of the Yalongjiang. Interestingly, this is despite the obvious lack of strong Neoproterozoic age proportions at Panzihua-2 immediately following the incorporation of the Yalongjiang (Figure 2.7B). Fuliang and Yichang have elevated incorporation of the Wujiang tributary (Figure 2.7B - purple) grains in the mixing model. This is notable given the Wujiang River only accounts for ~8% of the total catchment area at the sample locations. Figure 2.7 shows these two samples both have slightly higher than average Paleoproterozoic age zircons and may be why Wujiang, which shares this characteristic, is favored in the model. Samples at both Yibin and Yueyang-2 mirror the results observed in Figure 2.7, where higher than average concentrations of particular age modes of the most immediately incorporated tributaries leads the mixture model to include higher than expected tributary concentrations.

Discussion

Each analysis of zircon ages explored here demonstrates that the zircon U/Pb age distribution of the Yangtze River is established early in its upper reaches near the sampling location of Panzhihua-2 and remains continuous downstream. This refutes the claim of He et al., (2014) who argue that the tributaries of the Han, Xiang and Jialing Rivers constitute the largest contributions

of sediment to the Yangtze. Their conclusion relies heavily on a coarse grouping of zircon age components and just eight bedrock units to characterize the structural blocks of the Yangtze catchment, a total that we have expanded upon and refined here. Our more robust bedrock dataset, Gaussian component analysis, and multiple analytical techniques to explore zircon age distributions argue for the more tectonically active and steeper topographic regions of the Yangtze Catchment to dominate the sediment budget of the modern river.

The K-S test demonstrates consistent shared provenance for the vast majority of the trunk stream samples along the length of the Yangtze fluvial system. This argument is bolstered by the rejection of the K-S test null hypothesis in most trunk-to-tributary comparisons, demonstrating the lack of impact tributaries have on the trunk stream. If the contributed in sediment in equal amounts, the incremental addition of zircon from tributaries should result in a measurable change in zircon age distributions and would be noted moving downstream. The K-S test, Likeness, CPR, and component deviations from the mean trunk values all point towards a uniform character of the detrital zircon component downstream of Panzhihua. The few trunk samples that do exhibit large variations in components occur immediately downstream of specific tributaries (Figure 2.6B). It is plausible to assume the upward spike in zircon contributions is indicative of higher than average erosion or so-called zircon fertility from these tributaries. However, following these jumps in contribution from the nearest upstream tributary (often just tens of kilometers upstream), the signal is consistently absent at the next downstream trunk sample (Figure 2.6B). This most likely suggests poor homogenization of the tributary and trunk sediments at the sampling locality. For the remaining samples, the deviations from mean trunk stream values are essentially impossible to distinguish from the noise of random sampling (Figure 2.6C).

MDS analysis also supports a zircon source for trunk of the Yangtze derived primarily from the upper portions upstream of Panzhihua. Within MDS space, the progressive incorporation and dominance of zircon ages from downstream tributaries would result in a drift in zircon ages across MDS space. Instead, we observe the majority of trunk stream samples clustering together in MDS space centered on the Panzhihua trunk stream samples suggesting little deviation in zircon age downstream of those sampling localities. The tributaries nearest the trunk cluster are also primarily tributaries of the northwest Yangtze catchment, indicting they are important zircon sources.

Our mixture models, both of bedrock mixtures and upstream tributary mixtures further support our supposition of a quickly established and maintained zircon age distribution for the Yangtze. In the bedrock model, we find that high concentrations of eastern Tibetan Plateau bedrock units yields the highest likeness values of any mixture model, reaching likenesses near the proposed threshold of 72±6% of shared provenance established by Satkoski et al. (2013). Although we do not test all possible mixtures for samples containing >11 possible contributing sources, nor can we guarantee that similar age distributions are not substituted at the expense of the "correct" source, the corroborating results of the bedrock mixture model with the previously described methods suggests a high confidence in the overall results of the bedrock-mixing model. The U/Pb age distribution of the Yangtze is fixed after the river traverses the upper reaches of the Yangtze, which largely sources the Songpan Ganze Terrane and the Longmenshan (i.e. the catchment of upstream of Panzihua-2, and the Yalongjiang, Minjiang, Daduhe, and Jialingjiang tributaries). Thus, the high exhumation rates at the eastern margin of the Tibetan Plateau (Kirby et al. 2002; Wang, 2012; Densmore et al. 2007) provide much of the Yangtze's overall sediment load. This is consistent with well-documented large sediment flux to valleys

(Parker et al., 2011) after large earthquakes. Such persistent, far-traveled, geochemical signals that traverse 1000s of kilometers of lowlands are not unique to the Yangtze, as is evidenced by data from the Amazon River (e.g. Dobson et al., 2001; Wittmann et al., 2011). Importantly, our results are consistent with those with other detrital studies of the Yangtze, which focus on non-zircon systems. Zhang et al. (2014) characterized Pb isotopic composition of potassium feldspar and demonstrated erosion of the Longmenshan and neighboring regions are the important sediment suppliers to the middle-lower Yangtze. The recent high-resolution petrographic and heavy-mineral analysis of Vezzoli et al. (2016) finds that left-bank tributaries draining the topographic front of the Longmenshan and Qinling Mountains (believed to be a major source of sediment to the Songpan Ganze Terrane (Weislogel et al., 2010) are the principle contributors to sediment reaching the East China Sea. Both studies note the higher contributions of these tributaries and regions correlates well with well with their slope steepness, precipitation, stream power, and tectonic hazard (Vezzoli et al., 2016; Zhang et al., 2014).

Finally, the results of the fluvial sediment-mixing model (Figure 2.7B) are not inconsistent with the previously established results that the sediment of the trunk stream and not the downstream tributaries dominates the U/Pb age signal of trunk samples. The majority of subsequent trunk stream samples following Panzhihua are best described by mixtures of almost exclusively trunk stream sediments. Notable exceptions, such as samples near Yibin and Yueyang-2 can be attributed to high proportions of particular components linked closely to recently incorporated tributaries that do not maintain consistently high proportions downstream.

Based on our analysis, the interpretation of enhanced erosion within the Han, Jialing, and Xiang river catchments due to anthropogenic activity proposed by He et al. (2014) cannot be

substantiated. In no analysis performed in this paper is there evidence that these tributaries contribute disproportionately to the overall trunk stream catchment. This mischaracterization of zircon sources is likely the result of only considering broad age ranges and over generalized bedrock age distributions. The notable increase in contributions associated with Neoproterozoic zircon related to the South China block in downstream samples is the one exception to the dominance of the upper and northern reaches of the Yangtze. However, the contributions of the South China block never exceed 20% in optimal mixtures, averaging ~11%, which closely resembles the 6-10% areal proportions of the Xiangjiang and Ganjiang tributaries that source the South China Block. Without more data to distinguish Longmenshan from South China Neoproterozoic ages, it is difficult to determine whether these Neoproterozoic zircons are correctly grouped with the South China units or merely incorrect substitutions of their western Longmenshan counterpart.

Our analysis of provenance is limited exclusively to U/Pb zircon ages and could potentially be refined with a second layer of data such as cooling ages (e.g. Reiners et al. 2005), εHf (e.g. Andersen et al. 2011), or using Th/U ratios (e.g. Wang et al. 2014). Other limitations endemic to nearly all regional and continental scale detrital zircon provenance include potentially incomplete descriptions of zircon ages from source terranes, since these are typically complex composites of igneous, metamorphic and sedimentary rocks. Here, we have attempted to more robustly characterize the bedrock units of the Yangtze Catchment with an exhaustive compilation of bedrock zircon geochronology. Even with this compilation, it is difficult to completely discount spatial heterogeneity in zircon concentration (fertility) (Moecher and Samson, 2006; Malusà et al., 2015) or age spectra and thus may not be an accurate representation when combined. The problem is only exacerbated given the size of the Yangtze watershed (~1.8

million km^2). For example, despite the Wu and Yuan River catchments both encompassing a significant portion of South China block, their zircon ages are strikingly different. The Wu River mixture (Appendix II; Figure II.2.) is predominantly derived from Sichuan Basin despite its relatively minor areal contribution to the Wu's catchment. The Yuan River catchment does not contain the Sichuan Basin and results in a very different mixture despite the shared South China Block catchment. This implies either that the Sichuan Basin is exhuming faster than the South China Block or that there is greater abundance of zircons in the Sichuan Bedrock relative to the South China Block. However, the consistency in our results from method to method, as well as independent constraints on exhumation and erosion rates, and independent provenance data, support our conclusion that the upper reaches dominate the supply of zircon, and thus sediment to the Yangtze River.

Conclusions

We reinterpret the Yangtze River detrital zircon data of He et al. (2014) concluding that the upper Yangtze, and more specifically the catchment sourcing zircon from the northwestern portion of the basin, are the largest contributors of sediment to the Yangtze River. He et al. (2014) interpreted the Yangtze detrital zircon data to represent an increase in erosion rates in three tributaries of the Yangtze, the Han, Xian and Jialing Rivers, related to Holocene human disturbance and high specific stream power. Our interpretation is supported by the results of K-S test, likeness and CPR analysis, Gaussian component analysis, and mixing models of bedrock and fluvial distributions. The U/Pb age-distributions of trunk samples are established approximately 400 km downstream of the first bend of the Yangtze at Panzhihua (Figure 2.1) and maintained throughout the rest of the river. The majority of trunk stream samples are best described by high percentages of both the Songpan Ganze Terrane and the Longmenshan

consistent with K-feldspar and petrographic and heavy mineral analysis of Zhang et al. (2014) and Vezzoli et al. (2016), respectively. The tributaries of the Yalong, Min, Dadu, and Jialing Rivers help establish and maintain this signal for the remainder of the catchment. Intersample KS-Tests and dissimilarity measures establish a clear high degree of similarity between trunk-to-trunk sample comparisons, a fact further supported in MDS of the distributions. We argue that if specific downstream tributaries contributed disproportionate zircon fluxes to the main stream, there would be evidence seen in one more of the systematic approaches of detrital analysis performed here. However, there is no evidence of significant variation within the overall trunk stream sample distributions downstream of Panzhihua that cannot be explain by poor homogenization of recently incorporated tributaries. Our comprehensive approach can be applied to any detrital zircon provenance system as it relies on multiple quantitative comparison techniques.

Acknowledgments
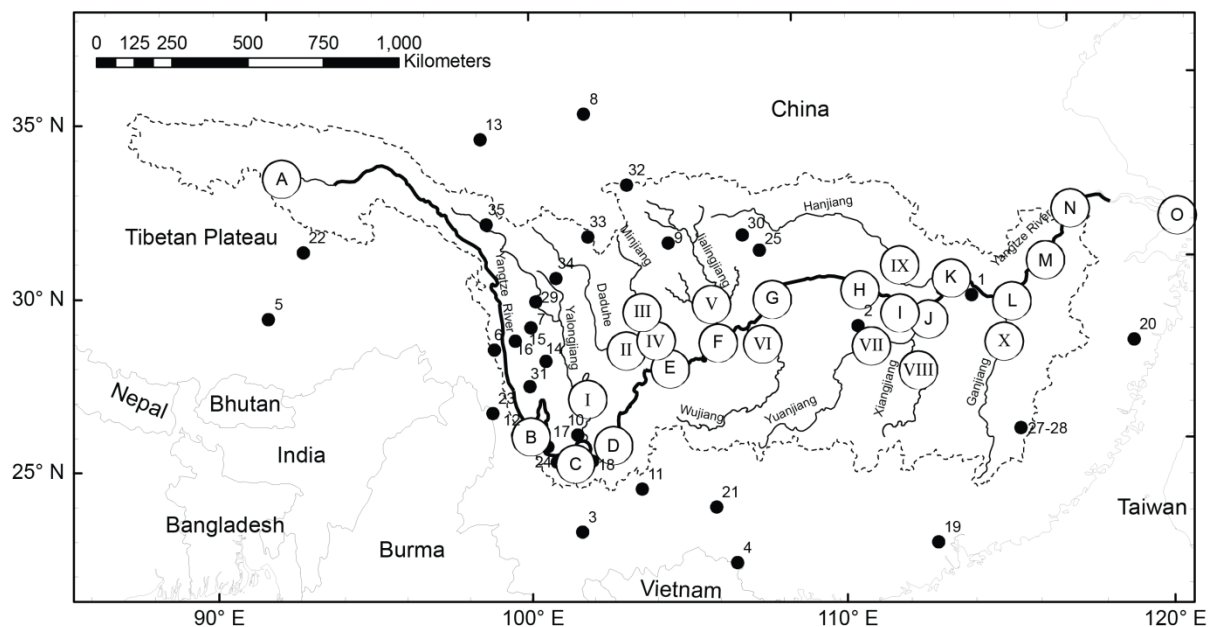
Figures

Figure 2.1. The Yangtze River catchment and sampling locations. Letters are for the trunk stream location of river sediment samples and roman numerals are for the tributary samples from He et al. (2013 and 2014). Black dots indicate the approximate sampling locations of potential bedrock source zircon age components (For bedrock names and references, see Appendix II; Figure II.1.). Source sampling locations may represent geologically contiguous units. Trunk Samples: A - Tuotuohe; B - Shigu (First Bend of Yangtze); C - Panzhihua-1; D - Panzhihua-2; E - Yibin; F - Chongqing; G- Fuliang; H - Yichang; I - Yueyang-1; J - Yueyang-2; K - Wuhan; L - Hukou; M - Datong; N - Nanjing; O - Changxing Island. Tributary Samples: I - Yalongjiang; II - Daduhe; III - Minjiang-1; IV - Minjiang-2; V - Jialingjiang; VI - Wujiang; VII - Yuanjiang; VIII – Xiangjiang; IX - Hanjiang; X – Ganjiang. Sample B at Shigu contains data from both He et al., (2014) and Kong et al., (2012).
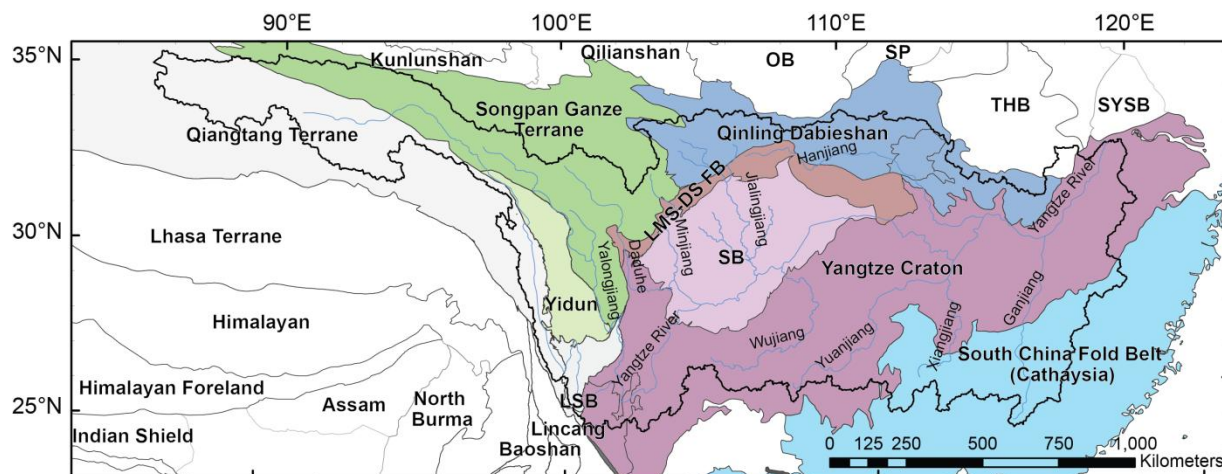
Figure 2.2. Geologic Terrane Map for the Yangtze River catchment. Terranes are colored if they are areally extensive in the Yangtze River catchment (Bold Black Line). OB = Ordos Basin; SP = Shanxi Plateau; THB = Taikang Hefei Basin; SYSB = Subei Yellow Sea Basin; LSB = Lanping Simao Basin.

A. Tuotuohe

B. Shigu (First Bend)

C. Panzhihua-1

I. Yalongjiang

D. Panzhihua-2

II. Daduhe

E. Yibin

III. Minjiang-1

F. Chongqing

IV. Minjiang-2

G. Fuling

V. Jialingjiang

H. Yichang

VI. Wujiang

I. Yueyang-1

VII. Yuanjiang

J. Yueyang-2

VIII. Xiangjiang

K. Wuhan

IX. Hanjiang

L. Hukou

X. Ganjiang

M. Datong

N. Nanjing

O. Changxing Isl.

Probabilities

Downstream

Age (Ma)

Age (Ma)
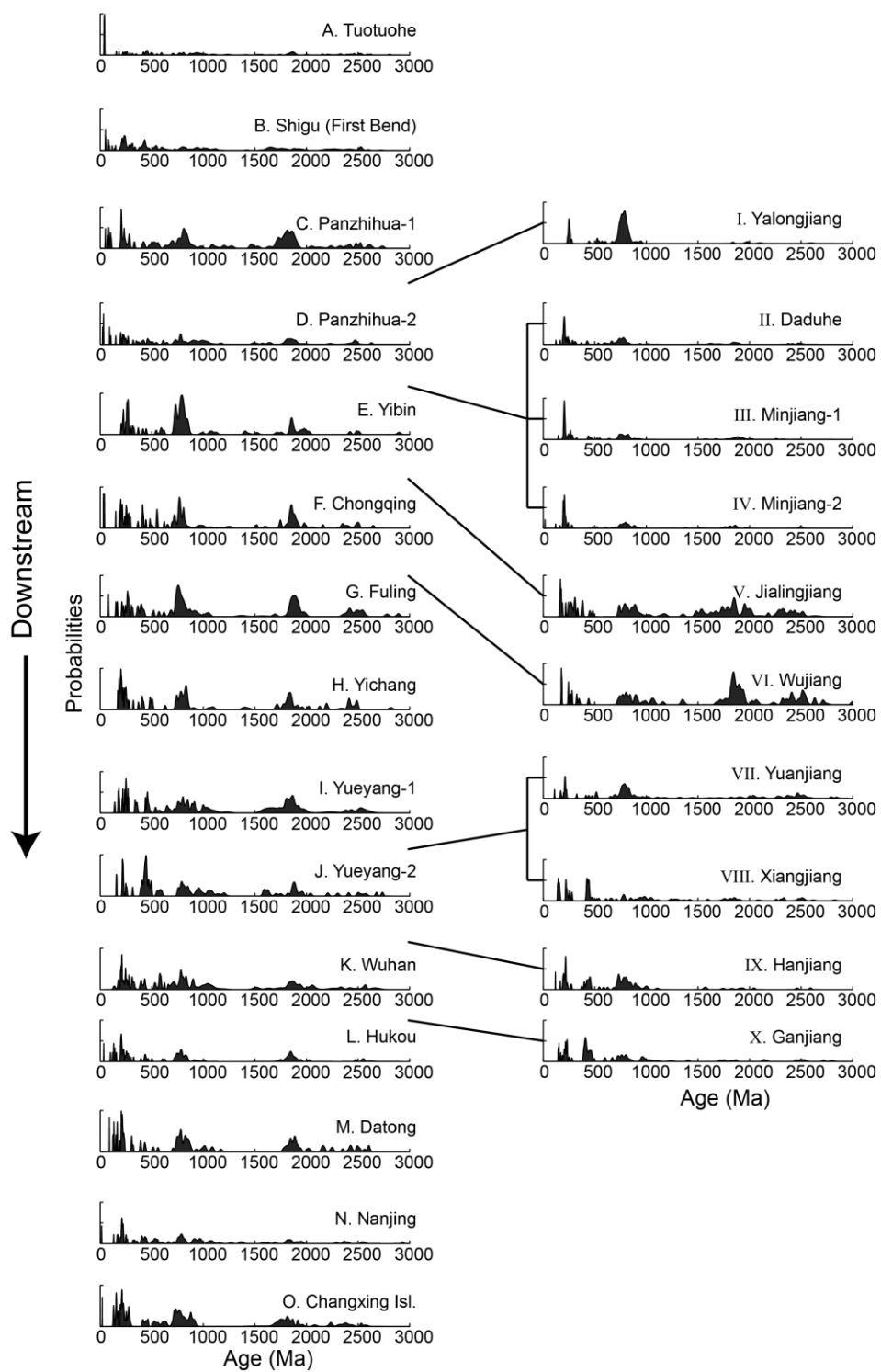
Figure 2.3. Probability density curves for each of the Yangtze River samples. On the Right are the 15 trunk stream samples and the left are the ten tributaries samples. Groups and solid lines extending from the tributaries indicate approximate confluence of these tributaries to the trunk stream.
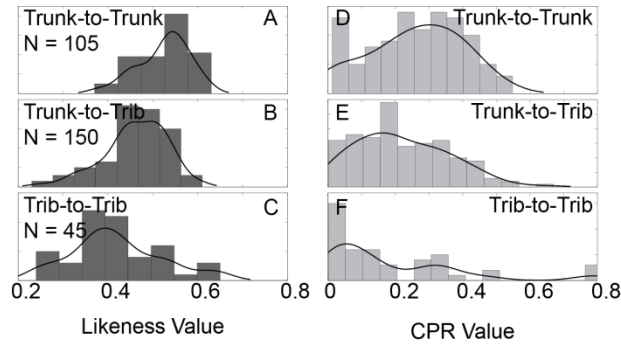
Figure 2.4. Intersample likeness and CPR values. Results of using the Likeness comparison metric (left) and CPR values (right) for trunk -to-trunk, trunk-to-tributary, and tributary-to-tributary intersample comparisons. N equals the number of comparisons per histogram. Higher values indicate higher similarity between pairwise comparisons. Note the trunk-to-trunk comparisons yield on average higher comparison values than all other sample type combinations.
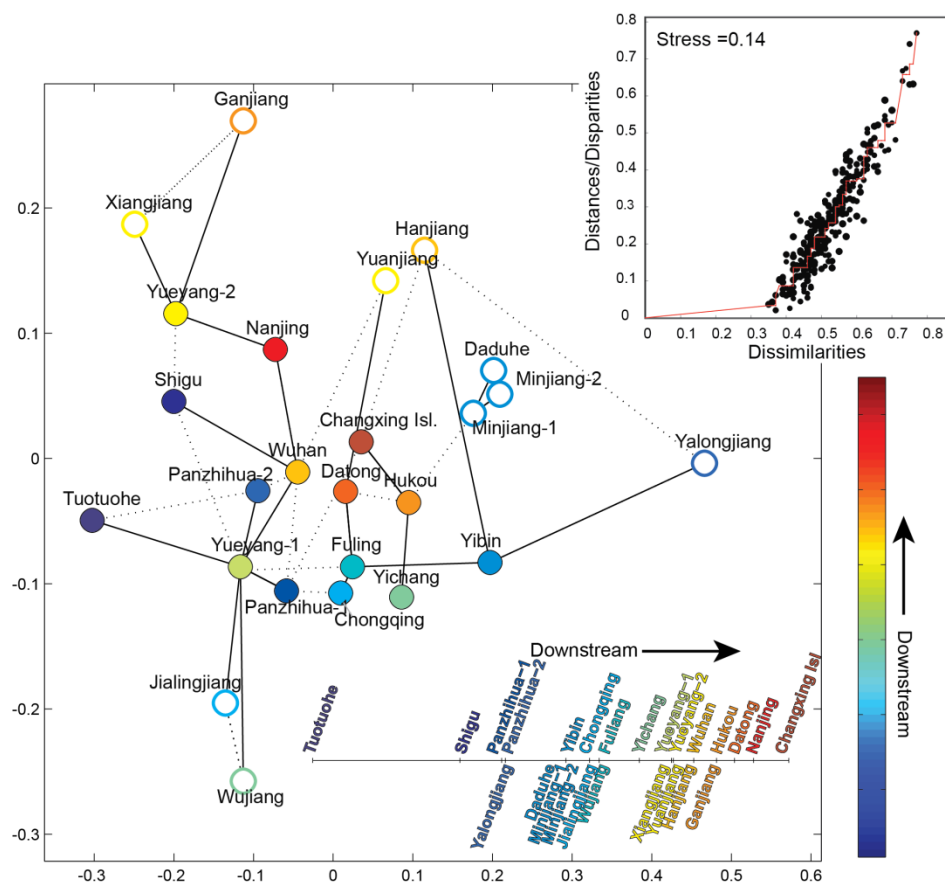
Figure 2.5. Multidimensional scaling plot of Yangtze River data. The nonmetric MDS plot (main) and Shepard Plot (inset) for the translated dissimilarities (likeness) for the Yangtze River dataset. Trunk stream samples are given as filled colors with warmer colors indicating further downstream sampling; Tributary point edge colors indicate downstream location. Solid and dashed lines indicate the closest neighbors and second closest neighbors in likeness, respectively. (Inset) The Shepard plot for the given data. Points represent the scatter plot of the measured dissimilarities (likeness values) vs. the distances in MDS space. Because the MDS is nonmetric, the monotonic function which best translates the data (red line) is calculated numerically. Better fits plot closer along function line. A stress value of ~0.14 indicates a fair translation of the data (Kruskal, 1964a) into MDS space.
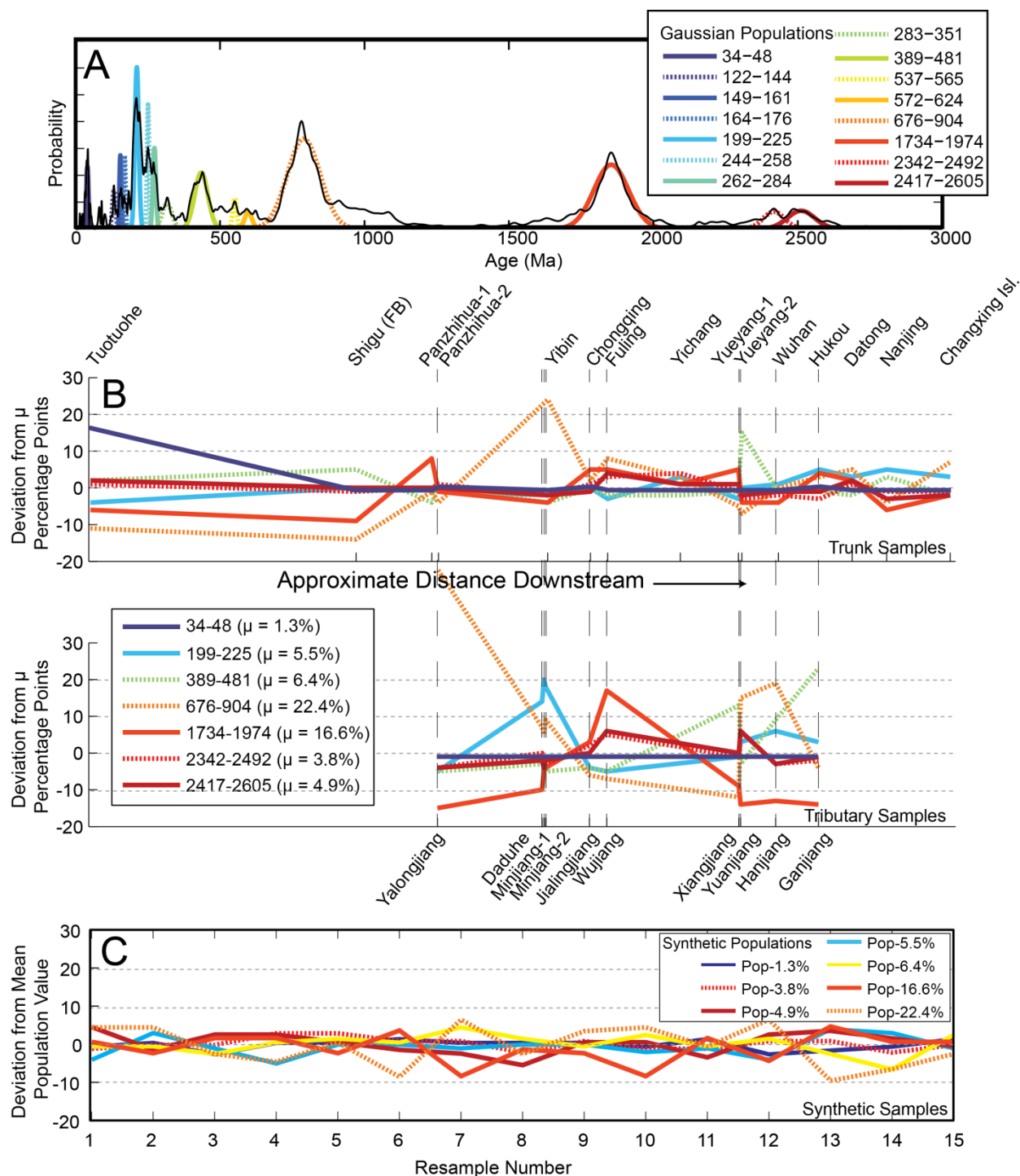
Figure 2.6. Gaussian breakdown of the Yangtze River dataset and deviations from means.

A) The black line indicates the summed curve of all trunk stream samples of the Yangtze River.

The colored curves are the Gaussian curves which best describe the overall variance of the

dataset. The range of each curve at $\pm 2\sigma$ from the mean value is given in the legend. B) The deviations (in percentage points) in proportion of the seven components, which account for >75% of the overall variance of the Yangtze River, at each sampling location from the mean value (μ) of that component. μ is given as a percentage in the legend). Top are trunk samples; bottom are tributary samples. Vertical dashed lines indicate the confluence point of the tributaries. Note the Daduhe and Minjiang Tributaries share a confluence point as do the Xiangjiang and Yuanjiang tributaries. C) Model of deviation plot for synthetic unique components with proportions equivalent and color coordination to the seven components in B. Note the similarity in curve shapes to trunk samples of B.

Figure 2.7. Mixture model results for the Yangtze River dataset. The Yangtze catchment outlined with the heavy black line; tributaries are outlined by thin black lines. Model results for mainstream samples are labeled with roman numerals (See Figure 2.1) Pie charts represent optimal mixtures of bedrock (A) and fluvial (B) components for each sample. A – Model results of mainstream samples of the Yangtze River mixed using bedrock zircon age data. Trunk stream samples contain disproportionate zircons from the Songpan Ganze Terrane and Longmenshan. Major Geologic Terranes are colored and labeled as follows: QT – Qiangtang Terrane; SPGT – Songpan Ganze Terrane; SB - Sichuan Basin ; TU – Transitional Unit; YC – Yangtze Craton;

CA-SC – Cathaysia-South China; QDS – Qinling Dabie Shan Fold Belt; LMS – Longmenshan Fold Belt; Y – Yidun Unit; NYB – Nanyang Basin. Geologic Terranes modified from Burchfiel and Zhiliang (2013) and Hearn et al. (2000). B – Results of mainstream samples of the Yangtze River using its upstream fluvial samples as sources. Colored map regions represent the corresponding catchments for each tributary and correspond with colors of the pie chart. Trunk stream samples within the pie charts are represented as red outlined 'slices' and show continual, disproportionate inclusion of ages derived trunk rather than tributary sources.

Sample Name	Upstream to the Left (Trunk Samples)															Upstream to the left (Tributary Samples)									
	A. Tuotuohe	B. Shigu	C. Panzhihua-1	D. Panzhihua-2	E. Yibin	F. Chongqing	G. Fuling	H. Yichang	I. Yueyang-1	J. Yueyang-2	K. Wuhan	L. Hukou	M. Datong	N. Nanjing	O. Changxing Is.	I. Yalongjiang	II. Daduhe	III. Minjiang-1	IV. Minjiang-2	V. Jialingjiang	VI. Wujiang	VII. Yuanjiang	VIII. Xiangjiang	IX. Hanjiang	X. Ganjiang
A. Tuotuohe	-	F	F	F	-	F	F	F	F	F	F	F	F	F	F	-	-	-	-	-	-	-	F	-	-
B. Shigu		-	F	-	-	-	F	-	-	-	F	-	F	F	F	-	-	-	-	-	-	-	F	-	-
C. Panzhihua-1			-	F	-	F	F	F	F	F	F	-	F	-	-	-	-	-	-	F	-	F	-	-	-
D. Panzhihua-2				-	-	F	F	F	F	F	F	F	F	F	F	-	-	-	-	-	-	F	F	-	-
E. Yibin					-	F	-	F	-	F	F	-	F	F	F	-	-	-	-	-	-	-	-	F	-
F. Chongqing						-	F	F	F	F	F	F	F	F	F	-	-	-	-	-	-	F	F	-	-
G. Fuling							-	F	F	F	F	-	F	-	-	-	-	-	-	F	-	F	-	-	-
H. Yichang								-	F	F	F	F	F	F	F	-	-	-	-	-	-	F	F	-	-
I. Yueyang-1									-	F	F	-	F	-	-	-	-	-	-	F	-	F	-	-	-
J. Yueyang-2										-	F	-	F	F	F	-	-	-	-	-	-	-	F	-	-
K. Wuhan											-	F	F	F	F	-	-	-	-	-	-	F	-	-	-
L. Hukou												-	F	F	F	-	F	F	F	-	-	-	F	-	F
M. Datong													-	F	F	-	-	-	-	-	-	F	-	-	-
N. Nanjing														-	F	-	-	-	-	-	-	-	F	-	F
O. Changxing Island															-	-	-	F	F	-	-	-	F	-	-
I. Yalongjiang																-	-	-	-	-	-	-	-	-	-
II. Daduhe																	-	F	F	-	-	-	-	-	-
III. Minjiang-1																		-	F	-	-	-	-	-	-
IV. Minjiang-2																			-	-	-	-	-	-	-
V. Jialingjiang																				-	-	-	-	-	-
VI. Wujiang																					-	-	-	-	-
VII. YuanJiang																						-	-	-	-
VIII. Xiangjiang																							-	-	F
IX. Hanjiang																								-	F
X. Ganjiang																									-

Note: F = Fail to reject the null hypotheis
Shaded = Tributaries within the upstream catchment

Table 2.1. Results of the K-S test. Trunk stream samples are given as bold labels, tributaries are italicized. A value of F indicates the K-S test failed to reject the null hypothesis that the two sample distributions were derived from the same distribution, while a dash indicates a rejected null hypothesis. Results falling below and to the left of the bold line (shaded area) within the tributary-to-trunk portion of the table are tributaries that fall within the trunk stream catchment indicated by the row.

Chapter 3. Multidimensional scaling in detrital zircon studies - examples from platform, basin, and passive margin settings of North America

Submitted as:

Wissink, G.K., Wilkinson, B., Hoke, G.D. (2016). Multidimensional scaling in detrital zircon studies - examples from platform, basin, and passive margin settings of North America. GSA Bulletin (in review)

Abstract

Development of high efficiency and low cost techniques for the acquisition of U/Pb ages has led to the rapid expansion of detrital zircon analysis and interpretation over the last several decades. This abundance of information affords unparalleled means to better understand histories of sediment dispersal, but also requires effective approaches for qualitative and quantitative interpretation. Multidimensional scaling (MDS) is one of the more recent approaches for visualizing and understanding U/Pb age data and is applied by translating the dissimilarities between sample U/Pb age distributions into Euclidean space, with greater distances between sample points equating to greater dissimilarities. Here we examine several important issues in the application of MDS to detrital zircon research; these include: 1) different methods of representing intra-sample variation and intra-sample dissimilarity in grain ages 2) the consequences of random sampling and dating a limited number of grains on MDS results, and 3) the effects on MDS differentiation among samples with varying degrees of overlapping, shared, and unique age components. We then apply this methodology to several real-world detrital zircon datasets in order to illustrate the usefulness of the approach in the interpretation of detrital zircon age data. Results from both synthetic and real-world examples suggest that the application of MDS mapping to detrital zircon data affords significant advantages in the geologic interpretation of grain ages.

Introduction

Zircon is a common accessory mineral in clastic sedimentary deposits, making it widely used in provenance analysis. Its durability, resistance to chemical and physical weathering, high concentrations of U and Th, and low concentrations of initial Pb make it a robust geochronometer and thus a useful mineral for provenance. The widespread use of single-grain detrital zircon age data are, in large part, due to the development of rapid and inexpensive age acquisition techniques, primarily through laser ablation inductively coupled mass spectrometry (LA-ICP-MS). LA-ICP-MS compromises the higher analytical precision of Thermal Ionization Mass Spectrometry for the ability to determine the ages of hundreds of zircon grains per day. As the number of zircon grains analyzed per sample and the number of samples per study grows, the management, visualization, and interpretation of such data becomes increasingly challenging. Efficient, effective, and meaningful techniques to envisage, compare, and evaluate zircon U/Pb age distributions has therefore garnered considerable attention. This is particularly critical in the representation of differences among detrital zircon samples arrayed over broad geographic regions and/or through geologic time.

What are the best approaches to illustrate the variation within a suite of samples arrayed in time and/or in space? Most commonly, differences in sample grain ages are evaluated qualitatively by visual comparison. However, given the growing size of datasets and increasing desire for more robust characterization of inter-sample variation, differences in zircon age-frequency distributions are increasingly being treated more quantitatively. This allows one to examine such variation within an entire detrital dataset, as opposed simply to sample pairs. Methodologies employed thus far include mixture modeling (e.g. Sambridge and Compston, 1994), hierarchical cluster analysis (e.g. Sircombe and Hazelton, 2004), principal component

analysis (e.g. Fedo et al., 2003; Sircombe, 2000), and age spectrum deconvolution (Sambridge and Compston, 1994). Additional insight can be obtained from multidimensional scaling (Vermeesch, 2013).

The multivariable ordination method, called multidimensional scaling (MDS), significantly enhances the capability to visualize differences among samples based on quantified pairwise differences in their zircon age-frequency distributions (Vermeesch, 2013). Here, using zircon ages from both synthetic-model and real-world datasets, we assess strengths of the MDS approach by exploring changes in ordination that result from: 1) choice of pairwise dissimilarity metric, 2) sample complexity (i.e. number of age components in a sample), and 3) issues associated with random sampling. In the following, we employ the terms 'age component' to represent a suite of grain ages comprising a single mode, 'age population' as a suite of grains encompassing one or more age components, and a 'sample' as grain ages determined for a limited number of grains drawn at random from some population of nearly infinite size. In this construct, age components are analogous to classic source provinces (e.g. Grenvillian) whereas populations comprise one or (usually) more Gaussian components.

Variation in grain ages

In order to characterize spatial and temporal differences in zircon ages among various samples using multidimensional scaling, two rather independent steps must first be taken. These are: 1) the implementation of one of several methodologies for representing the relative abundances of different age components in an individual sample, and 2) the application of one or more of a number of metrics by which to quantify the degree of dissimilarity between any pair of samples based on the abundances of ages present in each. With these pairwise differences among

samples in hand, it is then possible to visualize degrees of sample age differences in time and/or space.

Representation of Sample Ages

Intra-sample abundances of different grain ages have long been represented as age frequency distributions (AFD; e.g. Machado et al., 1996), as probability density functions (PDF; e.g. Dodson et al., 1988) or as Kernel Density Estimations (KDE; e.g. Sircombe and Hazelton, 2004). Each approach strives to identify the presence of one or more age components within some sample, the relative frequencies of which can then be further interpreted in some geologic context. The application of any of the three approaches necessitates the imposition of certain assumptions and biases. The determination of AFDs requires utilization of some bin size (Figure 3.1A). Determination of PDFs involves the summed probabilities of measured grain ages and their associated Gaussian analytical uncertainties, and hence implicit in the method is the rather specious notion that that calculated age abundance (e.g. probability density) is somehow related to analytical error (Figure 3.1B). Representation of sample ages as KDEs is accomplished by arranging the measurements in a similar sense to that in an age frequency distribution, over which is imposed a kernel of predetermined bandwidth (Figure 3.1C), and the shape of the KDE function is highly dependent on the chosen kernel (band) width. Some use uniform predefined bandwidths, (e.g., Andersen, 2014), some adaptive bandwidths that vary by age (e.g. Breiman et al., 1977), while still others employ various algorithms to identify the 'optimal bandwidth' for a given distribution of ages (Botev et al., 2010; Botev, 2007; McPhillips and Brandon, 2010)

In theory, zircon ages in any sample reflect the differential contribution of one or more genetic zircon age components, each representing some duration-restricted zircon growth event

whose ages were acquired during the formation of some source province. To the degree that this is correct, the absolute importance of any one or several genetic age components can be quantified by imposing best-fit Gaussian distributions to any sample AFD, PDF, or KDE (Figure 3.1D). Regardless of the approach employed to characterize *inter*-sample variation, it is this characterization of *intra*-sample grain age abundances that ultimately serves as the basis for distinguishing variation among samples and their representation as geologically meaningful changes in the histories of sediment dispersion.

Calculation of Differences among Sample Age Distributions

A variety of approaches have been employed to quantitatively represent the differences in grain age distributions among sample pairs (e.g. Figure 3.2A). Such comparison techniques (e.g. Figure 3.2) include the Kolmogorov-Smirnov (K-S) Test that determines whether a statistically significant difference exists between two distributions (e.g. Press et al., 1988), PDF overlap that examines the proportion of age intervals that contain some number of zircon ages from either distribution (Gehrels, 2000), and PDF similarity that calculates the portions of two distributions with overlapping ages (Gehrels, 2000). The K-S statistic is not widely used to describe degrees of difference between two distributions, as it was designed to evaluate the probability that two samples are drawn from the same distribution. However, Vermeesch (2013) suggests that the maximum difference between two cumulative age frequency distributions (Figure 3.2B), a metric which serves as the basis for the K-S Test, is a useful measure of sameness among sample zircon ages in the context of MDS.

An alternative approach for measuring sample dissimilarities employs the determination of degrees of correlation (e.g. the Pearson product-moment correlation, or R^2 value) between

sample ages through cross-plots of PDFs (Figure 3.2C; Saylor et al., 2013) or cumulative ages

frequencies (Wilk and Gnanadesikan, 1968). In practice, such comparison through correlation

can be based on either frequencies or cumulative frequencies, and either of these could be

derived from age abundances, their PDFs, their KDEs, or their best-fit Gaussian distributions.

Lastly, more inclusive metrics of inter-sample difference are exemplified by the percent

area mismatch approach (Amidon et al., 2005a, 2005b) and closely-associated sample-to-sample

Likeness statistic (Satkoski et al., 2013). Both of these measures are determined by summing, at

some temporal scale of resolution, the absolute value of differences between all "coeval" age

frequencies (Figure 3.2D).

Multidimensional scaling (MDS)

Multidimensional scaling is an iterative ordination technique that graphically represents

the relative dissimilarities among samples arrayed in N-dimensional space, typically two. MDS

is not new to geologic applications (e.g. Doveton, 1976; Hayward and Smale, 1992; Honarkhah

and Caers, 2010; Hounslow and Morton, 2004). Indeed, paleontologists have been using the

technique for decades to visualize relative dissimilarity among fossil assemblages based on the

abundances of included species (e.g. Brower et al., 1978; Prentice, 1980; Shi, 1993). Over the

past several years, there has been a significant increase in its application to detrital zircon

datasets (Arboit et al., 2016; Spencer and Kirkland, 2015; Vermeesch and Garzanti, 2015;

Vermeesch, 2013). In the case of detrital zircons, data are generally presented in two dimensions

(though we will demonstrate the possible additional benefits of a third dimension), with each

plotted point representing one sample's distribution of grain ages and the distance between points

reflecting the degree of dissimilarity between those samples. In so doing, MDS reduces datasets

with large numbers of variables (in this case, age components) into relatively simple visualizations that describe the dispersion among samples. As multiple variables are collapsed into 2D and 3D space, some distortion of their N-dimensional configuration occurs and the degree of distortion is measured by a goodness-of-fit statistic, often called stress.

In the context of detrital geochronology, MDS transforms a matrix of pairwise dissimilarities of sample zircon age distributions into coordinates in Euclidean space. In essence, it takes the differences between zircon age distributions and creates a spatial distribution of sample points that are spaced as a function of their dissimilarities. The axes of MDS maps are unitless, and the orientation of the MDS map is arbitrary; only the relative proximities and distances between points have meaning. It is important to note that here we apply MDS purely as a visualization and interpretation aiding technique, meant to help identify overall relationships between samples that are otherwise difficult to indentify using more commonly used techniques.

Intersample dissimilarities are transformed into Euclidean distances, resulting in a disparity matrix of fitted distances (*d*) using a transformation function (*f*) applied to a matrix of dissimilarities (*δ*). For two samples, *i* and *j,* this can be represented as:

$$d_{ij} \approx f\left(\delta_{ij}\right) \quad (1)$$

where $f(\delta_{ij})$ is a monotonically-increasing function that transforms the dissimilarities to 'disparities' or fitted distances. MDS uses the disparities to produce a configuration of points in N-dimensions. If $f(\delta_{ij}) = \delta_{ij}$ (i.e. if the disparity transformation is the same as the identity matrix) and if the dissimilarities are metric, then the configuration of points can be solved via linear

algebra (Carroll and Arabie, 1980), and is known as classical MDS or principle component analysis.

Metric and nonmetric MDS

The two variants of MDS used in detrital age analysis are metric and nonmetric MDS. Metric MDS, a superset of classical MDS (Torgerson, 1952) and also known as principal coordinate analysis, simultaneously calculates configurations of the matrix *d* and the fit of the transformation via eigenanalysis (Torgerson, 1952; Borg and Groenen, 2005). Metric MDS, in its application to zircon ages, maximizes the linear relationship between measures of sample-to-sample dissimilarities and calculated disparities. For nonmetric MDS, the rank of the dissimilarities (ordinal data), not the absolute differences, is approximated (Kruskal, 1964a, 1964b). The transformation function (*f*) can be any nonparametric function as long as it is monotonically-increasing. Because the data are ordinal in nonmetric MDS, the implicit assumption of metric MDS that there is a true configuration of *d* is eliminated. Solutions to nonmetric MDS are solved numerically (e.g. isotonic regression) and iteratively, by finding first an optimal monotonic transformation of σ, then minimizing the stress between the scaled data by testing multiple configurations, stopping when the configuration most closely matches $f(\sigma)$ (Kruskal, 1964a). Configurations are evaluated by a loss function, which is minimized while best preserving the ordinal dissimilarities. It is important to note that in nonmetric MDS, only the ranks of dissimilarities are truly preserved in the disparities, and thus MDS distances determined using nonmetric MDS will hold far less significance than those of metric MDS with respect to the original sample-to-sample dissimilarities. The advantage however, is that nonmetric MDS assumes nothing about the underlying distribution.

Loss Function/Goodness-of-Fit

Both metric and nonmetric MDS are evaluated by a loss function, or goodness-of-fit (GOF) criterion, for the best achieved configuration for a given matrix of dissimilarities (δ). For metric MDS, the loss function is calculated simultaneously with the calculated configuration of $f(\sigma)$; for nonmetric MDS, the loss function is minimized numerically to optimize the configuration solution. A commonly-used loss function, stress (*S;* Kruskal, 1964), can be expressed as:

$$S = \sqrt{\frac{\sum_{i,j}(f(\delta_{ij})-d_{ij})^2}{\sum_{i,j}d_{ij}{}^2}} \qquad (2)$$

For nonmetric scaling, the normalization is to the sum of squares of interpoint distances, whereas in metric scaling, stress is normalized by the sum of squares of the dissimilarities. Other loss functions include is squared stress, which follows formula (2), but the normalization parameter is raised to the fourth power, and Sammon's Stress (Sammon, 1969).

A strength of MDS is that the particular choice of metric versus nonmetric MDS, or the particular measure of loss function, does not drastically change the resulting Euclidean transformation for detrital sample comparisons (see Appendix III. examples). We wish to suppose, however, that an actual configuration of the data exists based on inter-sample dissimilarities as populations should theoretically represent some fixed mixture of components. It is ideal if the distances between coordinates to approximate actual dissimilarity measured values, thus metric MDS is more appropriate. Lastly, metric MDS provides a global solution that won't get trapped in a local optima (stress minimum) and require changes in the initial configuration to find the true, optimal solution. We therefore focus on the application of metric MDS and utilize

stress (*S*) as the loss function as it is the most well-established.

Often included in evaluation of the goodness of an MDS fit is the Shepard plot, a diagram using Cartesian coordinates to display values of the interpoint distances (disparities; *d*) against the non-transformed dissimilarities (*δ*). In a Shepard Plot, if points fall along a 1:1 line for metric scaling or along the nonparametric function for nonmetric scaling, the MDS solution likely represents well the real differences among samples. A final feature of MDS plots are nearest-neighbor and second-nearest neighbor lines, which reflect least and second least dissimilar pairings; these can also aid in the visual interpretation of MDS scaling (Vermeesch, 2013).

Dissimilarities and Multidimensional Scaling

As noted above, the initial steps affecting an MDS analysis are selecting some representation of samples ages (frequency, PDF, KDE, Gaussian fit) and choosing some measurement of sample-to-sample dissimilarity that serves as the basis for MDS visualization. Vermeesch (2013) outlined the requirements for good measures of age population dissimilarity, positing that the chosen metric should be: 1) independent of sample size; 2) non-negative; 3) symmetric [$δ_{ij} = δ_{ji}$]; and 4) exhibit triangular inequality [$δ_{ik} ≤ δ_{ij} + δ_{jk}$]. In the construct of detrital geochronology, the measure of dissimilarity should also linearly scale with proportions of different age components that are incorporated into various sand populations. As also noted previously, we use the word 'component' as some modal age equivalent to that of the simplest bedrock source (i.e. plutonic zircon without recycling). The Mazatzal-Yavapai, Amarillo-Wichita, and Grenvillian (Figure 3.1D) zircon ages are examples of such 'components'. Clastic units containing one or more components comprise populations of grain ages; a (presumably more or less homogeneous) unit of the Devonian Temple Butte Formation of the Grand Canyon (Figure 3.1) displays a population of grain ages. Any limited number of grain age analyses drawn

from some population (stratal unit) embodies a sample, which is then represented by a point in

an MDS plot. For example, 100 or so ages drawn from the Temple Butte or Surprise Canyon

Formations of the Grand Canyon are samples of infinitely larger populations of grain ages

(Figure 3.2).

To a first order, the way zircon U/Pb age distributions are described, whether as age

distributions, PDFs, KDEs, or as Gaussian fits (e.g. Figure 3.1), has a major effect on how intra-

sample dissimilarities are calculated. Moreover, the choice of particular method used can

drastically change how distributions are evaluated for dissimilarity. The KDE (Figure 3.1B) and

PDF (Figure 3.1C) for a sample of the top of the Devonian Temple Butte Formation in the Grand

Canyon (Gehrels, Blakey, et al., 2011), for example, are quite different despite the fact that they

represent the same grain age frequencies (e.g. the arguably single component at ~1400Ma in

Figure 3.1B vs. the apparent multiple components at ~1400Ma in Figure 3.1C) . Any

computation of dissimilarities between the two curves of Figure 3.1B and 1C (KDE and PDP)

would be suspect as they are calculated in fundamentally different ways. For a choice of either

KDEs or PDFs, the nature of intra-analytical comparisons requires uniformity of initial

parameters. For example, the kernel bandwidths of KDEs should be uniform for all dissimilarity

calculations. While optimal bandwidth algorithms (e.g. Botev, 2007; Botev et al., 2010;

McPhillips and Brandon, 2010) may provide more statistically robust bandwidths for a given

distribution, they will vary, potentially by 10s of millions of years from sample to sample of a

single dataset. For PDFs, analytical uncertainty is directly related to methods of data acquisition

and therefore dissimilarity measures of PDFs derived by thermal ionization mass spectrometry

ages versus laser ablation inductively coupled plasma mass spectrometry ages are suspect.

The selection of method by which to represent differences between sample age frequencies (e.g. Figure 3.2) also affects the choice of measure of dissimilarity. For cumulative data, the commonly used dissimilarity measure in provenance studies is the maximum difference between cumulative frequencies (MDCF; Figure 3.2B); this is the measure widely used in computing the p value for the Kolmogorov-Smirnov Test (Press et al., 1987), and is the metric used by Vermeesch (2013). Other measures of difference exist for sample KDEs and PDFs but, in principle, all attempt the same thing, to quantify the differences between sample ages. Here, in addition to MDCF, we examine cross-plot R^2 values (CPR; Figure 3.2C ; Saylor et al., 2013) and likeness (LK; Figure 3.2D; Satkoski et al., 2013), as each satisfies the parameters outlined by Vermeesch (2013).

Evaluating Dissimilarity Measures

Although each of these three dissimilarity measures (MDCF, LK, and CPR) satisfy the criteria described by Vermeesch (2013), it is not immediately apparent which produces the MDS ordination reflecting the truest representation of dissimilarity within a dataset. To examine the impact of different metrics of dissimilarity on MDS mapping, we construct a simple, three-component model. The three components are defined by Gaussian distributions of 100 ± 10, 200 ± 10, and 300 ± 10 Ma, and mixed in increments of thirds, resulting in 10 populations (Figure 3.3). The two-dimensional MDS map generated from such a model should resemble a ternary diagram with each single-component sample (representing 100% of one component) positioned at vertices, and all distances between sample points being near some multiple of one-third the distance between any of the three vertices. This requires the calculated intersample dissimilarities to be linearly-correlated with the percentage of each component (Figure 3.3).

Using metric MDS and stress (*S*) as the loss function, we produce MDS configurations based on dissimilarities measured as LK (Figure 3.3A), CPR values also known as cross-correlation (Figure 3.3B), and MDCF (Figure 3.3C). Of the three measures (Figure 3.3), LK results in clearly the best approximation to the ternary nature of the model dataset with nearly uniform spacing between all points in the plot. The stress of this translation (*S* = 0.07) only suggests a good, but not excellent fit (based on Kruskal (1964a)'s rule of thumb for the goodness of fit for *S*; 0 = Perfect, 0.025 = Excellent, 0.05 = Good, 0.1 = Fair, 0.2 = Poor). It is not possible in two dimensions to distribute perfectly all 10 points. For each sample, there exists four or more equally dissimilar samples, which, ideally, would be plotted equidistantly but cannot in 2D; this is a product of three variables (age components) involved in the dataset. For example, a truly optimal configuration would require each sample point falling along an edge of the diagram to be equidistant from its opposite vertex, a feat not possible without outward curvature of the edge and poorer fit of the remaining sample points or additional dimensions. However, *S* =0.07 suggests a good fit to the data and the ternary representation provides the optimal 2D approximation for the dissimilarities. The configurations for CPR and MDCF both define components as vertices and have stresses comparable to LK (*S* = 0.08), but both are less accurate representations of the model data. For mixed multi-modal populations, CPR results in clustering of populations closer to their most similar vertices; this results in decidedly unequal spacing among points. For MDCF, the vertices are similarly established, but the mixed data are clearly displaced toward the 200 Ma component.

In order to further explore relations between choice of dissimilarity metric and differences among model age populations, we calculate the LK, CPR, and MDCF values between the three component model populations noted above, and plot these measures of

dissimilarity against the known proportions of components within each sample. Using one-tenth mixing proportions (Figure 3.4A), we demonstrate that LK yields a perfectly linear correlation in ideal populations with the proportion of component present in the sample and the measured LK value of the sample against that component. Using CPR values as a measure, samples with lesser degrees of end-member component mixing (e.g. 0 - 40%) yield higher CPRs (more dissimilar values) than expected; the opposite relation exists for samples with higher degrees of component mixing (60 - 100%). In essence, the utilization of CPR imposes an apparent 'pull' towards the MDS vertices (Figure 3.4A).

Utilization of MDCF produces even poorer correlation between component proportion and dissimilarity, with significant scatter of lower than expected dissimilarities for a proportion of mixed component comparisons. Because cumulative distributions are continuous functions, the summation of any age leads to an increase in the cumulative distribution (Figure 3.4C). An important caveat lies in comparing age distributions with 'sandwiched' age populations; that is, one population contains components that are both younger and older than some other component of intermediate modal age exclusively present in the other population (Figure 3.4B). In such cases, cumulative frequencies will cross below a cumulative value of unity (Figure 3.4C), forcing the calculated MDCF value to be less than unity, despite containing no overlapping ages. Most real-world samples are composed of grains drawn from a number of components representing several sediment provinces. Moreover, any sample containing a significant contribution of, e.g., 100 Ma grains, is no more or less likely to be mixed with a 200 Ma component than with a 300 Ma component. As a result, MDS configurations using CPR and MDCF yield equally accurate representations of the dissimilarities, but not the distributions of grain ages. Hence, S values are similar for all three dissimilarities, despite obvious variations in their 2D configurations. Given

that neither CPR nor MDCF yield the same linear relationship between degree of component incorporation and measure of dissimilarity that is attained using LK, and given the significant likelihood of encountering this 'sandwiching' effect in real detrital data, we judge LK to be the best metric of sample-to-sample dissimilarity for MDS.

Synthetic Data

Employing LK as the measure of dissimilarity, and stress (S) as the loss function in metric MDS mapping, we can now explore the influences of several variables common to detrital geochronology on MDS. These are: 1) the effects of considering a limited number of zircon ages sampled at random from some nearly infinite population, 2) the degree of dissimilarity that must exist between pairs of age frequencies before MDS can no longer effectively assess real sample differences; 3) the effects of the random sampling of both unique and shared age components among pairs of age frequencies 4) the effects of random sampling on variably overlapping age components; and 5) the effects of multiple components on MDS mapping with respect to increasing MDS dimensionality.

Effect of Limited Sample Size –

What is the influence of considering a limited number of grain ages, presumably drawn at random from some nearly infinite population, on MDS mapping? One major source of uncertainty associated with detrital geochronology studies is random sampling error, imposed by the limitation of sampling and analysis of a finite number of detrital grains from essentially infinitely large pools of grains. The question of the 'correct' number of grains needed to accurately represent the population of ages in any deposit has plagued the geochronology community for some time (Dodson et al., 1988; Vermeesch, 2004; Pullen et al., 2014). Most

studies currently strive to analyze about 100 grains per sample, with the assumption that fewer ages (and their derived abstraction as PDFs or KDEs) may produce incomplete or distorted representations of the actual distribution of population ages. The influence of this number on MDS mapping can be explored by examining MDS maps of samples of multiple components versus those samples drawn from one component. With respect to the 3-component model described above (Figure 3.3; 100 ± 10, 200 ± 10, and 300 ± 10 Ma), we consider 100 ages drawn at random from mixtures of these end-members. Moreover, because ages comprising these model components do not include associated analytical errors requisite for calculation of PDFs, we represent sample age frequencies as KDEs with a bandwidth at 10Ma.

Plots based on one and three samples, each comprising 100 random age draws from the 10 original perfectly-distributed mixtures (e.g. Figure 3.3A) closely replicate the actual MDS spatial configuration (Figure 3.5). However, differences comparing randomly drawn samples and the ideal populations are larger for samples containing two or more age components (Figure 3.5A). While not surprising, this difference lends itself to a consideration of the real meaning of 'clustering' in MDS space. Visually, some distributions from single-draw samples, such as group 1 in Figure 3.5A, appear to be more similar while samples from group 2 appear to be less so. By model formulation, we know this is not the case, and this degree of clustering simply reflects the effect of the random sampling of 100 grain ages containing more- or less-heterogeneous grain ages.

For this reason alone, caution should be used when interpreting the significance of data clustering in MDS plots. This effect is greatly reduced when considering three 100-age samples per population (Figure 3.5B), as the mean of each set of 'triplets' falls approximately at the node for the ideal population. Samples of shared provenance in this case are easily distinguishable.

Multiple samples would serve to reduce uncertainties associated with limited numbers of age determinations, and the corollary that measuring more grains per sample should help reduce random sampling uncertainties.

Despite the incertitude associated with limited numbers of random samples, MDS adequately characterizes dissimilarities among model populations (Figure 3.5). It is worthwhile to explore what degree of dissimilarity renders MDS ineffective in assessing sample differences at the level of 100 grains per sample. This can be explored by examining the impact of limited sampling of model populations with variable degrees of component dissimilarity.

Limited sampling of variable proportions of shared components

The effect of random sampling of populations with shared but unequal proportions of age components is an important issue in interpreting detrital geochronological data. Because sampling numbers are finite, the proportions of particular age components are inherently variable in any sample. This aspect of detrital zircon age data perhaps favors approaches focused more on determinations of component (and presumed associated provenance) presence or absence (Gehrels, Blakey, et al., 2011) rather than interpretations based on their relative abundances, but also brings focus to the issue of just how different the proportions of two distinct, non-overlapping age components in a 100-grain sample need to be in order to ascertain their relative contributions. We approach this question by considering variable proportions of two age components (100 ± 10 and 200 ± 10Ma) in order to generate five sets of population pairings, each containing a bimodal population of varying component proportions (Figure 3.6). From each bimodal population, three samples of 100 ages each were randomly drawn. Thus, for each of five MDS analyses, we compare six samples total, three each from the two bimodal populations

(Figure 3.6). For simplicity, one population contains equal proportions of the two age

components, while components in the second population vary in increments of 5% per MDS

analysis (Figure 3.6). This results in an incremental LK change of 0.05 among the five model

MDS sets, starting at an initial dissimilarity likeness value of 0.05 between the 50-50 and 45-55

populations (Figure 3.6; column 1). On the basis of 10 iterations for each of the 5 model sets, it

seems apparent that a LK value of 0.20 or greater is needed to effectively differentiate

populations in MSD space (Figure 3.6). That is to say, sample pairs in which there is less than

20% overlap of KDEs determined at a fixed bandwidth will not be visually separated in MDS

space.

Limited sampling of variable proportions of different components

Following a similar construct, we can examine how quickly MDS differentiation occurs

between random samples drawn from two populations that contain one shared and one unique

component, each. We consider three age components (100 ± 10, 200 ± 10, and 300 ± 10 Ma) and

let the 200 ± 10 Ma component be shared in equal proportion between the two populations. The

100 ± 10 and 300 ± 10 Ma components are unique to one or the other population, respectively

(Figure 3.7). We again consider the average degree of differentiation among 10 iterations of each

model set (Figure 3.7). The consequence of these model datasets is that MDS differentiation only

becomes apparent as LK meets or exceeds a value of ~0.1 (mixtures B and C), and demonstrates

that MDS mapping is far more sensitive to the inclusion of unique age components (Figure 3.7)

than the variably-shared populations discussed above (Figure 3.6).

The dependency of MDS visualization on the exclusivity of different age components

may be both a boon and a nuisance to detrital geochronologists. A 5% difference in the

abundance of some unique component (LK = 0.05) among different model populations was enough to produce differentiation in the randomly drawn, 100-age, samples in one of the ten model iterations. In some instances, the ability to potentially identify unique contributions from individual provenances that represent relatively small variance in zircon sample age distributions may be of considerable geologic importance. However, the limited number of grain ages typically drawn at random from some infinitely larger multimodal population may result either in the inclusion or exclusion of certain age components, purely from random sampling and the effect of that sampling on MDS mapping.

Unique age components in detrital zircon data can also be an artifact of the depiction of zircon sample age data. Representation of zircon ages from the sample of the Devonian Temple Butte Formation in the Grand Canyon as a KDE (Figure 3.1C), for example, might be taken as evidence of the presence of several distinct age components. However, when these same ages are represented as a PDF (Figure 3.1B), the number of identifiable age components is roughly halved. The reason for this is that width and 'inclusion' of ages in PDFs is directly dependent on analytical uncertainty in zircon age determination, whereas the shape of the KDE functions is highly dependent on bandwidth. In the case of the Temple Butte sample, average analytical errors (n = 100; errors range 45.1 ± 22.4 Ma) are greater than the 10 Ma bandwidth used to calculate the KDE. It is therefore essential for MDS users to examine the sorts of representations applied to their data to weigh the strengths and weakness of each style of representation, and to consider how these may affect MDS mapping. Here, we consider perfect age distributions with no analytical uncertainties. As a result, model results almost surely yield greater MDS differences than would be the case for real-world datasets comprising true U/Pb ages.

Nonetheless, representations of age data as PDF frequencies provide a valuable baseline against which to evaluate MDS mapping.

Random Sampling of Overlapping Distributions

Given that the inclusion of a unique age component in grain age populations serves to improve the resolving power of MDS, we might then ask if there is a limit of age overlap between two populations that can be resolved by MDS. To address this question, we consider two unimodal populations (essentially components), whose mean ages differ by increments of 1Ma (Figure 3.8). As before, each distribution is resampled 3 times, at 100 ages per sample, and then evaluated using MDS (Figure 3.8). In this example, MDS appears to have considerable power to resolve different age components, even if their mean ages are only slightly different (<3%). Moreover, the validity of this result appears less dependent on component standard deviations than the mean ages of the components in question. To some detrital geochronologists, this outcome may be disconcerting. Significant differences in ages may exist between 'cogenetic' zircons formed in pluton cores versus pluton margins (e.g. Schoene et al., 2012), or along an volcanic arc (e.g. Reid et al., 2007), and analytical uncertainties of zircon age measurements are typically several percent that of measured age (e.g. ~100 Ma for a 1 Ga age). In this regard, it is important to note that if a third population were included, one whose mean age differed greatly from those comprising the overlapping distributions, then the less dissimilar samples would be sufficiently close in MDS space that their difference would be seemingly negligible compared to the magnitude of difference established by the far more dissimilar component as the actual distance between the cluster is small (~0.1 dimensionless units).

The apparent sensitivity of MDS mapping to differences in mean age does, however,

argue for the importance of MDS users to consider how differing representations of probabilities, as PDFs or KDEs, might influence perceptions of component mean values. As noted above, the dependence of PDFs on analytical uncertainties can easily skew population modes by several million years and several percent. KDEs, on the other hand, with the dependency on measured ages and bandwidths, may lead to possibly unique but overlapping age components being smoothed into one. Conversely, truly cogenetic age components might be divided if the kernel bandwidth is too small.

For all these 100-age models, chance groupings or clusters may occur in perfectly homogenous distributions. Although less common when only three samples are drawn from each population (e.g. Figure 3.5B), these incidences become more frequent with greater numbers of samples. This difficulty gives rise to the suggestion that more weight perhaps be given to determining the presence or absence of different age components rather than to assessing their apparent abundances (e.g. Fedo et al., 2003; Andersen, 2005). It therefore seems sensible that users of MDS plots challenge and evaluate the reality of sample 'clusters' as possible coincidences of random sampling. On a similar note, clusters of samples that include an outlier (because we known the origin of each sample in the model) are also common in larger MDS configurations, a phenomenon also associated with random sampling. We suggest that the presence of such outliers in clusters when source is known, should serve to temper conclusions based on MDS visualizations of unknown samples, where conclusions should be limited to general characteristics of such plots and not inclusion of a single sample within such a cluster.

Numbers of Components and MDS Dimensionality

Thus far, we have only considered systems composed of two and three endmember age

components. In practice, however, an MDS user may wish to examine distributions containing four or more such components. It is important to reiterate that a component is defined as a unimodal population; a unique contributor of grain-ages to one or more samples of a dataset, presumably reflecting in its simplest the contribution of grains of delimited ages from some source province. A theoretical set of data comprised of various mixtures of four equally-dissimilar components (e.g. 100 ± 10, 200 ± 10, 300 ± 10, and 400 ± 10 Ma), requires a spatial MDS configuration of four equidistant points. To achieve this configuration (in which equally-distinct components are evenly spaced), N-1 dimensions are required. As we noted above, only with 2 components can MDS perfectly configure the dissimilarities of detrital samples in two dimensions. While MDS is often characterized as a useful tool by which to evaluate generalities large datasets containing multiple components, the N-1 dimensional requirement potentially limits the application of MDS for multi-component detrital zircon datasets.

Here we briefly show how a four-component model projected onto a 2D MDS surface can result in incorrectly transformed configurations, and further show how this problem is significantly resolved when scaling to 3D. To do so, we use a mixture model based on quarters of the four age components noted above (similar to the method described above for three-component ideal mode; Figure 3.3). We will then translate the dissimilarity matrix of this dataset into 2D (Figure 3.9A) and 3D (Figure 3.9C) MDS configuration. Theoretically, a properly translated four-component data set plot should resemble a tetrahedron (triangular pyramid); the configuration required to equally space the four vertices. Distances between points should be some multiple of one-fourth the distance between any of the four vertices.

2D MDS essentially tries to project the triangular pyramid into the two available dimensions. In this instance, nearest neighbor lines seem directed towards one of the

tetrahedron's corners, the projected peak of the pyramid (Figure 3.9A). The essence of the poor

fit of 4 components in 2D space is further highlighted by the corresponding Shepard plot (Figure

3.9B), with poor linear agreement between LK and distances, and the elevated and poor stress

value ($S = 0.23$). While the vertices do indeed represent each of the four age components, the

internal character of the data are highly suspect, as the distances between points do not correlate

well with dissimilarities, as evidenced by the 'long' neighbor lines connecting 'least-dissimilar'

points over great MDS distances (Figure 3.9A) and large vertical scatter in the Shepard plot.

Conversely, a 3D MDS translation of the same data reproduces the predicted pyramidal shape

and uniform spacing of sample points. Moreover, the stress value is good at $S = 0.9\%$ (does not

equal 0 for the same reasons as 3 component example above) and the Shepard plot (Figure 3.9D)

shows the far better correlation between distances and dissimilarities and highlighting the more

correct dimensionality for the data.

We have attempted to illustrate strengths and weaknesses of MDS mapping in the study

of detrital zircon ages employing various mixtures of idealized model components. For two and

three component systems, MDS is very effective at translating dissimilarities into distances in 2D

space, and four component systems are readily evaluated in three-dimensional space. Generally,

the desired effect in detrital zircon provenance studies is to characterize a single shift in

provenance (e.g. Vermeesch, 2013); which may not require increasing dimensionality or low S

values. While this is often the case, here we do urge caution and careful evaluation of the dataset

when applying MDS to detrital zircon age datasets.

Phanerozoic Examples from North America

We have considered various aspects of model age distributions derived from variable mixtures of ideal components with no analytical uncertainties. Our goal in utilizing this approach is in part to develop a better feeling for the formulation of MDS visualizations from detrital zircon age data, and in part to highlight those aspects of such data that most significantly influence MDS maps. While modeled data provide a valuable baseline against which to evaluate MDS mapping, we conclude by considering MDS analyses of three real-world datasets. Our intent here is to demonstrate the utility of the approach in highlighting sample age variation in both time and in space. The particulars of such differences would of course then serve as the basis for further investigation of the regions in question.

The Colorado Plateau

Remarkable exposures of Paleozoic and Mesozoic strata across the Colorado Plateau offer a nearly unparalleled opportunity to examine changes in detrital zircon provenance of Cambrian through Jurassic sandstones across of the southwestern United States. Recent LA-ICP-MS determinations of 2,529 zircon U/Pb grain ages from 26 Paleozoic samples (Gehrels, Blakey, et al., 2011) and 3,444 grain ages from 36 Triassic and Jurassic samples (Dickinson and Gehrels, 2009, 2008) afford an excellent opportunity to compare more traditional representations of grain ages with those derived through the application of MDS.

As noted by Gehrels et al. (2011), detrital zircons from Cambrian through Devonian strata yield mainly 1.7 and 1.4 Ga ages derived from basement rocks of the Yavapai-Mazatzal Province and the Amarillo-Wichita uplift, respectively. Mississippian through Permian rocks contain predominantly 1.1 Ga and younger Paleozoic grains derived from the Grenville and

Appalachian orogen, respectively. Mesozoic sands record a greater number of age components but exhibit little directional upsection stratigraphic/secular variation (Dickinson and Gehrels, 2008, 2009).

Given the multiple components within the detrital samples that vary in their presence and proportions upsection, as well as the relatively large number of samples, an MDS plot in 3-dimensions affords an opportunity view clear changes in provenance in stratigraphic sequence in a single plot. MDS mapping of age differences among these 65 samples reveals that differences among samples (LK values calculated amongst PDFs) as revealed on axis one largely correlate with stratigraphic position (Figure 3.10B). Sample ages also define three general clusters, which correspond closely with those age groups that could be discerned qualitatively from sample age abundances. In particular, the three clusters in the MDS visualization (Figure 3.10B) are coincidentally almost exactly the same as the groupings of Cambrian through Devonian, Mississippian through Permian, and Mesozoic that are apparent in sample PDFs (Figure 3.10A). Upsection, these are: 1) zircons derived from Yavapai-Mazatzal Province and the Amarillo-Wichita sources; 2) the grains with a significant admixture of Grenvillian zircons; and 3) Grenvillian grains with a significant admixture of Appalachian zircons. Similar clusters can be approximated in 2-dimensions; however, the additional dimension more clearly demonstrates the upsection variations.

Moreover, those samples that exhibit somewhat anomalous distances in MDS mapping also become apparent in sample PDFs. Among these are an early Jurassic (Moenave Formation; Utah) sample which contains an anomalously high concentration (40 of 93 grains, 43%) spanning only 40 Ma of the late Paleozoic (202-242 Ma; labeled 1 in Figure 3.10B), and two Late Cretaceous samples (north eastern New Mexico and south western Utah) which are

dominated by ~1.7 Ga Mazatzal-Yavapai ages, the only two Mesozoic samples in this compilation containing significant numbers of pre-Grenville grains (labeled 2 in Figure 3.10B). While the specifics of the geologic history of these localities have surely served to give rise to these deviations, it is their clear deviance in MDS that serves to bring their differences into sharper view.

The Bighorn Basin

Dissimilarities in abundances of different age components in any population of zircon grains potentially reflect changes in the tectonic history of basins or of variations in climate and sea level, all of which possibly impact paleogeography and sediment dispersal patterns. May et al. (2013) have recently compiled zircon age data from Phanerozoic units exposed in the Bighorn Basin of Wyoming in order to better understand the tectonostratigraphic evolution of that region. Based on 4,104 U/Pb detrital zircon ages from 44 samples, they subdivided Upper Mississippian through Paleocene units into four "tectonostratigraphic assemblages" based on perceived patterns in sample zircon age frequencies: 1) a Paleozoic–Triassic proximal continental margin assemblage, 2) a Jurassic–early Cretaceous (early Albian) assemblage associated with organization of Cordilleran orogeny; 3) a late Cretaceous (late Albian through Maastrichtian) interior seaway foreland basin assemblage, and 4) a Paleogene assemblage accumulated during structural segmentation during the Laramide orogeny. Owing to the fact that these interpretations are largely based on qualitative inspection of probability density plots, and because of the abundance of zircon age data generated during the study, it serves as an excellent case study to which to apply MDS. A three dimensional MDS plot should prove adequate in resolving such a four component system. Are the four hypothesized "assemblages" apparent in MDS visualizations, and are differences among these samples sufficient to affect separation between

presumably genetic clusters in MDS?

Conclusions based on visual examination of sample PDFs are largely confirmed by quantitative evaluation via MDS. Three of the four proposed assemblages are well-resolved by MDS. The posited fourth assemblage, comprising three Paleogene samples, does not separate as a distinct group or cluster. Each of the resolved assemblages contains either a unique component or component with anomalously high proportions. The samples of the fourth assemblage, however, share components with each of the stratigraphically older assemblages, likely contributing to its poor differentiation. In addition, with MDS mapping as a guide, it is apparent that differences that serve to differentiate the first (Paleozoic) and second (lower Mesozoic) assemblages are much less than those that serve to distinguish the second from the third (upper Cretaceous) assemblage; the clusters appear closer together in MDS space indicating that mean populations are less dissimilar. Qualitative differences among sample PDFs support this conclusion; abundant Grenvillian (~1.1 Ga) grains persist upsection through Paleozoic and lower Mesozoic units, but are largely absent above the early Albian Greybull Sandstone at the top of association (the sample 22, Figure 3.11A).

In addition to largely furnishing verification of the actuality of most of the tectonostratigraphic assemblages identified by May et al. (2013), MDS provides two additional insights in the interpretation of detrital zircon data. It serves to identify those samples within any assemblage that are least dissimilar to those in any other, and it allows for a visualization of the relative degrees of difference between groups of samples; both provide motivation for the further examination of spatial and/or temporal attributes that might not be apparent in the absence of MDS.

The Gulf Coast

In addition to better understanding secular differences among various zircon samples, such as those upsection in the Colorado Plateau and Bighorn Basin, MDS should be equally useful in the discrimination of lateral heterogeneities within stratal units of similar age. To this end, we conclude by examining age data from samples of the Paleocene Wilcox Formation collected from along ~2,000 km of its outcrop belt, extending northwest from western Alabama to the head of the Mississippi embayment south of St. Louis, Missouri, and then southwest toward San Antonio, Texas (Blum and Pecha, 2014).

Cenozoic-scale persistence of several major fluvial axes supplying sediment to the northwestern Gulf of Mexico coastal plain (e.g. Galloway et al., 2011) served to impart prominent along-strike variation in the dominance of the same major age components comprising grains in the Colorado Plateau and Bighorn Basin (Figure 3.12A). Blum and Pecha (2014) report 2,564 ages from 27 along strike samples of the Wilcox Formation. Dominant age components consist of ~1.7 Ga Mazatzal-Yavapai, ~1.4 Ga Amarillo-Wichita, and younger Western Cordillera (~170 Ma) and Laramide (~60-75 Ma) province grains along the western third of the belt, and ~1.1 Ga Grenvillian grains along the eastern two-thirds of the section (Figure 3.12A). Once again, the multiple components and numerous samples provide an excellent application of 3D MDS configurations; 2D will not adequately represent the component variance of the detrital dataset. MDS mapping of these age data results in excellent agreement between qualitative assessments of lateral variations based on PDF inspection and variations based on quantified differences (Figure 3.12B). Variation in the MDS distribution of these 27 samples corresponds closely with position along the outcrop belt. Eastern sampled dominated by Grenville grains are

more closely clustered than other samples; more western samples are noticeably more dispersed, an aspect reflecting the incorporation of a larger number of modal ages (Figure 3.12A).

Conclusions

MDS has the potential to be a valuable resource in the tool belt of the detrital geochronology community. Proper recognition of its strengths and limitations is necessary, however, if valid conclusions are to be drawn from MDS data configurations. MDS based on synthetic data suggest that use of MDCF and CPR as dissimilarity measures can significantly distort resulting configurations. Use of LK results in a strong linear correlation with degrees of age component incorporation into various populations, and their sample-to-sample dissimilarity. MDS is more sensitive to the presence of unique age components than variable proportions of shared components; differences in as little as 5% can lead to MDS differentiation. However if a 5% difference is due to uncertainties attendant with random sampling, the resulting MDS configuration may exhibit significant divergence from reality. This is more likely when considering multi-modal populations or when considering under- or over-smoothed representations of sample age frequencies. MDS is also relatively sensitive to degrees of overlap of different age modes; as little as a 2% difference in the mean ages of different components can result in MDS differentiation. This effect also makes the choice of the function (KDE, PDF) used to calculate dissimilarities significant, as each will have an important effect on perception of the actuality of different modal ages. It is also critical for the user of MDS to recognize the possibility that more than two dimensions may be required to properly transform the dissimilarity matrix. A four-component system requires, at minimum, a third dimension to properly represent data; five requires a fourth dimension, and so on. Insufficient dimensions can lead to oversimplified solutions where inter-sample distances do not accurately represent inter-

sample dissimilarities. That said, in the case of detrital zircon, the number of components and how they relate to the contributing sources lie at the heart of the issue. MDS should be effective at configuring dissimilarities of samples derived from two multi-component sources, as this is essentially a two end-member mixing model. More sources and more components require increasing dimensions to effectively resolve variation in MDS. MDS does have considerable resolving power in detrital zircon datasets, but its application, like any other tool must be used with an understanding of its limitations. Use of MDS in conjunction with other analytical tools serves to improve the accuracy of interpretations and conclusions.

Application of MDS to three datasets representing sediment accumulation in North American platform, intermontane basin, and passive margin settings reveals that MDS mapping provides informative visualizations of relative differences among sample zircon ages and the degree to which these differences can be related to their disposition in time and/or space. In each application, MDS configurations in three-dimensions improved the resolving power due to the complexities of the detrital samples. MDS affords an important tool for understanding the nature of the distributions of zircon ages and ultimately, to the geologic processes and histories reflected in these sorts of data.

Acknowledgements
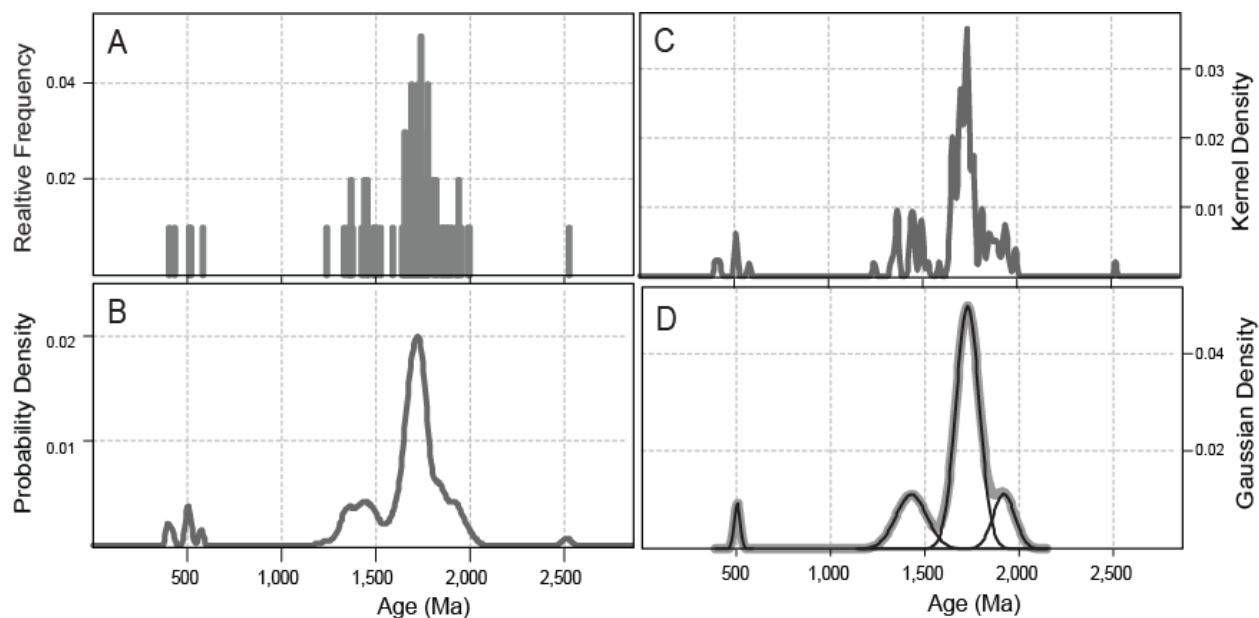
Figures

Figure 3.1. Four representations of within-sample variations in detrital zircon ages. In this case in a sample from the top of the Devonian Temple Butte Formation (n = 100) exposed in the Grand Canyon (Gehrels, Blakey, et al., 2011). A) Age frequency distribution (AFD) binned at 5 Ma; B) Probability Density Plot (PDF), where peaks (e.g. ~1,430 and 1,725 Ma) reflect abundant grains presumably derived from different (e.g. Amarillo-Wichita and Mazatzal-Yavapai) provinces. C) Kernel Density Estimation (KDE) derived using a fixed bandwidth of 10 Ma, and D) the resulting best-fit Gaussian distributions to four recognized age components (1,722, 1,426, 1,913, and 509 Ma) of the PDF, which account for 99% (88.3%, 3.4%, 4.6%, and 0.3%, respectively) of the observed variance in zircon ages for this sample
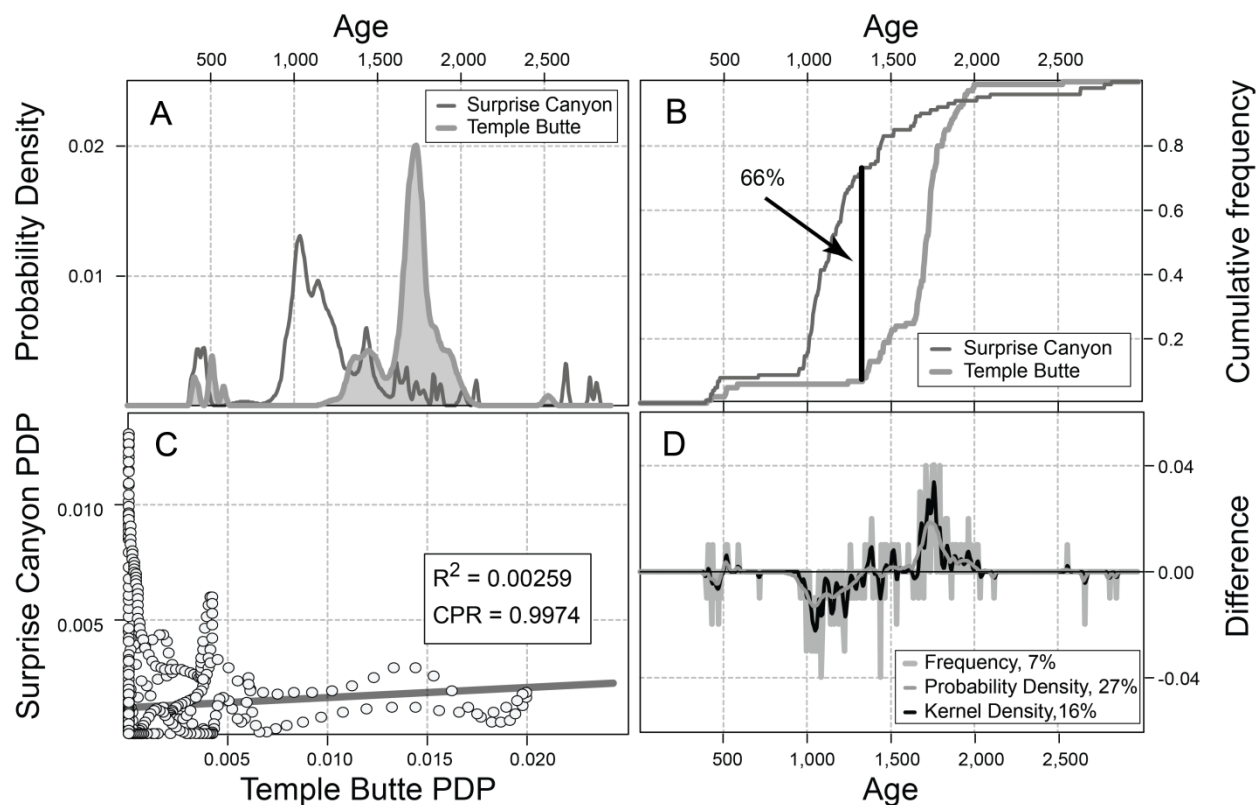
Figure 3.2. Examples of several measures of zircon age dissimilarity. Dissimilarities are

represented by two (rather dissimilar) samples from the Grand Canyon, one from the Devonian

Temple Butte Formation (as in Figure 3.1) and one from the Upper Mississippian Surprise

Canyon Formation (n = 101; also from Gehrels et al. (2011). A) PDFs showing dominance

~1,725 Ma Mazatzal and Yavapai ages in the Temple Butte sample replaced by ~1,035 Ma

grains of Grenvillian age in the Surprise Canyon sample. B) Intra-sample difference represented

as the maximum difference between cumulative frequency distributions of the two samples

(vertical black line), in this case, 66%. C) Inter-sample difference shown as the correlation (grey

line) of cross plot of the two PDFs (open circles). D) Dissimilarity between Temple Butte and

Surprise Canyon ages represented as differences between age frequencies (gray bars), PDF

values (gray curve), and KDE values (black curve). Each of these three measures might serve as

the basis for computation of inter-sample difference employing the Likeness (LK) metric (one minus the sum of all absolute differences divided by two). These are 7%, 27%, and 16%, respectively.
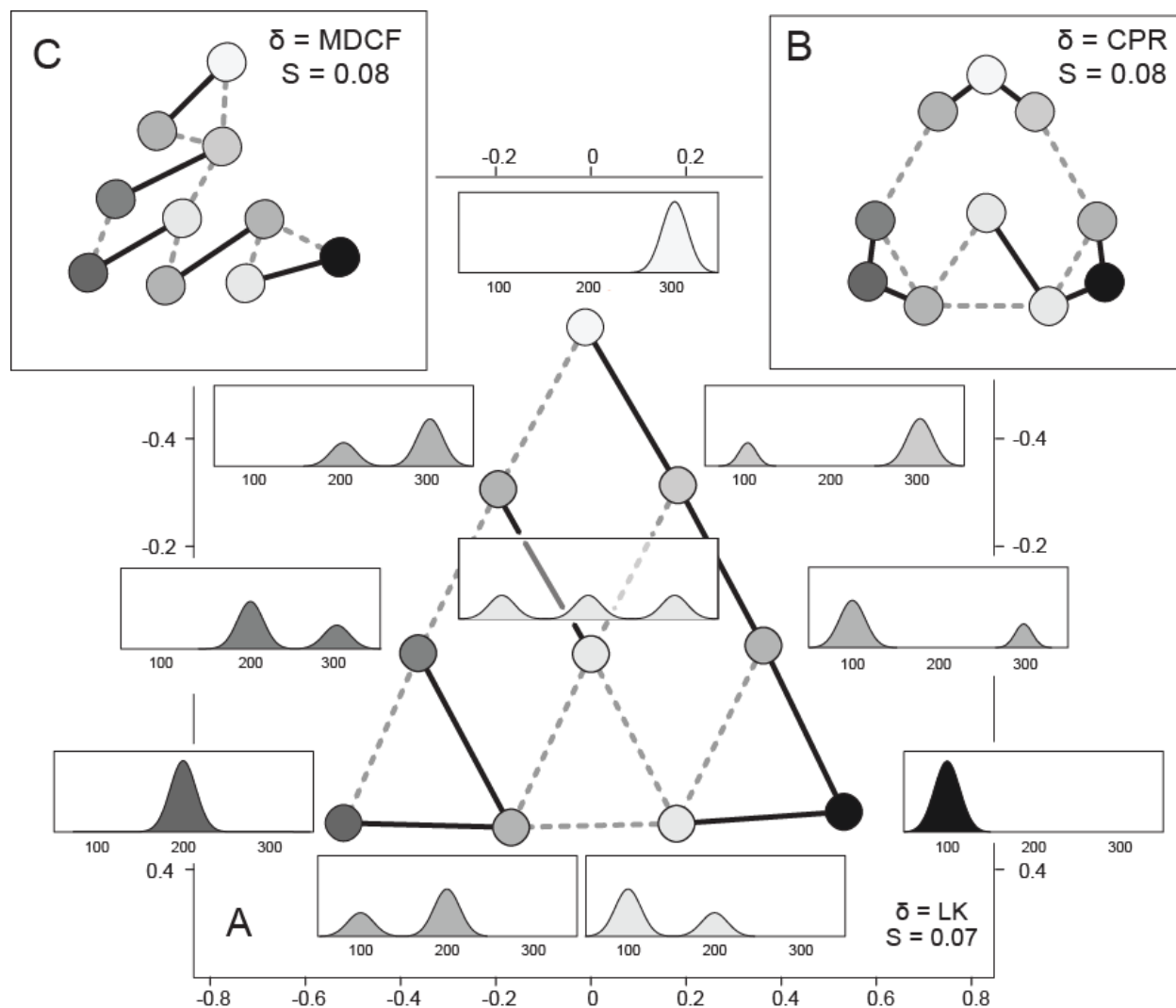
Figure 3.3. MDS configuration using varying dissimilarity measures. Metric MDS images employing different measures of dissimilarity (δ) based on variable mixing of three components (100 ± 10, 200 ± 10, and 300 ± 10 Ma) at 33.3% intervals. Rectangular insets are probability curves representing population ages for the nearest point in the MDS plot. Nearest neighbor lines (with respect to calculated dissimilarity) are solid back; second nearest neighbors are connected with dashed gray lines. *S* = Stress value. A) MDS using Likeness (LK). B) The same model dataset and parameters but using CPR as the measure of dissimilarity. C) As A and B, but using

the maximum difference between cumulative functions (MDCF) as the measure of dissimilarity.

Note that only LK (A) produces the theoretically correct (and desired) configuration.
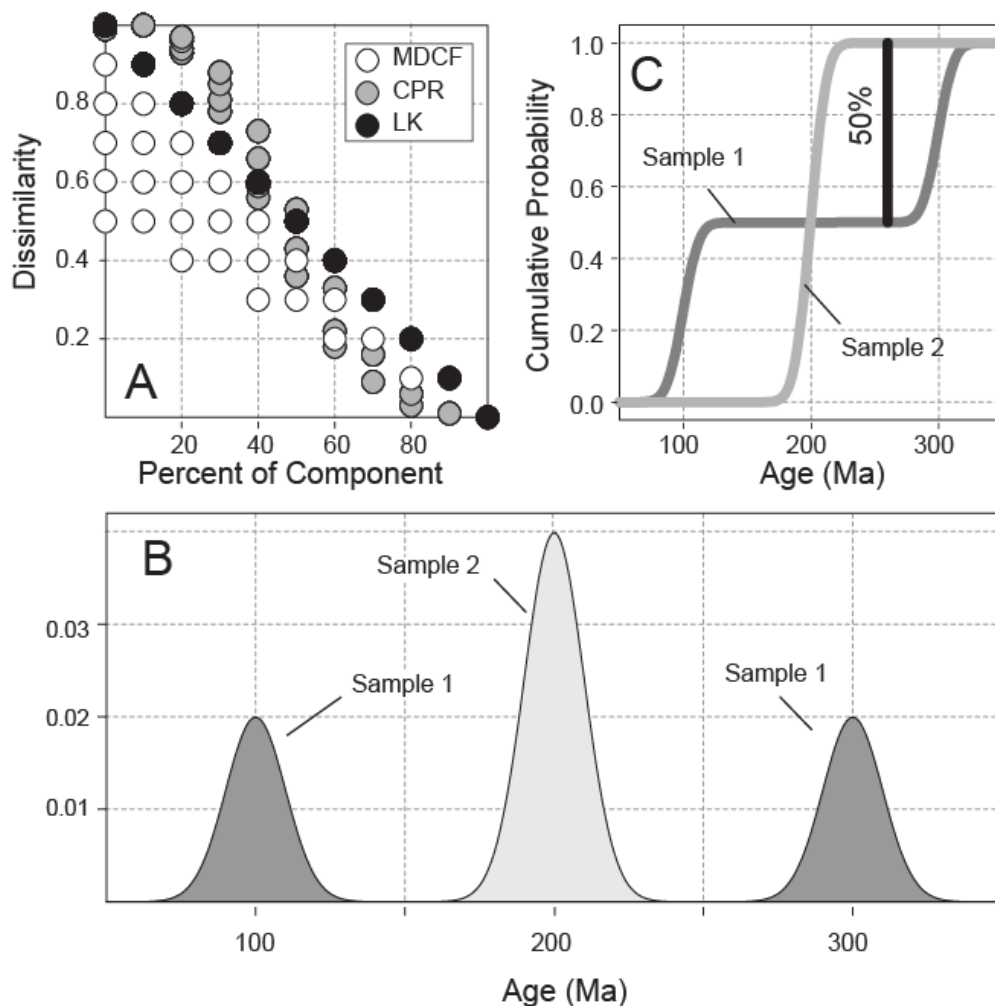
Figure 3.4. Differences in dissimilarity measures for MDS. Differences in dissimilarity measures based on variable mixing of three components (100 ± 10, 200 ± 10, and 300 ± 10 Ma) at 33.3% intervals (Figure 3.3). A) Percent of component in each of 10 model populations (X axis) versus calculated measures of dissimilarity. B) Probability curves of two hypothetical population age distributions. C) Cumulative amounts of each sample; note that the maximum difference is only 50% even though the two populations have no grain ages in common. Compare this with somewhat overlapping samples in Figure 3.2B with a MDCF of 66%.
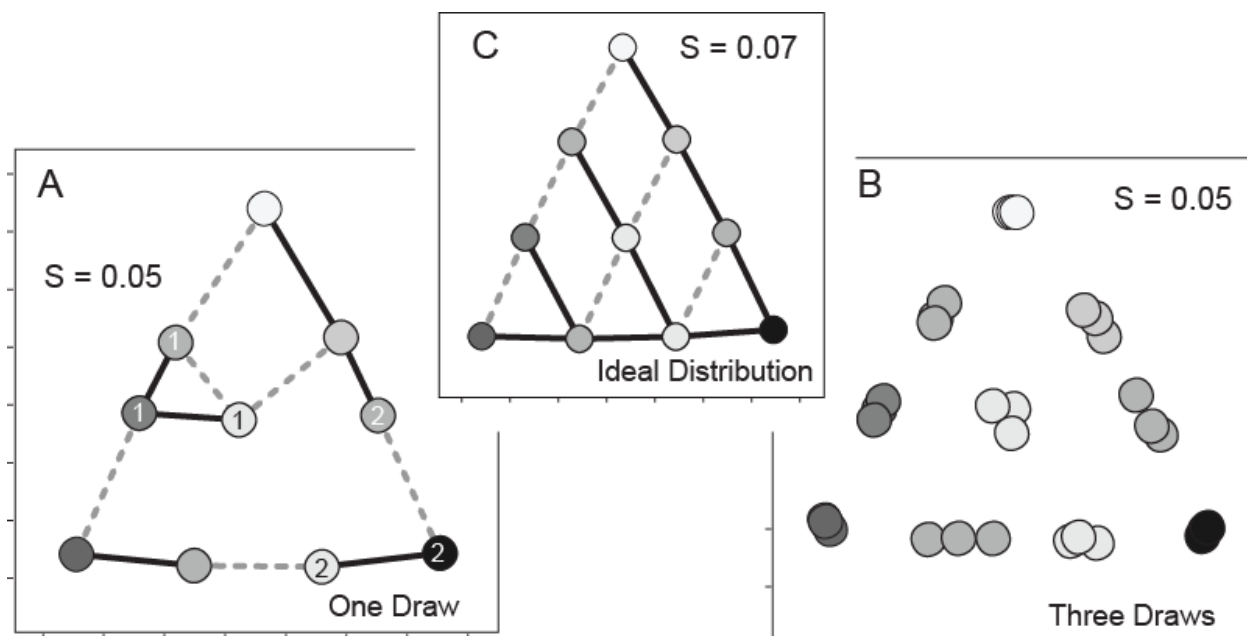
Figure 3.5. MDS configurations for randomly drawn samples. MDS configuration of samples

defined by 100 ages each (circles) drawn from the 10 three-component mixtures in Figure 3.3.

A- 1 sample from each population; B- 3 samples from each population; C- ideal MDS map (true

populations). Note that typical zircon age samples sizes (on the order 100 grains) closely

replicate the actual MDS map, but that variance in spacing is larger among samples containing 2

or 3 age components. Moreover, MDS separation based on 1 draw of 100 ages (A) suggests

lesser (samples containing more evenly-distributed components; e.g. "1") or greater (samples

containing greater proportions of an end-member component, e.g. "2") dissimilarity than actually

exists.
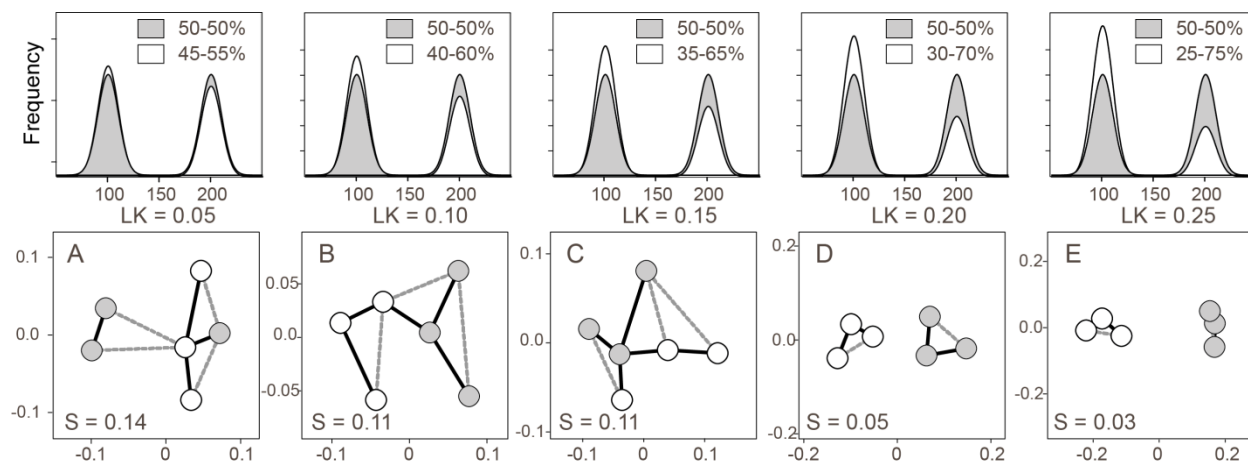
Figure 3.6. Models incorporating variable proportions of two age components. Probability curves affording 5 possible mixtures (columns) of 2 (upper row) age populations with variable contributions of 100 ± 10 Ma and 200 ± 10 Ma components. LK = Likeness values between population age frequencies. Bottom Row- averages of 10 metric MDS results, each comprising three, random, 100-age draws from the two distributions; S = Stress. Note that actual sample differences manifest as MDS separation only becomes apparent at likeness values in excess of ~0.2 (mixtures D and E).
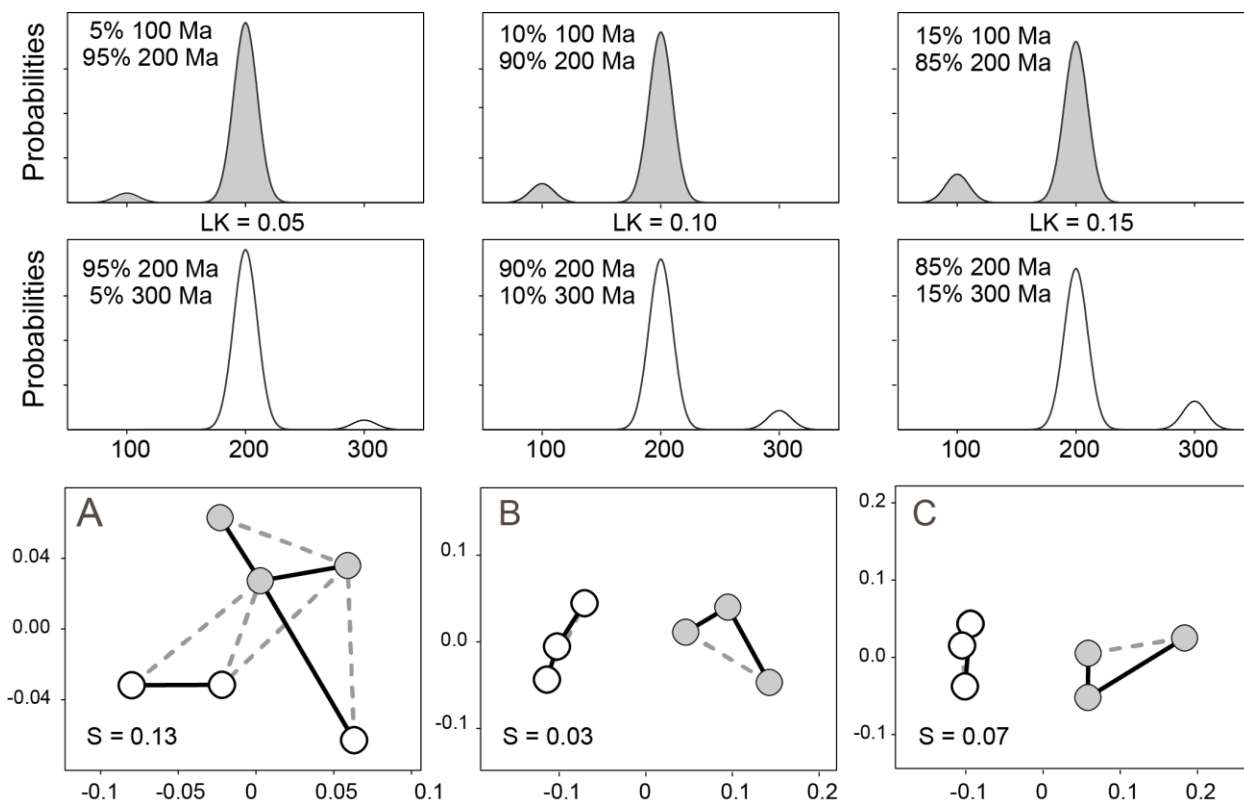
Figure 3.7. Models incorporating variable proportions of three age components. Probability curves affording 3 possible mixtures (columns) of 2 (upper and middle rows) bimodal age distributions with variable contributions of 100 ± 10, 200 ± 10 Ma, and 300 ± 10 Ma. LK = Likeness values between top and middle row frequencies. Bottom Row- averages of 10 metric MDS results, each comprising three, random, 100-age draws from each of the two distributions in each of the 5 sets of mixtures; *S* = Stress. Note that actual sample differences manifest as MDS separation only becomes apparent as likeness approaches a value of ~0.1 (mixtures B and C).
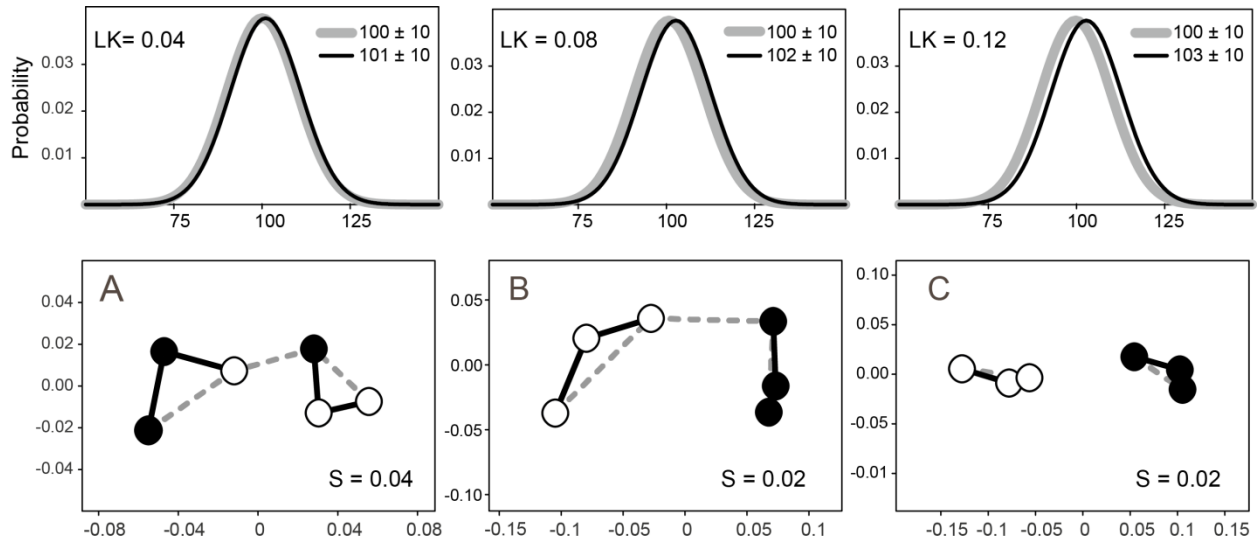
Figure 3.8. Models incorporating two distributions containing variably- overlapping age components. Top row- Idealized probability curves of the two (black and gray lines) unimodal distributions (LK = Likeness). Bottom Row- metric MDS plots for three 100-age draws from each of the two distributions (*S* = Stress). Note that sample differences manifest as MDS separation becomes increasingly apparent as likeness values decrease and mean age difference increases.
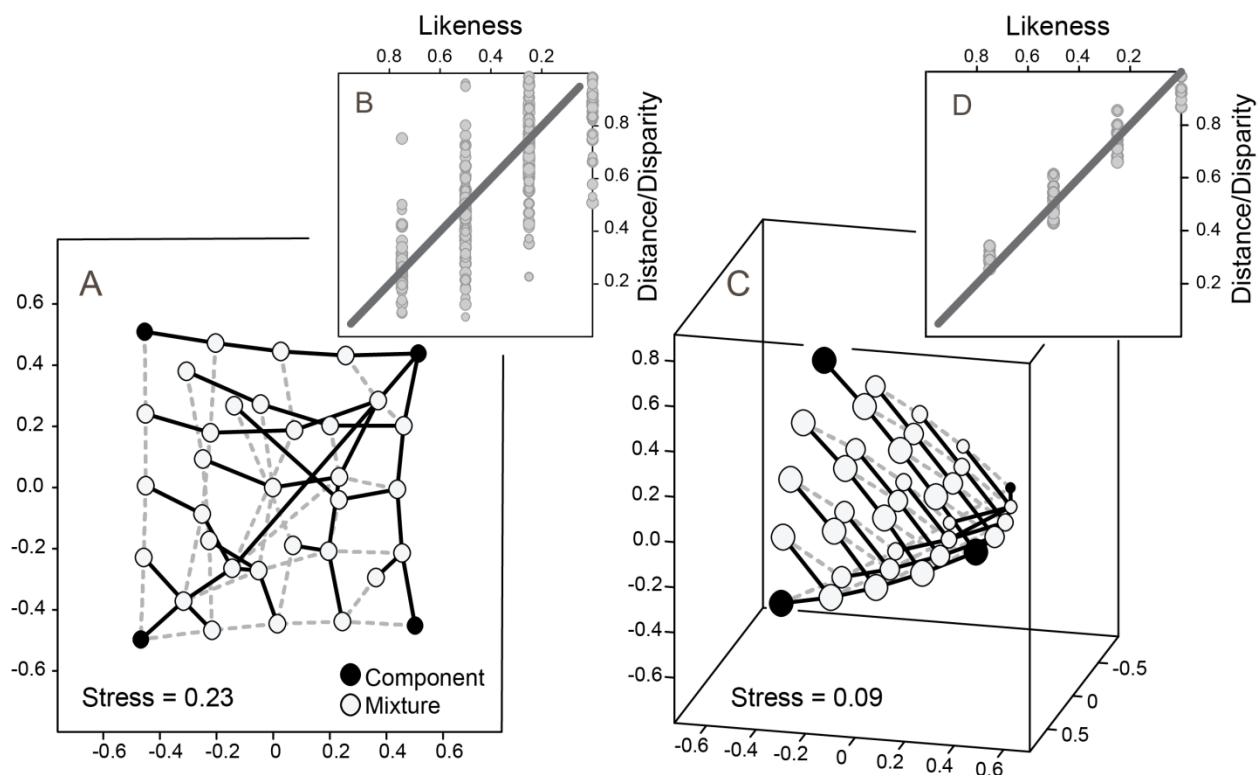
Figure 3.9. Two versus three dimensional MDS for four component mixtures. A- 2D MDS for a four component (100 ± 10, 200 ± 10, 300 ± 10, and 400 ± 10 Ma) mixture model (solid and dashed gray lines = nearest and next-nearest neighbors). B- Shepard plot for 2D MDS. The poor linearity between dissimilarities and distances indicates poor translation of the dissimilarity matrix. C- 3D MDS for the four component mixture model (circles size scaled to distance of point from viewer). D- Shepard plot for 3D MDS. The improved fit demonstrates the value of the added dimension in resolving sample differences.
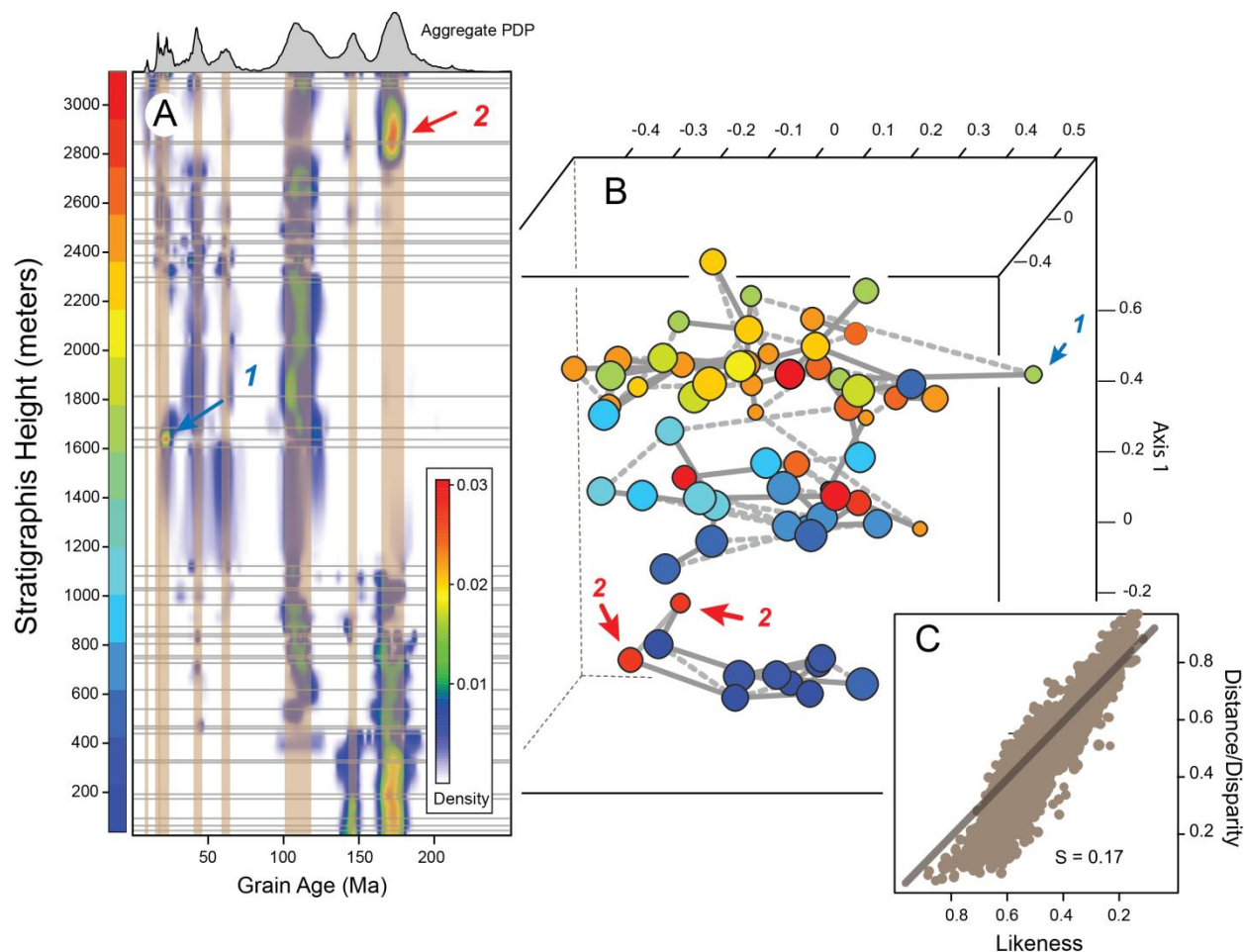
Figure 3.10. Detrital zircon analysis of sediment from the Colorado Plateau. Detrital zircon

ages from the Paleozoic (Gehrels, Blakey, et al., 2011)- Mesozoic (Dickinson and Gehrels, 2009,

2008) succession across the Colorado Plateau. A- Age probability density of 65 samples (black

horizontal lines) ranging from the Cambrian Tapeats Sandstone at the base through the Jurassic

Morrison Formation at the top. Predominant modal age components as vertical tan lines. B-

MDS plot of sample age dissimilarities colored by stratigraphic height. Samples points are scaled

for distance into page and nearest neighbor lines are positioned to reflect fore vs. background

sample points (solid and dashed gray lines = nearest and next-nearest neighbors; circles size

scaled to distances of points from viewer). Three sample clusters are: 1) dominated by ~1.7 Ga

Mazatzal-Yavapai and ~1.4 Amarillo-Wichita province grains (below ~420); 2) dominated by

~1.7 Ga Mazatzal-Yavapai and ~1.1 Grenvillian grains (between ~420 and 1,100 m); and 3)

dominated by ~1.1 Grenvillian and younger province grains (above ~1,100). Note several

obvious anomalies in both PDF (A) and MDS (C) visualizations. These are an early Jurassic

Moenave sample which contains numerous late Paleozoic grains ("1" and blue arrow in A and

B), and two Late Cretaceous samples which are dominated by ~1.7 Ga Mazatzal-Yavapai ages

("2" and red arrows in A and C). C- Shepard plot for the 3D MDS.
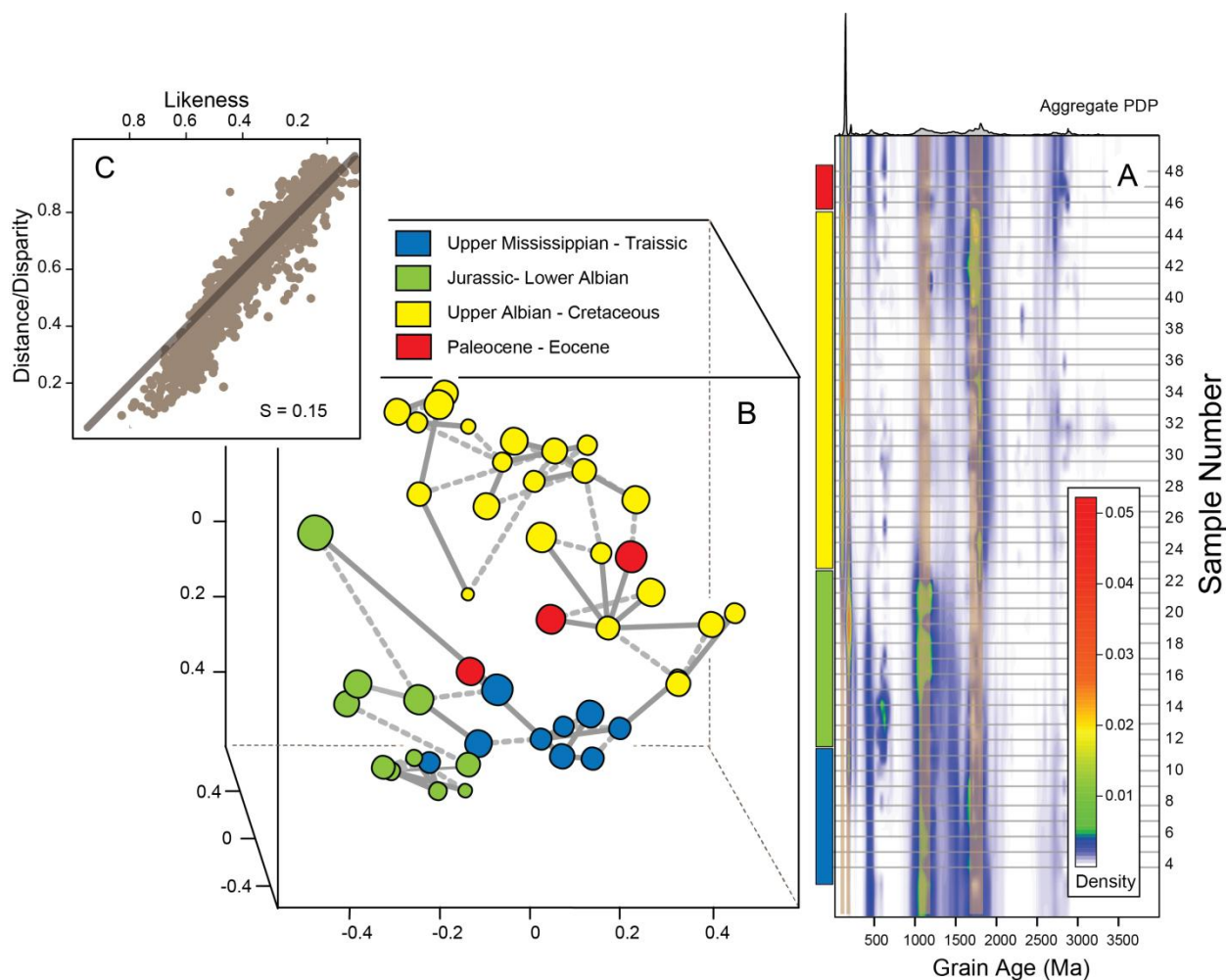
Figure 3.11 Detrital zircon analysis of sediment from the Bighorn Basin. Upper

Mississippian to Paleocene detrital zircon ages from the Bighorn Basin, Wyoming (May et al.,

2013). A- Probability densities of 44 samples (black horizontal lines). Dominant age components

as vertical tan lines. B- MDS plot of sample age dissimilarities colored by tectonostratigraphic

assemblage membership as inferred by May et al. (2013). Sample points are scaled to distance

into page and nearest neighbor lines are positioned to reflect fore vs. background sample points.

Three of the four assemblages are well-resolved by MDS: 1) Upper Mississippian - Triassic

samples (blue bar and points), 2) Jurassic - lower Albian samples (green bar and points), and 3)

upper Albian – Cretaceous samples (yellow bar and points). A posited fourth assemblage comprising three Paleogene samples (red bar and points) does not well segregate as a distinct population. Also note that the closer association between assemblage 1 (blue) and 2 (green) than between 2 and 3 (yellow) evident in MDS, can be seen in sample PDFs as a persistence of ~1.1 Ga Grenvillian grains through the first two. D- Shepard plot for the 3D MDS.
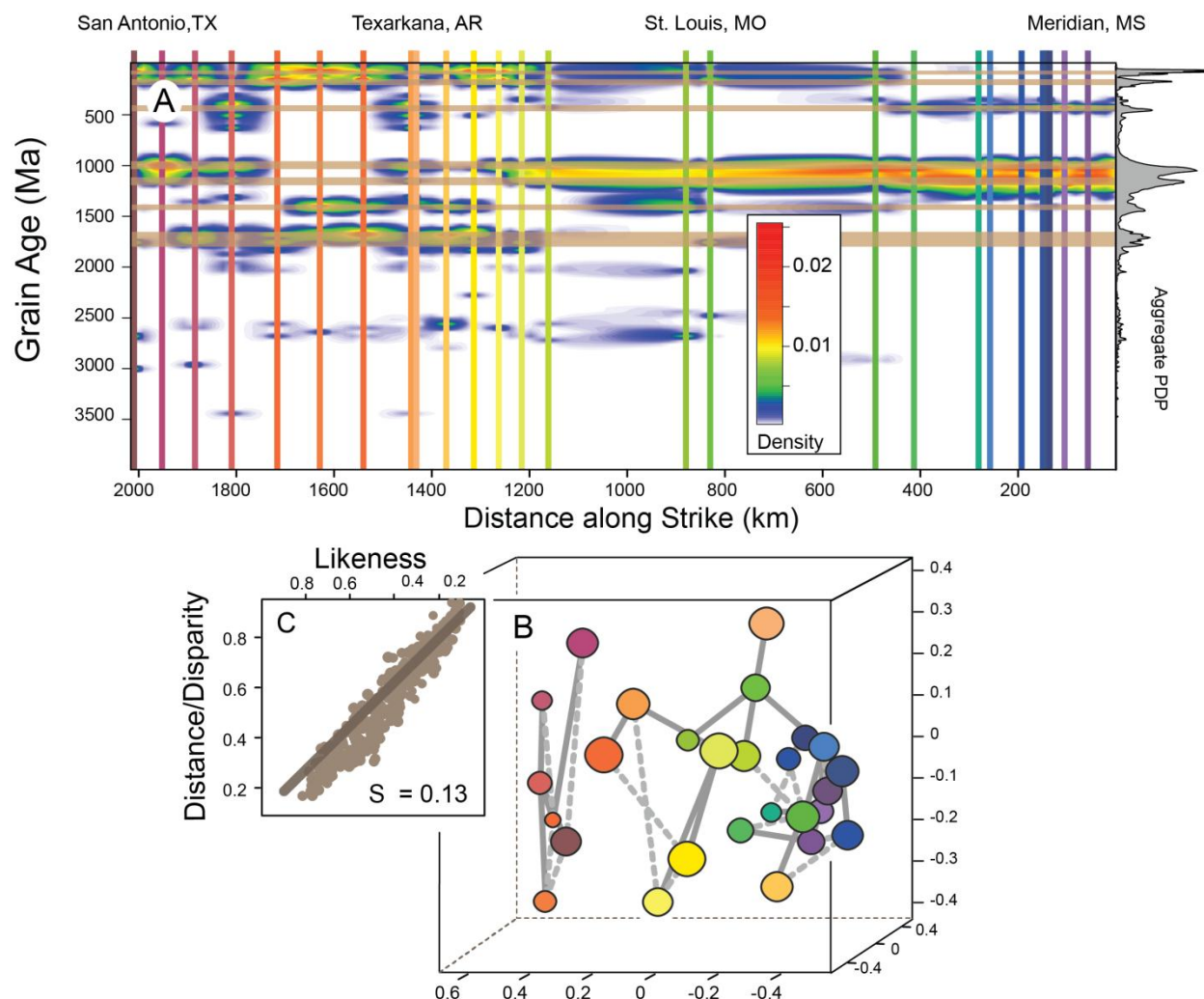
Figure 3.12. Detrital zircon analysis of sediment from the Wilcox Formation Lateral

variation in zircon ages along ~18,000 km of outcrop of the Paleocene Wilcox Formation from

near Meridian, MS, to St. Louis MO, to San Antonio, TX (Blum and Pecha, 2014). A- Age

probability density of 27 samples (vertical colored lines); dominant modal age components as

horizontal tan lines. Qualitatively, note abundant ~1.7 Ga Mazatzal-Yavapai, ~1.4 Amarillo-

Wichita, and Western Cordillera and Laramide grains along the western third of the transect

(left), and ~1.1 Grenvillian grains along the eastern two thirds of the section. B- MDS plot of

sample age dissimilarities colored by lateral geographic location (solid and dashed gray lines =

nearest and next-nearest neighbors; circles size scaled to distances of points from viewer). Note

strong correspondence of MDS and geographic separation among most samples. C- Shepard plot

for the 3D MDS.

Appendix I: Chapter 1

Figures
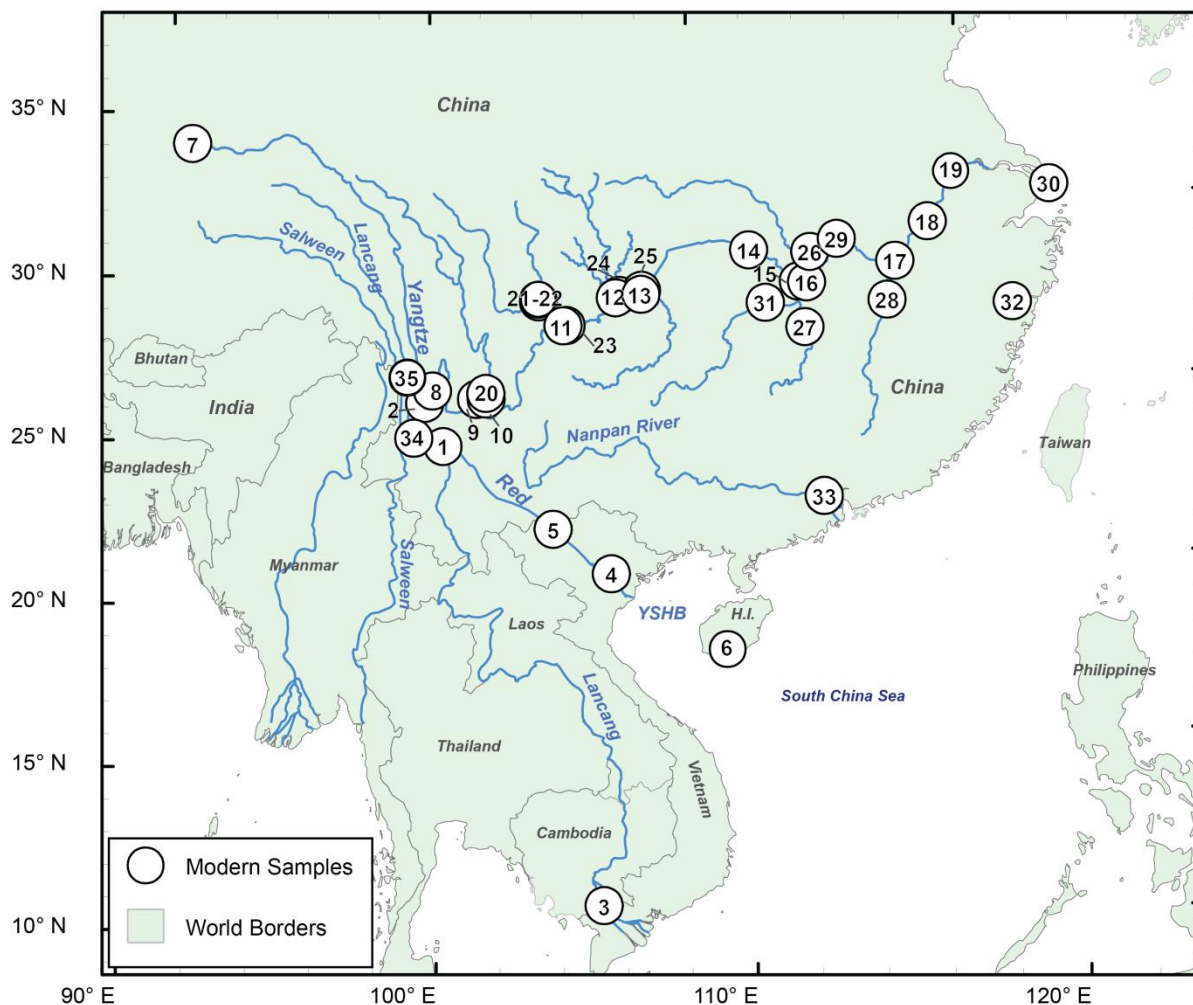
Figure I.1. Sample Locations of modern fluvial detrital samples. [1] Hong-11-01 (This study); [2] Mek-11-02 (This Study); [3] Lancang (Clift, Carter, et al., 2006); [4-5] Red River (van Hoang et al., 2009); [6] Hainan Island (Chen et al., 2014); [7-31] Yangtze River and Major Tributaries (He et al., 2013, 2014); [8] Yangtze River First Bend (He et al., 2013, 2014; Kong et al., 2012); [32] Ou River (Xu et al., 2007); [33] Nanpan River (Xu et al., 2007); [34-35] Lancang River (Chen et al., 2014)
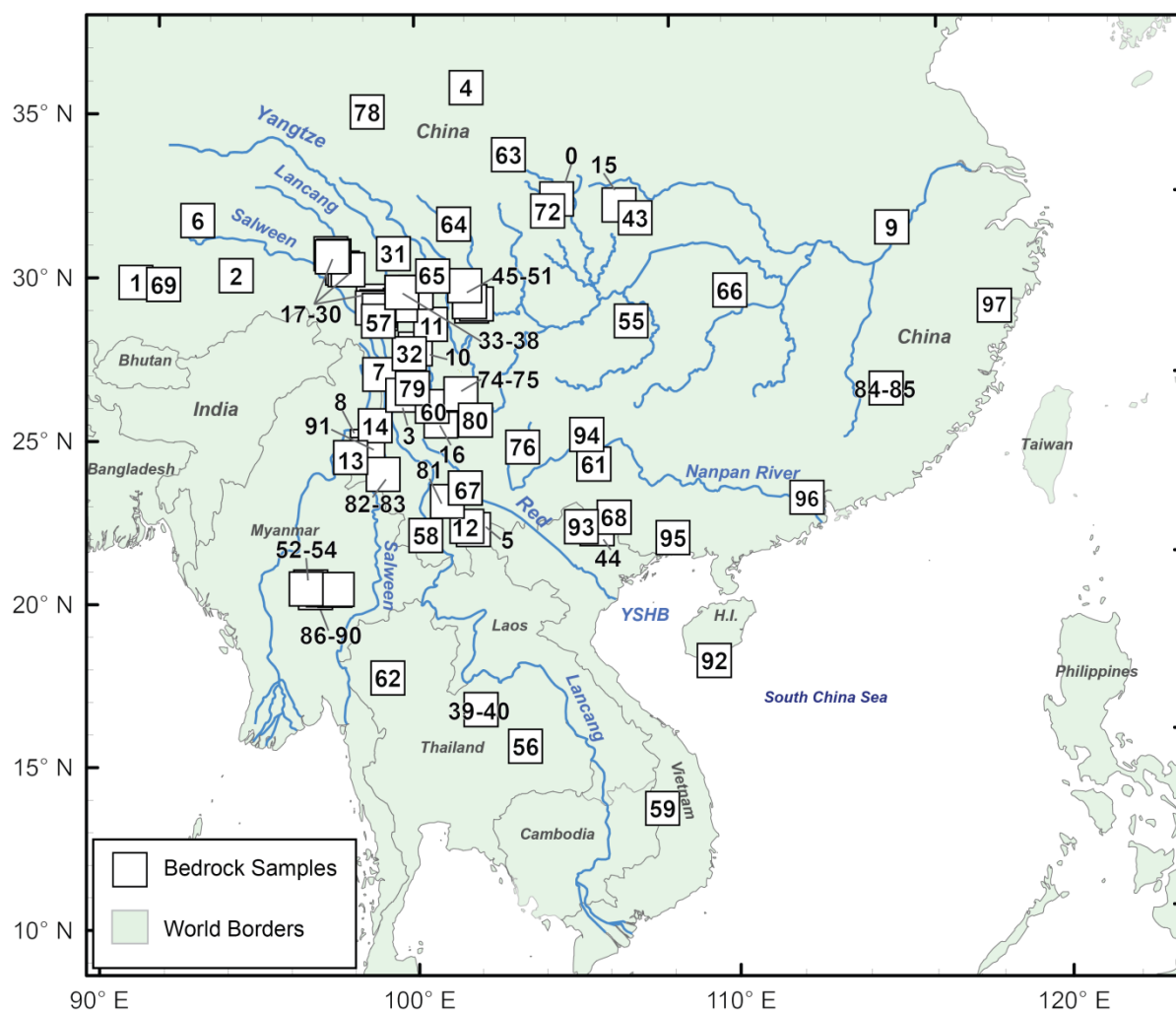
Figure I.2. Bedrock (sources) approximate locations. [0] Qinling-Dabieshan (Clift, Carter, et al., 2006; Hacker et al., 1998); [1-2] Lhasa Terrane (Leier et al., 2007; Clift, Carter, et al., 2006; Gehrels, Kapp, et al., 2011; Chu et al., 2006); [3] Jomda-Weixi Arc (Yang, Ding, et al., 2014); [4] Laji Shan (Lease et al., 2007); [5] Lanping Simao Basin (Wang, Liu, et al., 2014a); [6] Amdo Basement (Guynn et al., 2006; Zhang et al., 2013); [7] Gaoligong Batholith (Xu et al., 2012); [8] Tengliang and E. Yinjiang (Xu et al., 2012) [9] Chizhou Bedrock (Song et al., 2014); [10-11] Yidun Arc (Wang, Hu, et al., 2014); [12] Mengyejing Formation (Wang, Liu, et al., 2015); [13] Tengchong Block (Qi et al., 2015); [14] Jiaojiguanliangzi Formation (Cao et al., 2014); [15]

Jurassic SS Sichuan Basin (Luo et al., 2014); [16] Jurassic SS Yunnan (Su et al., 2014); [17-30] Qamdo Basin (Shang et al, in review); [31- 38] Yidun Terrane (Wang, Wang, et al., 2013; Reid et al., 2007; Peng et al., 2014b) (Shang et al, in review); [39] Loei (Burrett et al., 2014); [40] Indochina (Burrett et al., 2014); [41-42] Qiangtang Terrane (Gehrels, Kapp, et al., 2011) [43] Triassic SS Sichuan Basin (She et al., 2012); [44] NE Vietnam (Burrett et al., 2014); [45-54] Zheduo-Gonggar massif (Li, Chen, et al., 2015); [55] Yangtze Block (Su et al., 2014); [56] Khorat Plateau (Carter and Moss, 1999; Clift, Carter, et al., 2006; Carter et al., 2001; Carter and Bristow, 2003; Nagy et al., 2001); [57]Qiangtang Volcanics (Peng et al., 2014a; Zhai et al., 2013); [58] Lincang (Dong et al., 2013; Hennig et al., 2009); [59] Kontum (Clift, Carter, et al., 2006; Nagy et al., 2001); [60] Emeishan (Shellnutt, 2014); [61] Youjiang Basin (Yang et al., 2012); [62] Sukhothai (Burrett et al., 2014); [63-65] Songpan Ganze Terrane; [66] Yangtze Craton (Zheng et al., 2006; Li, 1999; Zhang et al., 2006a, 2006b; Gao et al., 2011) [67] Ailao Shan (Leloup et al., 1993, 1995; Lin et al., 2012; Cao et al., 2011; Clift, Carter, et al., 2006; Harrison and Leloup, 1996; Wang et al., 1998; Jolivet et al., 1999; Maluski et al., 2001); [68] Cathaysia (Li, 2005; Clift, Carter, et al., 2006; Xianhua et al., 1989); [69] Gangdese Arc (He et al., 2007; Wen et al., 2008; Ji et al., 2009); [70] Tarim Platform (Gehrels, Kapp, et al., 2011); [71] North China (Darby and Gehrels, 2006; Guan et al., 2002; Gao et al., 2004); [72] Longmenshan (Pei et al., 2009); [73] Qilian Shan (Gehrels, Kapp, et al., 2011; Gehrels et al., 2003); [74-75] Yanbian Terrane (Zhou et al., 2006; Sun et al., 2009); [76] Luliang (Zhuo et al., 2013); [77] Altunshan (Gehrels, Kapp, et al., 2011); [78] Kunlunshan (Chen et al., 2008; Gehrels, Kapp, et al., 2011); [80] Yangtze Craton West (Sun et al., 2009; Greentree and Li, 2008; Zhao et al., 2010); [81] Ailaoshan (Burrett et al., 2014); [82] Baoshan Granite (Liu et al., 2009); [83] W. Yingjiang (Xu et al., 2012); [84-85 South China (Wang et al., 2011; Li et al.,

2011) [86-90] Sibumasu Terrane (Cai et al., 2015); [91] W. Yingjiang (Xu et al., 2012); [92]

Hainan Island (Xu, Sun, Cai, et al., 2014); [93] Laojunshan (Feng et al., 2012, 2008); [94]

Guizhou (Zhou et al., 2009); [95] Darongshan (Chen et al., 2011); [96-97] Cathaysia (Xu et al.,

2007)
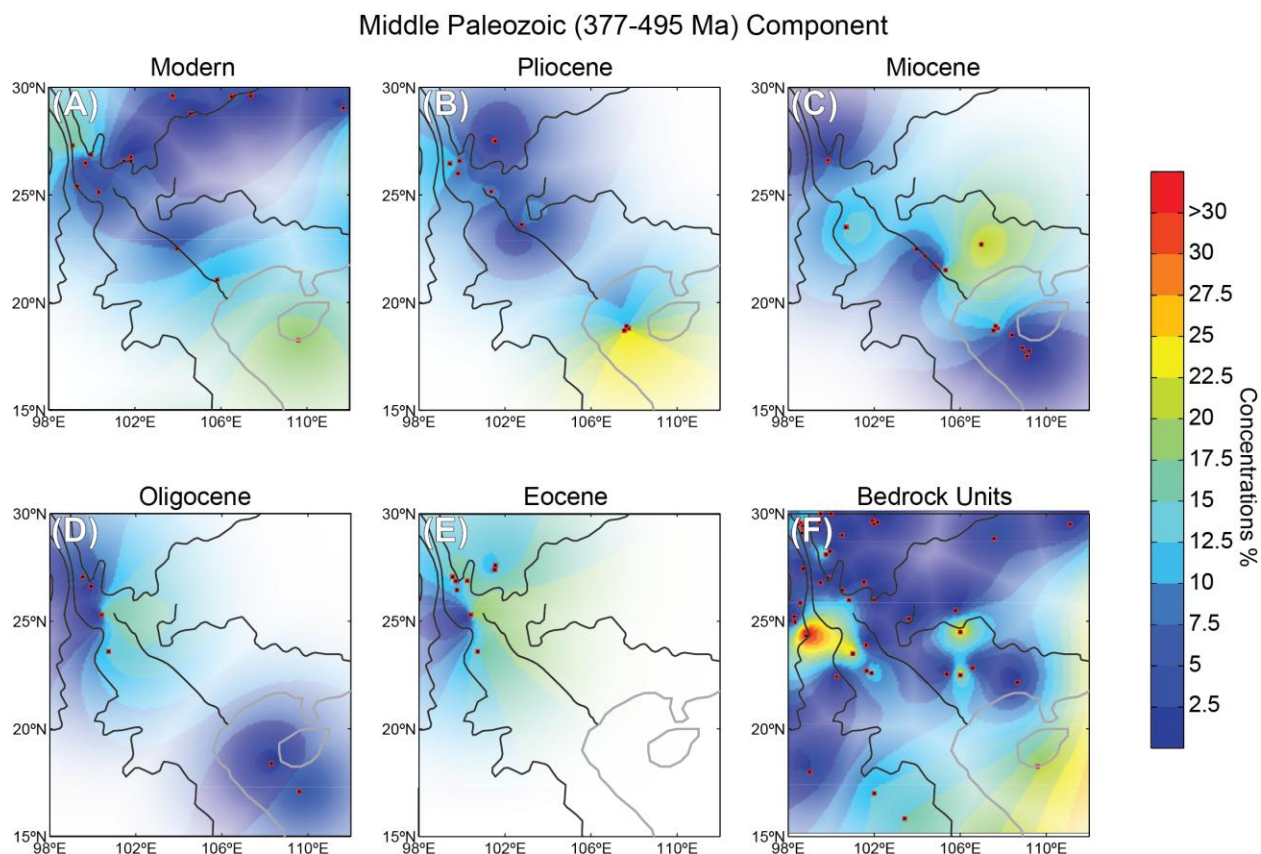
Figure I.3. Middle Paleozoic (377-495 Ma) Interpolation Concentration Maps. Each map represents a different sampling suite with (a) – (e) are interpolation maps based on depositional ages and (f) of bedrock units of depositional or emplacement age of Eocene or older. Interpolation points are indicated by small red dots. Colors are scaled to interpolated concentrations of zircon of Middle Paleozoic age for each depositional time slice. Population concentrations are in percents. Transparency of interpolation map increases with cubic distance from nearest sampling location.

Tables

Table I.1 U-Pb Geochronologic Analyses

Table. U-Pb geochronologic analyses.

Analysis	Apparent ages (Ma)						Samp
	206Pb*	±	207Pb*	±	206Pb*	±	#
	238U*	(Ma)	235U	(Ma)	207Pb*	(Ma)	
Dali-13-04-02	1655.6	127.2	1799.9	73.9	1971.5	15.1	13
Dali-13-04-03	1817.7	26.3	1849.7	14.5	1885.8	6.7	13
Dali-13-04-04	1027.7	16.5	1023.0	13.9	1012.7	25.9	13
Dali-13-04-06	250.6	3.2	243.7	9.3	177.0	95.7	13
Dali-13-04-07	327.5	6.8	330.5	9.4	352.3	57.7	13
Dali-13-04-09	874.8	37.7	885.8	27.9	913.5	21.1	13
Dali-13-04-10	444.1	7.3	433.3	19.3	376.7	117.3	13
Dali-13-04-100	1708.4	35.9	1719.9	20.0	1733.9	6.5	13
Dali-13-04-101	2521.4	45.7	2499.6	20.6	2481.9	6.6	13
Dali-13-04-102	250.3	11.7	240.4	27.7	145.0	282.3	13
Dali-13-04-103	291.0	5.8	286.3	12.0	247.4	100.1	13
Dali-13-04-104	883.7	15.3	885.9	11.3	891.5	9.9	13
Dali-13-04-105	247.5	2.8	248.5	13.6	258.1	139.0	13
Dali-13-04-11	514.1	21.2	582.9	22.1	860.8	52.7	13
Dali-13-04-12	1896.3	13.2	1885.7	9.5	1874.1	13.7	13
Dali-13-04-13	1742.3	96.0	1842.3	53.5	1957.1	3.5	13
Dali-13-04-14	839.0	11.0	834.1	18.9	821.3	62.9	13
Dali-13-04-15	192.9	8.4	231.6	56.2	645.1	584.1	13
Dali-13-04-16	247.7	9.0	237.6	13.2	138.5	117.4	13
Dali-13-04-18	244.8	6.3	237.8	12.1	169.0	118.3	13
Dali-13-04-19	181.4	15.3	312.4	94.7	1458.2	667.6	13
Dali-13-04-20	459.6	6.5	459.0	9.0	456.1	43.2	13
Dali-13-04-21	2022.0	119.1	2244.0	62.7	2453.0	16.1	13
Dali-13-04-22	806.9	20.4	799.3	22.1	777.9	62.2	13
Dali-13-04-23	443.4	8.8	438.3	11.4	411.5	54.9	13
Dali-13-04-25	408.0	7.7	410.9	15.9	426.9	95.6	13
Dali-13-04-26	686.1	6.6	694.7	8.3	722.5	27.5	13
Dali-13-04-27	2417.8	32.0	2479.7	14.8	2530.8	3.2	13
Dali-13-04-28	412.2	3.5	425.3	5.9	496.9	32.3	13
Dali-13-04-29	338.8	6.7	343.0	6.8	371.9	25.4	13
Dali-13-04-30	1909.0	39.5	1892.6	20.7	1874.6	6.2	13
Dali-13-04-31	255.8	4.0	260.8	9.0	306.0	81.7	13
Dali-13-04-32	2639.2	44.8	2624.6	19.7	2613.3	5.3	13

Dali-13-04-34	265.4	7.9	267.0	8.8	280.9	51.2	13
Dali-13-04-35	801.3	17.7	802.4	24.3	805.4	77.3	13
Dali-13-04-36	251.0	3.5	256.7	9.9	309.0	94.3	13
Dali-13-04-37	468.3	21.0	435.4	78.5	265.0	501.4	13
Dali-13-04-38	2414.7	16.9	2462.5	8.1	2502.1	4.2	13
Dali-13-04-39	290.8	7.5	279.2	17.4	183.0	154.6	13
Dali-13-04-40	257.8	9.2	245.9	45.9	133.1	491.1	13
Dali-13-04-41	252.5	4.4	255.8	8.1	285.6	71.1	13
Dali-13-04-42	1387.8	34.2	1409.8	21.0	1443.2	3.7	13
Dali-13-04-43	335.5	6.0	306.5	21.0	90.8	183.0	13
Dali-13-04-44	1815.9	13.7	1854.5	7.8	1898.2	4.9	13
Dali-13-04-45	734.8	26.6	734.0	30.2	731.6	91.6	13
Dali-13-04-46	250.5	4.9	262.9	12.1	374.7	108.6	13
Dali-13-04-47	174.8	3.8	176.0	6.1	193.1	71.3	13
Dali-13-04-48	217.0	2.2	220.6	3.7	258.5	35.5	13
Dali-13-04-49	2306.2	35.0	2400.2	33.6	2480.9	53.7	13
Dali-13-04-50	448.8	9.9	450.0	16.9	455.9	89.9	13
Dali-13-04-51	217.8	6.7	229.2	22.5	347.9	238.8	13
Dali-13-04-52	2013.0	26.0	2056.9	14.2	2101.2	10.2	13
Dali-13-04-54	914.9	15.6	919.3	14.3	929.7	30.6	13
Dali-13-04-55	940.9	12.5	956.7	10.3	993.3	17.3	13
Dali-13-04-56	227.6	6.1	250.2	8.0	467.4	52.1	13
Dali-13-04-57	292.8	8.6	283.0	41.8	202.8	389.0	13
Dali-13-04-58	175.1	4.0	171.6	17.0	122.5	248.9	13
Dali-13-04-60	364.8	3.7	370.7	5.8	408.0	34.5	13
Dali-13-04-61	443.3	13.6	448.0	15.0	472.6	58.9	13
Dali-13-04-62	2058.6	122.7	2282.3	64.7	2489.1	24.8	13
Dali-13-04-63	217.2	6.5	224.0	9.1	295.5	76.4	13
Dali-13-04-64	2350.7	15.8	2345.5	7.5	2340.9	3.1	13
Dali-13-04-65	272.6	6.2	295.3	19.6	479.3	161.1	13
Dali-13-04-66	1829.6	56.2	1850.4	30.1	1873.7	6.0	13
Dali-13-04-67	274.9	11.9	265.6	34.4	184.4	328.6	13
Dali-13-04-68	279.0	5.8	277.5	10.3	265.5	84.1	13
Dali-13-04-69	975.4	11.4	975.2	23.0	974.8	70.2	13
Dali-13-04-71	881.0	17.4	887.3	13.2	903.0	15.0	13
Dali-13-04-72	255.5	6.9	266.7	20.5	366.4	187.2	13
Dali-13-04-73	217.1	6.1	212.6	18.6	163.1	217.4	13
Dali-13-04-74	249.1	4.9	248.8	9.8	245.5	91.5	13
Dali-13-04-75	274.2	3.7	276.3	8.5	294.3	73.9	13
Dali-13-04-76	1803.2	10.1	1832.6	6.4	1866.1	7.4	13
Dali-13-04-77	930.2	14.5	925.9	14.8	915.7	36.5	13

Dali-13-04-78	983.6	13.3	986.2	11.2	991.7	20.4	13
Dali-13-04-80	758.2	11.5	759.1	10.5	762.0	24.0	13
Dali-13-04-81	245.8	4.6	251.0	15.8	299.1	155.9	13
Dali-13-04-82	233.5	12.7	252.6	21.0	434.1	169.4	13
Dali-13-04-83	437.7	8.7	443.9	11.4	476.3	53.6	13
Dali-13-04-84	538.5	34.0	620.9	31.2	934.4	27.1	13
Dali-13-04-86	276.6	8.7	291.1	9.5	409.4	42.9	13
Dali-13-04-88	1874.2	23.8	1866.6	19.1	1858.1	30.6	13
Dali-13-04-89	832.8	6.2	832.8	8.8	832.7	27.7	13
Dali-13-04-90	764.0	25.9	765.9	46.2	771.5	164.2	13
Dali-13-04-91	288.4	3.9	289.5	5.9	297.8	42.9	13
Dali-13-04-92	972.7	18.6	971.0	13.3	967.1	11.6	13
Dali-13-04-93	236.6	6.9	250.1	22.7	378.5	221.3	13
Dali-13-04-94	2210.7	112.1	2334.4	54.9	2444.4	6.0	13
Dali-13-04-95	256.6	5.1	251.6	12.3	204.6	119.0	13
Dali-13-04-96	896.1	15.9	885.0	17.9	857.3	49.0	13
Dali-13-04-98	2249.6	54.8	2392.9	26.6	2517.2	2.7	13
Dali-13-04-99	171.1	5.1	173.6	22.6	207.8	321.5	13
Hong-11-01-01	292.3	8.7	275.0	28.1	130.2	265.6	38
Hong-11-01-02	39.5	1.0	42.3	4.0	202.9	217.5	38
Hong-11-01-03	290.4	5.9	294.4	14.5	325.9	119.9	38
Hong-11-01-05	36.5	1.7	37.2	5.5	83.1	338.3	38
Hong-11-01-06	1605.2	17.3	1713.4	10.7	1848.3	7.7	38
Hong-11-01-07	501.5	47.5	522.5	44.8	615.2	104.3	38
Hong-11-01-08	1635.9	26.2	1710.4	15.5	1803.0	8.4	38
Hong-11-01-100	198.1	7.9	204.3	15.9	276.3	173.0	38
Hong-11-01-101	1713.1	12.7	1795.2	9.0	1892.0	11.8	38
Hong-11-01-103	1884.3	14.3	1886.2	7.8	1888.3	4.8	38
Hong-11-01-104	178.5	11.1	156.6	39.1	-164.0	660.9	38
Hong-11-01-105	441.8	3.0	445.8	7.1	466.5	41.1	38
Hong-11-01-11	36.7	2.0	39.3	7.7	204.9	449.9	38
Hong-11-01-12	176.7	5.0	177.8	10.8	191.8	138.2	38
Hong-11-01-13	189.3	1.7	194.5	15.4	257.7	199.2	38
Hong-11-01-15	1541.2	24.5	1547.6	15.8	1556.2	16.2	38
Hong-11-01-16	439.5	9.7	448.0	15.2	492.0	77.3	38
Hong-11-01-18	294.1	8.5	291.7	16.6	272.9	134.6	38
Hong-11-01-19	36.3	1.4	37.4	6.1	104.7	381.8	38
Hong-11-01-20	2143.1	30.0	2160.6	15.1	2177.3	6.6	38
Hong-11-01-21	1715.6	34.2	1719.4	19.6	1724.1	12.1	38
Hong-11-01-22	305.1	5.2	302.9	12.3	286.6	100.1	38

Hong-11-01-23	285.3	10.3	300.4	16.2	419.5	112.3	38
Hong-11-01-24	828.7	18.2	839.7	19.2	868.9	50.2	38
Hong-11-01-26	176.4	2.1	188.1	8.9	337.5	114.5	38
Hong-11-01-27	880.3	18.2	888.3	29.0	908.1	89.9	38
Hong-11-01-28	1888.3	26.0	1952.3	18.3	2020.9	24.8	38
Hong-11-01-29	1875.0	63.7	1889.7	34.9	1906.0	19.4	38
Hong-11-01-30	149.1	6.2	157.1	10.7	280.0	138.2	38
Hong-11-01-34	35.6	0.4	35.7	1.3	41.7	81.7	38
Hong-11-01-35	1124.6	27.7	1122.0	23.0	1117.0	41.1	38
Hong-11-01-36	36.1	0.6	40.4	1.8	304.9	97.5	38
Hong-11-01-38	1894.3	33.1	1888.4	18.0	1881.9	10.2	38
Hong-11-01-39	36.7	2.4	32.1	7.4	-302.6	580.9	38
Hong-11-01-414	1627.5	35.6	1638.0	20.2	1651.6	4.4	38
Hong-11-01-42	361.4	5.0	376.0	9.8	466.8	61.5	38
Hong-11-01-43	2003.3	72.3	2153.6	43.2	2300.2	41.3	38
Hong-11-01-44	36.1	1.5	40.6	4.1	316.5	214.8	38
Hong-11-01-46	967.8	39.9	975.7	27.9	993.5	7.8	38
Hong-11-01-47	1684.6	59.0	1770.6	33.4	1873.6	2.6	38
Hong-11-01-48	1003.7	42.5	1067.1	31.8	1199.0	29.7	38
Hong-11-01-49	36.8	0.8	36.7	2.7	31.3	172.1	38
Hong-11-01-50	177.1	5.6	181.5	20.0	239.4	267.7	38
Hong-11-01-51	179.4	4.7	175.4	15.3	121.3	214.6	38
Hong-11-01-52	187.1	3.9	192.1	4.6	254.1	35.4	38
Hong-11-01-53	2116.8	60.8	2158.1	30.1	2197.7	2.2	38
Hong-11-01-54	528.1	8.8	575.8	9.2	769.0	24.7	38
Hong-11-01-55	228.6	11.4	230.1	11.3	246.4	47.1	38
Hong-11-01-58	254.3	5.4	259.8	6.4	309.7	40.8	38
Hong-11-01-59	1940.8	70.0	2034.2	38.8	2130.2	25.2	38
Hong-11-01-60	318.9	7.8	339.4	22.6	481.7	164.0	38
Hong-11-01-61	400.9	21.1	395.9	19.3	366.8	50.8	38
Hong-11-01-62	35.6	1.1	36.7	4.9	113.7	311.8	38
Hong-11-01-63	254.9	4.3	249.7	10.9	201.0	107.0	38
Hong-11-01-64	268.0	12.9	243.7	59.4	15.9	657.1	38
Hong-11-01-65	268.0	3.3	271.7	6.0	304.0	49.8	38
Hong-11-01-66	36.8	1.4	37.6	6.4	90.2	406.0	38
Hong-11-01-67	1711.1	46.3	1773.1	26.3	1847.0	11.0	38
Hong-11-01-70	228.7	3.1	230.7	11.2	252.0	120.7	38
Hong-11-01-72	271.0	8.4	268.3	30.0	244.7	285.1	38
Hong-11-01-73	438.8	5.5	430.5	13.1	386.3	78.6	38
Hong-11-01-74	757.1	11.8	749.7	23.6	727.6	87.5	38
Hong-11-01-75	2767.9	64.7	2700.0	27.3	2649.7	5.9	38

Hong-11-01-76	371.8	4.6	373.9	21.8	386.5	153.9	38
Hong-11-01-77	396.7	4.6	389.5	10.0	347.1	64.6	38
Hong-11-01-79	2548.2	18.0	2526.0	8.1	2508.2	2.9	38
Hong-11-01-80	268.1	16.3	294.6	24.0	509.7	155.7	38
Hong-11-01-81	167.2	3.2	172.3	6.7	242.5	87.0	38
Hong-11-01-82	262.8	13.0	257.6	21.0	210.3	178.8	38
Hong-11-01-84	2243.1	26.7	2353.8	24.9	2451.2	39.3	38
Hong-11-01-85	35.8	1.0	33.8	5.2	-108.3	377.5	38
Hong-11-01-86	820.1	26.9	830.3	22.4	857.9	38.2	38
Hong-11-01-87	451.1	6.8	481.0	14.9	626.0	77.0	38
Hong-11-01-88	358.2	1.5	356.3	5.8	343.7	42.8	38
Hong-11-01-89	36.1	0.8	37.1	5.9	103.0	378.4	38
Hong-11-01-90	417.9	9.7	410.9	32.9	371.6	212.8	38
Hong-11-01-92	35.1	2.3	30.5	5.8	-320.7	467.0	38
Hong-11-01-93	253.3	6.3	231.1	24.8	10.3	282.8	38
Hong-11-01-94	888.5	64.3	881.4	47.0	863.7	38.9	38
Hong-11-01-95	250.3	2.9	255.9	7.4	307.0	69.2	38
Hong-11-01-96	262.5	2.7	264.2	8.9	278.8	84.3	38
Hong-11-01-97	181.5	4.2	179.6	12.3	154.6	166.6	38
Hong-11-01-98	649.6	29.8	673.0	24.5	751.9	25.5	38
Hong-11-01-99	36.6	0.4	38.3	1.6	150.3	95.3	38
Jian-11-06-01	457.3	10.8	458.3	31.0	463.1	178.5	9
Jian-11-06-02	229.2	5.1	192.4	54.6	-238.4	800.2	9
Jian-11-06-03	1861.3	11.0	1871.3	8.1	1882.5	12.1	9
Jian-11-06-05	1876.0	56.6	1868.9	29.7	1860.9	2.8	9
Jian-11-06-06	1844.5	26.8	1857.9	14.4	1872.9	3.8	9
Jian-11-06-07	383.9	10.1	378.8	30.4	347.9	209.1	9
Jian-11-06-08	275.9	8.0	270.6	32.2	225.1	307.1	9
Jian-11-06-10	529.0	19.5	535.1	26.5	561.3	110.7	9
Jian-11-06-101	40.4	2.4	41.1	4.1	81.3	194.6	9
Jian-11-06-102	41.0	1.2	39.1	2.7	-74.7	157.9	9
Jian-11-06-103	254.1	6.8	264.9	11.4	361.3	91.7	9
Jian-11-06-104	1815.1	32.8	1839.5	17.9	1867.2	6.7	9
Jian-11-06-105	244.8	9.0	241.0	18.2	203.6	176.3	9
Jian-11-06-106	440.3	6.2	446.5	9.8	478.9	50.6	9
Jian-11-06-108	222.1	5.0	230.2	11.8	313.9	119.5	9
Jian-11-06-109	932.5	20.6	938.9	24.3	953.9	64.9	9
Jian-11-06-11	1897.0	48.5	1891.2	26.0	1884.9	12.0	9
Jian-11-06-110	279.7	22.6	284.8	33.2	326.2	238.8	9
Jian-11-06-111	154.5	4.2	152.4	16.6	119.4	269.5	9

Jian-11-06-112	673.1	16.1	694.4	20.4	764.2	66.9	9
Jian-11-06-113	1761.0	31.5	1758.8	20.9	1756.1	26.3	9
Jian-11-06-114	402.4	13.1	396.0	26.5	358.8	166.2	9
Jian-11-06-12	272.7	6.1	281.1	46.2	351.8	424.5	9
Jian-11-06-13	247.5	9.3	236.2	33.3	125.0	362.8	9
Jian-11-06-14	330.2	6.0	334.7	20.9	365.6	159.6	9
Jian-11-06-15	233.0	7.6	217.0	23.5	46.8	277.2	9
Jian-11-06-16	849.8	27.8	884.2	22.4	971.5	30.0	9
Jian-11-06-17	2328.2	37.5	2449.6	18.2	2552.0	7.7	9
Jian-11-06-18	44.0	2.4	43.3	2.9	5.1	98.2	9
Jian-11-06-19	231.9	6.9	228.7	11.4	195.7	107.9	9
Jian-11-06-21	224.3	9.8	220.7	23.1	182.2	251.4	9
Jian-11-06-22	179.0	4.4	187.1	16.0	290.7	206.8	9
Jian-11-06-23	217.8	5.5	215.5	9.0	190.0	89.4	9
Jian-11-06-24	243.4	8.8	271.5	36.0	521.0	323.2	9
Jian-11-06-25	1001.5	20.4	1000.1	15.0	997.0	17.3	9
Jian-11-06-26	1859.0	43.3	1859.2	23.3	1859.5	9.8	9
Jian-11-06-27	890.2	41.1	900.1	30.6	924.7	28.0	9
Jian-11-06-28	1778.4	22.1	1822.6	12.3	1873.5	5.3	9
Jian-11-06-29	1886.8	52.7	1885.1	27.7	1883.2	5.6	9
Jian-11-06-30	456.0	21.0	447.2	57.3	402.7	339.7	9
Jian-11-06-31	898.6	52.0	925.5	38.3	990.1	23.2	9
Jian-11-06-32	1911.3	52.8	1890.7	27.4	1868.2	2.5	9
Jian-11-06-33	329.1	11.2	334.3	20.9	370.4	145.7	9
Jian-11-06-34	1772.8	58.6	1815.1	32.1	1864.1	6.0	9
Jian-11-06-36	38.6	1.4	38.8	2.4	52.8	124.5	9
Jian-11-06-37	2147.1	85.5	2316.5	44.5	2469.3	22.9	9
Jian-11-06-38	755.3	69.8	795.0	57.1	908.1	69.2	9
Jian-11-06-39	535.4	17.2	558.6	16.0	654.3	35.0	9
Jian-11-06-41	1784.7	38.0	1791.7	31.3	1799.9	51.1	9
Jian-11-06-43	248.6	9.5	240.7	18.9	164.8	184.6	9
Jian-11-06-45	222.8	5.6	228.4	9.3	287.3	86.0	9
Jian-11-06-46	215.3	5.8	219.1	13.9	260.8	149.7	9
Jian-11-06-48	36.3	2.1	35.0	5.2	-55.1	341.2	9
Jian-11-06-49	1531.5	95.2	1555.7	60.7	1588.6	56.9	9
Jian-11-06-50	796.6	20.9	808.0	29.4	839.7	93.4	9
Jian-11-06-51	370.7	20.9	367.4	19.7	346.8	61.7	9
Jian-11-06-52	1670.3	49.8	1679.2	41.5	1690.3	69.2	9
Jian-11-06-53	35.4	1.8	34.7	6.3	-11.0	429.2	9
Jian-11-06-54	213.6	4.4	214.3	7.4	222.1	75.2	9
Jian-11-06-57	1699.7	53.1	1772.0	29.9	1858.3	4.7	9

Jian-11-06-58	42.5	1.2	45.5	7.7	207.2	401.5	9
Jian-11-06-59	763.8	21.2	772.2	18.3	796.6	35.2	9
Jian-11-06-60	645.6	27.2	647.0	21.4	652.1	12.4	9
Jian-11-06-61	254.4	6.8	266.3	16.8	372.2	149.2	9
Jian-11-06-62	1858.9	73.9	1859.0	39.2	1859.1	6.8	9
~~Jian-11-06-63~~	~~1852.8~~	~~78.6~~	~~2013.5~~	~~63.2~~	~~2182.5~~	~~92.4~~	9
Jian-11-06-64	1665.4	44.1	1634.4	26.1	1594.6	21.0	9
Jian-11-06-65	2472.3	68.5	2438.0	30.9	2409.5	4.9	9
Jian-11-06-66	261.6	5.4	265.7	8.7	301.5	69.7	9
Jian-11-06-67	178.9	5.5	169.3	9.7	37.0	128.4	9
Jian-11-06-68	1927.9	10.5	1974.1	17.2	2022.8	33.3	9
Jian-11-06-69	439.1	12.0	443.7	30.2	467.6	175.3	9
Jian-11-06-70	1071.8	35.1	1068.3	23.8	1061.3	12.8	9
Jian-11-06-71	417.8	20.9	421.0	18.9	438.1	41.0	9
Jian-11-06-72	157.5	4.5	161.3	10.0	218.9	140.2	9
Jian-11-06-74	921.9	21.8	922.7	16.4	924.6	18.9	9
Jian-11-06-75	495.6	8.3	494.7	7.7	490.4	20.5	9
Jian-11-06-77	36.5	1.2	35.4	5.2	-35.3	352.4	9
Jian-11-06-78	286.4	19.8	300.1	39.3	407.4	300.1	9
Jian-11-06-79	43.5	1.5	45.9	5.1	171.7	253.6	9
Jian-11-06-81	2574.6	45.4	2549.2	20.7	2528.9	9.8	9
Jian-11-06-82	2659.2	133.2	2589.5	57.4	2535.5	5.9	9
Jian-11-06-83	2267.9	64.4	2402.4	31.2	2518.4	7.3	9
Jian-11-06-84	37.8	1.5	36.6	8.2	-40.6	549.3	9
Jian-11-06-85	1775.6	31.8	1812.9	18.5	1856.1	13.7	9
Jian-11-06-87	219.1	3.3	219.9	7.0	228.0	74.5	9
Jian-11-06-88	842.8	11.8	843.5	14.6	845.3	42.9	9
Jian-11-06-89	253.8	6.1	250.3	12.3	218.1	115.5	9
Jian-11-06-91	42.1	0.5	41.6	1.6	10.8	93.1	9
Jian-11-06-92	838.6	22.6	838.5	17.6	838.2	23.5	9
Jian-11-06-93	1320.4	26.3	1306.2	17.3	1282.8	16.1	9
Jian-11-06-94	909.5	17.8	912.8	13.7	920.9	18.6	9
Jian-11-06-95	275.7	10.8	277.2	31.1	289.9	278.9	9
Jian-11-06-96	265.5	9.1	264.0	11.4	251.2	79.3	9
Jian-11-06-97	425.5	3.5	422.7	9.1	407.4	55.5	9
Jian-11-06-98	1860.2	28.7	1859.5	15.3	1858.6	5.1	9
Jian-11-06-99	411.1	11.0	431.6	12.5	542.2	48.8	9
Jian-11-18-01	34.7	2.0	33.0	3.6	-88.7	235.7	8
Jian-11-18-02	37.2	1.0	34.1	5.9	-177.0	434.0	8
Jian-11-18-03	36.8	0.9	35.2	2.9	-73.3	193.3	8

Jian-11-18-04	35.3	0.9	36.5	3.4	115.5	217.1	8
Jian-11-18-05	37.3	1.1	37.0	3.6	19.4	228.5	8
Jian-11-18-06	37.4	2.3	39.6	6.9	172.4	392.7	8
Jian-11-18-07	36.0	0.6	36.0	2.4	32.8	157.6	8
Jian-11-18-08	36.8	0.5	36.6	2.0	24.7	131.3	8
Jian-11-18-09	36.4	1.3	36.6	8.2	47.4	542.5	8
Jian-11-18-10	35.8	0.6	31.6	4.3	-275.9	347.4	8
Jian-11-18-100	46.3	1.2	46.8	5.0	75.2	251.1	8
Jian-11-18-101	37.5	2.1	37.0	7.7	2.2	499.2	8
Jian-11-18-103	37.6	1.3	49.6	6.3	673.5	268.4	8
Jian-11-18-105	37.5	1.0	36.4	6.8	-39.9	463.1	8
Jian-11-18-106	35.8	0.8	37.9	3.8	169.9	230.7	8
Jian-11-18-107	35.9	0.8	35.1	2.2	-21.4	146.1	8
Jian-11-18-108	35.8	0.9	31.4	4.8	-289.1	392.4	8
Jian-11-18-109	35.7	0.6	35.0	4.9	-7.5	345.0	8
Jian-11-18-11	35.9	0.5	37.0	3.4	107.0	215.6	8
Jian-11-18-110	36.0	0.8	33.4	13.2	-153.1	1033.4	8
Jian-11-18-12	37.6	0.7	37.1	3.4	4.9	218.7	8
Jian-11-18-13	37.2	1.1	37.6	3.7	65.8	230.4	8
Jian-11-18-14	36.8	1.6	43.7	6.6	440.9	332.1	8
Jian-11-18-15	36.3	0.9	40.1	4.0	274.3	226.7	8
Jian-11-18-17	35.7	0.7	34.9	2.3	-15.9	155.0	8
Jian-11-18-18	36.5	1.6	34.6	3.4	-95.9	224.9	8
Jian-11-18-19	816.3	8.6	818.4	6.7	824.1	8.6	8
Jian-11-18-20	36.5	1.1	31.9	4.0	-302.6	316.3	8
Jian-11-18-21	386.7	21.0	467.1	54.0	884.5	276.0	8
Jian-11-18-22	36.7	1.6	35.4	5.7	-49.5	385.6	8
Jian-11-18-23	36.1	0.7	33.7	4.1	-136.3	302.0	8
Jian-11-18-24	37.1	1.2	38.9	4.3	148.2	255.2	8
Jian-11-18-25	224.9	11.7	279.3	13.4	764.4	28.4	8
Jian-11-18-26	226.9	4.7	215.8	13.4	96.6	155.4	8
Jian-11-18-27	36.8	1.1	40.3	3.1	254.0	170.5	8
Jian-11-18-29	36.3	1.2	35.9	3.7	12.1	243.1	8
Jian-11-18-30	35.9	0.8	37.4	2.7	134.1	166.3	8
Jian-11-18-31	35.8	1.4	34.7	6.6	-45.9	466.4	8
Jian-11-18-32	35.9	1.5	32.6	8.0	-201.2	623.6	8
Jian-11-18-33	35.1	1.0	35.7	3.6	78.3	234.0	8
Jian-11-18-34	37.6	0.8	37.5	6.1	35.4	393.9	8
Jian-11-18-35	36.3	3.0	36.3	6.3	35.4	377.0	8
Jian-11-18-37	38.1	1.3	32.8	5.6	-337.1	439.0	8
Jian-11-18-38	35.7	1.1	36.3	5.2	69.6	343.1	8

Jian-11-18-39	627.7	13.7	684.5	11.9	875.9	13.8	8
Jian-11-18-40	36.2	1.0	35.9	3.7	17.5	243.1	8
Jian-11-18-41	36.2	1.2	38.6	6.5	189.1	395.7	8
Jian-11-18-42	41.9	2.3	53.7	15.0	617.3	617.4	8
Jian-11-18-43	35.7	0.7	37.0	5.7	120.9	367.4	8
Jian-11-18-44	247.6	2.6	246.7	3.7	237.4	30.1	8
Jian-11-18-45	35.6	0.8	30.3	5.3	-369.2	457.8	8
Jian-11-18-46	36.6	1.9	35.5	4.4	-34.0	282.3	8
Jian-11-18-47	36.4	0.9	37.6	2.9	117.2	175.7	8
Jian-11-18-49	36.0	0.7	36.8	2.7	87.8	170.2	8
Jian-11-18-50	36.0	0.5	36.3	4.6	58.4	308.3	8
Jian-11-18-52	36.1	0.7	35.8	2.5	13.6	166.2	8
Jian-11-18-53	36.3	0.7	38.4	2.0	169.4	112.0	8
Jian-11-18-54	35.9	1.1	35.5	5.8	6.4	397.9	8
Jian-11-18-55	799.7	7.3	814.3	7.7	854.6	20.3	8
Jian-11-18-56	35.8	1.6	39.0	6.9	240.3	407.0	8
Jian-11-18-57	36.2	0.8	36.6	3.2	65.2	208.7	8
Jian-11-18-58	448.0	10.7	440.3	31.1	400.6	186.9	8
Jian-11-18-59	35.8	1.4	31.4	5.5	-290.1	447.5	8
Jian-11-18-60	36.1	1.5	34.8	7.0	-54.8	494.0	8
Jian-11-18-61	36.2	0.5	36.1	4.2	27.5	285.0	8
Jian-11-18-62	36.0	0.9	36.5	5.7	65.1	375.4	8
Jian-11-18-63	36.9	1.0	36.6	5.3	18.4	347.8	8
Jian-11-18-64	37.5	1.2	37.8	6.3	59.1	402.0	8
Jian-11-18-65	36.9	0.6	32.7	5.6	-267.7	446.9	8
Jian-11-18-66	37.0	1.0	41.0	2.8	282.2	146.0	8
Jian-11-18-67	855.2	20.4	854.3	15.5	852.0	18.1	8
Jian-11-18-68	721.1	29.6	748.6	23.1	831.6	10.4	8
Jian-11-18-69	37.2	1.0	40.9	7.2	263.0	412.2	8
Jian-11-18-70	1890.8	20.5	1890.8	11.4	1890.7	7.7	8
Jian-11-18-71	36.2	0.6	36.1	2.3	28.8	151.7	8
Jian-11-18-72	1923.0	54.3	1910.1	28.2	1896.1	4.0	8
Jian-11-18-73	35.5	0.6	34.7	5.2	-19.8	369.5	8
Jian-11-18-74	36.2	2.2	36.6	3.8	57.5	206.1	8
Jian-11-18-75	37.1	1.2	33.2	6.4	-237.7	489.2	8
Jian-11-18-76	36.0	1.9	34.1	8.5	-102.8	618.7	8
Jian-11-18-77	791.5	51.8	798.2	40.0	817.1	42.4	8
Jian-11-18-78	37.8	2.2	37.8	8.3	40.7	522.3	8
Jian-11-18-79	315.4	20.1	378.6	21.2	785.5	30.7	8
Jian-11-18-80	36.9	1.0	37.9	6.1	105.2	381.6	8
Jian-11-18-81	36.9	1.0	36.8	2.8	34.3	173.3	8

Jian-11-18-84	37.4	2.6	36.3	4.8	-33.8	281.8	8
Jian-11-18-85	37.0	1.0	35.2	3.4	-89.0	232.3	8
Jian-11-18-86	460.0	11.4	507.4	11.1	727.4	22.8	8
Jian-11-18-87	37.3	1.6	31.7	5.2	-370.4	418.6	8
Jian-11-18-88	36.5	0.9	38.6	4.1	168.5	247.6	8
Jian-11-18-89	37.5	1.3	35.4	7.2	-103.8	506.4	8
Jian-11-18-90	36.7	0.7	37.9	6.1	113.2	388.6	8
Jian-11-18-91	40.2	1.1	47.7	8.9	439.8	426.0	8
Jian-11-18-92	36.3	0.5	37.3	6.0	103.4	389.9	8
Jian-11-18-93	57.3	3.7	45.1	15.6	-562.5	962.6	8
Jian-11-18-94	36.4	1.7	40.8	4.5	306.1	230.9	8
Jian-11-18-96	37.2	0.9	34.3	8.4	-162.4	624.3	8
Jian-11-18-99	36.0	0.7	36.4	4.7	64.5	308.9	8
Jian-11-39-01	36.0	0.6	39.5	3.2	255.3	189.2	7
Jian-11-39-02	216.9	4.5	217.1	5.2	219.2	37.0	7
Jian-11-39-03	469.5	6.2	460.9	10.0	418.6	51.8	7
Jian-11-39-04	36.8	3.3	31.3	10.5	-375.9	877.6	7
Jian-11-39-05	39.8	1.5	42.2	3.0	177.8	144.0	7
Jian-11-39-10	36.0	1.7	35.2	3.0	-21.8	173.7	7
Jian-11-39-100	39.2	0.6	40.8	2.8	135.4	158.1	7
Jian-11-39-101	254.1	9.8	251.9	15.1	231.9	127.0	7
Jian-11-39-102	1911.9	147.8	1902.0	76.9	1891.2	4.7	7
Jian-11-39-103	37.9	1.9	35.4	10.1	-131.6	717.8	7
Jian-11-39-104	35.6	0.9	35.2	6.3	7.0	436.7	7
Jian-11-39-105	1605.5	34.3	1644.4	19.8	1694.6	6.2	7
Jian-11-39-106	39.5	1.9	39.6	6.7	46.4	399.0	7
Jian-11-39-107	35.8	1.6	35.2	9.0	-6.6	630.8	7
Jian-11-39-108	42.2	1.3	39.0	3.2	-152.6	190.3	7
Jian-11-39-109	461.9	8.2	467.5	16.0	494.7	84.9	7
Jian-11-39-11	37.9	1.2	40.3	7.8	186.8	456.7	7
Jian-11-39-110	41.5	0.9	42.2	3.8	80.0	211.0	7
Jian-11-39-112	37.5	2.8	40.3	12.9	210.5	755.0	7
Jian-11-39-114	38.2	0.7	34.9	2.2	-191.4	153.7	7
Jian-11-39-116	251.2	8.1	251.3	9.6	252.5	63.0	7
Jian-11-39-117	36.2	1.1	35.7	4.4	4.6	294.9	7
Jian-11-39-118	37.4	1.4	32.7	6.7	-293.3	524.7	7
Jian-11-39-119	36.3	0.8	38.5	3.0	176.2	175.9	7
Jian-11-39-12	39.4	1.8	34.7	4.4	-275.1	309.8	7
Jian-11-39-120	942.6	17.4	939.9	17.8	933.6	43.5	7
Jian-11-39-121	978.4	10.9	977.6	9.9	975.8	20.8	7

Jian-11-39-122	37.8	1.1	36.4	5.9	-56.3	395.9	7
Jian-11-39-123	2528.0	28.4	2685.2	13.0	2805.9	3.6	7
Jian-11-39-124	37.1	1.8	27.7	12.5	-731.1	1328.4	7
Jian-11-39-125	36.7	1.9	42.2	7.4	365.1	386.2	7
Jian-11-39-126	38.5	1.2	41.8	5.2	234.8	282.8	7
Jian-11-39-128	37.7	1.0	38.9	1.6	115.2	79.8	7
Jian-11-39-129a	41.4	1.5	42.2	3.6	88.7	189.3	7
Jian-11-39-129b	39.1	1.1	39.9	1.8	90.4	82.8	7
Jian-11-39-13	40.7	1.1	39.8	3.0	-13.2	175.8	7
Jian-11-39-130	38.5	1.1	40.1	3.1	136.8	173.3	7
Jian-11-39-133	194.4	10.3	198.7	10.2	251.1	38.9	7
Jian-11-39-134	38.8	0.5	37.3	1.3	-59.7	77.3	7
Jian-11-39-135	42.1	1.1	42.9	2.6	92.6	135.8	7
Jian-11-39-137	37.4	1.4	31.1	13.0	-433.5	1159.1	7
Jian-11-39-14	35.7	1.9	31.8	4.3	-256.9	321.1	7
Jian-11-39-15	37.1	2.5	42.0	9.9	333.7	529.1	7
Jian-11-39-16	37.2	1.2	36.6	6.4	-3.9	425.1	7
Jian-11-39-17	37.4	1.4	36.7	5.0	-8.0	324.9	7
Jian-11-39-18	38.4	1.9	37.0	2.7	-54.1	139.0	7
Jian-11-39-19	39.1	1.6	38.1	4.0	-30.2	241.2	7
Jian-11-39-20	1954.6	42.4	1910.5	21.9	1862.9	6.6	7
Jian-11-39-21	36.1	0.7	35.1	5.2	-30.6	366.0	7
Jian-11-39-22	40.1	3.0	40.7	5.8	78.1	300.6	7
Jian-11-39-23	39.8	1.2	40.3	3.1	65.9	171.6	7
Jian-11-39-24	38.4	1.0	40.8	4.7	180.4	267.5	7
Jian-11-39-27	36.9	1.0	34.7	7.6	-114.8	548.7	7
Jian-11-39-28	39.0	0.6	41.0	2.4	159.1	132.8	7
Jian-11-39-29	446.1	8.4	442.6	11.8	424.8	59.0	7
Jian-11-39-30	79.7	5.6	91.2	8.4	401.9	147.3	7
Jian-11-39-31	39.2	1.0	39.9	2.5	84.4	135.2	7
Jian-11-39-33	702.8	15.3	718.9	12.8	769.3	19.7	7
Jian-11-39-34	837.5	10.6	834.8	27.0	827.4	94.7	7
Jian-11-39-35	37.7	1.4	41.5	5.8	267.2	319.9	7
Jian-11-39-36	42.6	1.4	40.0	3.4	-109.1	197.2	7
Jian-11-39-37	338.4	7.3	345.2	16.6	391.1	117.6	7
Jian-11-39-38	37.7	0.9	37.1	3.2	-5.7	204.3	7
Jian-11-39-39	41.4	1.3	43.5	2.0	159.1	84.1	7
Jian-11-39-40	41.3	1.2	41.1	4.9	24.8	284.3	7
Jian-11-39-43	57.7	7.0	57.9	17.2	65.3	679.1	7
Jian-11-39-44	36.7	0.8	37.3	8.1	76.1	528.1	7
Jian-11-39-46	42.5	3.6	46.3	12.5	248.7	613.8	7

Jian-11-39-47	39.8	0.4	38.9	1.9	-17.2	117.4	7
Jian-11-39-50	36.9	1.3	29.2	8.3	-561.8	787.4	7
Jian-11-39-52	35.3	0.8	33.4	3.6	-99.5	260.4	7
Jian-11-39-53	39.5	1.4	40.8	5.5	118.2	311.8	7
Jian-11-39-54	42.7	0.6	41.6	2.9	-19.8	167.1	7
Jian-11-39-55	33.9	3.4	44.9	20.5	679.3	1025.7	7
Jian-11-39-56	37.5	0.9	36.8	4.9	-6.9	324.2	7
Jian-11-39-57	244.9	4.6	260.7	31.1	405.6	301.3	7
Jian-11-39-58	44.1	2.2	44.1	4.4	45.5	215.8	7
Jian-11-39-59	41.9	0.9	43.6	2.5	137.5	126.6	7
Jian-11-39-6	38.0	0.6	38.2	2.0	46.1	122.5	7
Jian-11-39-60	39.5	2.9	37.9	9.5	-65.2	606.1	7
Jian-11-39-61	36.8	2.3	33.0	8.5	-236.8	647.2	7
Jian-11-39-62	36.3	2.4	40.0	7.4	265.7	404.6	7
Jian-11-39-63	38.6	1.4	35.0	4.5	-202.5	313.2	7
Jian-11-39-64	36.6	2.1	44.0	9.9	467.2	496.0	7
Jian-11-39-65	38.2	2.4	40.7	9.0	193.0	506.2	7
Jian-11-39-66	43.5	6.7	58.6	26.5	729.5	977.4	7
Jian-11-39-69	43.0	3.2	35.0	11.2	-483.5	860.8	7
Jian-11-39-7	37.2	2.2	36.8	3.5	9.2	187.8	7
Jian-11-39-70A	42.3	2.5	41.3	3.1	-19.3	121.9	7
Jian-11-39-71	42.2	2.9	40.4	3.9	-67.2	175.4	7
Jian-11-39-72	34.6	2.1	25.3	13.0	-785.0	1545.1	7
Jian-11-39-74	2217.3	97.1	2283.1	52.1	2342.6	42.1	7
Jian-11-39-75	42.0	1.0	41.4	3.3	6.2	190.0	7
Jian-11-39-76	36.1	2.4	38.0	4.0	154.8	194.5	7
Jian-11-39-77	457.0	7.1	457.0	9.6	457.0	45.7	7
Jian-11-39-78	429.8	5.5	432.9	11.2	449.4	64.1	7
Jian-11-39-79	251.0	5.6	230.2	29.4	21.8	340.0	7
Jian-11-39-8	2294.3	81.7	2439.8	39.3	2563.3	7.0	7
Jian-11-39-80	38.5	1.0	41.3	3.6	210.1	200.1	7
Jian-11-39-81	33.9	4.0	35.9	6.1	174.7	289.8	7
Jian-11-39-82	38.7	0.6	37.7	3.4	-26.3	219.5	7
Jian-11-39-83	1746.2	23.9	1755.3	40.3	1766.2	83.3	7
Jian-11-39-84	43.4	0.5	44.7	2.6	112.9	137.5	7
Jian-11-39-84	270.2	10.4	333.5	12.7	802.2	43.7	7
Jian-11-39-85	43.3	1.3	45.5	3.2	163.0	154.0	7
Jian-11-39-87	41.4	0.5	41.5	2.3	42.2	133.4	7
Jian-11-39-89	38.2	0.7	37.2	3.0	-25.8	191.8	7
Jian-11-39-9	322.6	1.8	332.2	10.7	400.0	83.6	7
Jian-11-39-91	250.2	6.4	240.7	17.7	149.4	184.5	7

Jian-11-39-93	39.8	1.6	41.2	4.2	121.8	228.1	7
Jian-11-39-94	40.6	3.3	60.4	27.1	940.5	982.1	7
Jian-11-39-95	1847.8	64.1	1856.3	34.9	1865.9	16.7	7
Jian-11-39-97	253.1	5.0	265.1	12.5	372.5	111.9	7
Jian-11-39-98	39.1	1.1	39.0	4.9	32.1	301.0	7
Jians-13-05-01	1756.4	33.5	1728.6	20.6	1695.2	21.8	24
Jians-13-05-02	2279.0	37.2	2373.4	18.1	2455.6	5.7	24
Jians-13-05-03	1874.5	52.8	1849.7	29.8	1822.0	24.0	24
Jians-13-05-04	451.1	9.0	452.1	12.8	457.2	63.2	24
Jians-13-05-05	783.0	33.3	777.1	32.2	760.3	80.9	24
Jians-13-05-06	1846.4	9.6	1855.8	5.4	1866.4	3.7	24
Jians-13-05-08	506.5	6.8	547.1	13.9	720.2	63.1	24
Jians-13-05-09	875.2	16.5	882.7	17.8	901.7	46.2	24
Jians-13-05-10	1746.4	30.7	1741.0	39.8	1734.4	79.4	24
Jians-13-05-11	263.1	4.0	266.4	8.5	295.5	75.1	24
Jians-13-05-12	243.6	9.5	276.8	25.5	567.5	212.7	24
Jians-13-05-13	1905.8	20.9	1897.6	11.1	1888.6	4.2	24
Jians-13-05-14	2915.7	21.2	2925.4	9.3	2932.1	5.8	24
Jians-13-05-15	440.1	2.4	445.6	7.0	474.4	41.1	24
Jians-13-05-16	263.1	6.5	272.8	9.7	356.4	71.7	24
Jians-13-05-17	2498.5	28.8	2464.1	15.3	2435.9	15.2	24
Jians-13-05-18	1778.5	20.4	1766.9	39.3	1753.2	82.5	24
Jians-13-05-19	417.1	12.2	411.1	19.5	377.5	110.7	24
Jians-13-05-20	1964.6	47.5	2033.6	25.4	2104.4	12.3	24
Jians-13-05-21	1868.5	10.9	1862.4	7.7	1855.5	10.9	24
Jians-13-05-22	2408.9	19.8	2455.8	9.2	2494.8	2.4	24
Jians-13-05-23	276.9	3.8	280.0	7.7	306.2	63.8	24
Jians-13-05-24	1899.5	14.9	1895.3	7.8	1890.8	1.9	24
Jians-13-05-25	258.4	5.5	266.7	13.0	340.4	116.1	24
Jians-13-05-26	321.7	4.3	334.3	11.3	422.2	83.3	24
Jians-13-05-27	1895.5	10.0	1891.4	6.0	1886.9	6.0	24
Jians-13-05-28	247.3	2.0	254.8	5.8	323.6	55.6	24
Jians-13-05-29	1230.9	40.2	1227.4	25.7	1221.3	7.9	24
Jians-13-05-30	1733.1	25.3	1732.3	20.2	1731.3	32.5	24
Jians-13-05-31	256.1	2.0	259.1	8.1	286.2	79.3	24
Jians-13-05-32	1766.9	10.7	1766.1	8.4	1765.2	13.3	24
Jians-13-05-34	263.5	5.1	256.2	27.9	189.8	283.7	24
Jians-13-05-35	1797.3	47.4	1842.5	39.0	1893.9	62.0	24
Jians-13-05-36	465.3	42.1	468.9	53.7	486.6	238.5	24
Jians-13-05-37	1879.1	4.6	1877.3	3.1	1875.4	4.2	24

Jians-13-05-39	471.5	8.0	471.0	27.2	468.5	155.0	24
Jians-13-05-41	812.2	11.3	812.1	22.2	812.0	76.9	24
Jians-13-05-42	420.7	2.8	428.8	7.5	472.2	44.8	24
Jians-13-05-45	252.6	6.3	257.0	21.1	297.3	203.8	24
Jians-13-05-46	1599.6	60.1	1572.2	34.6	1535.6	15.1	24
Jians-13-05-47	1903.3	33.7	1890.4	18.1	1876.4	9.3	24
Jians-13-05-48	372.7	12.2	384.7	21.3	457.2	127.2	24
Jians-13-05-50	1879.4	18.8	1880.1	10.0	1880.9	3.5	24
Jians-13-05-53	1898.0	13.6	1892.5	7.5	1886.4	5.0	24
Jians-13-05-54	621.6	9.4	616.1	9.9	596.2	31.7	24
Jians-13-05-55	246.5	4.5	249.5	9.8	277.9	92.6	24
Jians-13-05-56	2203.1	26.2	2194.7	12.9	2186.8	5.3	24
Jians-13-05-57	1099.4	7.5	1098.4	5.6	1096.3	7.8	24
Jians-13-05-58	1974.9	15.3	1970.6	8.6	1966.1	7.3	24
Jians-13-05-59	241.7	4.5	250.1	10.8	329.2	101.5	24
Jians-13-05-60	1086.4	33.2	1105.4	25.5	1143.0	35.7	24
Jians-13-05-61	851.0	17.9	840.8	14.5	813.9	24.9	24
Jians-13-05-62	423.5	9.5	438.0	13.2	514.8	63.6	24
Jians-13-05-63	299.3	7.2	298.8	13.7	294.7	106.7	24
Jians-13-05-64	802.8	20.8	798.8	29.7	787.7	96.9	24
Jians-13-05-65	382.0	11.0	371.0	15.9	302.5	94.9	24
Jians-13-05-67	1924.9	27.4	1895.4	14.3	1863.2	4.8	24
Jians-13-05-68	2123.8	49.8	2234.5	27.2	2337.5	21.1	24
Jians-13-05-69	293.4	4.1	303.1	9.2	378.3	72.2	24
Jians-13-05-70	1899.0	27.5	1881.3	14.5	1861.9	5.1	24
Jians-13-05-71	1852.9	50.1	1874.4	27.5	1898.3	15.0	24
Jians-13-05-73	2562.9	21.1	2540.2	9.4	2522.1	3.1	24
Jians-13-05-74	1852.6	29.2	1848.8	15.5	1844.4	3.7	24
Jians-13-05-75	298.5	11.8	314.8	23.0	437.3	166.3	24
Jians-13-05-76	1892.9	41.1	1875.0	21.8	1855.3	8.8	24
Jians-13-05-77	1974.3	36.4	1955.3	18.6	1935.2	3.7	24
Jians-13-07-01	2201.4	184.4	2346.2	90.9	2474.7	13.1	23
Jians-13-07-02	814.3	15.0	819.6	38.8	833.8	137.7	23
Jians-13-07-03	813.6	24.1	835.7	47.3	894.9	158.8	23
Jians-13-07-04	255.5	4.8	263.4	12.1	334.2	109.7	23
Jians-13-07-05	1708.5	67.1	1676.7	43.1	1637.1	51.2	23
Jians-13-07-07	283.6	8.2	289.7	19.4	339.4	161.0	23
Jians-13-07-08	803.0	13.1	796.7	17.8	779.1	57.3	23
Jians-13-07-09	2629.1	99.5	2644.3	46.1	2655.9	27.9	23
Jians-13-07-10	795.1	7.3	805.1	9.5	833.2	29.2	23

Jians-13-07-102	830.8	4.8	833.0	8.2	839.0	27.0	23	
Jians-13-07-104	247.1	7.1	250.8	30.9	285.1	311.6	23	
Jians-13-07-12	1066.9	30.6	1100.0	33.1	1165.9	75.8	23	
Jians-13-07-13	247.5	5.1	243.5	9.2	205.4	85.1	23	
Jians-13-07-14	813.0	10.8	823.7	13.3	852.8	39.0	23	
Jians-13-07-16	1021.7	18.8	1035.5	20.0	1064.7	47.1	23	
Jians-13-07-17	807.2	29.0	855.4	31.1	982.6	76.9	23	
Jians-13-07-18	788.8	14.7	796.2	16.5	817.0	46.8	23	
Jians-13-07-19	834.1	20.9	826.2	30.3	805.0	97.3	23	
Jians-13-07-20	1642.8	37.6	1717.1	21.7	1808.9	5.8	23	
Jians-13-07-22	2705.2	39.9	2700.8	17.4	2697.5	5.9	23	
Jians-13-07-23	1236.2	16.3	1235.9	12.4	1235.5	19.0	23	
Jians-13-07-24	836.3	14.8	833.9	17.8	827.7	52.0	23	
Jians-13-07-25	1650.9	21.3	1724.5	13.2	1815.0	11.4	23	
Jians-13-07-26	296.6	5.8	295.0	8.0	282.6	55.1	23	
Jians-13-07-27	1432.2	46.3	1509.7	34.4	1620.1	46.2	23	
Jians-13-07-28	772.2	12.4	769.3	11.8	761.0	28.9	23	
Jians-13-07-29	830.7	29.5	855.3	45.2	919.8	140.8	23	
Jians-13-07-30	936.2	32.8	977.8	61.8	1072.5	182.7	23	
Jians-13-07-32	1709.2	22.5	1716.2	14.3	1724.8	15.6	23	
Jians-13-07-34	212.7	2.3	213.9	9.6	226.6	112.8	23	
Jians-13-07-35	833.0	22.0	830.6	24.7	824.2	69.3	23	
Jians-13-07-36	232.6	3.3	224.2	9.8	137.0	109.8	23	
Jians-13-07-37	442.7	5.1	442.2	16.0	439.5	95.8	23	
Jians-13-07-39	2119.0	151.2	2325.5	76.9	2512.0	12.6	23	
Jians-13-07-40	1880.2	31.9	1873.8	17.8	1866.7	13.0	23	
Jians-13-07-41	2312.1	72.0	2416.7	34.2	2506.1	4.1	23	
Jians-13-07-42	1354.9	32.2	1375.6	21.2	1407.8	19.0	23	
Jians-13-07-43	241.6	5.9	274.9	12.3	568.9	97.6	23	
Jians-13-07-44	1396.9	13.4	1401.9	9.8	1409.6	13.9	23	
Jians-13-07-46	779.2	35.4	779.5	33.0	780.4	76.9	23	
Jians-13-07-47	245.1	15.6	317.6	55.4	890.3	400.6	23	
Jians-13-07-48	820.7	14.6	818.6	32.5	812.7	114.4	23	
Jians-13-07-49	221.3	3.4	228.1	11.1	297.9	119.1	23	
Jians-13-07-50	247.9	5.5	246.6	13.8	234.2	135.5	23	
Jians-13-07-51	879.3	11.0	881.9	8.8	888.4	14.0	23	
Jians-13-07-53	1176.8	19.7	1173.1	23.6	1166.2	56.4	23	
Jians-13-07-55	212.9	5.4	207.0	10.2	140.8	113.3	23	
Jians-13-07-56	1863.6	40.8	1849.9	33.0	1834.4	53.5	23	
Jians-13-07-57	690.5	45.1	715.1	36.1	793.0	29.1	23	
Jians-13-07-58	439.4	4.1	453.3	9.2	524.3	51.1	23	

Jians-13-07-59	252.1	4.9	246.6	19.1	195.0	198.1	23	
Jians-13-07-60	805.3	8.0	805.0	17.2	804.2	61.1	23	
Jians-13-07-62	2120.2	32.1	2135.0	17.9	2149.3	16.2	23	
Jians-13-07-63	820.1	6.0	817.8	20.3	811.7	74.0	23	
Jians-13-07-64	998.1	17.3	1012.1	14.6	1042.6	26.3	23	
Jians-13-07-65	880.6	19.1	935.9	36.1	1068.5	109.0	23	
Jians-13-07-66	858.1	41.8	872.4	37.2	908.8	75.0	23	
Jians-13-07-67	1669.2	10.7	1667.7	9.7	1665.8	17.4	23	
Jians-13-07-69	447.7	5.4	454.4	13.7	488.1	77.9	23	
Jians-13-07-70	414.8	6.4	422.1	9.7	461.7	51.5	23	
Jians-13-07-73	445.4	8.1	463.1	21.3	552.1	118.3	23	
Jians-13-07-75	1879.0	6.6	1874.7	3.8	1869.9	3.1	23	
Jians-13-07-76	804.0	70.6	829.8	54.8	899.6	50.6	23	
Jians-13-07-77	887.3	7.3	886.2	6.7	883.4	14.7	23	
Jians-13-07-78	404.6	11.8	363.5	56.3	109.0	431.6	23	
Jians-13-07-79	1608.2	5.7	1662.4	4.0	1731.5	5.3	23	
Jians-13-07-80	222.3	2.1	223.4	7.8	235.0	87.4	23	
Jians-13-07-82	824.0	7.4	830.2	8.6	846.8	24.3	23	
Jians-13-07-83	833.0	8.7	849.7	14.3	893.7	45.7	23	
Jians-13-07-85	884.1	5.7	882.1	13.2	877.1	44.0	23	
Jians-13-07-87	521.1	25.6	909.1	33.0	2025.4	36.2	23	
Jians-13-07-88	297.9	3.0	308.9	11.4	392.7	92.9	23	
Jians-13-07-90	807.7	9.4	860.9	22.5	1000.3	74.7	23	
Jians-13-07-92	779.6	9.3	778.5	25.5	775.5	95.0	23	
Jians-13-07-93	1879.9	31.6	1870.3	51.6	1859.6	103.3	23	
Jians-13-07-94	596.9	57.0	689.3	59.5	1003.6	130.3	23	
Jians-13-07-95	2532.1	10.7	2515.3	7.1	2501.7	9.6	23	
Jians-13-07-96	818.0	6.4	828.1	12.6	855.5	43.0	23	
Jians-13-07-97	279.2	2.5	294.5	13.3	417.0	114.2	23	
Jians-13-07-98	466.8	7.6	460.3	11.7	428.0	59.3	23	
Jians-13-07-99	791.3	10.4	793.4	28.8	799.2	105.6	23	
Jians-13-08-02	1809.4	27.4	1798.9	15.1	1786.6	8.4	22	
Jians-13-08-03	840.3	7.6	837.9	14.2	831.4	47.8	22	
Jians-13-08-04	876.9	27.0	871.0	19.6	856.2	14.0	22	
Jians-13-08-05	282.3	7.7	278.9	13.1	250.2	106.1	22	
Jians-13-08-06	837.6	20.2	843.1	19.1	857.3	44.0	22	
Jians-13-08-07	1701.2	69.2	1763.3	43.7	1837.7	43.6	22	
Jians-13-08-08	989.2	15.5	995.6	13.2	1009.8	24.4	22	
Jians-13-08-09	832.4	9.9	830.2	11.1	824.3	31.2	22	
Jians-13-08-10	270.8	12.6	266.5	28.7	228.5	261.3	22	

Jians-13-08-101	850.1	14.4	853.8	17.9	863.4	52.1	22
Jians-13-08-103	1621.6	52.7	1596.1	32.4	1562.7	30.9	22
Jians-13-08-104	771.1	9.7	778.9	12.4	801.3	38.6	22
Jians-13-08-105	221.8	4.9	220.1	8.4	202.3	83.6	22
Jians-13-08-12	907.4	22.8	899.5	17.1	880.3	20.1	22
Jians-13-08-14	895.6	10.8	891.1	13.9	879.9	40.3	22
Jians-13-08-15	1720.7	25.4	1720.1	15.1	1719.5	12.6	22
Jians-13-08-17	832.5	9.6	827.4	9.4	813.8	23.5	22
Jians-13-08-18	1368.8	26.0	1395.2	18.9	1435.7	25.5	22
Jians-13-08-19	1753.8	16.8	1748.3	10.8	1741.7	13.0	22
Jians-13-08-20	821.2	12.4	813.0	26.8	790.5	94.8	22
Jians-13-08-21	913.7	15.4	904.7	13.3	882.7	26.7	22
Jians-13-08-22	823.0	13.1	832.3	12.3	857.0	28.2	22
Jians-13-08-23	1868.6	25.7	1874.5	13.7	1881.0	4.7	22
Jians-13-08-25	827.9	11.3	839.3	12.1	869.7	31.8	22
Jians-13-08-27	836.3	21.4	845.2	18.8	868.8	38.1	22
Jians-13-08-28	264.5	2.1	269.5	9.6	313.0	90.5	22
Jians-13-08-29	836.1	29.8	842.6	22.5	859.7	20.9	22
Jians-13-08-30	860.3	31.5	870.5	26.7	896.5	49.0	22
Jians-13-08-31	795.5	16.7	821.6	33.7	892.9	114.8	22
Jians-13-08-33	1047.1	20.8	1040.7	17.4	1027.2	32.0	22
Jians-13-08-36	912.2	12.2	906.9	12.9	893.8	32.9	22
Jians-13-08-38	3358.5	21.9	3340.2	8.4	3329.2	2.8	22
Jians-13-08-39	257.4	4.5	251.1	12.3	193.1	121.8	22
Jians-13-08-41	316.9	13.1	351.5	68.2	586.6	494.9	22
Jians-13-08-46	1369.1	7.6	1374.1	8.4	1381.9	17.8	22
Jians-13-08-47	1862.0	96.1	1883.4	57.8	1907.2	57.2	22
Jians-13-08-48	809.4	11.5	821.8	20.3	855.5	68.0	22
Jians-13-08-49	243.2	4.3	244.1	9.0	252.4	86.1	22
Jians-13-08-50	830.2	15.9	855.3	34.7	920.9	116.1	22
Jians-13-08-51	1010.2	26.1	1004.3	23.3	991.4	48.0	22
Jians-13-08-52	444.5	7.4	445.3	10.4	449.5	51.5	22
Jians-13-08-55	1042.7	22.8	1027.4	16.9	994.9	22.6	22
Jians-13-08-56	821.1	11.2	863.5	33.6	973.9	114.0	22
Jians-13-08-57	814.2	8.1	812.9	7.8	809.3	19.0	22
Jians-13-08-58	796.3	16.3	834.6	33.6	938.0	112.5	22
Jians-13-08-59	799.4	12.1	816.7	17.7	864.2	56.6	22
Jians-13-08-61	796.1	6.3	815.9	11.3	870.4	37.7	22
Jians-13-08-64	825.2	14.6	820.6	12.9	808.3	27.3	22
Jians-13-08-66	834.2	14.7	833.4	22.6	831.2	73.2	22
Jians-13-08-67	816.3	16.3	818.0	23.1	822.6	73.5	22

Jians-13-08-68	846.8	9.7	845.5	7.4	842.2	8.9	22
Jians-13-08-69	1920.8	25.2	1928.4	14.2	1936.5	11.4	22
Jians-13-08-71	270.4	5.4	264.4	13.5	212.0	125.7	22
Jians-13-08-74	1899.1	59.7	1906.7	31.8	1915.1	12.0	22
Jians-13-08-75	2628.0	39.5	2616.5	19.0	2607.6	14.3	22
Jians-13-08-76	1909.9	28.9	1896.0	15.9	1880.8	10.7	22
Jians-13-08-77	2343.6	39.2	2417.2	18.5	2479.7	4.4	22
Jians-13-08-78	819.1	11.6	812.8	20.3	795.6	69.1	22
Jians-13-08-79	820.2	18.5	824.2	19.3	835.0	50.7	22
Jians-13-08-81	806.7	10.8	807.9	21.6	811.1	75.6	22
Jians-13-08-82	813.5	14.1	811.6	26.2	806.3	90.4	22
Jians-13-08-83	887.3	14.0	885.8	12.8	882.2	28.1	22
Jians-13-08-84	1911.0	23.0	1897.3	12.0	1882.4	3.5	22
Jians-13-08-85	903.8	15.7	896.2	24.0	877.5	74.0	22
Jians-13-08-86	1751.9	34.1	1790.7	19.2	1836.2	9.1	22
Jians-13-08-87	2299.1	46.6	2316.2	22.6	2331.3	10.0	22
Jians-13-08-88	984.0	22.3	988.6	19.8	998.8	39.8	22
Jians-13-08-89	801.7	10.2	814.6	10.1	850.1	24.9	22
Jians-13-08-90	1436.9	14.0	1486.1	10.4	1557.1	14.6	22
Jians-13-08-91	810.8	16.8	816.7	16.0	832.8	37.7	22
Jians-13-08-93	1863.7	27.0	1855.7	48.1	1846.7	97.5	22
Jians-13-08-95	817.9	16.2	822.9	17.3	836.4	46.4	22
Jians-13-08-96	880.7	11.4	880.5	17.1	879.9	52.8	22
Jians-13-08-97	846.3	12.8	852.7	15.7	869.4	45.2	22
Jians-13-08-99	252.6	20.6	281.0	33.4	524.1	236.0	22
Jing-12-01-01	218.1	3.9	222.3	7.6	266.1	76.2	19
Jing-12-01-04	884.8	9.6	893.9	9.3	916.7	21.8	19
Jing-12-01-05	1274.8	31.2	1377.0	20.8	1539.2	11.2	19
Jing-12-01-07	2569.4	21.0	2557.8	9.6	2548.5	4.7	19
Jing-12-01-08	284.7	10.7	297.9	18.3	402.4	133.2	19
Jing-12-01-09	443.1	19.7	443.1	19.4	443.0	62.4	19
Jing-12-01-10	251.3	4.5	251.3	9.7	251.6	91.2	19
Jing-12-01-100	213.1	4.2	215.1	7.3	237.9	72.7	19
Jing-12-01-101	1007.1	19.7	1004.8	15.0	999.9	21.0	19
Jing-12-01-102	213.3	17.4	162.1	266.4	-534.6	0.0	19
Jing-12-01-103	246.7	7.7	234.9	19.2	117.9	202.6	19
Jing-12-01-105	949.8	13.3	948.4	12.2	944.9	26.2	19
Jing-12-01-106	1840.5	41.1	1861.4	22.2	1884.9	8.0	19
Jing-12-01-108	203.1	6.1	204.3	8.5	218.5	80.3	19
Jing-12-01-109	1754.8	28.3	1748.5	41.1	1740.9	83.8	19

Jing-12-01-10B	644.2	30.4	668.6	27.1	751.9	51.9	19
Jing-12-01-11	2537.9	37.9	2544.1	17.3	2549.0	7.0	19
Jing-12-01-111	212.5	3.3	214.9	3.9	241.3	28.5	19
Jing-12-01-115	967.5	14.0	973.5	11.5	986.9	20.1	19
Jing-12-01-119	1462.5	30.3	1471.8	19.8	1485.2	20.4	19
Jing-12-01-12	455.9	7.2	448.8	32.0	412.6	194.1	19
Jing-12-01-121	1309.6	34.4	1314.3	25.1	1322.1	34.3	19
Jing-12-01-122	933.4	15.9	936.0	12.0	942.2	14.4	19
Jing-12-01-123	960.7	32.9	948.2	24.0	919.3	25.6	19
Jing-12-01-124	2545.7	28.3	2544.3	13.3	2543.2	7.8	19
Jing-12-01-125	219.9	3.3	220.0	5.1	221.5	48.3	19
Jing-12-01-126	214.6	7.6	225.0	20.1	335.5	211.2	19
Jing-12-01-127	440.8	6.2	432.0	9.4	384.8	50.8	19
Jing-12-01-128	249.4	10.3	228.3	32.0	15.9	364.0	19
Jing-12-01-13	866.1	7.6	871.6	8.1	885.7	21.2	19
Jing-12-01-131	828.8	18.7	833.7	15.7	846.8	28.4	19
Jing-12-01-132	914.5	56.7	903.5	40.9	876.6	32.2	19
Jing-12-01-133	237.8	5.1	245.2	20.8	317.4	211.2	19
Jing-12-01-134	311.3	8.5	309.5	9.8	295.6	54.9	19
Jing-12-01-136	866.6	18.7	877.5	18.1	905.1	41.8	19
Jing-12-01-137	424.3	6.2	412.7	19.4	348.3	125.2	19
Jing-12-01-139	836.9	13.7	836.4	10.9	835.2	16.3	19
Jing-12-01-14	630.6	22.0	661.8	19.6	769.3	36.0	19
Jing-12-01-140	244.1	3.7	245.7	6.3	260.6	55.8	19
Jing-12-01-142	815.8	18.7	828.1	16.3	861.2	31.8	19
Jing-12-01-143	867.0	45.4	870.2	33.1	878.4	17.4	19
Jing-12-01-147	1606.3	78.2	1579.6	46.7	1544.1	35.6	19
Jing-12-01-148	440.4	20.8	504.7	83.5	807.7	430.5	19
Jing-12-01-15	874.9	14.3	875.4	12.9	876.8	27.5	19
Jing-12-01-150	1738.4	55.1	1749.9	30.8	1763.7	13.2	19
Jing-12-01-151	711.6	27.8	744.8	25.7	845.6	53.8	19
Jing-12-01-152	2346.5	39.4	2321.5	19.0	2299.6	9.9	19
Jing-12-01-153	437.2	6.6	440.6	8.7	458.6	41.1	19
Jing-12-01-154	343.3	4.9	336.3	20.1	288.4	157.1	19
Jing-12-01-155	795.4	66.8	838.1	53.1	953.0	53.5	19
Jing-12-01-158	241.7	4.7	240.6	15.1	229.5	156.6	19
Jing-12-01-16	413.0	4.4	411.7	8.4	404.4	50.0	19
Jing-12-01-161	455.6	10.0	455.2	11.9	453.1	51.1	19
Jing-12-01-162	221.6	7.2	228.1	20.4	295.1	216.0	19
Jing-12-01-17	279.4	8.3	299.8	39.1	461.9	328.3	19
Jing-12-01-19	433.5	10.2	431.0	21.2	417.8	123.3	19

Jing-12-01-20	1935.3	79.7	2068.6	48.1	2204.2	45.4	19
Jing-12-01-21	1886.7	55.6	1942.3	33.9	2002.1	34.6	19
Jing-12-01-22	862.8	18.1	855.6	17.3	837.1	41.2	19
Jing-12-01-23	1407.8	14.2	1382.5	14.3	1343.6	29.5	19
Jing-12-01-24	267.8	9.8	262.6	47.6	216.6	471.9	19
Jing-12-01-25	443.9	5.0	447.1	9.5	463.6	51.8	19
Jing-12-01-27	528.9	9.0	560.7	39.7	692.1	193.2	19
Jing-12-01-28	431.9	10.2	435.7	18.1	455.7	99.7	19
Jing-12-01-30	216.6	5.2	216.0	8.9	209.4	90.1	19
Jing-12-01-31	837.1	15.2	837.8	11.7	839.5	13.9	19
Jing-12-01-32	449.3	5.4	461.0	8.6	519.6	43.1	19
Jing-12-01-34	846.6	16.1	846.0	13.9	844.5	28.0	19
Jing-12-01-35	1939.5	126.7	1913.8	67.2	1886.0	33.3	19
Jing-12-01-36	1928.3	142.1	2111.8	76.0	2295.6	9.2	19
Jing-12-01-37	242.7	4.9	255.6	19.0	374.7	183.3	19
Jing-12-01-38	712.4	33.1	737.2	25.9	813.3	11.4	19
Jing-12-01-39	411.6	9.9	408.4	11.8	390.2	55.5	19
Jing-12-01-40	271.2	9.1	283.0	19.6	382.1	160.7	19
Jing-12-01-41	1740.8	16.7	1750.6	19.0	1762.4	36.4	19
Jing-12-01-42	274.4	8.1	274.2	14.0	272.3	113.9	19
Jing-12-01-44	768.9	24.5	856.1	26.0	1089.2	59.7	19
Jing-12-01-45	215.2	3.9	213.2	6.1	191.4	60.6	19
Jing-12-01-46	429.1	7.1	427.6	9.6	419.4	48.2	19
Jing-12-01-47	561.5	10.6	597.7	10.9	737.8	28.9	19
Jing-12-01-48	427.0	3.6	427.8	7.6	431.9	44.4	19
Jing-12-01-50	427.1	6.3	433.9	15.3	470.0	90.0	19
Jing-12-01-51	1398.6	101.3	1503.6	67.6	1654.9	56.3	19
Jing-12-01-52	398.6	5.3	408.9	7.8	467.5	40.9	19
Jing-12-01-53	822.6	11.7	839.6	13.9	885.1	39.5	19
Jing-12-01-54	2401.4	100.1	2436.7	47.7	2466.3	22.4	19
Jing-12-01-55	444.3	6.0	454.9	15.5	508.8	88.1	19
Jing-12-01-56	850.7	12.2	843.6	15.9	824.8	48.1	19
Jing-12-01-57	2088.9	33.7	2287.6	18.4	2470.3	12.2	19
Jing-12-01-58	365.6	5.3	364.4	8.9	356.7	56.4	19
Jing-12-01-59	161.6	3.3	164.1	16.5	200.0	248.6	19
Jing-12-01-60	255.8	12.3	251.3	44.0	209.6	446.7	19
Jing-12-01-61	222.5	6.0	211.5	20.5	90.9	247.0	19
Jing-12-01-62	218.3	5.1	219.8	9.0	236.1	90.0	19
Jing-12-01-65	853.6	36.7	868.1	27.6	905.1	24.3	19
Jing-12-01-66	411.2	7.7	391.5	25.3	276.6	173.4	19
Jing-12-01-67	243.9	13.7	244.4	14.3	248.6	75.0	19

Jing-12-01-68	1856.3	25.1	1858.3	15.5	1860.4	17.1	19
Jing-12-01-69	208.7	5.0	212.2	30.0	251.8	357.6	19
Jing-12-01-71	736.6	25.4	762.8	21.3	840.4	33.0	19
Jing-12-01-72	405.9	8.4	412.5	12.5	449.4	67.2	19
Jing-12-01-74	253.6	4.3	262.3	9.0	341.3	78.7	19
Jing-12-01-75	817.6	26.6	824.3	20.8	842.4	25.9	19
Jing-12-01-77	392.6	13.0	400.4	15.3	445.8	69.7	19
Jing-12-01-78	857.6	6.7	897.6	7.2	997.3	17.7	19
Jing-12-01-79	778.1	8.4	792.5	7.7	833.3	16.7	19
Jing-12-01-80	441.4	10.0	420.7	24.1	308.5	150.1	19
Jing-12-01-81	829.7	11.4	832.5	10.3	840.2	22.6	19
Jing-12-01-82	827.0	22.9	844.0	21.8	889.1	49.2	19
Jing-12-01-84	222.7	5.4	221.0	16.8	203.2	188.0	19
Jing-12-01-86	279.8	10.0	294.9	21.2	416.3	166.1	19
Jing-12-01-88	645.2	6.8	647.3	13.1	654.6	53.5	19
Jing-12-01-89	684.9	16.2	713.7	13.3	805.5	15.2	19
Jing-12-01-90	927.7	15.9	931.9	11.9	941.9	13.8	19
Jing-12-01-91	256.2	5.8	264.2	9.1	335.8	72.0	19
Jing-12-01-92	768.4	14.9	787.7	42.4	843.0	155.3	19
Jing-12-01-93	2004.4	23.8	1989.9	13.8	1974.8	13.5	19
Jing-12-01-94	142.7	3.1	130.4	13.0	-88.6	254.5	19
Jing-12-01-95	1010.0	37.2	1056.1	28.5	1152.5	34.8	19
Jing-12-01-96	1847.3	21.4	1847.0	11.7	1846.6	6.2	19
Jing-12-01-97	258.9	17.8	280.6	95.1	465.7	871.9	19
Jing-12-01-98	1811.5	26.3	1810.7	18.4	1809.7	25.5	19
Jing-12-01-Sl	571.4	7.4	569.1	7.7	559.6	24.8	19
Jing-12-05-01	437.7	13.6	455.5	37.0	546.4	209.3	18
Jing-12-05-03	311.8	8.5	318.8	9.1	370.3	41.6	18
Jing-12-05-05	388.7	2.5	396.6	3.0	443.0	14.2	18
Jing-12-05-06	214.4	7.6	220.4	9.6	285.6	74.0	18
Jing-12-05-07	241.5	4.5	240.6	11.5	232.1	116.5	18
Jing-12-05-08	808.3	22.0	817.5	17.0	842.7	17.8	18
Jing-12-05-09	843.3	18.8	844.6	16.7	848.1	34.6	18
Jing-12-05-100	277.5	13.1	288.4	15.4	377.5	85.4	18
Jing-12-05-102	237.4	4.0	232.8	12.2	186.4	130.3	18
Jing-12-05-103	1123.2	10.0	1111.5	11.1	1088.5	26.7	18
Jing-12-05-105	270.3	4.3	278.4	14.1	347.4	126.1	18
Jing-12-05-106	454.7	7.5	458.4	12.3	476.8	63.6	18
Jing-12-05-109	2504.7	48.5	2487.5	22.9	2473.5	13.3	18
Jing-12-05-11	714.3	15.6	721.9	23.7	745.4	84.1	18

Jing-12-05-110	272.1	3.1	268.5	10.5	237.3	99.2	18
Jing-12-05-111	19.7	2.6	-266.2	#NUM!	NA	NA	18
Jing-12-05-113	163.2	6.9	156.3	34.7	53.7	569.1	18
Jing-12-05-115	213.4	5.6	221.9	12.8	312.6	132.9	18
Jing-12-05-118	812.3	20.0	813.6	17.2	817.2	33.3	18
Jing-12-05-11B	1748.1	41.0	1800.5	23.4	1861.8	13.2	18
Jing-12-05-12	292.0	5.1	295.9	15.4	326.7	129.9	18
Jing-12-05-14	429.8	8.5	419.9	25.5	365.9	160.5	18
Jing-12-05-17	502.7	9.3	490.9	17.3	436.2	89.3	18
Jing-12-05-18	2062.5	77.6	2336.8	40.3	2585.9	4.5	18
Jing-12-05-19	226.4	8.5	231.2	11.1	280.2	85.8	18
Jing-12-05-22	579.0	10.8	579.2	25.3	579.8	117.2	18
Jing-12-05-23	666.2	35.2	724.3	48.9	908.4	157.0	18
Jing-12-05-24	501.4	21.8	562.9	21.1	819.9	38.3	18
Jing-12-05-28	183.7	3.3	184.6	11.7	195.3	155.7	18
Jing-12-05-30	1838.7	26.6	1953.1	14.7	2076.6	6.0	18
Jing-12-05-31	227.3	2.3	226.4	11.7	216.6	131.4	18
Jing-12-05-33	95.9	1.0	96.3	4.5	108.1	112.9	18
Jing-12-05-35	302.1	3.4	300.0	15.9	283.7	137.4	18
Jing-12-05-36	1881.1	23.0	2106.5	12.7	2334.5	4.3	18
Jing-12-05-38	78.5	3.2	71.1	28.7	-170.1	1078.3	18
Jing-12-05-39	513.8	9.8	515.9	12.5	525.4	52.2	18
Jing-12-05-40	173.2	2.6	177.1	6.4	229.7	83.4	18
Jing-12-05-41	432.3	6.8	439.1	10.7	474.9	56.0	18
Jing-12-05-44	437.3	6.8	418.0	20.5	313.1	131.1	18
Jing-12-05-45	225.5	4.7	224.8	15.1	217.7	166.5	18
Jing-12-05-47	359.3	17.2	416.3	65.9	745.7	397.1	18
Jing-12-05-49	1331.7	52.6	1366.0	34.1	1420.0	22.8	18
Jing-12-05-50	450.6	5.5	454.5	8.5	473.9	43.0	18
Jing-12-05-51	224.8	2.8	222.6	8.1	200.1	89.4	18
Jing-12-05-52	444.9	5.2	445.7	11.1	450.0	63.0	18
Jing-12-05-53	1852.8	147.3	1871.2	88.4	1891.6	86.1	18
Jing-12-05-54	963.1	10.0	961.3	19.0	957.1	58.2	18
Jing-12-05-56	219.0	5.1	216.7	8.4	192.2	83.7	18
Jing-12-05-57	1904.1	37.7	2174.6	20.6	2440.7	4.7	18
Jing-12-05-58	461.0	8.9	462.7	12.3	471.4	58.2	18
Jing-12-05-59	1564.0	45.6	1637.2	26.9	1732.5	6.8	18
Jing-12-05-60	223.6	9.7	227.3	26.7	266.7	284.1	18
Jing-12-05-61	313.2	24.1	337.9	25.0	511.4	82.2	18
Jing-12-05-63	168.2	7.1	184.8	37.3	402.4	489.4	18
Jing-12-05-66	403.4	6.6	405.2	7.6	415.4	34.1	18

Jing-12-05-67	199.2	5.5	199.2	11.8	199.3	137.7	18
Jing-12-05-68	842.0	21.2	923.1	16.5	1122.1	9.3	18
Jing-12-05-69	250.0	13.9	268.0	27.7	427.9	229.8	18
Jing-12-05-70	216.4	3.1	208.4	6.1	119.1	68.6	18
Jing-12-05-71	591.3	38.4	636.3	59.6	799.6	222.6	18
Jing-12-05-72	214.4	3.7	223.2	8.6	316.9	89.3	18
Jing-12-05-75	230.8	6.0	234.0	10.9	266.5	102.9	18
Jing-12-05-76	215.2	7.2	220.7	14.0	279.7	141.4	18
Jing-12-05-77	914.8	9.1	916.8	9.2	921.6	22.4	18
Jing-12-05-79	161.1	2.7	155.4	11.4	68.8	184.7	18
Jing-12-05-80	285.3	9.2	290.2	31.0	330.6	268.9	18
Jing-12-05-81	816.2	10.0	812.6	8.4	802.8	16.1	18
Jing-12-05-83	554.5	13.4	636.6	12.4	940.0	14.0	18
Jing-12-05-85	315.6	14.6	353.0	23.8	607.0	138.7	18
Jing-12-05-87	204.9	14.3	213.7	29.6	311.5	311.9	18
Jing-12-05-88	498.2	11.5	495.7	9.7	484.2	13.0	18
Jing-12-05-89	1856.7	43.5	1855.2	23.4	1853.5	9.1	18
Jing-12-05-90	389.3	11.9	383.7	19.7	349.5	119.8	18
Jing-12-05-91	152.4	2.8	155.7	5.7	205.9	81.5	18
Jing-12-05-92	1122.5	8.4	1108.9	14.7	1082.4	40.6	18
Jing-12-05-93	230.9	14.4	246.7	25.8	399.7	222.2	18
Jing-12-05-94	255.5	6.0	260.2	11.0	302.5	95.1	18
Jing-12-05-95	440.5	8.9	437.5	12.2	421.5	60.7	18
Jing-12-05-96	1218.6	31.8	1230.7	20.7	1251.9	8.9	18
Jing-12-05-97	1913.1	44.5	1894.8	23.3	1874.9	7.1	18
Jing-12-05-98	967.8	18.3	961.0	16.4	945.5	34.4	18
Jing-12-05-99	302.4	4.4	310.5	15.7	372.1	127.8	18
Jing-12-16-65	91.6	1.1	90.8	3.0	69.5	76.5	17
Jing-12-16-09	103.2	1.3	109.9	6.4	257.1	138.8	17
Jing-12-16-48	109.4	3.5	118.4	14.6	303.3	289.3	17
Jing-12-16-43	111.0	1.3	113.7	4.8	169.3	101.3	17
Jing-12-16-17.5	121.1	4.1	110.4	17.3	-114.8	401.3	17
Jing-12-16-95a	157.1	3.3	159.9	12.9	201.8	197.1	17
Jing-12-16-102	166.8	5.2	165.4	10.9	146.1	150.8	17
Jing-12-16-79	167.6	4.6	178.0	12.6	318.4	164.0	17
Jing-12-16-63	170.8	2.2	172.4	5.8	194.2	79.0	17
Jing-12-16-02	219.3	1.8	214.7	5.6	164.5	65.3	17
Jing-12-16-73	220.6	3.9	217.6	10.4	184.6	117.0	17
Jing-12-16-76	221.6	9.2	224.5	11.8	255.8	93.0	17
Jing-12-16-61	222.1	2.3	219.6	4.3	192.6	44.1	17

Jing-12-16-69	222.2	5.1	222.7	5.7	228.7	36.8	17
Jing-12-16-112	222.7	2.3	229.1	3.2	294.9	26.1	17
Jing-12-16-12	223.8	7.6	262.1	45.1	620.0	417.6	17
Jing-12-16-14	225.0	7.5	228.2	16.0	260.8	162.6	17
Jing-12-16-110	227.0	3.4	221.4	9.1	161.8	101.2	17
Jing-12-16-28	233.8	3.8	234.5	13.2	241.7	140.5	17
Jing-12-16-78	252.8	3.1	255.8	6.3	282.5	57.2	17
Jing-12-16-30	256.2	3.3	258.5	7.1	279.6	63.9	17
Jing-12-16-18	264.6	4.4	267.1	10.9	288.9	99.1	17
Jing-12-16-59	273.5	18.1	415.5	25.8	1306.5	66.7	17
Jing-12-16-52	277.7	3.5	259.1	13.2	94.1	132.9	17
Jing-12-16-85	281.3	15.6	306.3	16.9	501.4	65.4	17
Jing-12-16-62	286.4	3.5	278.6	21.7	213.8	204.4	17
Jing-12-16-68	287.7	4.3	302.2	10.8	415.7	85.9	17
Jing-12-16-38	303.5	6.6	300.2	14.9	274.4	120.9	17
Jing-12-16-44	316.1	5.3	319.2	6.6	342.1	37.9	17
Jing-12-16-41	319.3	13.3	303.4	53.8	182.4	471.3	17
Jing-12-16-95	323.6	6.4	341.6	9.9	465.6	61.1	17
Jing-12-16-60	328.0	12.2	331.3	13.3	354.5	62.3	17
Jing-12-16-64	330.3	16.7	330.4	48.3	331.2	371.8	17
Jing-12-16-42	339.4	5.0	331.1	13.2	273.1	101.0	17
Jing-12-16-57	351.0	13.1	399.5	13.9	691.0	36.1	17
Jing-12-16-55	360.9	7.6	362.0	14.0	368.6	91.8	17
Jing-12-16-25	396.8	23.9	557.7	29.9	1283.3	61.1	17
Jing-12-16-67	416.4	39.3	412.5	43.4	391.0	185.7	17
Jing-12-16-86	428.2	6.6	421.3	18.1	383.2	112.6	17
Jing-12-16-81	432.4	32.8	427.8	30.2	403.0	80.7	17
Jing-12-16-24	436.0	26.1	427.6	26.7	382.9	100.8	17
Jing-12-16-53	438.2	8.9	438.2	8.4	438.1	24.5	17
Jing-12-16-47	445.5	36.7	447.0	36.8	455.1	123.2	17
Jing-12-16-82	453.2	9.0	460.2	18.7	495.1	101.7	17
Jing-12-16-06	454.2	8.6	455.0	9.0	459.2	32.8	17
Jing-12-16-91	455.0	5.1	468.0	15.4	531.9	86.3	17
Jing-12-16-46	483.5	15.5	481.5	14.1	472.3	33.9	17
Jing-12-16-107	518.7	15.9	524.3	38.3	549.0	192.5	17
Jing-12-16-104	548.5	44.6	639.5	41.7	975.6	46.1	17
Jing-12-16-10	607.1	14.3	618.0	19.6	658.1	73.9	17
Jing-12-16-01	631.8	26.0	673.0	24.4	813.4	50.9	17
Jing-12-16-77	714.0	11.0	718.0	9.3	730.4	16.8	17
Jing-12-16-58	770.2	6.9	771.2	7.6	774.3	21.6	17
Jing-12-16-99	774.2	10.6	772.1	9.5	766.1	20.4	17

Jing-12-16-23	774.2	9.2	796.3	26.0	858.5	94.3	17
Jing-12-16-33	925.5	19.2	927.1	22.3	931.0	59.7	17
Jing-12-16-07	955.5	8.2	953.6	16.9	949.3	52.5	17
Jing-12-16-16	859.9	47.8	888.0	36.1	958.7	28.1	17
Jing-12-16-88	909.2	39.9	925.6	29.0	964.8	15.1	17
Jing-12-16-17	844.5	27.7	878.6	27.3	965.6	62.4	17
Jing-12-16-20	1002.9	9.6	1003.9	8.7	1006.2	18.2	17
Jing-12-16-08	960.7	53.3	985.5	42.0	1041.1	59.1	17
Jing-12-16-15	1090.9	48.9	1075.8	40.5	1045.5	74.3	17
Jing-12-16-11	1105.9	25.2	1098.4	17.1	1083.6	11.3	17
Jing-12-16-71	851.2	16.7	919.6	13.1	1087.4	11.2	17
Jing-12-16-56	1166.7	21.3	1169.0	20.5	1173.2	43.2	17
Jing-12-16-109	1065.1	19.6	1218.4	14.6	1501.2	9.5	17
Jing-12-16-90	1534.1	17.0	1605.0	10.4	1699.3	5.6	17
Jing-12-16-74	1347.1	27.8	1497.4	23.8	1717.3	36.8	17
Jing-12-16-22	1618.3	29.9	1713.2	23.8	1831.1	35.7	17
Jing-12-16-75	1867.5	18.4	1865.0	10.4	1862.3	7.9	17
Jing-12-16-29	1881.1	56.1	1876.0	29.9	1870.3	11.7	17
Jing-12-16-98	1923.5	30.2	1898.6	16.7	1871.4	12.3	17
Jing-12-16-50	1870.0	43.7	1873.9	23.1	1878.3	4.4	17
Jing-12-16-03	1895.7	14.3	1891.3	10.2	1886.5	14.6	17
Jing-12-16-87	2119.9	32.9	2299.0	16.6	2462.1	2.4	17
Jing-12-16-49	2264.3	14.4	2376.1	7.0	2473.5	2.4	17
Jing-12-16-13	2558.0	35.6	2542.0	23.3	2529.1	31.0	17
Jing-12-16-89	2556.4	26.3	2552.7	12.0	2549.7	5.2	17
Jing-12-24-01	161.4	4.9	146.0	16.9	-96.9	297.4	16
Jing-12-24-03	894.5	10.3	910.0	9.1	947.7	17.8	16
Jing-12-24-04	219.8	1.2	219.4	4.3	214.6	48.5	16
Jing-12-24-06	468.5	8.5	473.7	12.3	498.8	58.5	16
Jing-12-24-07	2456.7	20.5	2609.3	10.3	2729.9	7.4	16
Jing-12-24-09	232.9	19.6	262.2	48.8	533.1	425.2	16
Jing-12-24-10	548.8	28.9	546.3	23.7	535.5	24.2	16
Jing-12-24-100	394.4	31.5	479.9	44.6	912.7	170.2	16
Jing-12-24-101	2511.3	33.4	2515.6	15.5	2519.1	7.4	16
Jing-12-24-102	1864.9	19.0	1855.5	12.3	1845.0	15.1	16
Jing-12-24-103	329.7	7.8	326.1	19.0	300.7	145.5	16
Jing-12-24-104	445.3	7.1	425.8	32.6	321.9	210.0	16
Jing-12-24-105	967.6	31.8	964.4	22.7	957.1	17.9	16
Jing-12-24-11	852.2	44.8	876.4	37.4	938.2	61.2	16
Jing-12-24-12	984.1	23.7	975.3	17.7	955.3	22.9	16

Jing-12-24-14	965.7	11.4	966.9	19.8	969.6	59.5	16
Jing-12-24-15	431.9	24.0	474.6	22.7	686.9	37.1	16
Jing-12-24-16	1898.8	50.6	1885.9	28.6	1871.6	23.4	16
Jing-12-24-17	1768.2	26.8	1836.7	14.9	1915.2	4.3	16
Jing-12-24-18	272.8	5.9	294.0	12.6	465.7	98.1	16
Jing-12-24-19	994.2	24.1	995.4	17.4	997.9	16.1	16
Jing-12-24-21	160.6	4.6	165.6	11.4	236.4	158.9	16
Jing-12-24-22	988.6	23.9	983.2	19.9	971.1	36.4	16
Jing-12-24-23	156.7	2.9	156.1	6.2	146.5	90.8	16
Jing-12-24-25	402.1	12.7	401.2	17.6	396.1	93.7	16
Jing-12-24-26	255.8	10.2	227.3	43.6	-58.1	517.0	16
Jing-12-24-27	263.4	6.1	261.4	17.2	243.1	163.0	16
Jing-12-24-28	223.4	5.6	233.5	10.1	336.6	93.3	16
Jing-12-24-29	227.1	3.3	229.0	8.4	248.2	88.0	16
Jing-12-24-30	222.5	3.9	222.9	21.7	226.8	247.4	16
Jing-12-24-32	224.5	4.9	221.0	10.2	183.6	107.9	16
Jing-12-24-33	490.5	17.0	574.4	22.3	922.2	74.1	16
Jing-12-24-34	436.2	9.6	458.7	25.5	573.1	142.1	16
Jing-12-24-35	848.0	25.0	881.4	19.6	966.0	22.2	16
Jing-12-24-36	2238.5	62.7	2240.4	30.4	2242.2	9.8	16
Jing-12-24-37	710.4	17.0	710.3	40.6	710.1	160.1	16
Jing-12-24-38	223.0	4.4	218.5	11.0	170.4	122.4	16
Jing-12-24-39	2041.7	25.1	2092.9	14.8	2143.6	14.9	16
Jing-12-24-40	2573.7	45.5	2561.3	21.2	2551.5	12.6	16
Jing-12-24-41	222.4	9.3	224.8	11.2	250.5	81.7	16
Jing-12-24-42	874.8	47.6	879.3	40.4	890.8	75.1	16
Jing-12-24-43	2493.5	99.5	2514.8	45.7	2531.9	16.6	16
Jing-12-24-44	1911.5	34.4	1895.4	18.1	1877.7	6.6	16
Jing-12-24-47	797.3	13.5	804.5	15.3	824.5	43.2	16
Jing-12-24-48	911.0	40.6	921.2	31.5	945.7	42.3	16
Jing-12-24-49	291.8	4.5	294.4	9.2	315.4	73.8	16
Jing-12-24-50	219.1	2.8	227.8	5.1	318.2	48.7	16
Jing-12-24-51	223.0	5.5	232.1	11.4	326.2	111.0	16
Jing-12-24-52	2171.5	79.3	2316.8	39.3	2447.4	4.4	16
Jing-12-24-54	2413.2	38.3	2527.7	29.4	2621.0	41.9	16
Jing-12-24-55	760.1	49.4	786.0	39.6	860.1	44.9	16
Jing-12-24-56	458.8	12.3	462.8	19.5	482.6	98.5	16
Jing-12-24-57	249.5	5.7	252.1	7.9	276.6	61.1	16
Jing-12-24-59	1112.0	26.6	1133.9	46.1	1176.1	123.1	16
Jing-12-24-60	1055.3	40.9	1060.5	29.1	1071.3	28.0	16
Jing-12-24-61	222.3	4.8	221.6	10.6	213.1	112.9	16

Jing-12-24-62	218.9	4.0	217.7	6.5	204.7	64.6	16
Jing-12-24-63	753.9	39.9	788.4	31.3	887.5	21.8	16
Jing-12-24-64	106.3	1.8	91.9	10.7	-266.6	305.5	16
Jing-12-24-65	895.8	7.8	897.9	14.1	902.9	45.0	16
Jing-12-24-66	116.1	4.4	112.4	23.3	33.8	522.4	16
Jing-12-24-67	454.7	10.4	454.0	11.1	450.8	42.1	16
Jing-12-24-68	248.8	4.0	259.8	12.8	360.4	120.5	16
Jing-12-24-69	2043.6	41.2	2253.4	21.5	2449.8	4.8	16
Jing-12-24-70	532.4	9.4	538.7	19.8	565.4	95.3	16
Jing-12-24-71	2135.5	167.3	2272.2	88.7	2397.7	55.2	16
Jing-12-24-72	113.5	3.1	113.7	5.2	118.0	93.4	16
Jing-12-24-73	443.4	6.8	449.4	12.4	480.4	66.8	16
Jing-12-24-74	562.4	8.6	564.3	7.6	571.6	15.7	16
Jing-12-24-75	248.7	6.9	247.3	12.4	233.6	113.1	16
Jing-12-24-76	1825.7	47.5	1851.2	25.9	1880.0	10.2	16
Jing-12-24-78	231.7	5.5	223.1	10.8	133.4	112.6	16
Jing-12-24-80	259.3	8.9	253.6	31.4	201.9	315.5	16
Jing-12-24-83	244.9	7.3	246.6	16.1	263.5	154.2	16
Jing-12-24-84	264.3	5.1	258.8	14.1	209.7	135.9	16
Jing-12-24-85	2454.9	37.8	2471.0	17.4	2484.3	5.4	16
Jing-12-24-87	230.1	4.3	261.5	46.8	553.3	445.1	16
Jing-12-24-88	2358.6	48.6	2421.7	24.2	2475.2	15.2	16
Jing-12-24-89	1686.9	88.4	1766.9	50.0	1862.8	7.0	16
Jing-12-24-91	430.0	8.8	430.3	16.9	432.1	96.2	16
Jing-12-24-92	260.3	6.1	256.4	11.4	220.6	102.0	16
Jing-12-24-93	1856.6	36.5	1918.3	20.0	1985.8	9.5	16
Jing-12-24-94	527.4	30.7	695.4	31.8	1285.1	34.9	16
Jing-12-24-96	563.4	15.8	552.5	16.2	507.6	53.6	16
Jing-12-24-98	2121.3	38.5	2148.9	19.8	2175.4	10.8	16
Jing-12-24-99	704.0	27.0	733.0	21.4	822.8	14.0	16
Jing-12-25-91	154.5	12.2	185.8	54.3	604.9	683.8	15
Jing-12-25-82	157.2	1.6	157.5	4.8	161.9	72.9	15
Jing-12-25-73	211.6	5.3	208.7	9.9	175.8	106.8	15
Jing-12-25-72	212.1	6.1	223.8	9.4	348.7	82.3	15
Jing-12-25-74	212.2	6.5	206.1	19.9	137.6	240.6	15
Jing-12-25-89	215.4	5.1	229.3	23.1	374.2	247.7	15
Jing-12-25-111	215.8	3.8	210.3	13.3	149.4	158.5	15
Jing-12-25-16	216.5	4.6	216.3	18.3	214.0	212.2	15
Jing-12-25-64	217.0	4.6	219.9	7.3	251.5	68.6	15
Jing-12-25-116	217.1	1.5	219.9	8.9	250.8	102.2	15

Jing-12-25-54	217.3	3.0	216.1	6.0	202.6	63.9	15
Jing-12-25-128	217.7	2.3	217.2	9.8	212.3	113.3	15
Jing-12-25-17	218.0	3.9	219.5	4.9	235.9	37.9	15
Jing-12-25-98	218.4	3.2	216.6	6.0	196.3	62.7	15
Jing-12-25-120	219.4	2.4	223.1	11.7	262.4	131.6	15
Jing-12-25-24	220.4	8.5	231.8	11.2	349.7	83.6	15
Jing-12-25-100	220.4	3.9	221.3	5.6	230.3	50.0	15
Jing-12-25-76	220.8	6.2	219.5	14.0	205.5	150.5	15
Jing-12-25-22	220.9	3.8	232.9	12.7	355.9	132.5	15
Jing-12-25-11	221.3	1.8	224.3	9.2	256.0	103.5	15
Jing-12-25-21	221.4	5.4	225.4	7.9	268.0	69.9	15
Jing-12-25-12	221.8	8.0	216.4	20.3	158.9	229.0	15
Jing-12-25-109	222.0	1.5	224.7	5.6	252.6	61.5	15
Jing-12-25-122	222.1	3.7	222.4	6.1	225.3	58.9	15
Jing-12-25-138	222.5	4.8	221.8	10.5	214.3	110.7	15
Jing-12-25-90	223.0	2.5	219.1	10.1	176.6	116.9	15
Jing-12-25-81	223.9	2.1	219.8	9.0	175.9	103.3	15
Jing-12-25-25	225.6	4.0	220.0	7.4	160.3	77.4	15
Jing-12-25-41	225.6	2.7	224.0	4.0	206.9	36.3	15
Jing-12-25-19	226.7	7.7	222.4	8.3	177.7	54.2	15
Jing-12-25-45	227.4	3.2	227.4	4.0	227.7	31.5	15
Jing-12-25-139	227.8	8.1	245.3	17.3	416.5	158.3	15
Jing-12-25-39	228.6	1.9	232.2	7.1	267.8	76.4	15
Jing-12-25-97	229.2	5.0	234.4	15.1	286.9	157.3	15
Jing-12-25-57	229.4	6.3	228.3	6.7	217.1	40.0	15
Jing-12-25-70	231.7	5.6	230.0	14.5	213.2	153.5	15
Jing-12-25-124	232.3	17.3	259.5	32.3	513.6	261.8	15
Jing-12-25-52	237.7	6.6	238.6	9.0	247.1	72.3	15
Jing-12-25-117	248.7	5.2	252.4	7.2	287.4	55.0	15
Jing-12-25-63	259.5	9.1	282.6	29.7	477.9	255.1	15
Jing-12-25-58	263.5	4.1	265.5	15.3	283.2	145.8	15
Jing-12-25-79	333.7	14.1	319.8	16.7	219.7	98.7	15
Jing-12-25-106	340.2	11.7	318.8	68.5	165.0	586.3	15
Jing-12-25-51	349.0	33.8	411.5	39.3	779.1	125.7	15
Jing-12-25-59	366.6	7.2	366.1	8.8	363.2	46.3	15
Jing-12-25-130	376.1	18.1	384.8	19.8	437.2	82.7	15
Jing-12-25-43	409.5	32.9	433.5	30.7	563.2	58.5	15
Jing-12-25-125	412.7	6.3	413.3	8.3	416.4	41.3	15
Jing-12-25-66	416.3	30.3	511.7	31.8	964.6	50.9	15
Jing-12-25-01	437.8	8.8	441.8	37.4	462.9	227.4	15
Jing-12-25-112	441.6	11.1	442.2	12.3	445.1	50.0	15

Jing-12-25-62	442.2	8.5	436.5	11.9	406.7	60.5	15
Jing-12-25-136	443.0	11.3	448.2	11.0	474.8	32.3	15
Jing-12-25-47	444.7	10.6	457.8	18.0	524.0	92.1	15
Jing-12-25-103	446.4	8.0	450.8	9.5	473.3	40.3	15
Jing-12-25-61	452.7	10.1	464.5	10.9	523.5	39.8	15
Jing-12-25-134	474.9	14.0	474.8	12.5	474.4	26.2	15
Jing-12-25-37	476.9	7.4	471.3	12.0	443.7	61.2	15
Jing-12-25-53	494.5	9.5	490.5	16.0	472.0	80.0	15
Jing-12-25-86	536.0	11.5	598.5	12.8	843.0	36.0	15
Jing-12-25-44	542.9	18.4	588.6	19.0	769.0	49.3	15
Jing-12-25-14	571.7	10.4	604.6	9.0	730.0	11.7	15
Jing-12-25-35	590.7	16.3	634.2	18.8	792.6	57.2	15
Jing-12-25-129	601.3	7.0	613.1	5.9	657.0	9.6	15
Jing-12-25-110	690.8	19.6	740.6	16.5	894.3	19.6	15
Jing-12-25-113	727.2	35.5	759.6	33.2	856.1	71.2	15
Jing-12-25-32	739.1	44.1	800.0	35.5	973.5	23.0	15
Jing-12-25-08	766.8	11.5	767.9	24.7	771.1	90.5	15
Jing-12-25-18	790.9	21.9	783.1	29.2	760.9	94.5	15
Jing-12-25-26	796.7	64.8	845.7	51.3	976.5	45.1	15
Jing-12-25-31	808.9	38.9	824.2	31.3	865.5	44.0	15
Jing-12-25-68	857.7	19.6	885.8	16.7	956.8	29.2	15
Jing-12-25-42	956.6	29.4	958.1	21.3	961.6	18.1	15
Jing-12-25-33	972.0	12.4	974.8	9.1	981.0	9.4	15
Jing-12-25-133	990.7	15.8	996.1	13.5	1007.9	25.2	15
Jing-12-25-29	793.9	34.4	853.6	29.1	1012.2	41.5	15
Jing-12-25-34	821.1	17.5	878.2	13.8	1024.9	12.9	15
Jing-12-25-99	979.3	21.2	995.6	18.2	1031.8	33.5	15
Jing-12-25-40	1001.8	11.3	1011.7	16.5	1033.2	46.0	15
Jing-12-25-48	890.6	26.0	939.9	19.4	1057.6	9.7	15
Jing-12-25-07	1053.7	18.3	1062.1	15.6	1079.4	28.6	15
Jing-12-25-107	1078.8	35.9	1084.2	25.1	1095.0	20.8	15
Jing-12-25-132	872.8	43.5	941.8	33.4	1106.9	21.8	15
Jing-12-25-02	1121.5	16.1	1139.4	13.2	1173.8	22.0	15
Jing-12-25-71	1064.4	42.3	1101.1	33.2	1174.4	48.0	15
Jing-12-25-10	851.6	19.7	952.0	15.9	1192.1	13.6	15
Jing-12-25-09	1244.6	17.8	1248.9	12.2	1256.4	12.6	15
Jing-12-25-105	1175.8	28.1	1232.1	25.3	1332.2	46.3	15
Jing-12-25-06	1488.8	18.6	1523.4	11.1	1571.9	2.3	15
Jing-12-25-13	1882.9	42.6	1869.1	26.5	1853.8	30.3	15
Jing-12-25-05	1817.7	15.9	1845.6	8.8	1877.2	4.4	15
Jing-12-25-88	2001.4	26.8	1974.0	14.5	1945.5	10.4	15

Jing-12-25-131	1753.4	53.7	1918.9	30.3	2102.8	5.1	15
Jing-12-25-55	1667.9	40.5	1925.9	30.2	2216.4	37.4	15
Jing-12-25-101	1825.9	41.0	2050.6	22.9	2284.9	6.0	15
Jing-12-25-114	2137.7	83.5	2289.9	41.9	2428.6	6.3	15
Jing-12-25-137	2117.5	89.4	2294.9	45.4	2456.9	10.0	15
Jing-12-25-83	2492.3	16.5	2512.4	8.8	2528.8	8.7	15
Jing-12-25-28	2353.7	129.5	2453.9	60.8	2538.1	3.6	15
Jing-12-25-36	2364.9	116.6	2481.7	55.4	2578.7	15.9	15
Jing-12-25-03	2516.1	84.4	2579.9	38.4	2630.3	11.2	15
Jing-12-25-65	2865.6	19.0	2859.2	10.1	2854.7	10.9	15
Jing-13-01-01	427.3	38.8	451.4	34.5	576.1	26.1	20
Jing-13-01-02	439.1	9.1	418.1	74.4	303.6	496.5	20
Jing-13-01-03	451.0	12.8	503.4	16.3	749.2	60.1	20
Jing-13-01-04	178.8	2.7	177.6	9.6	161.6	133.4	20
Jing-13-01-05	1908.2	26.1	1895.9	14.1	1882.5	8.1	20
Jing-13-01-06	501.9	5.6	505.7	6.2	522.8	22.2	20
Jing-13-01-07	572.9	20.4	663.6	22.7	985.3	56.9	20
Jing-13-01-08	570.8	12.4	610.4	25.9	760.2	109.0	20
Jing-13-01-09	1434.6	24.4	1482.5	16.3	1551.7	16.3	20
Jing-13-01-10	1078.6	33.7	1087.4	24.5	1105.2	28.0	20
Jing-13-01-12	376.6	15.2	375.8	13.4	371.2	20.0	20
Jing-13-01-13	1681.3	84.6	1708.0	47.5	1741.0	10.2	20
Jing-13-01-14	869.4	56.9	907.2	42.2	1000.3	13.9	20
Jing-13-01-16	2572.4	56.8	2538.9	25.1	2512.2	4.8	20
Jing-13-01-17	178.8	4.9	179.9	7.3	193.5	80.4	20
Jing-13-01-18	266.9	8.9	268.1	16.1	278.3	136.2	20
Jing-13-01-19	451.5	10.3	451.5	13.1	451.4	60.4	20
Jing-13-01-20	1002.2	19.1	995.1	13.6	979.3	11.4	20
Jing-13-01-22	2544.6	27.8	2532.6	15.3	2522.9	16.4	20
Jing-13-01-24	122.6	6.1	116.5	18.7	-7.9	394.0	20
Jing-13-01-25	222.7	5.5	223.2	9.1	228.3	86.8	20
Jing-13-01-27	1812.9	28.5	1844.9	15.9	1881.3	8.7	20
Jing-13-01-29	219.4	4.4	221.5	12.0	245.0	130.8	20
Jing-13-01-30	176.5	5.7	122.1	44.0	-841.3	1121.4	20
Jing-13-01-32	988.1	14.6	988.5	11.4	989.4	16.8	20
Jing-13-01-33	484.6	12.9	482.1	11.7	470.6	28.4	20
Jing-13-01-34	115.3	2.0	116.6	7.2	143.0	148.6	20
Jing-13-01-36	276.5	3.2	277.7	12.5	287.7	114.9	20
Jing-13-01-37	288.5	4.0	284.8	9.7	254.3	83.2	20
Jing-13-01-38	221.1	3.9	223.1	8.0	243.9	82.8	20

Jing-13-01-39	434.6	20.6	460.1	100.1	589.0	584.5	20
Jing-13-01-40	312.9	8.1	338.1	10.1	515.5	51.1	20
Jing-13-01-42	162.2	2.8	155.0	11.8	46.4	192.0	20
Jing-13-01-43	184.2	6.7	175.0	27.1	53.2	395.1	20
Jing-13-01-44	2161.7	45.1	2314.4	23.3	2452.0	11.7	20
Jing-13-01-45	1762.5	78.2	1737.7	43.6	1707.9	24.0	20
Jing-13-01-46	156.4	3.8	158.5	20.0	190.4	313.6	20
Jing-13-01-48	1755.4	101.6	1814.8	56.2	1883.8	10.4	20
Jing-13-01-49	211.8	3.8	213.9	6.3	237.7	62.4	20
Jing-13-01-50	435.0	9.0	564.8	18.9	1129.3	75.8	20
Jing-13-01-51	1432.6	45.3	1490.5	27.8	1573.8	8.1	20
Jing-13-01-52	226.5	7.1	229.5	14.2	260.1	140.9	20
Jing-13-01-53	370.6	6.6	375.4	9.2	404.8	51.5	20
Jing-13-01-54	254.4	4.3	254.7	8.3	258.0	75.2	20
Jing-13-01-55	106.2	2.4	108.7	9.0	162.5	197.2	20
Jing-13-01-56	175.9	6.0	173.6	14.3	142.0	194.2	20
Jing-13-01-57	251.1	4.8	252.6	7.3	267.1	60.6	20
Jing-13-01-58	276.0	4.8	279.7	6.5	311.4	44.8	20
Jing-13-01-59	330.0	6.4	318.6	13.8	236.3	106.9	20
Jing-13-01-60	861.2	25.7	863.4	49.2	868.9	162.3	20
Jing-13-01-61	223.0	2.9	220.5	8.4	193.2	93.8	20
Jing-13-01-64	2543.2	50.4	2530.3	22.6	2519.9	5.6	20
Jing-13-01-65	1505.5	26.9	1520.5	16.9	1541.3	14.3	20
Jing-13-01-66	261.4	4.7	262.4	11.0	271.0	100.7	20
Jing-13-01-67	454.6	10.7	455.4	14.8	459.3	71.3	20
Jing-13-01-68	272.5	4.7	273.1	10.3	278.4	90.3	20
Jing-13-01-69	207.4	4.3	210.5	8.4	244.8	89.8	20
Jing-13-01-70	332.3	4.6	339.2	19.2	387.1	146.3	20
Jing-13-01-71	468.5	13.5	465.9	13.5	453.1	45.4	20
Jing-13-01-72	1869.9	10.3	1870.6	5.6	1871.3	2.5	20
Jing-13-01-73	239.8	13.0	247.3	19.4	319.1	156.4	20
Jing-13-01-74	433.9	9.9	447.1	31.9	515.2	187.0	20
Jing-13-01-75	296.1	8.1	289.9	12.6	239.9	95.1	20
Jing-13-01-77	117.9	4.0	111.4	16.0	-25.9	360.2	20
Jing-13-01-78	223.5	2.2	217.7	10.6	155.6	125.0	20
Jing-13-01-80	150.4	6.5	153.9	9.7	207.8	121.3	20
Jing-13-01-81	231.3	12.1	238.2	13.1	307.0	71.3	20
Jing-13-01-82	1917.8	53.1	1898.7	27.7	1877.8	6.9	20
Jing-13-01-83	438.9	7.5	443.4	22.7	466.5	134.7	20
Jing-13-01-84	533.1	4.2	544.2	6.3	590.7	27.1	20
Jing-13-01-85	168.1	2.9	172.5	14.0	233.4	200.6	20

166

Jing-13-01-86	329.1	6.2	332.6	13.5	356.5	98.5	20
Jing-13-01-87	2052.3	38.8	2255.4	21.9	2445.1	16.9	20
Jing-13-01-88	1891.5	24.3	1880.1	17.8	1867.6	26.3	20
Jing-13-01-89	2060.6	24.3	2083.0	12.3	2105.1	2.9	20
Jing-13-01-91	432.2	6.7	437.0	10.5	462.1	55.1	20
Lan-11-01-02	1788.6	68.7	1776.6	37.4	1762.5	13.2	37
Lan-11-01-03	445.6	10.6	444.1	11.0	436.3	40.1	37
Lan-11-01-05	304.7	21.3	306.6	40.6	321.1	309.8	37
Lan-11-01-06	288.6	10.6	299.1	10.7	382.2	37.5	37
Lan-11-01-07	263.9	4.6	275.8	11.9	377.4	103.5	37
Lan-11-01-08	461.5	11.4	494.6	23.4	650.8	115.8	37
Lan-11-01-10	78.5	2.8	70.6	8.7	-187.4	307.0	37
Lan-11-01-12	852.8	37.8	853.6	29.4	855.8	39.6	37
Lan-11-01-13	1383.8	90.2	1599.8	76.8	1897.1	111.2	37
Lan-11-01-14	1719.6	15.4	1733.8	9.3	1750.9	8.4	37
Lan-11-01-15	1768.5	59.0	1749.7	32.6	1727.5	15.7	37
Lan-11-01-16	1581.4	127.1	1701.7	85.9	1853.2	91.6	37
Lan-11-01-20	443.3	11.2	445.0	12.4	454.0	50.0	37
Lan-11-01-21	221.6	2.8	219.4	7.2	195.5	79.0	37
Lan-11-01-22	412.0	5.5	425.9	9.1	501.8	49.1	37
Lan-11-01-26	77.4	4.9	85.4	17.0	315.1	452.2	37
Lan-11-01-27	244.2	7.5	252.1	10.1	325.6	73.6	37
Lan-11-01-29	300.9	9.6	304.9	10.3	335.7	48.1	37
Lan-11-01-30	220.3	5.0	220.6	6.0	224.0	45.1	37
Lan-11-01-31	232.7	1.7	235.3	9.1	261.6	97.7	37
Lan-11-01-32	793.6	15.9	799.1	18.0	814.3	51.3	37
Lan-11-01-33	2209.8	35.4	2220.5	20.3	2230.4	21.1	37
Lan-11-01-34	316.3	2.2	320.4	4.9	350.5	37.1	37
Lan-11-01-35	112.5	1.6	113.4	2.4	133.3	38.9	37
Lan-11-01-36	715.7	56.0	752.1	45.1	862.2	40.1	37
Lan-11-01-37	2373.8	108.2	2439.8	50.5	2495.3	7.8	37
Lan-11-01-38	420.1	4.5	419.1	10.3	413.6	62.1	37
Lan-11-01-39	255.4	7.3	261.1	13.0	311.8	110.1	37
Lan-11-01-40	423.7	6.9	406.9	21.8	312.3	143.0	37
Lan-11-01-41	220.0	3.4	220.4	5.5	224.9	53.0	37
Lan-11-01-42	449.0	9.6	457.7	15.2	501.8	76.5	37
Lan-11-01-43	793.3	35.6	789.3	26.9	778.1	22.5	37
Lan-11-01-46	187.2	14.5	237.2	28.2	766.7	227.1	37
Lan-11-01-47	173.3	2.6	168.3	21.9	99.7	334.1	37
Lan-11-01-49	834.3	31.7	865.3	30.5	945.7	67.8	37

Lan-11-01-50	223.7	3.6	223.5	12.7	221.4	142.0	37
Lan-11-01-51	1766.6	27.8	1805.7	16.1	1851.1	11.6	37
Lan-11-01-52	2638.1	50.1	2641.3	22.0	2643.7	6.2	37
Lan-11-01-53	288.4	9.3	283.0	73.5	238.4	694.1	37
Lan-11-01-54	2518.1	18.5	2507.6	8.6	2499.2	4.3	37
Lan-11-01-55	122.4	2.3	126.3	11.8	200.0	227.6	37
Lan-11-01-56	234.6	8.4	231.3	13.0	197.9	119.0	37
Lan-11-01-58	755.8	5.9	757.5	13.6	762.7	50.6	37
Lan-11-01-59	239.8	3.0	241.9	4.9	262.4	43.3	37
Lan-11-01-60	1057.6	9.1	1063.6	8.2	1076.2	16.4	37
Lan-11-01-62	195.4	7.9	204.8	12.0	314.7	114.4	37
Lan-11-01-63	1126.3	10.2	1124.4	9.4	1120.7	19.3	37
Lan-11-01-64	217.1	6.0	230.8	18.2	373.0	188.2	37
Lan-11-01-65	310.9	3.5	312.2	6.6	321.8	49.4	37
Lan-11-01-66	2198.1	18.0	2157.6	10.1	2119.3	10.4	37
Lan-11-01-67	903.7	28.4	908.3	21.7	919.4	26.9	37
Lan-11-01-68	173.1	3.6	186.9	11.3	365.1	141.0	37
Lan-11-02-43	105.9	4.2	109.3	13.2	185.5	283.0	36
Lan-11-02-85	106.7	3.9	106.6	8.7	104.9	183.6	36
Lan-11-02-51	111.4	4.8	122.3	14.1	339.1	259.5	36
Lan-11-02-58	137.2	5.8	125.3	23.4	-93.7	479.5	36
Lan-11-02-33	212.0	13.7	223.5	21.5	346.3	191.6	36
Lan-11-02-80	212.3	4.6	216.9	9.8	266.5	104.2	36
Lan-11-02-42	213.6	4.2	210.5	6.1	175.4	59.2	36
Lan-11-02-02	217.9	8.6	224.3	16.1	291.6	158.5	36
Lan-11-02-96	223.3	3.6	227.5	7.2	271.0	72.0	36
Lan-11-02-89	223.8	13.7	236.2	21.5	361.5	182.1	36
Lan-11-02-13	225.6	13.9	238.9	30.7	371.4	293.4	36
Lan-11-02-91	225.7	5.4	234.4	11.3	322.8	109.6	36
Lan-11-02-77	226.1	10.2	234.4	27.2	318.6	277.4	36
Lan-11-02-57	230.1	4.7	232.4	5.9	255.8	44.3	36
Lan-11-02-30	233.1	4.6	228.5	14.3	182.0	156.1	36
Lan-11-02-64	235.4	7.8	216.0	30.3	9.3	367.4	36
Lan-11-02-84	237.3	3.4	246.4	10.4	333.7	103.1	36
Lan-11-02-45	253.3	3.4	249.5	10.4	213.6	104.6	36
Lan-11-02-90	254.7	3.4	245.1	7.0	153.8	68.5	36
Lan-11-02-21	260.1	16.1	266.7	19.4	325.2	120.7	36
Lan-11-02-106	261.5	5.4	260.6	7.6	251.7	58.4	36
Lan-11-02-103	263.4	7.6	275.9	22.4	383.6	198.1	36
Lan-11-02-14	269.5	5.6	265.8	12.9	233.6	117.6	36

Lan-11-02-107	270.5	4.2	276.5	17.8	328.2	163.1	36
Lan-11-02-75	271.1	4.4	265.5	8.2	216.7	71.9	36
Lan-11-02-04	276.0	5.6	276.8	8.4	283.7	63.8	36
Lan-11-02-55	276.3	2.9	274.7	8.2	261.3	73.9	36
Lan-11-02-10	276.5	3.8	280.5	14.3	313.7	128.9	36
Lan-11-02-65	309.9	4.6	313.4	8.1	339.6	58.4	36
Lan-11-02-59	337.3	8.2	338.4	13.0	346.0	84.9	36
Lan-11-02-38	343.2	9.3	372.3	25.6	557.8	168.9	36
Lan-11-02-34	367.2	4.8	354.8	15.0	274.3	110.6	36
Lan-11-02-100	390.6	20.9	414.9	58.2	552.4	354.5	36
Lan-11-02-16	401.3	6.5	398.1	25.5	379.5	170.4	36
Lan-11-02-03	423.3	8.3	430.9	28.7	471.9	175.6	36
Lan-11-02-08	435.3	3.4	424.6	11.4	366.4	71.8	36
Lan-11-02-104	438.5	4.4	438.7	6.5	440.1	33.0	36
Lan-11-02-05	442.5	6.5	442.7	8.3	444.1	39.1	36
Lan-11-02-81	442.6	7.1	446.7	10.9	467.7	55.9	36
Lan-11-02-18	443.0	9.0	453.1	15.3	504.4	79.9	36
Lan-11-02-26	444.9	8.6	447.1	20.8	458.6	119.6	36
Lan-11-02-112	452.6	16.6	445.3	22.1	408.1	107.8	36
Lan-11-02-79	459.2	7.9	459.1	11.7	458.2	57.8	36
Lan-11-02-63	520.3	8.2	506.7	13.6	445.5	66.7	36
Lan-11-02-105	593.6	23.0	665.9	20.7	918.9	24.9	36
Lan-11-02-19	700.0	35.8	727.5	29.0	813.1	29.4	36
Lan-11-02-23	700.3	26.0	741.5	32.3	867.8	97.8	36
Lan-11-02-32	714.8	44.0	779.2	35.7	968.4	15.8	36
Lan-11-02-61	716.5	21.6	719.1	27.3	727.1	89.9	36
Lan-11-02-108	749.8	26.7	753.4	27.7	763.9	75.4	36
Lan-11-02-83	788.6	8.5	785.4	12.6	776.4	41.9	36
Lan-11-02-22	826.8	18.0	838.3	25.4	869.1	78.9	36
Lan-11-02-62	848.5	17.4	844.1	44.0	832.5	153.6	36
Lan-11-02-68	938.8	22.4	929.4	16.1	907.1	13.4	36
Lan-11-02-74	891.7	28.7	897.7	20.8	912.2	11.7	36
Lan-11-02-67	934.4	9.0	930.8	10.3	922.2	27.5	36
Lan-11-02-49	951.4	24.1	944.3	55.1	927.9	175.3	36
Lan-11-02-87	882.3	35.4	899.4	39.8	941.7	104.4	36
Lan-11-02-48	918.3	13.4	926.0	15.4	944.4	40.9	36
Lan-11-02-70	975.5	13.9	974.8	10.0	973.3	9.0	36
Lan-11-02-07	986.1	20.7	986.5	22.9	987.4	57.8	36
Lan-11-02-35	985.6	12.3	1006.2	9.5	1051.2	12.9	36
Lan-11-02-110	1736.0	17.6	1729.8	10.3	1722.3	8.1	36
Lan-11-02-72	1786.9	26.5	1777.6	14.9	1766.6	9.8	36

Lan-11-02-17	1625.5	38.3	1688.3	24.8	1767.2	25.6	36
Lan-11-02-111	1662.6	82.8	1734.6	83.8	1822.7	151.2	36
Lan-11-02-78	1774.4	57.5	1801.4	31.4	1832.9	6.7	36
Lan-11-02-76	1833.6	32.2	1838.7	17.3	1844.4	4.3	36
Lan-11-02-82	1873.5	14.4	1866.2	9.3	1858.1	11.5	36
Lan-11-02-15	1751.5	9.5	1806.9	5.8	1871.3	5.5	36
Lan-11-02-69	1813.9	51.0	1842.6	27.6	1875.2	6.0	36
Lan-11-02-56	1888.8	13.0	1883.1	7.2	1876.8	4.8	36
Lan-11-02-09	1897.7	36.9	1891.2	19.6	1884.1	7.6	36
Lan-11-02-60	1861.8	12.7	1874.7	7.1	1889.0	4.7	36
Lan-11-02-27	2094.2	18.1	2088.0	9.1	2081.8	3.0	36
Lan-11-02-114	2193.7	37.8	2169.9	18.5	2147.5	6.1	36
Lan-11-02-11	1631.6	122.2	1875.7	78.4	2157.9	59.9	36
Lan-11-02-113	2301.1	14.4	2270.3	8.1	2242.7	8.5	36
Lan-11-02-31	2455.0	32.5	2462.9	15.1	2469.4	6.3	36
Lan-11-02-12	2470.8	43.2	2475.4	20.2	2479.2	9.8	36
Lan-11-02-39	2417.1	18.7	2465.2	8.9	2505.2	4.4	36
Lan-11-02-28	2557.6	38.8	2534.3	17.4	2515.7	5.1	36
Lan-11-02-50	2533.6	34.2	2535.5	15.9	2537.0	8.1	36
Lan-11-02-52	2568.0	29.4	2553.0	14.8	2541.2	12.7	36
Lan-11-02-20	3063.8	20.4	3043.7	20.8	3030.4	31.8	36
Lan-11-02-102	3028.1	43.1	3074.6	18.4	3105.1	10.5	36
Lan-11-04-02	858.4	8.5	869.4	23.2	897.6	79.0	35
Lan-11-04-03	1919.3	46.3	1897.3	24.2	1873.3	7.1	35
Lan-11-04-05	229.7	2.7	234.1	3.9	279.3	32.0	35
Lan-11-04-06	1727.2	33.4	1714.2	38.7	1698.5	76.0	35
Lan-11-04-07	353.9	26.5	343.2	34.8	271.6	209.8	35
Lan-11-04-102	236.5	9.3	238.4	25.4	257.5	259.1	35
Lan-11-04-103	1555.8	28.8	1681.1	17.6	1841.2	8.7	35
Lan-11-04-104	2113.7	30.8	2087.1	16.9	2060.9	14.8	35
Lan-11-04-106	717.9	20.3	733.0	40.1	779.6	148.6	35
Lan-11-04-107	479.8	8.4	462.4	19.8	376.7	112.5	35
Lan-11-04-109	110.0	8.0	93.7	19.0	-304.6	513.5	35
Lan-11-04-110	238.9	4.0	240.5	10.5	256.7	105.3	35
Lan-11-04-111	258.0	5.5	247.6	19.3	150.2	199.7	35
Lan-11-04-112	827.2	9.6	821.3	11.7	805.2	34.9	35
Lan-11-04-113	258.8	7.7	255.6	9.7	226.1	70.4	35
Lan-11-04-115	776.7	13.1	772.6	12.7	760.7	31.7	35
Lan-11-04-117	281.7	17.6	329.2	33.4	680.7	214.3	35
Lan-11-04-118	241.5	4.7	245.9	10.9	288.4	105.0	35

Lan-11-04-119	262.5	3.5	262.9	9.0	266.7	83.5	35
Lan-11-04-12	445.5	13.2	449.6	15.4	470.7	65.0	35
Lan-11-04-120	1861.8	57.9	1871.3	30.7	1881.9	4.1	35
Lan-11-04-121	474.2	13.0	477.2	26.4	491.7	139.4	35
Lan-11-04-122	1880.1	34.8	1885.8	18.5	1892.1	6.3	35
Lan-11-04-123	1752.6	45.0	1756.8	26.3	1761.7	21.1	35
Lan-11-04-126	239.1	3.2	237.5	6.0	221.7	58.2	35
Lan-11-04-127	918.4	21.0	916.8	19.6	912.7	43.7	35
Lan-11-04-129	208.3	5.6	210.8	8.5	238.5	82.0	35
Lan-11-04-13	124.0	1.5	116.2	12.8	-42.1	283.5	35
Lan-11-04-130	1296.6	34.7	1299.9	26.2	1305.3	39.3	35
Lan-11-04-131	212.4	4.8	210.6	19.6	191.3	234.2	35
Lan-11-04-135	366.9	8.0	390.2	30.5	530.8	200.3	35
Lan-11-04-14	1919.4	26.9	1904.7	15.3	1888.8	13.5	35
Lan-11-04-15	258.2	4.4	261.5	7.3	290.9	61.1	35
Lan-11-04-17	2061.0	115.0	2235.0	65.9	2398.3	55.4	35
Lan-11-04-18	122.4	2.3	119.7	9.6	65.6	196.7	35
Lan-11-04-21	462.2	5.3	442.1	30.5	338.7	191.2	35
Lan-11-04-22	245.7	7.4	246.9	9.6	258.0	72.1	35
Lan-11-04-23	222.2	7.2	220.8	10.8	205.8	100.4	35
Lan-11-04-26	1815.2	26.9	1837.7	15.0	1863.3	8.9	35
Lan-11-04-27	261.2	20.6	256.3	60.1	211.6	593.7	35
Lan-11-04-33	417.0	9.7	414.9	9.2	403.5	27.5	35
Lan-11-04-35	242.5	10.0	239.4	19.6	209.1	189.6	35
Lan-11-04-40	2344.3	48.1	2334.4	22.8	2325.7	8.1	35
Lan-11-04-41	1101.3	27.6	1098.0	18.6	1091.4	9.9	35
Lan-11-04-44	573.5	27.2	630.4	25.1	840.5	41.3	35
Lan-11-04-48	1412.2	34.5	1423.4	21.0	1440.3	6.3	35
Lan-11-04-49	451.6	5.4	451.7	6.0	452.0	24.3	35
Lan-11-04-51	1787.9	30.8	1773.1	29.3	1755.7	52.7	35
Lan-11-04-52	224.4	3.6	216.6	12.2	133.5	141.9	35
Lan-11-04-53	422.7	10.0	419.6	11.2	402.8	48.1	35
Lan-11-04-54	952.0	25.9	948.4	20.8	940.0	34.2	35
Lan-11-04-57	216.5	6.7	220.1	19.7	259.2	216.9	35
Lan-11-04-58	247.4	4.0	242.8	8.4	199.1	81.7	35
Lan-11-04-59	172.9	3.3	164.1	16.4	38.8	256.2	35
Lan-11-04-60	269.3	3.6	267.6	6.2	252.3	51.5	35
Lan-11-04-61	902.1	21.9	907.4	17.4	920.1	26.4	35
Lan-11-04-62	447.0	16.3	456.7	21.8	505.9	100.7	35
Lan-11-04-64	2329.3	48.8	2430.4	23.3	2516.2	6.4	35
Lan-11-04-66	1880.4	21.3	1893.0	18.3	1906.8	30.3	35

Lan-11-04-67	1677.1	33.7	1731.5	23.1	1797.8	28.7	35
Lan-11-04-68	227.3	4.0	224.9	12.9	199.8	143.0	35
Lan-11-04-70	323.2	7.7	319.4	14.4	291.3	106.8	35
Lan-11-04-71	224.6	3.5	225.8	10.1	238.3	109.4	35
Lan-11-04-72	251.5	2.8	257.1	6.9	308.3	64.4	35
Lan-11-04-73	1808.7	24.2	1815.3	21.2	1823.0	36.1	35
Lan-11-04-74	917.4	27.1	915.0	22.2	909.3	38.4	35
Lan-11-04-75	797.9	40.5	843.8	44.6	966.6	114.6	35
Lan-11-04-76	435.6	5.1	434.6	10.4	429.4	60.1	35
Lan-11-04-77	2492.9	21.6	2503.5	11.8	2512.1	12.3	35
Lan-11-04-78	214.5	7.8	216.6	9.1	239.7	64.3	35
Lan-11-04-79	316.7	8.9	284.0	47.4	22.2	457.5	35
Lan-11-04-80	234.8	4.0	228.8	9.1	168.0	95.5	35
Lan-11-04-82	1766.6	14.2	1769.2	9.3	1772.3	11.6	35
Lan-11-04-83	1011.9	12.2	1011.0	10.0	1009.1	17.5	35
Lan-11-04-84	300.4	12.5	285.1	37.0	161.0	335.2	35
Lan-11-04-86	157.2	10.4	142.5	34.3	-96.2	619.5	35
Lan-11-04-87	450.3	12.2	452.6	19.8	464.4	102.5	35
Lan-11-04-89	217.6	3.8	219.7	6.9	241.7	69.8	35
Lan-11-04-91	953.9	38.2	946.4	28.9	928.9	38.1	35
Lan-11-04-92	298.2	8.5	297.6	14.5	292.4	109.8	35
Lan-11-04-94	271.4	10.7	271.5	21.7	272.2	187.8	35
Lan-11-04-96	936.6	9.7	931.9	8.5	921.0	17.5	35
Lan-11-04-97	247.8	10.5	246.0	21.3	228.2	202.7	35
Lan-11-04-99	1003.1	15.0	993.8	17.2	973.5	44.7	35
Lij-12-01-01	440.8	2.8	450.7	9.1	501.5	53.3	14
Lij-12-01-02	228.4	10.9	238.3	31.2	337.3	314.9	14
Lij-12-01-05	253.7	2.3	251.1	6.2	226.1	60.2	14
Lij-12-01-07	1773.4	11.6	1772.2	9.4	1770.7	15.4	14
Lij-12-01-08	1743.5	78.0	1827.2	43.3	1924.0	3.1	14
Lij-12-01-09	248.9	12.3	264.6	20.5	406.1	161.5	14
Lij-12-01-10	986.0	7.4	984.6	10.5	981.4	29.8	14
Lij-12-01-100	236.5	2.7	243.1	6.7	307.5	65.4	14
Lij-12-01-101	1862.8	43.2	1875.5	22.9	1889.6	3.7	14
Lij-12-01-102	815.5	9.7	813.5	14.4	808.1	46.7	14
Lij-12-01-103	289.6	3.9	297.4	12.2	359.0	101.9	14
Lij-12-01-105	1807.2	21.1	1821.2	23.1	1837.3	43.1	14
Lij-12-01-12	395.2	8.3	408.7	21.7	485.6	134.3	14
Lij-12-01-14	1714.4	35.1	1781.5	19.8	1861.1	5.9	14
Lij-12-01-15	300.2	4.2	305.8	12.1	348.9	98.8	14

Lij-12-01-16	855.5	19.7	851.6	18.0	841.4	39.8	14
Lij-12-01-17	425.2	7.7	429.0	8.1	449.6	30.6	14
Lij-12-01-18	899.9	45.1	908.8	33.3	930.5	28.2	14
Lij-12-01-19	250.7	6.5	335.2	21.1	972.8	140.5	14
Lij-12-01-20	934.6	13.3	933.0	13.2	929.4	31.3	14
Lij-12-01-22	1252.8	57.1	1240.5	40.0	1219.3	48.6	14
Lij-12-01-23	764.9	7.6	763.9	17.1	760.9	63.6	14
Lij-12-01-26	2521.7	42.2	2505.1	19.1	2491.6	6.2	14
Lij-12-01-27	261.3	4.5	267.3	17.2	320.2	161.8	14
Lij-12-01-29	1869.5	45.1	1866.9	23.8	1863.9	3.7	14
Lij-12-01-30	878.3	9.0	888.1	8.9	912.7	21.3	14
Lij-12-01-31	417.4	9.7	425.9	25.0	472.3	149.7	14
Lij-12-01-32	445.4	7.4	446.8	8.4	454.5	35.0	14
Lij-12-01-33	243.8	3.6	245.2	12.2	258.8	124.2	14
Lij-12-01-34	718.8	14.3	739.1	34.5	801.0	130.3	14
Lij-12-01-35	761.1	52.3	779.8	40.3	833.4	28.7	14
Lij-12-01-36	239.1	5.8	241.7	11.8	266.8	112.7	14
Lij-12-01-37	346.6	4.5	350.0	14.8	372.9	108.3	14
Lij-12-01-38	2391.4	55.0	2531.1	26.1	2645.1	8.6	14
Lij-12-01-39	174.6	5.8	163.9	27.5	10.8	432.7	14
Lij-12-01-40	59.9	0.7	62.1	4.0	148.2	154.1	14
Lij-12-01-41	541.2	8.5	529.2	33.9	477.4	178.4	14
Lij-12-01-42	1437.2	23.0	1451.1	14.9	1471.6	13.5	14
Lij-12-01-43	234.0	4.0	228.6	12.2	173.3	133.5	14
Lij-12-01-44	1130.6	17.3	1126.4	13.9	1118.5	23.7	14
Lij-12-01-45	241.2	10.2	243.1	26.7	261.2	266.9	14
Lij-12-01-46	207.3	13.0	262.4	51.1	788.9	448.5	14
Lij-12-01-47	212.1	2.6	215.3	8.2	250.2	92.4	14
Lij-12-01-48	1106.5	15.6	1101.1	10.5	1090.4	5.6	14
Lij-12-01-49	248.0	3.5	234.8	18.0	104.1	200.7	14
Lij-12-01-50	1619.6	25.6	1617.2	14.9	1614.0	8.0	14
Lij-12-01-51	2401.9	44.6	2442.3	21.1	2476.1	8.3	14
Lij-12-01-52	2579.9	77.3	2603.2	34.5	2621.4	9.8	14
Lij-12-01-53	1057.8	21.2	1051.4	17.9	1038.0	33.3	14
Lij-12-01-55	247.8	4.1	257.8	9.9	349.9	90.5	14
Lij-12-01-57	2981.8	61.0	3157.6	25.2	3271.3	6.9	14
Lij-12-01-58	244.0	3.2	241.7	11.4	219.8	118.5	14
Lij-12-01-59	792.5	9.3	803.2	8.0	833.0	15.3	14
Lij-12-01-60	1687.1	30.7	1701.8	17.4	1719.9	7.5	14
Lij-12-01-61	1689.6	9.7	1757.7	5.7	1839.6	3.8	14
Lij-12-01-62	774.5	21.9	780.0	38.7	795.7	135.3	14

Lij-12-01-63	251.3	2.8	252.0	4.4	258.7	37.4	14
Lij-12-01-64	256.8	10.9	289.6	19.1	564.1	136.0	14
Lij-12-01-65	433.9	2.1	438.2	6.5	460.6	38.7	14
Lij-12-01-66	636.9	15.4	649.0	17.5	691.3	55.8	14
Lij-12-01-67	250.6	4.0	271.7	47.0	457.9	439.0	14
Lij-12-01-69	220.9	3.0	221.6	13.0	229.0	147.9	14
Lij-12-01-70	567.4	11.0	569.6	9.7	578.4	19.8	14
Lij-12-01-71	215.5	2.5	216.9	7.5	231.5	84.3	14
Lij-12-01-72	823.5	4.0	824.0	4.6	825.1	13.3	14
Lij-12-01-73	829.3	3.0	829.1	3.9	828.6	11.7	14
Lij-12-01-74	423.9	6.1	421.7	11.1	410.0	63.4	14
Lij-12-01-75	1988.3	17.2	2068.0	9.8	2148.5	8.1	14
Lij-12-01-76	792.8	18.7	821.2	35.9	898.9	121.0	14
Lij-12-01-77	289.7	13.1	270.2	27.3	105.0	249.4	14
Lij-12-01-78	1910.6	15.0	1901.5	9.5	1891.6	11.3	14
Lij-12-01-79	234.2	3.2	231.1	6.5	200.3	65.1	14
Lij-12-01-81	870.1	16.7	880.6	39.7	907.0	132.3	14
Lij-12-01-82	412.7	5.8	419.2	16.7	455.0	102.9	14
Lij-12-01-83	2551.3	44.5	2563.7	20.6	2573.5	10.7	14
Lij-12-01-85	248.1	11.5	239.4	50.3	155.5	547.2	14
Lij-12-01-86	465.9	9.2	466.7	29.9	470.7	171.0	14
Lij-12-01-87	255.2	5.5	242.8	42.1	125.4	459.0	14
Lij-12-01-88	62.1	2.1	68.7	10.2	303.1	343.7	14
Lij-12-01-89	219.3	4.9	221.8	16.2	247.7	180.1	14
Lij-12-01-90	442.1	14.6	452.0	18.7	502.8	84.2	14
Lij-12-01-91	1937.2	19.1	1966.8	11.0	1998.0	9.5	14
Lij-12-01-92	717.4	9.1	743.9	8.0	824.6	14.2	14
Lij-12-01-93	838.9	22.5	838.8	27.9	838.5	82.7	14
Lij-12-01-94	259.7	10.8	273.1	23.0	389.6	194.1	14
Lij-12-01-95	820.8	12.4	831.8	14.1	861.3	39.4	14
Lij-12-01-96	254.4	3.9	242.4	18.9	127.1	202.8	14
Lij-12-01-97	486.4	11.0	502.7	26.0	577.7	133.2	14
Lij-12-01-99	390.2	8.6	382.2	26.8	333.7	183.8	14
Lij-12-01-S06	1910.2	18.5	1907.6	13.2	1904.7	18.8	14
Lim-12-05-1	219.4	11.3	229.4	13.3	333.0	86.3	3
Lim-12-05-10	327.9	5.6	331.8	17.2	358.8	131.2	3
Lim-12-05-100	444.0	23.4	443.8	20.6	442.6	39.3	3
Lim-12-05-101	419.1	5.8	423.7	19.0	448.8	117.9	3
Lim-12-05-102	411.5	4.0	415.3	8.3	436.5	49.7	3
Lim-12-05-103	423.8	15.8	417.4	24.8	382.7	138.4	3

Lim-12-05-104	317.0	12.2	282.6	58.8	6.7	571.6	3
Lim-12-05-105	214.8	2.5	213.1	10.2	194.5	120.1	3
Lim-12-05-107	1847.4	34.9	1877.0	19.2	1909.9	9.9	3
Lim-12-05-108	245.6	4.5	256.9	11.9	360.9	110.1	3
Lim-12-05-109	341.7	7.1	341.1	16.9	337.4	123.1	3
Lim-12-05-11	233.1	5.1	237.5	14.0	281.7	142.4	3
Lim-12-05-110	458.0	13.1	455.6	12.4	443.8	35.8	3
Lim-12-05-111	787.1	45.2	792.2	33.7	806.5	11.5	3
Lim-12-05-112	126.3	2.3	130.6	3.5	209.6	51.8	3
Lim-12-05-113	422.3	6.8	423.3	8.1	428.3	37.2	3
Lim-12-05-115	837.5	11.9	837.2	9.1	836.3	10.7	3
Lim-12-05-116	417.8	5.9	418.5	10.0	422.7	56.1	3
Lim-12-05-117	258.5	5.3	250.7	13.9	178.4	137.9	3
Lim-12-05-118	1029.4	7.1	1020.2	8.2	1000.5	20.9	3
Lim-12-05-119	441.0	4.6	432.9	12.2	390.2	73.6	3
Lim-12-05-12	779.8	15.9	793.4	17.6	831.9	48.9	3
Lim-12-05-120	248.8	2.9	242.2	9.4	178.3	97.3	3
Lim-12-05-121	250.9	4.4	262.3	8.9	365.8	77.1	3
Lim-12-05-122	934.5	16.4	924.7	12.6	901.2	17.9	3
Lim-12-05-124	264.7	3.8	246.7	15.8	78.5	167.3	3
Lim-12-05-125	1169.8	28.6	1159.8	44.6	1141.1	116.7	3
Lim-12-05-126	246.4	3.1	247.3	9.2	256.4	91.4	3
Lim-12-05-127	1801.6	29.5	1814.8	49.6	1830.0	100.7	3
Lim-12-05-128	1875.2	22.1	1862.7	13.8	1848.8	15.8	3
Lim-12-05-13	2435.0	19.7	2430.4	10.5	2426.5	9.9	3
Lim-12-05-130	1922.5	15.7	1904.7	8.4	1885.3	4.7	3
Lim-12-05-131	421.3	12.1	420.0	16.3	413.2	82.4	3
Lim-12-05-132	215.3	5.6	218.5	8.6	253.0	80.5	3
Lim-12-05-133	216.8	8.6	213.4	16.0	175.9	170.2	3
Lim-12-05-134	434.3	16.7	435.4	18.0	441.4	70.6	3
Lim-12-05-135	221.7	3.1	220.4	19.8	206.4	230.0	3
Lim-12-05-136	743.8	15.4	763.4	15.9	821.1	41.7	3
Lim-12-05-14	3192.9	57.2	3143.8	22.1	3112.6	3.4	3
Lim-12-05-15	949.4	21.5	962.8	21.5	993.6	49.6	3
Lim-12-05-16	449.8	7.6	445.2	11.6	421.7	60.3	3
Lim-12-05-17	824.9	13.6	830.0	20.3	843.7	65.1	3
Lim-12-05-18	279.9	6.6	277.1	19.8	253.5	179.3	3
Lim-12-05-19	253.7	4.3	237.2	24.8	76.1	276.2	3
Lim-12-05-21	482.0	14.2	557.3	13.5	878.1	14.8	3
Lim-12-05-22	864.0	9.0	864.5	9.2	865.6	23.4	3
Lim-12-05-24	999.7	16.7	995.7	12.5	986.9	16.5	3

Lim-12-05-25	840.3	9.5	838.7	16.4	834.3	54.4	3
Lim-12-05-26	197.9	3.2	210.1	10.4	349.2	117.9	3
Lim-12-05-27	255.2	9.1	258.8	21.2	291.5	195.1	3
Lim-12-05-28	264.2	10.1	271.9	14.9	338.6	109.8	3
Lim-12-05-29	551.9	9.5	550.7	9.6	545.8	29.9	3
Lim-12-05-3	275.4	8.6	300.6	29.1	500.9	236.4	3
Lim-12-05-30	229.7	6.3	227.2	11.3	201.2	111.9	3
Lim-12-05-31	263.0	5.8	259.6	11.5	229.2	104.2	3
Lim-12-05-32	2258.4	23.6	2309.9	13.0	2355.8	12.3	3
Lim-12-05-33	1756.9	27.1	1775.0	15.0	1796.3	6.0	3
Lim-12-05-34	2207.7	39.8	2302.6	21.1	2388.0	15.7	3
Lim-12-05-35	476.2	12.5	467.1	27.4	422.4	151.5	3
Lim-12-05-36	1991.0	28.2	1957.0	14.7	1921.1	7.0	3
Lim-12-05-37	249.2	2.4	248.5	8.5	242.5	86.1	3
Lim-12-05-38	873.4	30.9	866.3	23.9	848.2	33.4	3
Lim-12-05-39	2651.2	28.5	2592.2	13.4	2546.3	9.4	3
Lim-12-05-4	297.5	4.5	284.6	22.6	179.8	209.2	3
Lim-12-05-40	1044.2	14.0	1040.4	16.3	1032.3	41.0	3
Lim-12-05-42	901.3	13.2	895.6	18.5	881.6	55.5	3
Lim-12-05-43	836.9	12.1	829.5	20.4	809.7	68.0	3
Lim-12-05-44	1881.5	31.4	1857.4	25.0	1830.5	40.1	3
Lim-12-05-45	906.8	23.7	899.5	31.3	881.6	91.6	3
Lim-12-05-46	225.6	5.4	219.9	11.8	159.8	127.5	3
Lim-12-05-47	1132.3	17.7	1261.4	19.1	1489.0	38.3	3
Lim-12-05-48	390.0	8.3	307.1	47.4	-283.1	455.2	3
Lim-12-05-49	1498.2	75.6	1585.4	47.4	1703.3	30.9	3
Lim-12-05-5	462.0	4.2	471.7	15.5	519.2	87.6	3
Lim-12-05-50	221.5	5.2	223.1	8.5	239.2	81.1	3
Lim-12-05-51	464.9	4.5	469.6	21.1	492.7	121.6	3
Lim-12-05-53	837.9	10.4	831.3	15.8	813.7	51.2	3
Lim-12-05-54	2243.3	31.6	2223.8	16.7	2205.8	13.9	3
Lim-12-05-55	1067.5	10.5	1057.4	8.0	1036.6	11.7	3
Lim-12-05-56	435.8	5.7	437.5	11.6	446.7	66.0	3
Lim-12-05-57	443.4	6.5	445.5	8.4	456.7	38.7	3
Lim-12-05-58	1631.0	17.6	1631.6	15.5	1632.3	27.2	3
Lim-12-05-59	2497.7	46.0	2464.0	21.7	2436.3	12.7	3
Lim-12-05-6	691.6	18.9	723.6	16.8	824.1	31.8	3
Lim-12-05-60	844.9	12.9	840.7	11.2	829.6	22.4	3
Lim-12-05-61	226.0	3.3	231.5	6.5	288.1	62.8	3
Lim-12-05-62	213.2	7.6	229.1	15.0	395.6	143.2	3
Lim-12-05-63	245.4	3.1	247.7	14.5	270.1	148.3	3

Lim-12-05-64	967.3	13.4	968.4	23.1	970.9	69.0	3
Lim-12-05-65	231.0	5.5	229.4	10.6	212.9	105.2	3
Lim-12-05-66	241.1	5.7	249.7	15.5	331.5	149.8	3
Lim-12-05-67	221.2	11.7	229.9	15.9	319.5	125.6	3
Lim-12-05-68	434.3	9.7	445.3	16.7	502.7	88.8	3
Lim-12-05-69	249.2	4.3	245.2	18.3	207.1	191.0	3
Lim-12-05-70	232.0	2.2	232.6	5.1	238.6	51.9	3
Lim-12-05-72	779.2	4.2	782.9	5.6	793.4	18.0	3
Lim-12-05-73	214.5	3.0	212.8	6.9	194.1	77.4	3
Lim-12-05-74	467.4	11.2	508.4	15.3	697.3	61.8	3
Lim-12-05-75	222.4	4.2	210.6	15.7	80.9	191.0	3
Lim-12-05-76	247.1	4.3	247.7	13.5	253.0	135.6	3
Lim-12-05-77	928.2	18.4	928.1	13.6	927.9	14.3	3
Lim-12-05-78	820.3	13.9	824.4	11.3	835.6	17.8	3
Lim-12-05-8	1750.5	17.7	1766.1	12.6	1784.7	17.6	3
Lim-12-05-80	433.2	8.9	435.6	27.4	448.6	165.2	3
Lim-12-05-81	1929.6	17.0	1911.9	8.9	1892.7	2.7	3
Lim-12-05-82	224.9	3.0	226.2	8.3	239.8	89.0	3
Lim-12-05-83	426.9	9.3	434.9	22.9	477.5	134.2	3
Lim-12-05-85	1872.4	19.0	1877.5	14.1	1883.1	21.0	3
Lim-12-05-86	2453.4	55.4	2473.2	25.6	2489.5	8.3	3
Lim-12-05-87	913.4	18.2	910.5	16.6	903.5	36.2	3
Lim-12-05-88	257.5	8.6	255.4	36.6	235.8	367.1	3
Lim-12-05-89	2611.9	41.9	2713.2	22.2	2789.6	21.3	3
Lim-12-05-9	773.6	17.7	792.0	15.0	844.2	25.9	3
Lim-12-05-90	1261.3	23.6	1416.7	19.7	1658.7	28.5	3
Lim-12-05-92	415.1	4.4	420.8	7.5	452.5	41.8	3
Lim-12-05-93	229.6	3.3	227.9	14.9	210.5	166.5	3
Lim-12-05-95	783.0	7.3	794.7	10.6	827.5	34.5	3
Lim-12-05-98	477.5	23.8	511.6	21.7	667.0	33.4	3
Lim-12-05-99	540.2	2.6	535.8	7.6	516.9	38.8	3
Lim-12-05-99B	264.4	5.9	268.7	15.9	306.4	144.9	3
Lim-12-26-100	218.5	6.1	202.2	17.5	15.0	219.6	2
Lim-12-26-99	219.8	5.1	216.2	10.6	177.0	114.8	2
Lim-12-26-97	220.7	3.3	226.0	9.0	280.7	95.6	2
Lim-12-26-47	224.7	1.9	229.1	7.2	274.9	78.3	2
Lim-12-26-94	227.0	7.4	231.3	11.3	275.2	99.0	2
Lim-12-26-68	229.1	5.2	212.9	8.5	37.3	90.1	2
Lim-12-26-63	238.2	8.8	243.7	14.7	297.1	128.8	2
Lim-12-26-82	241.6	2.6	242.7	5.1	253.3	47.9	2

Lim-12-26-01	246.6	9.8	175.7	63.7	-698.5	1123.7	2
Lim-12-26-112	246.9	3.2	248.7	6.1	266.5	56.2	2
Lim-12-26-67	249.2	4.6	236.8	13.5	116.2	143.6	2
Lim-12-26-32	249.2	5.2	243.3	7.5	186.0	63.2	2
Lim-12-26-90	249.4	3.5	251.1	10.7	267.2	104.7	2
Lim-12-26-13	251.3	4.9	260.0	7.7	339.1	61.0	2
Lim-12-26-17	251.3	3.3	253.1	6.3	269.9	56.4	2
Lim-12-26-79	253.1	5.4	255.0	8.4	273.2	68.7	2
Lim-12-26-88	253.1	6.1	247.3	12.8	192.9	123.0	2
Lim-12-26-70	253.3	3.1	253.4	12.4	254.8	123.5	2
Lim-12-26-14	253.9	9.5	249.8	11.4	211.0	79.6	2
Lim-12-26-74	254.5	3.3	248.9	10.3	196.0	104.5	2
Lim-12-26-73	255.1	6.6	259.4	23.7	298.8	229.3	2
Lim-12-26-07	258.0	6.1	266.6	12.3	343.1	105.6	2
Lim-12-26-28	258.8	2.5	255.8	17.2	227.8	174.7	2
Lim-12-26-66	259.9	2.9	257.1	11.7	231.7	115.8	2
Lim-12-26-49	260.4	7.0	267.8	16.3	333.4	144.0	2
Lim-12-26-16	263.5	1.8	264.6	8.6	274.3	82.9	2
Lim-12-26-77	264.2	4.9	262.7	10.8	249.4	98.2	2
Lim-12-26-76	265.7	6.0	265.1	12.0	259.6	105.4	2
Lim-12-26-44	266.1	20.7	344.7	71.5	914.9	481.4	2
Lim-12-26-110	272.2	4.4	273.0	7.0	280.5	54.8	2
Lim-12-26-20	274.8	4.9	274.0	6.2	267.4	42.4	2
Lim-12-26-48	280.6	5.8	279.9	9.3	273.8	72.1	2
Lim-12-26-54	281.1	6.4	276.8	39.4	240.5	372.9	2
Lim-12-26-85	283.3	2.9	297.1	10.0	407.1	83.4	2
Lim-12-26-04	288.5	7.0	280.1	20.8	210.4	188.6	2
Lim-12-26-21	293.9	3.6	293.9	6.0	294.0	45.3	2
Lim-12-26-39	310.8	3.4	308.2	7.3	289.3	57.0	2
Lim-12-26-78	311.6	9.4	321.2	16.7	390.8	117.3	2
Lim-12-26-26	316.6	2.3	323.5	4.2	373.1	29.4	2
Lim-12-26-83	336.9	10.3	346.4	18.1	410.4	119.1	2
Lim-12-26-35	338.3	5.8	324.0	20.2	221.9	163.8	2
Lim-12-26-24	391.2	11.1	399.4	21.0	446.7	125.3	2
Lim-12-26-57	406.7	4.8	400.8	6.9	366.5	38.7	2
Lim-12-26-05	430.2	5.3	439.2	8.9	487.0	47.1	2
Lim-12-26-69	437.8	3.4	450.8	10.6	517.7	61.3	2
Lim-12-26-72	448.8	8.0	472.9	28.8	591.8	160.6	2
Lim-12-26-71	450.2	14.3	450.3	17.0	450.8	74.0	2
Lim-12-26-75	451.9	20.3	444.7	20.1	407.8	69.1	2
Lim-12-26-87	460.5	4.8	443.3	13.9	354.5	84.0	2

Lim-12-26-34	461.2	7.5	460.4	10.4	456.5	50.1	2
Lim-12-26-55	462.7	6.9	459.6	13.0	443.7	70.2	2
Lim-12-26-91	471.7	11.8	481.3	14.5	527.0	60.5	2
Lim-12-26-107	478.0	6.7	471.8	15.8	442.2	87.4	2
Lim-12-26-02	498.8	6.9	506.3	6.7	540.2	19.0	2
Lim-12-26-109	546.8	18.5	561.5	18.6	621.7	53.2	2
Lim-12-26-40	623.1	11.6	647.9	15.0	735.4	51.6	2
Lim-12-26-62	671.2	21.4	695.0	17.3	772.6	15.8	2
Lim-12-26-93	712.6	57.9	756.3	46.9	887.9	39.3	2
Lim-12-26-56	712.6	16.2	735.7	19.4	806.5	58.9	2
Lim-12-26-81	712.9	21.7	778.8	17.7	972.7	10.4	2
Lim-12-26-03	775.5	5.6	773.9	6.8	769.4	21.1	2
Lim-12-26-11	782.3	40.4	822.0	31.3	930.8	19.4	2
Lim-12-26-92	825.8	11.1	815.9	18.1	789.0	60.8	2
Lim-12-26-95	848.1	24.6	846.0	20.2	840.3	34.7	2
Lim-12-26-27	861.9	7.6	857.4	10.5	845.5	32.1	2
Lim-12-26-59	919.2	25.1	915.3	18.3	905.9	15.8	2
Lim-12-26-61	985.2	15.7	985.4	11.4	986.0	11.5	2
Lim-12-26-105	1031.0	64.9	1018.1	46.4	990.5	48.1	2
Lim-12-26-19	1005.5	17.2	1000.9	13.5	991.0	20.7	2
Lim-12-26-101	990.5	14.7	991.4	10.3	993.5	6.3	2
Lim-12-26-23	892.8	17.3	924.7	13.5	1001.5	16.8	2
Lim-12-26-80	1031.3	9.2	1031.5	7.7	1031.8	14.2	2
Lim-12-26-111	1025.9	21.1	1028.9	19.9	1035.2	42.7	2
Lim-12-26-12	1078.0	35.1	1069.2	23.7	1051.4	11.8	2
Lim-12-26-96	1122.8	19.1	1117.6	12.9	1107.5	8.9	2
Lim-12-26-98	1169.5	21.2	1184.5	14.2	1212.0	9.3	2
Lim-12-26-50	1385.4	24.3	1446.2	16.3	1536.6	15.7	2
Lim-12-26-103	1862.6	32.5	1867.3	17.8	1872.6	9.8	2
Lim-12-26-30	1900.2	48.4	1897.1	25.7	1893.6	10.5	2
Lim-12-26-09	1873.0	26.0	1884.9	13.9	1897.9	4.3	2
Lim-12-26-51	1959.5	25.0	1933.7	12.9	1906.2	4.0	2
Lim-12-26-106	578.8	36.3	1072.4	45.6	2285.2	36.2	2
Lim-12-26-108	2286.8	43.5	2292.5	20.7	2297.6	4.7	2
Lim-12-26-53	2236.4	66.0	2430.2	32.3	2596.7	2.7	2
Lim-12-26-15	3304.7	80.4	3435.9	30.5	3513.3	1.9	2
Lim-12-42-02	1308.1	13.8	1333.0	11.3	1373.1	19.0	1
Lim-12-42-03	437.7	8.8	442.9	7.8	469.8	13.2	1
Lim-12-42-04	767.7	11.3	767.2	11.0	765.7	27.9	1
Lim-12-42-05	442.6	15.2	443.4	31.7	447.5	179.8	1

Lim-12-42-06	888.1	9.8	901.7	11.9	935.2	33.2	1
Lim-12-42-07	1722.8	81.3	1787.8	45.3	1864.4	6.7	1
Lim-12-42-08	225.9	1.8	227.1	5.2	239.9	55.6	1
Lim-12-42-09	230.6	5.1	233.2	8.6	258.9	79.9	1
Lim-12-42-10	1866.4	40.9	1876.9	21.7	1888.6	4.4	1
Lim-12-42-12	247.8	4.4	245.5	10.1	223.5	98.3	1
Lim-12-42-13	433.6	4.3	431.5	8.4	420.2	48.0	1
Lim-12-42-15	2427.4	53.1	2402.7	57.6	2381.8	96.9	1
Lim-12-42-16	216.5	4.7	216.6	10.7	216.9	116.0	1
Lim-12-42-17	228.0	2.5	228.1	6.0	229.0	62.5	1
Lim-12-42-18	813.1	17.6	827.4	19.1	865.9	51.3	1
Lim-12-42-19	750.4	23.4	790.0	20.1	903.6	32.4	1
Lim-12-42-20	225.3	2.0	229.6	5.3	274.1	55.6	1
Lim-12-42-21	2353.3	24.7	2422.1	11.7	2480.5	3.6	1
Lim-12-42-22	376.0	17.7	407.3	18.6	588.5	58.3	1
Lim-12-42-23	215.3	2.8	229.9	17.1	382.8	184.2	1
Lim-12-42-24	1877.9	18.3	1884.1	10.4	1891.0	8.2	1
Lim-12-42-25	967.1	17.1	971.9	13.2	982.8	18.6	1
Lim-12-42-26	256.8	10.2	252.6	11.0	213.9	63.9	1
Lim-12-42-27	1226.5	35.2	1247.0	27.7	1282.6	43.0	1
Lim-12-42-28	223.4	3.6	226.6	6.4	259.4	61.7	1
Lim-12-42-29	225.4	2.9	230.8	8.0	286.1	83.1	1
Lim-12-42-30	1884.0	18.5	1877.6	10.8	1870.5	10.1	1
Lim-12-42-31	797.1	11.5	798.0	19.6	800.7	67.1	1
Lim-12-42-32	1725.5	37.0	1766.6	20.6	1815.4	4.7	1
Lim-12-42-33	214.5	1.7	215.8	4.3	229.3	48.2	1
Lim-12-42-34	216.4	3.1	223.2	6.5	295.5	66.3	1
Lim-12-42-34B	590.7	14.4	590.9	24.9	591.7	107.0	1
Lim-12-42-35	309.0	5.0	317.5	32.4	380.3	265.4	1
Lim-12-42-36	225.9	2.2	225.1	3.8	216.9	36.7	1
Lim-12-42-37	220.2	3.1	220.9	10.3	228.6	115.7	1
Lim-12-42-39	2360.8	80.4	2365.3	38.8	2369.2	20.0	1
Lim-12-42-40	223.7	4.6	223.6	8.5	222.8	85.0	1
Lim-12-42-41	944.6	75.3	951.6	58.1	967.7	78.4	1
Lim-12-42-42	225.5	2.5	241.3	19.9	397.2	206.2	1
Lim-12-42-43	213.5	2.8	219.8	7.9	288.6	86.1	1
Lim-12-42-45	225.9	3.4	227.4	8.0	243.1	83.6	1
Lim-12-42-46	227.4	2.5	226.8	6.7	220.2	71.5	1
Lim-12-42-47	528.2	6.9	530.3	11.3	539.6	51.9	1
Lim-12-42-48	266.3	7.2	250.5	22.0	104.3	225.0	1
Lim-12-42-49	221.9	5.2	234.5	23.7	362.3	250.6	1

Lim-12-42-50	1946.2	15.9	1956.9	9.1	1968.1	8.0	1
Lim-12-42-52	241.1	2.7	243.0	16.3	262.0	171.0	1
Lim-12-42-54	336.9	8.3	362.4	13.8	529.6	82.2	1
Lim-12-42-55	1348.8	63.0	1539.6	41.4	1812.5	12.6	1
Lim-12-42-56	216.0	2.6	225.1	7.8	321.9	82.9	1
Lim-12-42-57	955.0	46.0	956.2	33.2	959.0	28.4	1
Lim-12-42-58	889.0	10.4	906.8	8.4	950.3	12.8	1
Lim-12-42-59	240.7	4.6	239.6	10.5	228.6	104.4	1
Lim-12-42-60	373.6	2.8	378.4	7.8	407.5	52.6	1
Lim-12-42-61	227.4	5.5	237.2	13.3	335.5	130.9	1
Lim-12-42-62	245.8	5.7	257.1	9.9	361.9	81.8	1
Lim-12-42-63	2348.2	47.2	2356.6	22.1	2363.9	5.1	1
Lim-12-42-64	288.1	10.1	266.2	50.0	77.3	504.6	1
Lim-12-42-65	1883.2	15.0	1877.5	8.1	1871.1	4.3	1
Lim-12-42-67	333.4	15.9	355.6	20.4	503.5	103.4	1
Lim-12-42-68	1324.7	15.1	1317.7	9.7	1306.3	7.3	1
Lim-12-42-69	1827.8	28.0	1848.6	15.2	1872.0	5.8	1
Lim-12-42-70	217.8	3.8	213.0	10.5	160.3	121.3	1
Lim-12-42-71	1490.5	17.9	1539.7	11.6	1607.8	11.0	1
Lim-12-42-72	255.3	3.9	274.1	12.3	437.5	108.2	1
Lim-12-42-74	280.6	7.2	292.0	29.8	384.1	257.6	1
Lim-12-42-75	515.3	9.1	516.0	19.2	519.1	96.0	1
Lim-12-42-76	186.2	6.0	202.8	9.9	401.0	95.5	1
Lim-12-42-76B	215.1	3.7	232.0	14.0	407.2	145.4	1
Lim-12-42-82	2147.5	14.3	2149.5	7.6	2151.4	5.8	1
Lim-12-42-83	1876.2	16.5	1877.9	9.3	1879.8	7.1	1
Lim-12-42-84	1887.1	20.0	1876.3	11.1	1864.3	7.8	1
Lim-12-42-85	238.9	1.8	237.6	11.9	225.6	129.0	1
Lim-12-42-86	218.4	2.8	215.7	10.0	186.4	116.1	1
Lim-12-42-87	232.0	4.1	242.1	19.7	341.8	203.7	1
Lim-12-42-89	1587.7	42.3	1723.2	33.9	1892.0	50.0	1
Lim-12-42-90	1905.0	8.1	1888.9	5.5	1871.3	7.4	1
Lim-12-42-91	1906.3	23.0	1894.3	12.2	1881.0	4.9	1
Lim-12-42-92	369.6	5.1	350.8	20.5	227.9	156.4	1
Lim-12-42-93	2603.2	44.4	2623.7	20.1	2639.6	9.1	1
Lim-12-42-94	2533.0	29.5	2523.4	13.4	2515.6	5.4	1
Luhe-11-18-100	213.1	3.5	211.7	19.5	196.1	234.0	21
Luhe-11-18-101	994.2	20.0	993.4	15.7	991.7	24.1	21
Luhe-11-18-102	1125.0	33.3	1120.7	44.8	1112.6	115.0	21
Luhe-11-18-104	219.7	4.5	194.9	25.4	-94.8	349.3	21

Luhe-11-18-105	324.1	4.8	327.5	8.6	351.6	60.9	21
Luhe-11-18-35	34.2	4.1	34.3	6.6	41.3	365.8	21
Luhe-11-18-4	756.0	11.4	761.2	34.5	776.6	131.2	21
Luhe-11-18-45	284.2	4.6	285.2	35.9	293.9	328.4	21
Luhe-11-18-46	33.4	3.0	49.0	19.3	900.6	842.2	21
Luhe-11-18-48	43.4	1.6	83.7	24.0	1472.6	575.8	21
Luhe-11-18-51	782.1	15.1	780.5	37.5	776.1	138.2	21
Luhe-11-18-52	33.9	2.7	29.9	15.1	-280.4	1360.6	21
Luhe-11-18-53	428.6	9.1	433.2	12.0	457.7	57.5	21
Luhe-11-18-58	917.6	15.5	940.4	34.3	994.0	107.4	21
Luhe-11-18-59	34.2	1.9	49.4	6.6	871.3	261.3	21
Luhe-11-18-60	33.0	0.9	31.4	3.9	-93.1	302.9	21
Luhe-11-18-61	34.1	2.6	36.1	12.2	172.4	804.1	21
Luhe-11-18-62	34.8	1.4	37.1	6.9	192.6	434.5	21
Luhe-11-18-63	2404.5	72.5	2511.7	33.7	2599.5	3.6	21
Luhe-11-18-65	37.5	2.8	41.0	7.3	246.2	383.7	21
Luhe-11-18-66	32.8	1.4	32.1	4.3	-23.2	313.5	21
Luhe-11-18-67	852.6	22.0	851.6	18.6	849.1	34.4	21
Luhe-11-18-68	422.9	9.6	424.5	14.0	433.4	73.4	21
Luhe-11-18-69	36.0	3.8	32.6	14.5	-214.8	1156.5	21
Luhe-11-18-71	213.0	3.4	214.3	5.1	227.7	48.2	21
Luhe-11-18-72	370.7	6.4	368.8	26.1	356.6	186.4	21
Luhe-11-18-73	33.2	4.2	47.8	20.4	854.8	907.2	21
Luhe-11-18-75	249.8	4.4	233.2	34.5	69.6	393.9	21
Luhe-11-18-76	2270.4	37.7	2546.6	18.8	2774.6	6.9	21
Luhe-11-18-78	33.5	2.4	26.7	9.9	-550.9	1022.8	21
Luhe-11-18-79	32.9	1.6	35.6	9.0	222.6	590.4	21
Luhe-11-18-80	32.6	1.4	36.4	5.0	290.8	305.1	21
Luhe-11-18-81	33.3	4.0	53.8	26.1	1099.1	1027.4	21
Luhe-11-18-82	32.4	1.1	29.2	8.0	-225.2	707.5	21
Luhe-11-18-83	32.3	1.7	38.0	7.3	417.2	422.2	21
Luhe-11-18-84	573.1	23.0	593.4	27.3	671.7	93.7	21
Luhe-11-18-85	33.7	0.5	38.4	4.7	340.2	282.5	21
Luhe-11-18-86	34.8	1.3	33.3	5.9	-72.4	429.8	21
Luhe-11-18-87	2581.1	25.4	2566.2	11.5	2554.5	5.1	21
Luhe-11-18-88	33.7	1.4	40.1	6.4	439.9	349.2	21
Luhe-11-18-90	814.8	30.3	810.3	28.8	798.2	69.1	21
Luhe-11-18-91	32.4	1.1	34.4	8.4	173.3	579.3	21
Luhe-11-18-92	450.3	4.5	460.2	7.8	510.3	40.2	21
Luhe-11-18-94	33.8	1.5	35.0	5.9	118.8	391.0	21
Luhe-11-18-95	34.0	1.7	36.9	3.6	229.0	202.6	21

Luhe-11-18-96	33.3	1.3	37.7	3.7	326.2	207.6	21
Luhe-11-18-97	2375.3	64.1	2437.1	29.9	2489.1	3.7	21
Luhe-11-18-98	221.1	7.6	214.7	14.2	145.5	150.8	21
Luhe-11-18-99	1006.6	12.3	1014.2	9.3	1030.6	12.0	21
Mek-11-02-01	239.9	4.6	241.8	7.4	260.6	65.2	39
Mek-11-02-02	259.7	2.4	262.8	4.3	289.9	37.0	39
Mek-11-02-03	243.7	4.8	255.3	12.8	363.6	119.9	39
Mek-11-02-04	321.4	10.1	424.8	16.8	1033.6	72.9	39
Mek-11-02-06	238.1	2.7	237.4	12.3	230.6	132.0	39
Mek-11-02-08	242.3	2.8	248.0	10.4	301.9	104.7	39
Mek-11-02-09	522.9	19.7	580.5	18.2	812.6	27.0	39
Mek-11-02-10	243.1	3.7	242.3	8.0	234.5	77.4	39
Mek-11-02-11	243.5	3.9	239.2	10.4	197.4	106.2	39
Mek-11-02-12	929.9	34.6	950.7	25.0	999.2	13.8	39
Mek-11-02-13	240.3	2.8	233.7	13.8	167.7	151.9	39
Mek-11-02-15	2139.0	64.2	2311.8	32.8	2468.1	12.2	39
Mek-11-02-16	553.4	6.4	600.3	8.4	781.7	29.8	39
Mek-11-02-17	1041.1	45.0	1049.0	31.1	1065.5	16.2	39
Mek-11-02-18	244.3	4.2	249.7	13.8	300.9	136.2	39
Mek-11-02-19	242.9	5.8	241.7	17.9	230.3	184.0	39
Mek-11-02-21	238.2	3.1	237.3	9.3	228.7	96.6	39
Mek-11-02-22	240.0	2.2	254.0	18.4	385.6	182.7	39
Mek-11-02-23	385.6	24.0	411.8	25.4	561.2	84.5	39
Mek-11-02-24	279.1	7.3	280.8	13.2	295.2	106.2	39
Mek-11-02-25	245.3	2.9	249.0	12.4	283.9	125.5	39
Mek-11-02-26	276.3	12.0	306.1	18.9	539.4	122.5	39
Mek-11-02-27	238.4	4.2	238.6	5.6	240.3	44.9	39
Mek-11-02-29	241.8	2.8	242.2	11.5	245.9	119.6	39
Mek-11-02-30	334.6	8.9	343.3	10.4	402.6	51.7	39
Mek-11-02-31	243.5	4.2	260.1	18.5	412.3	175.6	39
Mek-11-02-32	243.3	2.1	242.9	8.7	238.6	90.6	39
Mek-11-02-35	591.4	10.4	593.7	24.1	602.3	108.8	39
Mek-11-02-36	620.4	11.0	619.3	13.3	615.5	46.8	39
Mek-11-02-39	250.9	4.0	257.5	8.4	318.0	75.6	39
Mek-11-02-40	270.6	9.8	295.9	16.7	500.2	117.4	39
Mek-11-02-41	1245.9	36.7	1337.1	26.1	1486.3	25.7	39
Mek-11-02-42	249.8	8.4	252.2	17.7	273.9	163.5	39
Mek-11-02-43	249.5	6.0	254.8	9.1	304.3	72.4	39
Mek-11-02-44	249.4	4.3	257.5	16.5	331.6	160.3	39
Mek-11-02-45	242.2	4.8	243.6	16.9	257.1	173.4	39

Mek-11-02-46	912.9	37.2	977.7	27.6	1126.2	10.3	39
Mek-11-02-47	248.6	5.2	250.9	9.6	272.1	86.1	39
Mek-11-02-48	266.4	6.5	267.1	12.1	273.3	103.7	39
Mek-11-02-49	471.1	21.7	758.9	27.7	1737.5	37.0	39
Mek-11-02-50	251.5	4.9	253.9	7.3	275.9	58.9	39
Mek-11-02-52	917.4	54.3	928.1	39.1	953.5	20.4	39
Mek-11-02-53	249.8	5.2	251.2	7.8	264.2	64.5	39
Mek-11-02-55	322.0	16.2	335.2	22.8	428.4	135.7	39
Mek-11-02-56	2033.3	63.7	2193.2	38.7	2346.2	38.8	39
Mek-11-02-57	297.7	11.5	498.2	53.9	1570.8	246.4	39
Mek-11-02-58	249.7	6.2	256.7	10.4	321.3	87.3	39
Mek-11-02-59	249.3	5.1	252.5	7.0	282.4	53.3	39
Mek-11-02-60	173.8	7.4	209.0	9.6	626.9	58.5	39
Mek-11-02-61	248.2	2.4	242.9	17.3	191.8	184.6	39
Mek-11-02-62	250.3	3.8	246.3	14.0	208.1	144.5	39
Mek-11-02-63	252.1	5.5	251.6	11.5	246.8	107.4	39
Mek-11-02-64	258.0	5.6	251.5	14.5	190.8	142.2	39
Mek-11-02-65	255.4	5.3	253.6	9.8	236.7	88.1	39
Mek-11-02-66	484.8	15.2	537.8	14.1	769.5	17.6	39
Mek-11-02-68	236.5	5.4	253.6	16.7	415.1	158.1	39
Mek-11-02-69	515.3	26.3	586.0	26.1	870.5	51.5	39
Mek-11-02-70	253.3	6.4	250.5	16.0	224.0	155.9	39
Mek-11-02-72	446.3	7.0	449.9	10.9	468.3	55.5	39
Mek-11-02-73	253.2	7.6	253.2	13.0	253.3	113.8	39
Mek-11-02-74	249.7	4.3	249.1	8.4	243.3	77.6	39
Mek-11-02-76	283.5	18.1	346.9	84.0	796.5	593.4	39
Mek-11-02-77	254.3	10.1	262.9	11.9	340.0	72.8	39
Mek-11-02-78	250.5	9.7	248.6	18.9	231.0	176.3	39
Midu-11-01-01	1811.0	42.7	1837.8	24.3	1868.3	17.1	34
Midu-11-01-02	835.0	7.4	841.1	7.4	857.3	18.3	34
Midu-11-01-03	1445.5	66.0	1604.2	41.7	1819.4	15.4	34
Midu-11-01-04	307.1	6.5	313.7	9.9	362.6	67.3	34
Midu-11-01-05	797.7	11.6	813.0	9.4	854.8	13.2	34
Midu-11-01-06	250.7	1.9	253.9	10.1	283.9	101.4	34
Midu-11-01-08	1637.5	107.9	1746.8	62.4	1880.2	8.0	34
Midu-11-01-09	232.0	5.2	234.1	11.6	255.6	116.8	34
Midu-11-01-10	428.5	6.2	430.0	11.4	438.1	64.2	34
Midu-11-01-100	1482.3	32.0	1633.0	19.7	1833.0	3.4	34
Midu-11-01-101	777.0	6.7	778.3	7.8	782.0	23.2	34
Midu-11-01-102	254.1	5.6	255.4	11.0	267.8	98.5	34

Midu-11-01-103	317.4	9.2	325.5	18.7	383.9	135.3	34
Midu-11-01-106	318.9	4.9	317.7	12.8	308.3	101.1	34
Midu-11-01-107	400.2	4.6	399.2	13.5	393.2	87.8	34
Midu-11-01-108	252.8	4.4	246.5	10.4	187.4	102.4	34
Midu-11-01-109	227.9	7.8	214.4	29.7	68.0	358.2	34
Midu-11-01-11	256.8	5.8	250.8	17.3	195.8	173.0	34
Midu-11-01-111	1878.6	29.2	1873.9	15.9	1868.6	9.4	34
Midu-11-01-112	1189.3	20.4	1197.1	16.7	1211.1	28.7	34
Midu-11-01-113	1874.5	67.9	2194.1	37.6	2507.8	5.7	34
Midu-11-01-114	538.6	21.8	520.0	20.6	439.1	62.9	34
Midu-11-01-115	1334.6	76.6	1520.3	50.7	1789.3	18.0	34
Midu-11-01-12	1050.8	25.2	1047.2	17.5	1039.8	13.3	34
Midu-11-01-13	259.7	7.3	263.0	16.2	292.7	145.4	34
Midu-11-01-14	2549.7	28.2	2543.1	12.7	2537.9	4.6	34
Midu-11-01-15	547.9	14.1	530.5	71.2	456.4	379.6	34
Midu-11-01-17	472.9	8.2	465.9	15.4	431.4	82.5	34
Midu-11-01-18	1849.1	25.3	1859.5	13.7	1871.2	5.6	34
Midu-11-01-20	948.1	11.8	949.0	9.1	951.1	13.1	34
Midu-11-01-20B	1225.5	17.8	1221.7	14.6	1215.2	25.4	34
Midu-11-01-21	792.1	18.8	793.7	23.6	798.1	72.7	34
Midu-11-01-22	826.7	37.4	840.3	29.9	876.3	41.8	34
Midu-11-01-23	2211.4	25.8	2213.7	13.5	2215.8	10.4	34
Midu-11-01-24	1948.7	31.5	1921.0	16.7	1891.2	8.3	34
Midu-11-01-25	756.9	21.0	776.4	30.4	832.8	99.6	34
Midu-11-01-26	415.0	32.3	384.2	75.1	202.3	516.6	34
Midu-11-01-28	824.2	9.1	826.0	10.2	830.8	28.3	34
Midu-11-01-29	173.7	5.3	163.1	14.9	12.6	226.2	34
Midu-11-01-30	412.9	9.8	416.0	10.8	433.2	45.0	34
Midu-11-01-33	761.4	7.5	761.6	11.9	762.4	41.4	34
Midu-11-01-34	721.2	23.7	748.9	24.3	832.4	62.5	34
Midu-11-01-36	193.2	4.7	195.2	5.4	219.7	41.5	34
Midu-11-01-37	157.9	3.1	161.9	5.7	220.9	75.7	34
Midu-11-01-38	416.0	7.4	417.1	10.4	423.4	54.2	34
Midu-11-01-39	405.2	7.3	404.4	14.9	400.1	91.2	34
Midu-11-01-40	161.4	2.7	166.3	14.4	236.5	213.5	34
Midu-11-01-41	1784.9	56.4	1833.2	30.8	1888.5	4.5	34
Midu-11-01-42	145.5	3.2	151.8	5.0	251.3	63.5	34
Midu-11-01-43	435.2	12.8	453.9	15.3	549.9	62.2	34
Midu-11-01-44	1325.2	3.7	1362.0	5.1	1420.2	11.6	34
Midu-11-01-45	448.2	14.4	450.4	15.5	461.5	58.6	34
Midu-11-01-46	806.2	9.3	817.7	8.8	849.0	20.6	34

Midu-11-01-47	357.3	15.9	357.6	46.6	359.6	334.2	34
Midu-11-01-48	2587.8	119.0	2760.3	55.6	2888.9	28.7	34
Midu-11-01-50	230.1	5.6	218.7	16.7	98.2	192.9	34
Midu-11-01-50A	464.7	5.1	467.3	6.8	479.8	31.3	34
Midu-11-01-51	160.4	5.0	159.8	7.9	150.8	100.7	34
Midu-11-01-53	435.6	5.8	433.7	7.4	423.7	35.3	34
Midu-11-01-54	2076.4	148.2	2355.9	78.0	2607.4	27.1	34
Midu-11-01-55	290.8	5.7	282.8	21.4	217.3	196.1	34
Midu-11-01-56	486.5	17.6	478.9	16.6	442.5	48.6	34
Midu-11-01-57	2397.0	48.7	2400.1	24.3	2402.8	17.4	34
Midu-11-01-59	943.1	16.4	942.2	13.1	940.1	21.5	34
Midu-11-01-60	836.5	18.6	840.0	17.8	849.2	42.4	34
Midu-11-01-61	1864.5	21.2	1863.3	11.2	1861.8	1.8	34
Midu-11-01-62	248.6	4.8	229.8	10.5	41.5	112.4	34
Midu-11-01-63	431.7	5.6	432.5	8.3	437.1	42.9	34
Midu-11-01-64	1812.2	38.3	1822.8	20.6	1834.8	3.3	34
Midu-11-01-65	1701.1	43.5	1670.1	24.5	1631.2	13.3	34
Midu-11-01-66	916.2	30.6	928.8	22.3	958.6	15.9	34
Midu-11-01-67	442.6	9.3	447.4	30.3	472.3	179.0	34
Midu-11-01-69	248.0	7.1	238.7	25.7	148.2	275.9	34
Midu-11-01-70	963.1	23.9	969.6	17.5	984.3	17.3	34
Midu-11-01-71	265.1	5.6	266.1	7.8	275.0	58.4	34
Midu-11-01-72	1839.7	62.7	1851.0	33.7	1863.7	10.8	34
Midu-11-01-74	980.7	14.8	979.7	13.6	977.4	28.9	34
Midu-11-01-75	266.5	4.5	276.6	9.1	362.4	75.4	34
Midu-11-01-76	1887.8	19.0	1881.5	11.6	1874.7	12.3	34
Midu-11-01-77	434.7	14.6	439.6	23.9	465.3	126.8	34
Midu-11-01-78	270.6	7.0	256.3	12.7	127.8	117.0	34
Midu-11-01-79	1145.5	27.1	1132.1	19.2	1106.5	22.5	34
Midu-11-01-80	226.3	3.9	230.7	5.3	275.2	43.2	34
Midu-11-01-81	169.1	3.0	168.1	8.7	153.7	124.9	34
Midu-11-01-82	2007.7	34.7	2007.4	19.4	2006.9	16.5	34
Midu-11-01-84	2340.4	37.5	2320.4	20.8	2302.8	21.2	34
Midu-11-01-85	184.1	14.3	215.3	42.7	571.9	450.4	34
Midu-11-01-86	436.9	4.1	437.5	6.3	440.7	33.3	34
Midu-11-01-87	830.6	7.3	828.0	6.5	821.0	13.7	34
Midu-11-01-88	177.4	2.9	173.6	6.5	122.7	88.1	34
Midu-11-01-89	1320.8	21.2	1315.5	16.6	1306.8	26.9	34
Midu-11-01-90	2539.3	79.3	2568.8	35.4	2592.1	3.4	34
Midu-11-01-91	402.5	21.4	431.7	24.6	590.9	94.4	34
Midu-11-01-92	1853.6	51.1	1866.2	27.5	1880.2	10.5	34

Midu-11-01-93	817.0	10.6	828.9	8.1	861.1	8.3	34
Midu-11-01-94	200.3	2.9	207.4	6.6	288.9	73.9	34
Midu-11-01-95	225.1	4.1	228.1	5.2	259.2	39.9	34
Midu-11-01-96	1919.9	76.5	1888.5	41.4	1854.1	26.0	34
Midu-11-01-97	418.8	14.8	421.0	13.0	433.1	22.4	34
Midu-11-01-98	247.4	6.6	241.4	28.9	183.7	307.9	34
Midu-11-01-99	164.5	2.9	162.9	7.6	139.0	110.9	34
Midu-11-02	559.4	5.2	561.2	8.3	568.5	36.3	33
Midu-11-02-01	37.4	0.8	39.5	2.2	170.8	123.7	33
Midu-11-02-02	35.8	6.5	37.1	6.7	123.0	84.1	33
Midu-11-02-03	72.6	2.8	72.1	2.9	57.0	32.3	33
Midu-11-02-03	36.0	3.3	37.0	3.5	104.8	65.3	33
Midu-11-02-04	36.6	1.2	37.6	2.4	98.7	131.7	33
Midu-11-02-05	40.8	3.1	46.9	8.1	369.2	362.9	33
Midu-11-02-05	57.1	1.0	57.1	1.0	57.4	18.5	33
Midu-11-02-06	36.8	0.5	37.2	1.0	66.7	57.4	33
Midu-11-02-11	36.2	0.5	36.6	1.1	63.7	67.5	33
Midu-11-02-12	93.8	1.2	94.8	2.5	120.7	58.8	33
Midu-11-02-12	75.1	2.2	75.5	3.9	90.5	106.9	33
Midu-11-02-13	35.6	0.3	36.3	2.1	87.5	138.5	33
Midu-11-02-14	65.2	3.8	66.6	8.9	117.1	294.6	33
Midu-11-02-15	35.9	0.6	36.1	1.3	51.0	74.4	33
Midu-11-02-15	466.1	4.6	459.7	19.3	427.4	114.3	33
Midu-11-02-16	38.4	3.3	39.5	3.5	106.9	68.8	33
Midu-11-02-16	35.3	0.6	35.5	1.9	51.1	121.3	33
Midu-11-02-17	35.4	1.0	36.3	6.1	94.0	402.8	33
Midu-11-02-18	35.6	1.1	33.8	6.9	-90.5	507.4	33
Midu-11-02-19	37.2	0.6	39.1	1.9	154.3	111.7	33
Shi-12-01-01	469.4	12.7	474.9	25.7	501.4	135.9	5
Shi-12-01-02	1909.3	61.0	1893.7	31.7	1876.5	2.9	5
Shi-12-01-03	1123.6	28.9	1113.0	22.2	1092.3	34.1	5
Shi-12-01-04	222.1	6.2	228.5	13.2	295.1	131.7	5
Shi-12-01-05	255.4	2.9	261.9	5.9	321.1	51.7	5
Shi-12-01-06	472.7	14.3	476.0	14.7	491.8	50.2	5
Shi-12-01-07	1066.0	15.4	1071.3	11.9	1082.2	17.3	5
Shi-12-01-08	1002.1	18.4	1017.4	13.0	1050.4	7.2	5
Shi-12-01-10	220.6	2.2	216.0	5.8	166.0	65.2	5
Shi-12-01-11	312.1	5.1	327.1	27.9	435.1	219.6	5
~~Shi-12-01-12~~	~~1893.1~~	~~33.9~~	~~2051.4~~	~~63.0~~	~~2214.5~~	~~118.7~~	5

Shi-12-01-14	1526.0	79.3	1528.2	46.6	1531.2	16.7	5
Shi-12-01-15	1799.7	33.4	1831.7	18.3	1868.3	6.2	5
Shi-12-01-16	2717.8	72.1	2801.6	31.3	2862.4	8.4	5
Shi-12-01-17	83.1	4.4	79.6	9.6	-22.0	274.6	5
Shi-12-01-18	259.0	7.3	255.5	35.3	223.8	356.5	5
Shi-12-01-19	220.3	7.8	214.3	23.3	148.5	269.8	5
Shi-12-01-20	985.6	12.6	999.9	29.0	1031.4	88.0	5
Shi-12-01-21	259.6	5.8	255.7	18.1	220.1	177.7	5
Shi-12-01-22	1726.8	104.8	1790.4	65.7	1865.3	65.0	5
Shi-12-01-23	1910.1	34.4	1896.1	19.6	1880.8	16.8	5
Shi-12-01-24	344.6	9.5	338.1	14.2	293.3	92.3	5
Shi-12-01-25	220.6	3.0	218.4	7.6	195.3	84.0	5
~~Shi-12-01-26~~	~~2356.4~~	~~45.1~~	~~2458.6~~	~~37.6~~	~~2544.2~~	~~56.3~~	5
Shi-12-01-27	454.6	7.1	453.3	15.6	446.7	87.7	5
Shi-12-01-29	785.6	13.5	781.2	13.7	768.5	36.4	5
Shi-12-01-30	44.6	1.5	41.3	10.6	-143.2	651.5	5
Shi-12-01-31	1924.1	25.1	1897.1	13.6	1867.7	8.4	5
Shi-12-01-32	444.2	9.3	443.3	14.9	438.5	78.6	5
Shi-12-01-33	223.0	9.0	217.5	17.5	158.0	186.3	5
Shi-12-01-34	44.4	1.4	46.5	5.7	159.7	286.8	5
Shi-12-01-35	1110.9	20.7	1098.2	16.6	1073.1	28.4	5
Shi-12-01-36	734.7	29.5	730.9	30.2	719.2	83.6	5
Shi-12-01-38	1934.5	34.8	1900.4	18.2	1863.3	6.9	5
Shi-12-01-39	438.0	6.8	433.8	15.1	411.4	88.5	5
Shi-12-01-40	753.1	8.0	753.5	9.0	754.7	26.7	5
Shi-12-01-41	239.1	12.2	208.3	72.2	-127.5	967.0	5
Shi-12-01-42	2526.6	61.9	2509.7	27.7	2496.1	4.9	5
Shi-12-01-43	463.8	8.1	458.4	13.2	431.4	68.6	5
Shi-12-01-44	45.5	0.9	45.7	4.0	55.2	210.1	5
Shi-12-01-45	1913.6	38.1	1897.6	26.5	1880.2	37.0	5
Shi-12-01-46	262.7	5.7	261.1	14.3	247.2	134.2	5
Shi-12-01-47	443.9	16.7	435.7	17.8	392.4	70.5	5
Shi-12-01-48	1514.0	39.9	1491.4	26.4	1459.4	31.1	5
Shi-12-01-49	1870.8	31.0	1863.8	16.7	1855.9	7.7	5
Shi-12-01-50	260.5	6.2	260.7	8.2	262.7	59.9	5
Shi-12-01-51	2114.7	38.0	2146.7	19.2	2177.6	7.8	5
Shi-12-01-52	1936.0	41.1	1902.5	21.5	1866.0	8.4	5
Shi-12-01-53	2549.4	21.7	2515.0	9.9	2487.3	4.5	5
Shi-12-01-54	956.5	17.1	954.8	18.9	950.9	48.6	5
Shi-12-01-55	178.6	10.0	154.0	33.7	-210.9	580.8	5
Shi-12-01-56	428.5	11.0	422.9	29.0	392.8	178.3	5

Shi-12-01-57	431.2	15.8	434.1	17.6	449.5	71.8	5
Shi-12-01-58	241.6	11.6	241.9	17.4	244.4	148.3	5
Shi-12-01-59	251.4	20.0	256.7	20.6	305.6	93.9	5
Shi-12-01-60	371.5	21.0	377.1	148.6	411.6	1095.8	5
Shi-12-01-61	535.7	11.5	538.0	16.1	547.7	68.8	5
Shi-12-01-62	248.5	9.8	239.7	22.3	154.1	226.4	5
Shi-12-01-63	774.1	13.5	768.4	12.7	751.8	30.9	5
Shi-12-01-64	423.4	7.8	424.0	13.0	426.8	72.1	5
Shi-12-01-65	1644.0	72.7	1744.1	41.8	1866.2	4.3	5
Shi-12-01-68	230.9	2.4	234.9	7.4	275.1	77.0	5
Shi-12-01-69	1929.0	27.8	1922.6	15.5	1915.8	11.9	5
Shi-12-01-70	752.1	27.0	759.4	28.0	780.8	75.9	5
Shi-12-01-71	458.2	4.2	457.7	6.3	455.3	31.6	5
Shi-12-01-72	1823.3	17.9	1833.6	14.8	1845.3	24.0	5
Shi-12-02-01	413.2	21.7	424.2	34.7	484.9	185.5	4
Shi-12-02-02	2713.2	122.7	2864.3	55.0	2972.4	24.9	4
Shi-12-02-04	983.0	20.8	986.0	23.6	992.4	60.1	4
Shi-12-02-05	445.0	9.9	433.3	16.7	371.6	93.1	4
Shi-12-02-06	1712.7	79.5	1754.6	77.4	1804.9	138.2	4
Shi-12-02-07	41.7	0.9	41.7	3.2	37.7	182.3	4
Shi-12-02-08	41.0	0.9	42.7	6.0	137.8	336.8	4
Shi-12-02-09	40.3	1.3	40.9	3.7	78.4	207.7	4
Shi-12-02-10	1616.5	22.5	1640.9	22.4	1672.3	41.7	4
Shi-12-02-100	362.7	11.1	372.2	12.7	431.9	57.8	4
Shi-12-02-101	255.6	13.6	240.7	26.1	97.5	258.1	4
Shi-12-02-102	395.9	26.6	404.9	24.7	456.3	58.1	4
Shi-12-02-103	801.7	29.1	794.5	33.8	774.5	100.5	4
Shi-12-02-104	1888.9	42.2	1956.9	23.9	2029.6	16.9	4
Shi-12-02-105	1619.1	75.4	1601.6	47.7	1578.6	50.5	4
Shi-12-02-106	271.9	7.2	272.1	15.3	274.1	133.7	4
Shi-12-02-107	42.2	1.2	43.7	3.4	129.2	173.2	4
Shi-12-02-108	42.7	1.1	44.6	2.7	148.7	130.6	4
Shi-12-02-109	41.7	1.3	42.4	4.0	87.7	217.4	4
Shi-12-02-11	40.1	0.8	42.3	3.0	166.3	161.4	4
Shi-12-02-110	2062.0	76.3	2038.9	38.6	2015.6	13.9	4
Shi-12-02-111	41.8	1.0	39.7	3.7	-88.2	228.3	4
Shi-12-02-112	819.8	29.0	823.6	22.6	834.0	28.7	4
Shi-12-02-113	41.3	1.6	41.2	3.8	38.3	203.6	4
Shi-12-02-114	1718.6	64.9	1886.1	37.0	2075.9	5.3	4
Shi-12-02-115	42.1	3.2	38.9	11.4	-152.1	730.5	4

Shi-12-02-13	216.9	3.6	224.5	9.0	304.4	94.8	4
Shi-12-02-14	40.2	1.2	54.4	6.1	735.7	236.6	4
Shi-12-02-15	755.1	13.3	785.3	21.9	872.2	73.5	4
Shi-12-02-17	887.5	14.4	910.6	15.2	967.1	37.6	4
Shi-12-02-18	455.5	17.1	443.7	21.1	383.2	98.8	4
Shi-12-02-21	759.6	24.2	753.0	55.0	733.5	207.3	4
Shi-12-02-22	1638.1	22.8	1637.4	12.8	1636.3	2.6	4
Shi-12-02-23	1457.8	21.0	1454.8	12.6	1450.4	5.3	4
Shi-12-02-24	256.1	7.6	242.9	30.9	116.8	330.3	4
Shi-12-02-25	530.8	22.7	533.5	22.5	544.9	67.6	4
Shi-12-02-26	596.6	33.4	699.9	30.2	1047.4	22.2	4
Shi-12-02-27	549.3	27.4	539.8	30.2	500.1	109.9	4
Shi-12-02-28	304.2	14.0	329.0	15.5	508.8	63.0	4
Shi-12-02-29	249.3	5.5	251.0	13.0	267.2	123.7	4
Shi-12-02-30	305.7	11.2	317.4	32.2	404.1	251.6	4
Shi-12-02-32	40.4	1.0	39.1	4.0	-44.8	245.7	4
Shi-12-02-33	964.3	51.5	972.6	36.5	991.3	18.9	4
Shi-12-02-34	423.9	4.3	432.0	5.5	475.5	25.2	4
Shi-12-02-35	1683.4	57.7	1694.2	36.1	1707.6	36.8	4
Shi-12-02-36	419.5	22.9	434.4	21.8	514.4	55.1	4
Shi-12-02-37	1743.6	65.8	1743.3	40.8	1742.9	42.5	4
Shi-12-02-38	1866.4	28.8	1872.1	15.7	1878.4	8.0	4
Shi-12-02-39	247.9	9.1	257.1	19.5	342.2	175.3	4
Shi-12-02-40	269.6	8.8	269.8	9.7	271.7	53.9	4
Shi-12-02-42	2033.4	53.4	2291.0	27.9	2529.5	2.8	4
Shi-12-02-43	1407.6	27.3	1407.8	43.4	1408.0	100.9	4
Shi-12-02-44	40.9	1.5	40.2	5.1	-3.5	298.1	4
Shi-12-02-46	284.0	8.9	291.6	9.4	352.5	41.4	4
Shi-12-02-47	1915.9	44.8	1909.9	24.3	1903.4	14.4	4
Shi-12-02-48	42.0	2.4	51.7	12.8	529.3	550.3	4
Shi-12-02-49	456.5	18.8	452.5	21.3	432.3	89.0	4
Shi-12-02-50	41.2	0.9	51.8	11.6	575.4	503.6	4
Shi-12-02-51	42.4	1.2	37.3	4.9	-282.4	337.7	4
Shi-12-02-52	329.1	16.1	327.9	17.4	319.7	83.3	4
Shi-12-02-53	260.0	10.6	265.3	22.1	312.1	193.2	4
Shi-12-02-54	451.5	18.2	490.5	42.9	677.4	218.7	4
Shi-12-02-55	278.6	6.2	272.9	10.7	223.8	89.4	4
Shi-12-02-56	2739.4	66.2	2739.8	29.3	2740.1	14.0	4
Shi-12-02-57	261.3	14.1	260.6	51.2	254.3	500.7	4
Shi-12-02-58	270.0	5.6	269.6	10.9	265.5	93.4	4
Shi-12-02-59	252.5	7.2	253.7	11.0	264.3	91.4	4

Shi-12-02-60	575.3	17.8	630.8	17.4	835.1	37.6	4
Shi-12-02-61	441.6	19.8	424.5	27.9	332.4	149.2	4
Shi-12-02-62	2245.2	48.8	2370.9	24.0	2480.9	7.6	4
Shi-12-02-63	1749.6	66.0	1723.5	63.8	1691.9	117.3	4
Shi-12-02-64	1919.7	46.8	1906.1	25.1	1891.2	14.0	4
Shi-12-02-66	1998.2	36.0	2002.6	18.4	2007.1	4.2	4
Shi-12-02-67	252.3	7.7	241.7	24.5	140.4	258.3	4
Shi-12-02-68	275.5	10.1	275.7	14.6	277.5	108.5	4
Shi-12-02-69	538.8	15.4	557.6	15.7	635.0	45.5	4
Shi-12-02-70	1057.4	17.3	1063.0	14.0	1074.6	23.1	4
Shi-12-02-71	248.3	9.3	252.8	14.4	294.4	118.1	4
Shi-12-02-72	262.7	9.2	307.7	17.4	665.1	118.1	4
Shi-12-02-73	282.4	13.4	273.4	25.2	197.3	216.7	4
Shi-12-02-74	41.2	3.0	43.9	5.5	192.9	243.8	4
Shi-12-02-75	476.7	11.9	558.8	12.5	908.7	27.9	4
Shi-12-02-76	41.6	1.5	43.2	5.0	130.7	264.1	4
Shi-12-02-77	232.9	4.3	235.3	5.8	259.0	46.8	4
Shi-12-02-78	260.3	4.7	265.2	16.7	308.8	157.2	4
Shi-12-02-79	255.1	4.0	260.6	5.3	310.6	37.8	4
Shi-12-02-81	1216.7	23.8	1213.8	16.1	1208.6	14.7	4
Shi-12-02-82	42.3	1.7	49.6	8.4	418.6	381.2	4
Shi-12-02-83	42.0	1.9	119.6	20.6	2210.9	310.2	4
Shi-12-02-84	231.4	6.1	238.2	14.7	306.3	145.7	4
Shi-12-02-85	773.3	25.9	798.1	21.1	868.2	28.6	4
Shi-12-02-86	429.1	5.4	419.4	30.4	366.1	197.5	4
Shi-12-02-87	232.9	8.2	257.2	21.5	484.7	193.8	4
Shi-12-02-88	255.8	6.9	251.6	9.4	212.4	73.7	4
Shi-12-02-89	931.9	19.3	924.5	30.2	906.7	91.7	4
Shi-12-02-90	812.2	32.2	824.7	25.5	858.7	33.0	4
Shi-12-02-91	449.0	15.3	430.3	23.5	330.9	129.5	4
Shi-12-02-92	250.7	6.2	244.9	17.2	189.3	174.0	4
Shi-12-02-93	1883.4	76.7	1875.3	40.3	1866.2	6.5	4
Shi-12-02-94	224.4	6.5	222.5	8.4	201.5	69.8	4
Shi-12-02-97	1887.7	39.9	1869.6	22.0	1849.5	15.1	4
Shi-12-02-98	41.1	0.9	41.6	3.1	68.6	171.2	4
Shi-12-02-99	450.2	8.4	451.7	12.0	459.7	59.4	4
Yany-13-02-01	212.0	5.2	203.9	27.2	111.4	343.6	29
Yany-13-02-02	536.6	7.5	539.2	8.5	549.9	30.7	29
Yany-13-02-03	213.1	3.3	215.1	5.6	237.5	55.7	29
Yany-13-02-04	411.7	6.3	410.1	8.3	400.7	41.8	29

Yany-13-02-05	525.0	8.9	518.5	38.4	490.3	205.4	29
Yany-13-02-07	210.3	4.4	206.9	5.6	168.2	48.7	29
Yany-13-02-08	761.8	9.6	761.5	7.8	760.5	12.0	29
Yany-13-02-09	439.8	6.5	440.7	7.6	445.3	32.8	29
Yany-13-02-10	774.4	16.5	786.1	28.1	819.6	96.4	29
Yany-13-02-100	1893.9	53.1	1885.9	28.0	1877.2	7.9	29
Yany-13-02-101	215.3	4.9	209.1	12.4	140.0	144.8	29
Yany-13-02-102	365.9	19.7	379.8	43.0	465.7	275.1	29
Yany-13-02-103	456.0	10.6	466.8	16.4	520.1	80.7	29
Yany-13-02-104	2194.9	74.7	2156.5	36.4	2120.1	11.7	29
Yany-13-02-105	257.6	6.3	260.1	9.0	282.4	69.6	29
Yany-13-02-106	1862.5	15.8	1874.0	9.9	1886.8	11.2	29
Yany-13-02-107	319.0	8.0	315.9	17.9	292.8	139.1	29
Yany-13-02-108	1246.7	24.6	1243.9	16.7	1239.0	16.8	29
Yany-13-02-109	1767.7	41.8	1769.7	23.7	1772.0	15.1	29
Yany-13-02-11	774.8	12.5	775.5	24.7	777.5	88.8	29
Yany-13-02-111	274.9	12.0	344.3	60.6	844.1	425.1	29
Yany-13-02-112	1903.7	43.3	1896.7	22.7	1888.9	5.9	29
Yany-13-02-113	970.2	25.2	971.8	18.6	975.4	21.0	29
Yany-13-02-114	620.5	14.5	638.6	38.7	703.1	165.8	29
Yany-13-02-115	1136.4	49.5	1157.4	34.4	1196.7	29.9	29
Yany-13-02-116	210.0	2.0	213.3	12.4	249.2	146.7	29
Yany-13-02-117	212.4	3.5	209.7	9.7	180.1	112.6	29
Yany-13-02-118	495.9	15.6	496.8	29.9	501.0	151.3	29
Yany-13-02-119	212.0	5.0	218.7	13.9	291.5	152.4	29
Yany-13-02-12	801.6	10.8	803.8	18.7	809.9	64.0	29
Yany-13-02-120	87.3	2.2	91.7	5.9	207.6	143.2	29
Yany-13-02-13	2271.8	23.8	2332.1	14.3	2385.3	16.3	29
Yany-13-02-14	510.9	8.6	511.3	7.7	513.1	17.5	29
Yany-13-02-15	1870.3	23.3	1856.5	13.6	1841.0	12.6	29
Yany-13-02-16	1781.0	19.8	1843.4	11.0	1914.7	4.6	29
Yany-13-02-17	214.3	3.7	224.1	6.1	329.1	56.3	29
Yany-13-02-18	1517.8	13.3	1654.6	11.0	1832.9	16.7	29
Yany-13-02-20	210.7	4.1	214.2	19.1	253.4	223.9	29
Yany-13-02-21	790.7	22.1	791.9	26.2	795.3	78.2	29
Yany-13-02-22	1895.3	32.1	1888.9	17.1	1881.8	7.4	29
Yany-13-02-23	215.9	8.9	214.7	20.0	201.4	219.6	29
Yany-13-02-24	212.8	4.6	215.1	14.8	240.0	169.2	29
Yany-13-02-25	90.0	1.9	91.9	5.8	140.9	145.5	29
Yany-13-02-26	1888.3	20.9	1870.8	11.3	1851.4	6.1	29
Yany-13-02-27	88.7	1.7	86.5	4.0	26.4	106.6	29

Yany-13-02-28	654.2	21.9	656.2	37.9	662.8	150.3	29
Yany-13-02-29	802.5	15.8	809.7	18.0	829.5	51.3	29
Yany-13-02-30	795.4	14.5	791.6	28.5	780.9	101.0	29
Yany-13-02-31	1786.8	14.5	1830.3	8.1	1880.2	3.9	29
Yany-13-02-32	1815.0	75.4	1834.3	46.4	1856.2	48.5	29
Yany-13-02-33	214.7	4.3	211.5	15.9	175.6	188.2	29
Yany-13-02-34	256.3	4.4	259.4	7.7	288.1	65.2	29
Yany-13-02-35	1874.7	30.9	1870.6	16.5	1866.0	5.6	29
Yany-13-02-36	271.6	10.8	282.4	28.9	372.4	248.5	29
Yany-13-02-37	413.6	24.8	435.4	26.5	552.5	91.6	29
Yany-13-02-38	256.8	3.2	263.1	6.7	319.9	59.4	29
Yany-13-02-39	106.0	0.9	110.5	3.0	209.1	63.6	29
Yany-13-02-40	88.5	1.1	90.0	3.1	128.4	79.7	29
Yany-13-02-41	1019.1	16.2	1017.2	20.6	1013.0	54.9	29
Yany-13-02-42	216.9	6.0	220.9	11.4	263.6	114.8	29
Yany-13-02-44	2176.4	24.3	2317.0	12.5	2443.3	6.3	29
Yany-13-02-45	1656.0	34.3	1651.2	19.3	1645.2	5.1	29
Yany-13-02-46	765.1	15.1	766.3	13.0	769.8	25.4	29
Yany-13-02-47	273.0	8.3	263.6	20.2	181.1	189.2	29
Yany-13-02-48	766.6	10.6	769.0	27.4	776.0	102.4	29
Yany-13-02-49	219.5	9.4	220.9	24.5	235.8	267.6	29
Yany-13-02-50	480.0	7.1	481.4	7.9	488.2	30.3	29
Yany-13-02-51	211.9	5.5	204.4	16.2	119.0	197.5	29
Yany-13-02-52	468.3	8.8	487.8	16.0	580.9	78.8	29
Yany-13-02-53	415.0	11.1	429.2	16.3	505.8	82.7	29
Yany-13-02-54	234.4	3.2	241.4	9.4	309.4	94.1	29
Yany-13-02-55	2277.1	25.4	2344.8	13.5	2404.2	10.9	29
Yany-13-02-56	219.2	3.5	217.9	10.1	204.1	113.9	29
Yany-13-02-57	89.7	2.4	88.2	5.8	48.7	151.2	29
Yany-13-02-58	281.2	8.4	288.6	41.6	349.0	369.8	29
Yany-13-02-59	212.1	1.9	216.2	3.0	260.5	28.9	29
Yany-13-02-60	262.5	4.9	269.8	13.6	333.3	123.3	29
Yany-13-02-61	2296.8	33.4	2298.1	15.8	2299.3	4.0	29
Yany-13-02-62	86.6	1.6	106.0	37.3	568.1	831.5	29
Yany-13-02-63	865.9	33.9	860.1	44.2	845.2	132.6	29
Yany-13-02-64	1940.8	33.8	1912.8	17.9	1882.6	8.7	29
Yany-13-02-65	1686.6	53.6	1763.5	30.5	1855.9	8.0	29
Yany-13-02-66	336.9	7.6	336.1	22.8	330.6	173.4	29
Yany-13-02-67	631.4	13.7	633.2	12.2	639.8	26.3	29
Yany-13-02-68	544.5	26.2	600.9	70.0	819.8	305.6	29
Yany-13-02-69	291.0	6.6	291.0	10.3	290.6	77.1	29

Yany-13-02-71	288.0	7.3	276.2	15.5	177.4	136.7	29
Yany-13-02-72	851.4	12.6	841.3	14.5	814.6	41.6	29
Yany-13-02-73	1872.8	66.2	1871.3	36.4	1869.6	22.0	29
Yany-13-02-74	1096.4	17.0	1092.9	22.5	1086.1	58.2	29
Yany-13-02-75	753.4	25.8	772.7	24.0	829.1	53.5	29
Yany-13-02-76	2392.5	49.2	2431.3	22.8	2464.0	4.5	29
Yany-13-02-77	749.5	10.2	756.5	10.5	777.4	28.4	29
Yany-13-02-78	317.8	5.4	319.1	11.1	329.0	83.1	29
Yany-13-02-79	88.2	2.1	87.4	16.1	64.5	458.1	29
Yany-13-02-80	88.3	2.3	87.9	4.9	78.2	124.4	29
Yany-13-02-82	278.8	9.2	275.3	9.6	245.4	48.3	29
Yany-13-02-83	1826.1	20.4	1826.4	12.5	1826.8	13.3	29
Yany-13-02-84	2363.1	62.0	2490.8	29.2	2596.7	4.1	29
Yany-13-02-85	89.8	1.5	89.8	6.3	92.1	168.0	29
Yany-13-02-86	1803.0	41.6	1792.6	26.0	1780.6	29.1	29
Yany-13-02-87	461.1	7.3	458.8	10.9	447.0	54.9	29
Yany-13-02-88	1665.2	19.1	1747.8	10.9	1848.0	2.2	29
Yany-13-02-89	302.3	16.4	337.4	40.0	586.7	277.8	29
Yany-13-02-90	226.1	18.9	245.6	43.8	436.0	407.2	29
Yany-13-02-91	1707.7	40.2	1780.3	22.7	1866.5	7.1	29
Yany-13-02-92	804.8	16.5	798.4	21.9	780.5	69.3	29
Yany-13-02-94	1827.0	78.7	1822.2	49.4	1816.6	56.0	29
Yany-13-02-95	2382.7	64.3	2448.2	30.6	2503.1	12.6	29
Yany-13-02-96	2156.8	58.5	2312.3	29.3	2452.7	7.4	29
Yany-13-02-97	216.2	6.1	215.4	11.1	206.1	115.0	29
Yany-13-02-98	212.4	5.5	207.0	26.5	145.5	327.9	29
Yany-13-02-99	804.7	23.0	828.1	52.8	891.6	182.4	29
Yany-13-04-01	884.7	27.0	894.1	28.7	917.6	73.1	31
Yany-13-04-02	1760.2	36.1	1812.2	20.2	1872.6	8.3	31
Yany-13-04-03	1303.6	42.9	1429.1	40.2	1621.3	70.3	31
Yany-13-04-04	445.7	24.6	449.0	27.4	465.4	109.5	31
Yany-13-04-05	592.4	14.2	587.1	19.8	566.5	79.7	31
Yany-13-04-06	1759.2	23.5	1763.6	27.1	1768.9	52.1	31
Yany-13-04-07	322.3	8.0	339.6	26.4	459.6	195.5	31
Yany-13-04-08	289.3	7.3	288.1	18.2	279.0	155.0	31
Yany-13-04-09	1107.3	10.1	1110.5	7.0	1116.7	5.8	31
Yany-13-04-10	213.8	7.1	208.1	8.6	144.4	71.6	31
Yany-13-04-100	207.0	4.2	205.7	8.9	191.0	100.7	31
Yany-13-04-101	438.7	11.3	445.4	14.4	480.0	65.3	31
Yany-13-04-102	209.9	2.0	211.7	2.8	232.8	25.8	31

Yany-13-04-103	776.5	15.0	783.3	16.3	802.5	45.6	31
Yany-13-04-104	475.9	14.5	472.0	13.9	453.2	42.1	31
Yany-13-04-106	1846.3	113.8	1859.7	60.6	1874.8	5.3	31
Yany-13-04-107	1841.4	12.1	1864.2	6.9	1889.7	5.3	31
Yany-13-04-108	535.5	12.7	556.0	16.4	640.6	62.9	31
Yany-13-04-109	1785.1	96.6	1791.5	68.5	1798.9	95.7	31
Yany-13-04-11	1895.9	34.4	1890.5	18.1	1884.7	5.3	31
Yany-13-04-110	1746.5	50.1	1809.1	27.7	1882.0	3.2	31
Yany-13-04-111	1746.8	18.3	1795.2	11.0	1852.0	9.4	31
Yany-13-04-112	209.5	4.2	209.5	11.9	209.9	137.8	31
Yany-13-04-12	334.4	11.5	319.3	43.8	210.9	363.0	31
Yany-13-04-13	211.8	4.2	206.7	9.3	148.9	107.4	31
Yany-13-04-14	1912.0	28.2	1895.4	14.8	1877.4	4.3	31
Yany-13-04-15	1161.4	18.0	1159.2	12.0	1155.1	7.2	31
Yany-13-04-16	219.3	6.3	213.0	9.6	144.3	94.7	31
Yany-13-04-17	649.0	10.1	656.8	12.3	684.0	42.0	31
Yany-13-04-18	1076.1	27.3	1069.3	20.0	1055.4	25.1	31
Yany-13-04-19	508.1	20.7	517.0	64.5	556.8	336.0	31
Yany-13-04-20	212.1	4.5	207.3	10.4	153.8	119.2	31
Yany-13-04-22	213.9	7.4	205.0	34.5	103.7	433.9	31
Yany-13-04-24	2410.4	23.2	2396.1	14.7	2384.0	18.8	31
Yany-13-04-25	2038.9	44.2	2222.9	22.9	2397.0	4.7	31
Yany-13-04-26	212.7	4.1	212.0	11.8	204.0	136.0	31
Yany-13-04-27	1778.4	16.8	1815.7	10.9	1858.8	12.6	31
Yany-13-04-28	2115.7	47.6	2300.7	24.1	2469.3	3.9	31
Yany-13-04-29	253.4	4.4	244.5	18.3	160.3	192.6	31
Yany-13-04-30	236.1	4.3	246.2	7.9	343.2	69.7	31
Yany-13-04-31	211.4	3.0	212.7	12.5	226.8	147.6	31
Yany-13-04-34	433.3	16.1	435.2	15.8	444.9	51.0	31
Yany-13-04-35	442.9	11.8	452.2	24.4	499.7	133.9	31
Yany-13-04-36	402.5	13.3	408.1	16.0	440.0	73.7	31
Yany-13-04-37	812.3	65.1	839.8	50.1	913.2	41.7	31
Yany-13-04-38	1963.0	27.9	1972.4	14.5	1982.2	3.8	31
Yany-13-04-39	272.0	3.3	273.2	17.0	283.4	159.8	31
Yany-13-04-41	250.7	6.9	234.7	34.8	77.7	390.7	31
Yany-13-04-44	422.2	28.3	426.6	26.3	450.4	66.1	31
Yany-13-04-45	1880.1	18.9	1877.5	10.3	1874.6	6.0	31
Yany-13-04-46	769.3	13.1	778.2	44.4	803.8	166.8	31
Yany-13-04-47	1741.0	19.4	1757.6	14.8	1777.3	22.5	31
Yany-13-04-48	211.8	5.9	212.5	15.9	220.5	181.1	31
Yany-13-04-49	214.4	4.4	213.0	10.1	198.0	111.9	31

Yany-13-04-50	213.5	3.0	215.5	13.9	237.5	161.7	31
Yany-13-04-51	982.8	34.2	998.7	29.6	1033.9	55.8	31
Yany-13-04-52	609.3	11.4	618.9	9.6	654.2	14.1	31
Yany-13-04-53	806.8	33.8	801.6	27.2	787.3	42.7	31
Yany-13-04-54	812.2	17.2	825.9	19.5	863.1	54.3	31
Yany-13-04-55	328.5	18.5	323.3	30.3	286.1	212.9	31
Yany-13-04-56	242.1	3.7	237.9	13.1	196.7	138.8	31
Yany-13-04-57	315.3	3.0	319.5	9.0	349.7	71.2	31
Yany-13-04-58	219.4	3.6	220.7	8.6	234.6	92.3	31
Yany-13-04-60	801.5	19.6	800.1	23.3	796.2	69.7	31
Yany-13-04-61	597.8	20.1	638.5	17.5	785.6	23.5	31
Yany-13-04-62	88.2	1.8	95.8	7.7	287.3	187.0	31
Yany-13-04-63	840.6	12.9	839.5	15.2	836.5	43.6	31
Yany-13-04-64	1870.4	16.6	1880.6	8.9	1891.9	2.8	31
Yany-13-04-65	747.8	28.5	757.6	52.8	786.5	189.6	31
Yany-13-04-66	822.2	20.5	825.4	17.4	834.2	32.5	31
Yany-13-04-67	475.7	7.2	470.8	11.4	446.6	57.5	31
Yany-13-04-68	207.6	2.1	200.9	8.4	123.6	105.3	31
Yany-13-04-69	611.2	11.3	606.7	10.4	589.8	25.8	31
Yany-13-04-70	530.3	21.4	562.4	20.7	694.4	48.8	31
Yany-13-04-71	829.9	12.7	842.8	32.9	877.1	113.9	31
Yany-13-04-72	2622.1	61.3	2601.1	26.9	2584.8	6.7	31
Yany-13-04-73	251.7	8.2	250.7	9.2	241.6	56.2	31
Yany-13-04-74	1904.9	36.3	1888.4	19.1	1870.2	5.5	31
Yany-13-04-75	1865.4	57.7	1871.2	30.8	1877.5	9.2	31
Yany-13-04-76	402.5	5.4	405.2	6.1	420.5	27.2	31
Yany-13-04-77	216.4	7.6	205.5	38.1	81.9	482.5	31
Yany-13-04-80	282.9	6.4	286.8	11.9	318.2	94.3	31
Yany-13-04-81	1876.2	62.4	1878.2	33.1	1880.5	8.6	31
Yany-13-04-82	88.4	1.6	89.1	4.1	108.4	106.1	31
Yany-13-04-83	442.2	5.4	445.0	8.2	459.7	42.3	31
Yany-13-04-84	1877.8	33.6	1874.0	17.8	1869.8	5.4	31
Yany-13-04-85	248.3	6.8	251.7	20.6	283.5	202.2	31
Yany-13-04-86	222.4	7.1	247.3	29.9	490.7	292.6	31
Yany-13-04-87	210.8	5.9	213.3	17.5	240.0	199.6	31
Yany-13-04-88	216.2	6.8	218.4	17.0	242.4	185.2	31
Yany-13-04-89	88.9	1.5	91.0	7.9	145.5	209.5	31
Yany-13-04-90	1450.9	107.9	1508.5	65.4	1590.5	9.9	31
Yany-13-04-91	265.0	8.6	260.6	37.9	221.0	375.7	31
Yany-13-04-92	407.2	12.6	393.3	19.2	312.2	112.5	31
Yany-13-04-94	209.8	3.2	207.5	8.6	182.1	100.5	31

Yany-13-04-96	1816.8	33.9	1995.1	36.1	2185.2	61.5	31
Yany-13-04-97	438.0	17.1	455.9	22.0	547.5	96.3	31
Yany-13-04-98	88.2	3.5	87.9	6.8	81.7	165.3	31
Yany-13-04-99	812.0	16.4	802.6	23.8	776.5	77.9	31
Yany-11-07-100	787.3	12.0	794.6	37.9	815.3	140.0	32
Yany-11-07-101	298.9	9.6	290.2	23.6	221.2	202.8	32
Yany-11-07-102	800.2	8.4	800.0	25.3	799.4	92.9	32
Yany-11-07-103	216.8	2.7	219.7	6.1	250.8	64.3	32
Yany-11-07-11	460.3	10.0	478.0	29.6	563.9	162.3	32
Yany-11-07-12	773.8	7.1	779.1	9.8	794.3	31.6	32
Yany-11-07-13	214.3	10.2	209.9	11.0	159.9	75.4	32
Yany-11-07-14	451.0	7.6	453.0	9.7	462.9	44.1	32
Yany-11-07-16	2416.1	87.9	2436.7	40.5	2453.9	6.4	32
Yany-11-07-17	807.1	15.8	808.9	13.8	813.8	27.7	32
Yany-11-07-18	429.7	5.1	438.6	11.4	485.9	65.5	32
Yany-11-07-19	318.0	9.5	315.2	9.7	294.4	43.0	32
Yany-11-07-2	2586.1	32.3	2650.9	14.6	2700.7	5.1	32
Yany-11-07-21	357.2	8.7	358.1	9.7	364.1	45.3	32
Yany-11-07-22	464.6	4.2	466.0	9.3	473.1	51.0	32
Yany-11-07-23	2604.7	64.5	2564.4	28.5	2532.6	7.9	32
Yany-11-07-24	1786.4	26.3	1822.7	14.9	1864.3	9.1	32
Yany-11-07-25	261.5	4.4	265.1	8.4	297.6	71.7	32
Yany-11-07-26	800.4	11.0	802.1	26.6	806.7	95.7	32
Yany-11-07-27	85.5	3.1	90.5	25.5	223.8	688.7	32
Yany-11-07-28	810.9	7.0	815.0	9.9	826.2	31.3	32
Yany-11-07-29	272.6	4.7	276.5	11.0	309.0	95.8	32
Yany-11-07-3	308.7	9.2	314.1	16.9	354.5	123.2	32
Yany-11-07-30	208.1	4.2	202.8	9.5	141.4	111.7	32
Yany-11-07-31	769.0	5.4	761.9	11.4	741.0	42.3	32
Yany-11-07-32	785.2	15.3	784.2	18.5	781.5	56.2	32
Yany-11-07-33	784.7	10.8	777.5	25.0	756.8	91.9	32
Yany-11-07-34	316.2	3.9	308.5	14.8	250.6	124.8	32
Yany-11-07-35	214.0	4.1	213.0	14.8	201.8	173.1	32
Yany-11-07-36	2147.9	34.2	2137.5	17.5	2127.6	10.1	32
Yany-11-07-37	2362.1	45.8	2415.5	24.4	2460.7	21.6	32
Yany-11-07-38	370.4	8.1	361.0	10.4	301.4	58.8	32
Yany-11-07-39	211.8	3.6	216.8	8.0	270.9	85.5	32
Yany-11-07-4	209.2	2.0	211.7	3.2	239.9	31.1	32
Yany-11-07-40	437.6	26.8	433.5	26.6	411.8	91.9	32
Yany-11-07-41	214.5	8.3	214.1	19.1	210.4	210.7	32

Yany-11-07-42	439.2	19.8	432.1	27.1	394.4	137.3	32
Yany-11-07-43	211.9	4.0	213.9	10.1	235.6	112.4	32
Yany-11-07-44	771.2	21.2	776.0	51.1	789.6	188.1	32
Yany-11-07-45	287.2	26.9	331.5	27.6	655.8	39.7	32
Yany-11-07-46	1626.3	25.4	1723.1	15.4	1842.7	9.9	32
Yany-11-07-48	1916.8	13.7	1900.5	9.3	1882.7	12.6	32
Yany-11-07-49	205.2	4.3	204.1	14.7	191.7	177.7	32
Yany-11-07-50	221.3	6.9	214.2	15.0	136.4	166.4	32
Yany-11-07-51	1924.3	48.9	1895.6	26.1	1864.3	13.8	32
Yany-11-07-54	798.3	17.5	804.6	19.0	822.2	51.9	32
Yany-11-07-55	368.2	6.0	361.0	8.8	314.6	54.0	32
Yany-11-07-56	786.6	20.6	782.5	19.7	770.9	48.8	32
Yany-11-07-57	794.3	29.0	790.5	21.9	779.9	18.6	32
Yany-11-07-58	1817.3	25.0	1845.2	14.1	1876.8	8.9	32
Yany-11-07-59	2191.8	91.2	2189.2	44.3	2186.8	8.7	32
Yany-11-07-61	758.0	15.2	769.9	42.2	804.4	157.7	32
Yany-11-07-62	2589.4	48.0	2550.7	21.4	2520.1	7.5	32
Yany-11-07-64	2389.1	16.9	2359.1	8.7	2333.3	7.5	32
Yany-11-07-66	821.4	6.8	821.2	14.4	820.5	50.3	32
Yany-11-07-67	500.6	18.5	507.1	20.4	536.7	73.6	32
Yany-11-07-68	208.7	3.3	208.4	12.0	204.8	142.7	32
Yany-11-07-69	257.7	7.3	235.6	28.2	20.8	314.9	32
Yany-11-07-7	444.1	13.2	443.6	17.1	441.2	80.8	32
Yany-11-07-70	90.0	6.4	89.6	10.2	78.2	227.2	32
Yany-11-07-72	820.2	10.7	820.8	26.6	822.5	94.4	32
Yany-11-07-73	767.6	31.5	765.3	25.4	758.5	39.2	32
Yany-11-07-74	769.0	11.3	782.5	17.2	821.2	57.4	32
Yany-11-07-75	338.6	6.0	342.4	11.8	368.4	81.7	32
Yany-11-07-76	1914.3	33.7	1890.9	17.5	1865.2	2.8	32
Yany-11-07-77	1920.9	77.7	1883.9	40.6	1843.3	13.6	32
Yany-11-07-79	433.2	12.4	439.6	15.6	473.5	71.7	32
Yany-11-07-82	518.3	13.5	538.0	23.5	622.2	106.4	32
Yany-11-07-83	798.0	19.8	795.1	28.5	786.9	93.2	32
Yany-11-07-84	2911.9	93.4	2842.2	38.3	2793.2	7.8	32
Yany-11-07-85	1854.5	17.3	1859.3	9.5	1864.6	5.5	32
Yany-11-07-86	1905.3	34.5	1896.6	18.2	1887.1	6.5	32
Yany-11-07-87	85.3	4.1	82.3	9.2	-3.8	257.9	32
Yany-11-07-89	418.3	7.2	421.6	11.2	439.7	60.3	32
Yany-11-07-9	89.0	5.0	92.4	5.6	179.4	67.7	32
Yany-11-07-90	800.6	9.6	809.2	19.0	832.9	65.9	32
Yany-11-07-91	217.0	5.5	215.6	11.2	200.5	120.0	32

Yany-11-07-93	219.2	7.2	216.2	9.6	183.3	84.2	32
Yany-11-07-94	215.0	3.0	218.0	9.5	250.4	107.1	32
Yany-11-07-95	582.8	10.6	587.1	10.0	603.8	25.8	32
Yany-11-07-96	1917.0	37.6	1896.9	19.7	1874.8	7.0	32
Yany-11-07-97	272.4	3.8	270.1	10.6	250.9	97.6	32
Yany-11-07-98	212.5	3.0	214.4	7.6	235.8	84.5	32
Yany-11-07-99	773.9	11.6	771.9	11.7	766.0	30.9	32
Yany-13-03-01	211.3	3.0	202.9	15.3	106.4	193.4	28
Yany-13-03-02	538.2	13.0	519.3	34.2	436.8	179.0	28
Yany-13-03-03	88.6	1.4	90.9	3.8	151.2	95.2	28
Yany-13-03-04	1672.3	19.0	1759.9	11.0	1865.5	5.1	28
Yany-13-03-05	751.2	9.8	760.6	18.1	788.1	65.0	28
Yany-13-03-06	233.7	4.7	232.9	16.9	225.1	181.4	28
Yany-13-03-07	208.4	3.8	206.0	25.9	178.3	322.6	28
Yany-13-03-08	87.0	4.0	82.8	9.1	-36.7	253.3	28
Yany-13-03-09	2472.8	45.3	2571.5	27.8	2650.2	33.0	28
Yany-13-03-12	814.6	4.3	814.5	7.9	814.2	27.0	28
Yany-13-03-13	2446.3	48.5	2404.8	29.6	2369.9	37.0	28
Yany-13-03-14	1699.6	12.1	1710.0	18.7	1722.7	38.7	28
Yany-13-03-15	899.1	62.8	915.7	46.8	955.8	40.8	28
Yany-13-03-16	1893.0	52.4	1889.4	27.9	1885.3	11.9	28
Yany-13-03-17	240.9	1.6	242.8	8.7	261.4	91.6	28
Yany-13-03-18	211.9	2.5	208.8	11.4	173.5	137.7	28
Yany-13-03-19	1840.8	16.3	1857.3	9.1	1875.9	6.2	28
Yany-13-03-20	2304.0	30.4	2379.6	14.7	2444.9	5.4	28
Yany-13-03-21	222.0	2.8	226.0	13.7	267.9	152.3	28
Yany-13-03-22	87.6	0.9	84.6	2.8	-0.3	79.2	28
Yany-13-03-23	250.3	6.8	259.9	17.1	348.2	156.4	28
Yany-13-03-24	90.8	1.3	89.9	4.4	66.2	116.3	28
Yany-13-03-25	1775.4	10.3	1818.7	5.8	1868.6	2.5	28
Yany-13-03-26	2123.2	26.0	2102.0	13.2	2081.3	7.1	28
Yany-13-03-27	217.5	2.7	220.3	9.8	250.4	110.7	28
Yany-13-03-28	1691.7	19.3	1719.2	41.4	1752.8	88.2	28
Yany-13-03-29	99.3	5.6	149.8	30.6	1049.9	431.9	28
Yany-13-03-30	253.2	6.6	237.0	36.6	78.6	408.9	28
Yany-13-03-31	265.3	11.4	287.4	57.2	471.2	501.7	28
Yany-13-03-32	255.4	4.7	260.7	15.2	308.1	144.2	28
Yany-13-03-33	531.0	5.1	519.1	18.0	466.7	95.7	28
Yany-13-03-35	90.9	1.3	97.0	5.2	249.8	125.7	28
Yany-13-03-36	214.7	3.7	207.6	10.9	127.5	130.9	28

Yany-13-03-38	1068.9	26.5	1075.4	20.1	1088.8	27.8	28
Yany-13-03-39	217.1	1.6	221.1	5.2	264.0	57.7	28
Yany-13-03-40	2271.5	10.0	2458.5	5.4	2617.0	4.4	28
Yany-13-03-41	294.7	4.5	282.1	28.8	178.9	271.2	28
Yany-13-03-42	88.1	1.3	85.8	5.1	21.3	144.2	28
Yany-13-03-43	457.3	10.1	461.3	22.7	481.3	125.2	28
Yany-13-03-44	799.3	10.0	819.7	18.3	875.3	61.5	28
Yany-13-03-45	267.8	1.7	269.6	5.6	284.6	52.4	28
Yany-13-03-46	798.9	6.4	794.1	18.6	780.7	68.6	28
Yany-13-03-47	370.5	7.2	345.8	39.5	182.8	311.3	28
Yany-13-03-48	994.3	4.9	1015.2	6.0	1060.5	15.4	28
Yany-13-03-49	215.2	6.1	215.4	11.5	217.5	120.0	28
Yany-13-03-50	774.4	6.7	774.6	8.0	775.4	24.2	28
Yany-13-03-51	88.4	1.6	88.7	6.3	97.9	169.4	28
Yany-13-03-52	211.6	1.0	209.8	4.8	189.5	57.6	28
Yany-13-03-54	411.2	14.9	502.0	85.1	940.8	437.3	28
Yany-13-03-55	1509.0	18.6	1649.4	12.3	1833.3	10.7	28
Yany-13-03-56	92.5	3.1	90.8	23.6	46.2	653.4	28
Yany-13-03-59	1682.2	46.1	1714.3	27.0	1753.7	17.6	28
Yany-13-03-60	86.9	5.5	71.8	19.4	-404.5	722.1	28
Yany-13-03-61	86.1	3.5	88.0	7.6	138.3	188.1	28
Yany-13-03-62	219.5	5.0	216.7	15.3	186.4	174.8	28
Yany-13-03-63	219.6	3.7	220.3	13.3	227.9	150.6	28
Yany-13-03-64	250.1	7.2	235.3	17.7	90.2	187.1	28
Yany-13-03-65	763.5	5.8	761.5	18.3	755.5	69.9	28
Yany-13-03-66	502.9	7.9	513.5	10.2	561.2	42.0	28
Yany-13-03-67	90.0	1.9	92.5	4.4	156.8	106.4	28
Yany-13-03-68	1848.0	24.0	1861.6	13.3	1876.8	8.0	28
Yany-13-03-70	1484.5	13.0	1631.3	8.7	1826.1	7.9	28
Yany-13-03-71	2096.6	31.4	2199.7	22.0	2297.2	29.4	28
Yany-13-03-72	1825.4	23.4	1828.0	17.0	1830.9	24.7	28
Yany-13-03-73	416.1	4.4	419.0	13.6	434.9	84.8	28
Yany-13-03-74	209.8	4.4	213.5	11.5	254.0	128.0	28
Yany-13-03-75	2491.1	44.3	2498.0	20.3	2503.5	7.5	28
Yany-13-03-76	562.7	5.0	562.7	6.0	562.8	22.5	28
Yany-13-03-76B	258.5	7.3	253.2	54.6	204.4	567.8	28
Yany-13-03-77	776.1	14.2	782.6	30.4	801.1	109.4	28
Yany-13-03-78	1509.2	38.8	1654.1	26.4	1843.4	26.8	28
Yany-13-03-80	531.9	10.0	530.5	16.2	524.7	74.6	28
Yany-13-03-81	778.3	14.1	783.9	24.0	799.9	82.6	28
Yany-13-03-82	227.5	7.8	227.8	9.3	231.6	67.3	28

Yany-13-03-83	2636.1	19.6	2662.8	9.7	2683.2	8.0	28
Yany-13-03-84	2628.4	24.7	2657.8	11.9	2680.2	8.8	28
Yany-13-03-85	448.5	8.0	441.4	15.3	405.1	86.0	28
Yany-13-03-86	90.4	2.7	84.4	7.5	-82.6	214.4	28
Yany-13-03-87	2010.3	29.1	1998.6	15.2	1986.5	7.7	28
Yany-13-03-88	207.0	5.4	198.3	11.3	95.9	134.4	28
Yany-13-03-89	442.5	7.4	441.4	10.9	436.0	55.8	28
Yany-13-03-90	330.7	7.5	421.7	9.3	955.5	27.2	28
Yany-13-03-91	1889.8	30.3	1889.2	16.8	1888.5	11.5	28
Yany-13-08-01	230.3	2.9	231.3	8.0	241.3	83.7	30
Yany-13-08-02	450.6	6.1	448.5	18.9	437.8	111.5	30
Yany-13-08-03	2283.0	14.1	2406.2	6.8	2512.2	1.5	30
Yany-13-08-04	216.2	4.9	211.6	37.1	160.2	454.2	30
Yany-13-08-05	87.2	1.4	89.4	9.0	146.6	243.4	30
Yany-13-08-06	794.0	14.2	787.5	12.9	769.2	29.4	30
Yany-13-08-07	1905.9	19.5	1900.0	11.4	1893.5	11.1	30
Yany-13-08-09	936.7	12.3	936.5	9.8	935.9	15.2	30
Yany-13-08-10	88.7	1.4	90.7	7.3	144.1	195.2	30
Yany-13-08-100	88.5	4.2	98.8	11.2	356.8	246.5	30
Yany-13-08-101	217.7	11.0	215.9	11.6	196.4	72.1	30
Yany-13-08-102	468.1	11.1	471.0	23.5	484.7	126.7	30
Yany-13-08-103	1171.3	35.3	1158.4	24.4	1134.2	25.2	30
Yany-13-08-104	431.0	7.8	466.5	29.1	645.3	162.4	30
Yany-13-08-105	794.1	13.7	793.5	12.5	791.6	28.0	30
Yany-13-08-12	217.2	6.7	215.4	13.7	196.0	146.4	30
Yany-13-08-14	222.4	4.7	231.6	14.4	326.2	149.9	30
Yany-13-08-15	219.0	5.7	220.2	14.5	233.1	158.2	30
Yany-13-08-16	956.7	12.8	955.7	9.5	953.3	10.4	30
Yany-13-08-17	1924.5	25.5	1917.3	14.6	1909.4	13.1	30
Yany-13-08-18	1987.8	18.4	1989.4	11.4	1991.0	13.3	30
Yany-13-08-19	786.9	21.2	780.8	28.7	763.3	93.2	30
Yany-13-08-20	770.6	16.9	771.0	23.8	772.2	78.6	30
Yany-13-08-21	292.8	10.9	245.1	60.2	-189.7	695.2	30
Yany-13-08-22	1766.9	56.0	1817.1	30.9	1875.1	9.2	30
Yany-13-08-23	88.8	2.5	82.7	10.1	-91.2	305.3	30
Yany-13-08-24	1864.7	32.2	1870.3	23.9	1876.6	35.3	30
Yany-13-08-25	430.7	18.3	428.3	17.4	415.1	53.2	30
Yany-13-08-26	1881.4	33.4	1874.6	17.6	1867.2	3.5	30
Yany-13-08-27	216.2	4.1	212.2	18.7	168.2	223.6	30
Yany-13-08-28	818.5	16.8	820.6	13.6	826.5	21.5	30

Yany-13-08-29	1938.7	16.8	1907.3	10.0	1873.3	10.7	30
Yany-13-08-30	217.2	3.1	221.1	6.3	262.6	64.8	30
Yany-13-08-31	90.0	3.3	85.4	6.8	-40.3	179.3	30
Yany-13-08-32	86.6	6.2	79.8	7.6	-119.6	167.3	30
Yany-13-08-34	256.8	12.5	247.1	36.9	156.2	378.2	30
Yany-13-08-35	1062.9	12.8	1054.3	8.7	1036.5	5.3	30
Yany-13-08-37	92.2	6.1	91.3	6.2	68.3	55.9	30
Yany-13-08-38	260.2	5.1	258.3	12.0	241.2	112.5	30
Yany-13-08-39	216.0	6.9	210.5	13.6	149.5	149.7	30
Yany-13-08-40	87.9	2.3	84.9	10.4	3.0	302.5	30
Yany-13-08-43	205.9	9.8	204.0	10.1	182.1	60.4	30
Yany-13-08-44	1609.2	37.6	1612.2	23.5	1616.2	22.7	30
Yany-13-08-45	209.7	9.6	208.5	15.3	195.0	154.0	30
Yany-13-08-46	2450.7	39.2	2473.7	18.4	2492.7	7.9	30
Yany-13-08-47	210.6	4.7	210.8	10.9	213.4	122.2	30
Yany-13-08-48	1926.5	23.5	1906.7	12.5	1885.2	5.9	30
Yany-13-08-49	89.8	2.8	88.4	4.3	49.9	95.3	30
Yany-13-08-50	222.7	19.5	216.6	19.1	150.7	93.4	30
Yany-13-08-51	824.5	17.7	821.5	38.6	813.6	135.1	30
Yany-13-08-52	206.1	12.9	206.6	16.7	211.6	145.3	30
Yany-13-08-53	759.4	17.1	771.8	37.7	808.0	137.3	30
Yany-13-08-54	212.3	7.6	203.7	37.9	105.7	481.6	30
Yany-13-08-55	767.6	15.1	771.1	13.5	781.2	28.7	30
Yany-13-08-56	1858.0	60.5	1869.6	32.5	1882.4	12.4	30
Yany-13-08-57	1121.6	26.7	1121.0	20.1	1119.7	28.2	30
Yany-13-08-58	2452.1	29.5	2471.4	13.9	2487.3	6.6	30
Yany-13-08-60	788.4	28.6	803.2	29.3	844.4	75.1	30
Yany-13-08-62	215.4	7.1	203.4	25.8	65.9	324.3	30
Yany-13-08-63	1528.8	28.0	1665.8	17.7	1843.1	11.8	30
Yany-13-08-64	778.9	28.6	775.6	48.5	766.3	169.6	30
Yany-13-08-65	805.3	34.6	825.3	32.1	879.6	69.9	30
Yany-13-08-66	814.2	22.8	832.9	49.9	883.2	171.0	30
Yany-13-08-68	1703.8	23.4	1780.5	13.5	1871.6	6.3	30
Yany-13-08-69	972.5	29.8	978.9	23.5	993.4	35.6	30
Yany-13-08-70	764.6	11.2	763.8	11.2	761.5	29.3	30
Yany-13-08-71	1615.6	31.5	1719.5	18.4	1848.4	4.7	30
Yany-13-08-72	209.6	6.1	212.9	7.3	249.3	56.1	30
Yany-13-08-73	456.6	33.1	501.3	45.0	710.8	181.6	30
Yany-13-08-74	1645.1	30.8	1643.9	18.3	1642.4	13.8	30
Yany-13-08-75	1893.0	57.4	1924.2	32.0	1958.0	21.7	30
Yany-13-08-76	216.3	7.2	190.1	29.1	-124.1	408.7	30

Yany-13-08-77	800.5	17.7	797.3	17.3	788.3	43.3	30
Yany-13-08-78	213.9	6.7	206.2	16.4	118.7	193.6	30
Yany-13-08-79	1764.9	31.7	1815.6	18.3	1874.2	12.2	30
Yany-13-08-80	212.1	8.3	208.4	15.0	167.0	161.0	30
Yany-13-08-81	891.3	74.4	911.1	69.1	959.6	147.3	30
Yany-13-08-82	449.3	7.0	454.0	11.4	477.9	58.6	30
Yany-13-08-83	264.9	8.0	238.4	39.5	-15.1	446.6	30
Yany-13-08-84	331.9	10.5	322.6	58.0	256.0	480.5	30
Yany-13-08-85	87.5	7.0	96.5	24.7	326.6	590.1	30
Yany-13-08-86	444.5	8.1	443.2	15.6	436.3	87.3	30
Yany-13-08-87	1005.0	22.3	1003.2	22.0	999.4	50.6	30
Yany-13-08-88	404.8	7.0	392.8	14.7	322.4	94.3	30
Yany-13-08-89	1972.9	153.3	1927.8	78.1	1879.7	6.6	30
Yany-13-08-90	477.6	15.2	484.3	20.1	516.4	89.1	30
Yany-13-08-91	745.8	33.0	780.7	26.0	881.7	19.1	30
Yany-13-08-92	734.0	31.5	730.7	26.9	720.3	51.7	30
Yany-13-08-93	2753.6	92.4	2788.8	40.1	2814.4	14.5	30
Yany-13-08-94	2338.9	54.5	2334.7	25.8	2331.1	8.7	30
Yany-13-08-95	841.5	22.8	831.3	26.7	804.0	77.9	30
Yany-13-08-96	286.7	17.0	282.0	43.0	243.3	379.9	30
Yany-13-08-97	821.4	14.9	814.1	12.5	794.2	23.9	30
Yany-13-08-98	1055.3	89.1	1100.7	63.0	1191.6	39.3	30
Yany-13-08-99	1884.7	24.1	1880.2	12.8	1875.1	4.5	30
Yany-13-08-S41	422.4	11.7	411.7	14.0	352.4	67.3	30
Yany-13-11-01	809.5	8.5	826.0	15.4	870.9	51.6	27
Yany-13-11-02	805.9	10.5	804.6	18.4	801.0	63.1	27
Yany-13-11-03	778.5	11.1	778.7	12.3	779.3	35.6	27
Yany-13-11-04	805.3	10.3	811.2	35.8	827.7	130.8	27
Yany-13-11-05	753.6	8.7	755.4	22.5	760.7	85.1	27
Yany-13-11-06	779.3	11.2	780.1	15.2	782.2	49.1	27
Yany-13-11-07	765.9	8.2	776.8	19.6	808.3	71.6	27
Yany-13-11-08	651.7	6.1	687.9	6.5	808.3	17.9	27
Yany-13-11-09	227.6	2.5	227.8	6.1	230.3	63.6	27
Yany-13-11-10	804.0	11.8	809.0	38.2	823.0	139.3	27
Yany-13-11-11	764.9	14.0	761.6	28.3	751.6	103.6	27
Yany-13-11-12	809.3	5.1	807.0	5.6	800.6	15.6	27
Yany-13-11-13	538.0	5.2	530.3	19.7	497.4	102.8	27
Yany-13-11-14	764.2	10.1	763.9	13.8	762.9	45.6	27
Yany-13-11-15	816.2	7.6	812.1	10.8	800.8	34.6	27
Yany-13-11-17	795.4	6.8	788.0	18.0	767.1	66.6	27

Yany-13-11-18	831.9	10.9	839.5	24.3	859.6	83.4	27
Yany-13-11-20	768.0	30.3	792.5	24.5	862.1	31.6	27
Yany-13-11-21	808.3	16.8	803.1	16.6	788.4	42.4	27
Yany-13-11-22	821.4	12.3	831.1	15.2	857.2	44.8	27
Yany-13-11-23	783.6	8.4	782.3	12.5	778.6	41.8	27
Yany-13-11-24	779.5	11.0	778.2	18.0	774.5	62.1	27
Yany-13-11-25	796.0	3.9	797.1	5.5	800.1	17.9	27
Yany-13-11-28	760.5	13.3	757.9	28.4	750.3	105.1	27
Yany-13-11-30	791.3	10.2	789.1	12.8	782.8	39.9	27
Yany-13-11-32	811.9	5.3	812.6	13.6	814.6	48.8	27
Yany-13-11-33	692.7	5.9	716.6	8.8	792.1	30.6	27
Yany-13-11-34	806.4	5.9	803.6	11.1	796.0	38.5	27
Yany-13-11-35	768.9	13.4	763.7	47.1	748.3	181.3	27
Yany-13-11-36	718.7	6.1	733.8	7.2	780.3	21.8	27
Yany-13-11-37	767.2	7.1	766.2	8.6	763.4	26.6	27
Yany-13-11-38	788.9	7.6	781.4	11.5	760.1	39.1	27
Yany-13-11-39	779.7	8.5	798.5	13.9	851.2	46.3	27
Yany-13-11-40	783.6	8.8	794.5	7.8	825.2	15.8	27
Yany-13-11-41	775.2	5.1	784.3	12.3	810.1	44.7	27
Yany-13-11-42	18.3	0.6	14.8	5.3	-519.4	989.9	27
Yany-13-11-43	785.5	21.8	805.2	24.6	860.1	68.5	27
Yany-13-11-44	784.2	8.9	794.3	8.3	822.8	18.8	27
Yany-13-11-45	794.1	29.9	792.4	42.1	787.5	137.2	27
Yany-13-11-46	774.9	6.8	767.9	17.3	747.7	64.7	27
Yany-13-11-48	781.4	10.7	780.4	32.6	777.5	122.4	27
Yany-13-11-50	783.2	9.1	789.4	12.2	807.1	38.6	27
Yany-13-11-51	803.9	12.5	811.1	14.9	830.9	43.6	27
Yany-13-11-52	752.7	14.3	756.2	21.1	766.7	71.9	27
Yany-13-11-53	803.1	9.6	816.0	14.0	851.5	44.9	27
Yany-13-11-54	741.7	18.9	753.0	18.1	786.5	43.3	27
Yany-13-11-55	927.0	24.2	963.3	18.9	1047.1	23.0	27
Yany-13-11-56	755.9	35.7	774.9	35.6	830.0	88.5	27
Yany-13-11-57	807.9	12.9	811.8	12.9	822.6	32.8	27
Yany-13-11-58	760.7	12.1	758.9	12.5	753.7	34.2	27
Yany-13-11-59	791.5	10.3	804.8	19.0	841.8	65.1	27
Yany-13-11-60	776.7	32.9	792.9	25.4	838.7	22.6	27
Yany-13-11-61	763.3	17.5	765.1	29.0	770.3	101.4	27
Yany-13-11-62	802.2	16.5	805.0	14.0	812.5	26.3	27
Yany-13-11-63	885.1	17.7	916.1	20.1	991.5	51.8	27
Yany-13-11-66	802.7	13.2	803.3	12.2	804.9	27.4	27
Yany-13-11-67	751.8	12.8	750.5	17.4	746.6	57.9	27

Yany-13-11-68	669.8	15.4	694.1	12.6	773.7	12.9	27
Yany-13-11-69	775.8	19.3	773.2	19.8	765.7	53.4	27
Yany-13-11-70	530.2	12.6	544.6	18.0	605.4	75.1	27
Yany-13-11-71	719.9	25.5	732.8	20.4	772.2	22.8	27
Yany-13-11-73	1228.3	29.0	1233.6	21.7	1242.9	30.8	27
Yany-13-12-01	758.7	13.5	787.1	31.4	868.4	112.2	26
Yany-13-12-04	825.7	6.3	827.1	9.6	830.9	31.2	26
Yany-13-12-05	689.1	11.7	694.1	13.3	710.6	41.0	26
Yany-13-12-07	770.4	12.5	772.9	41.2	780.1	156.2	26
Yany-13-12-08	777.7	14.1	768.9	15.1	743.6	42.9	26
Yany-13-12-09	755.6	5.9	771.1	15.3	816.3	56.4	26
Yany-13-12-11	774.8	14.9	798.9	35.5	866.9	126.4	26
Yany-13-12-12	919.0	14.6	921.0	21.6	926.0	64.6	26
Yany-13-12-13	769.1	13.5	768.6	18.4	767.2	60.1	26
Yany-13-12-14	822.2	13.4	831.7	20.0	857.2	63.6	26
Yany-13-12-15	793.8	11.5	799.7	48.3	816.2	179.7	26
Yany-13-12-16	981.7	33.5	969.2	29.9	940.9	62.6	26
Yany-13-12-17	758.4	12.6	779.9	22.3	842.0	76.9	26
Yany-13-12-18	768.9	58.0	808.5	49.5	919.3	78.9	26
Yany-13-12-19	801.6	7.7	796.8	9.7	783.4	29.9	26
Yany-13-12-20	727.6	20.4	736.2	22.7	762.5	66.8	26
Yany-13-12-21	772.5	21.0	776.2	34.5	786.6	118.9	26
Yany-13-12-25	845.5	10.6	844.2	9.4	840.6	19.8	26
Yany-13-12-26	769.8	17.9	776.2	21.5	794.9	65.1	26
Yany-13-12-28	775.0	11.8	793.3	17.6	845.0	57.4	26
Yany-13-12-29	483.3	10.1	489.3	17.8	517.5	89.0	26
Yany-13-12-30	1038.3	17.3	1040.5	16.0	1045.2	33.7	26
Yany-13-12-31	858.2	22.1	861.4	16.8	869.4	18.7	26
Yany-13-12-32	821.4	24.4	834.6	26.4	869.9	70.5	26
Yany-13-12-33	773.8	15.3	768.0	27.8	751.1	99.4	26
Yany-13-12-34	776.0	11.7	796.3	52.4	853.6	194.6	26
Yany-13-12-35	2098.1	27.3	2264.4	14.7	2418.2	9.7	26
Yany-13-12-37	754.7	28.9	770.7	23.0	817.5	26.7	26
Yany-13-12-39	767.9	26.8	774.4	21.0	793.0	24.5	26
Yany-13-12-40	781.1	19.4	773.4	26.2	751.4	85.9	26
Yany-13-12-41	1103.2	84.1	1102.3	56.6	1100.5	27.0	26
Yany-13-12-42	727.6	13.3	742.0	36.7	785.8	140.9	26
Yany-13-12-43	796.0	23.1	810.0	29.5	848.9	89.5	26
Yany-13-12-44	1799.0	68.7	1843.8	38.0	1894.8	16.0	26
Yany-13-12-49	788.0	27.6	802.4	45.5	842.7	152.2	26

Yany-13-12-50	813.1	17.6	818.6	37.0	833.6	128.7	26
Yany-13-12-51	781.3	18.4	773.8	36.3	751.9	131.6	26
Yany-13-12-54	957.3	21.0	964.2	37.2	980.0	111.7	26
Yany-13-12-55	778.7	18.0	783.8	25.3	798.5	82.6	26
Yany-13-12-56	802.4	20.6	803.6	18.2	807.0	38.0	26
Yany-13-12-57	2534.3	115.6	2568.2	53.5	2595.1	24.8	26
Yany-13-12-58	276.4	17.5	315.1	46.0	612.6	341.0	26
Yany-13-12-60	797.3	19.1	793.1	23.0	781.3	69.8	26
Yany-13-12-62	795.4	7.8	788.3	10.1	768.1	32.2	26
Yany-13-12-64	829.8	47.1	832.1	37.1	838.2	51.1	26
Yany-13-12-65	751.5	9.3	752.9	10.7	757.1	32.4	26
Yany-13-12-66	770.0	14.2	763.5	13.9	744.6	35.7	26
Yany-13-12-67	839.3	37.7	830.9	29.1	808.4	37.8	26
Yany-13-12-69	789.2	23.5	789.9	26.9	792.0	78.5	26
Yany-13-12-70	791.1	21.5	801.5	27.8	830.5	85.5	26
Yany-13-12-71	828.2	15.6	821.0	12.9	801.5	22.9	26
Yany-13-12-72	792.0	7.7	790.5	12.1	786.0	40.7	26
Yany-13-12-73	775.2	10.1	782.6	10.3	803.5	27.1	26
Yany-13-12-74	796.9	15.3	794.2	26.8	786.6	92.5	26
Yany-13-12-75	780.0	15.2	777.6	14.5	770.6	35.7	26
Yany-13-12-76	779.1	12.5	778.0	13.2	774.6	36.2	26
Yany-13-12-77	775.6	11.1	772.6	11.0	764.0	28.4	26
Yany-13-12-78	761.1	11.0	756.0	11.0	741.1	29.2	26
Yany-13-12-79	754.7	8.8	751.0	15.6	740.2	56.4	26
Yany-13-12-80	768.5	12.9	764.1	18.8	751.3	63.6	26
Yany-13-12-82	614.5	4.9	631.8	7.7	694.4	30.0	26
Yany-13-12-84	2002.4	43.3	2018.5	25.7	2035.0	26.7	26
Yany-13-12-85	973.3	21.5	974.2	16.1	976.2	20.1	26
Yany-13-12-86	775.9	13.7	774.5	12.2	770.3	26.3	26
Yany-13-12-87	794.7	17.6	801.8	14.8	821.6	26.9	26
Yany-13-13-01	771.6	6.9	769.2	14.6	762.4	53.3	25
Yany-13-13-02	793.8	19.2	797.0	29.1	806.1	96.3	25
Yany-13-13-04	817.7	5.3	817.5	7.1	817.2	22.4	25
Yany-13-13-05	822.5	11.7	826.7	22.9	837.8	78.3	25
Yany-13-13-06	788.7	12.8	801.7	30.1	838.1	107.1	25
Yany-13-13-07	822.5	27.1	845.6	25.5	906.6	56.2	25
Yany-13-13-09	798.1	9.0	797.0	34.9	794.0	130.2	25
Yany-13-13-10	769.9	10.5	779.4	37.0	806.8	139.3	25
Yany-13-13-100	792.8	13.5	800.9	32.4	823.4	115.9	25
Yany-13-13-101	773.7	9.0	770.3	17.2	760.5	62.0	25

Yany-13-13-12	531.6	9.9	531.6	22.2	531.2	109.7	25
Yany-13-13-13	735.0	17.4	768.1	14.9	866.0	23.9	25
Yany-13-13-14	789.1	9.8	789.8	11.7	791.8	35.0	25
Yany-13-13-17	778.0	24.6	776.0	55.8	770.3	205.0	25
Yany-13-13-18	788.9	6.3	789.5	10.6	791.2	36.4	25
Yany-13-13-19	767.7	8.5	772.9	15.3	788.0	54.0	25
Yany-13-13-20	779.4	7.6	789.4	23.1	817.8	85.2	25
Yany-13-13-21	778.9	8.3	792.9	10.7	832.5	32.8	25
Yany-13-13-22	805.6	5.6	806.9	9.8	810.3	33.5	25
Yany-13-13-23	765.2	12.7	772.5	35.6	793.7	132.9	25
Yany-13-13-25	768.1	6.1	776.0	22.1	798.7	83.7	25
Yany-13-13-26	800.2	7.9	809.4	11.6	835.0	37.3	25
Yany-13-13-27	862.0	9.1	856.0	13.3	840.4	41.8	25
Yany-13-13-30	796.7	9.6	811.1	26.4	850.8	94.6	25
Yany-13-13-31	755.1	4.1	766.1	7.9	798.3	28.5	25
Yany-13-13-32	739.3	29.2	764.0	26.1	837.1	51.6	25
Yany-13-13-33	2965.0	46.0	3105.6	19.3	3197.7	7.6	25
Yany-13-13-34	258.7	4.3	254.1	17.6	211.4	177.1	25
Yany-13-13-35	778.2	8.3	792.0	26.1	831.2	96.0	25
Yany-13-13-36	760.1	8.2	781.9	19.3	844.7	69.7	25
Yany-13-13-37	963.6	18.1	968.5	15.3	979.4	27.8	25
Yany-13-13-39	772.4	10.2	779.9	12.7	801.3	39.4	25
Yany-13-13-40	787.0	7.4	778.3	22.6	753.4	85.3	25
Yany-13-13-42	798.3	8.4	802.5	23.8	814.3	86.5	25
Yany-13-13-44	957.2	13.6	979.8	12.0	1031.0	23.3	25
Yany-13-13-45	1424.6	54.7	1529.3	34.2	1677.1	10.9	25
Yany-13-13-46	787.3	12.4	787.1	14.1	786.3	40.8	25
Yany-13-13-47	780.6	6.7	774.7	13.0	757.9	46.7	25
Yany-13-13-49	777.2	8.6	779.2	8.4	785.2	21.1	25
Yany-13-13-50	776.7	16.8	808.7	30.9	897.8	104.0	25
Yany-13-13-52	783.1	9.4	784.9	15.5	790.1	53.0	25
Yany-13-13-53	814.9	6.3	810.9	18.2	799.9	66.0	25
Yany-13-13-54	769.2	4.9	762.2	10.1	741.6	37.1	25
Yany-13-13-55	797.1	23.2	816.9	38.6	871.2	127.5	25
Yany-13-13-56	790.6	14.6	786.1	25.5	773.2	89.1	25
Yany-13-13-58	764.7	14.6	764.8	16.6	765.2	49.2	25
Yany-13-13-61	856.1	35.3	846.1	26.1	819.9	23.2	25
Yany-13-13-62	773.4	14.8	765.9	25.1	743.9	88.7	25
Yany-13-13-63	770.7	13.8	775.1	15.8	787.9	46.4	25
Yany-13-13-65	267.3	7.6	268.6	14.5	280.3	124.3	25
Yany-13-13-66	212.1	4.8	216.0	27.6	258.6	323.0	25

Yany-13-13-67	769.3	10.4	768.6	20.9	766.6	76.0	25
Yany-13-13-68	756.3	12.4	759.8	46.4	769.9	179.2	25
Yany-13-13-69	766.1	12.6	775.7	26.8	803.4	96.7	25
Yany-13-13-70	792.3	13.3	796.9	23.9	809.7	82.4	25
Yany-13-13-72	791.7	18.1	805.3	27.8	843.3	90.8	25
Yany-13-13-73	811.5	26.5	825.3	28.1	862.5	73.7	25
Yany-13-13-74	767.5	11.2	767.5	13.5	767.4	41.7	25
Yany-13-13-76	858.4	13.3	858.0	12.7	856.9	30.0	25
Yany-13-13-77	800.8	9.1	806.0	14.7	820.3	49.2	25
Yany-13-13-78	794.2	22.7	800.7	21.7	818.8	51.9	25
Yany-13-13-79	816.8	14.0	817.3	22.2	818.5	73.4	25
Yany-13-13-80	801.2	28.2	802.7	29.6	806.8	79.5	25
Yany-13-13-81	800.4	19.8	812.1	17.1	844.4	33.0	25
Yany-13-13-85	539.7	12.6	570.3	13.0	694.2	36.4	25
Yany-13-13-87	795.6	16.7	796.5	21.5	798.9	66.7	25
Yany-13-13-88	783.8	10.0	782.7	10.8	779.6	30.4	25
Yany-13-13-89	801.4	10.4	814.3	25.4	849.8	89.9	25
Yany-13-13-90	782.2	12.4	773.5	13.9	748.6	40.9	25
Yany-13-13-91	795.4	17.4	806.7	42.4	838.0	151.2	25
Yany-13-13-92	374.4	8.8	401.2	12.7	558.6	64.6	25
Yany-13-13-93	1885.2	25.4	1865.2	14.0	1842.9	9.2	25
Yany-13-13-95	837.1	12.6	826.6	9.9	798.4	14.3	25
Yany-13-13-98	802.7	32.3	817.8	32.9	859.0	83.0	25
Yany-13-13-99	766.0	19.7	770.4	38.5	783.2	138.6	25

Table I.2. Sample Locations

Sample Name	Deposit Age	Latitude	Longitude
Dali-13-04	N2	26.00115	99.81805
Hong-11-01	Modern	25.140171	100.3168
Jian-11-06	N1	26.593921	99.847463
Jian-11-18	N1	26.621358	99.849063
Jian-11-39	N1	26.621358	99.849063
Jians-13-05	N2	23.6689	102.84065
Jians-13-07	N2	23.62689	102.78594
Jians-13-08	N2	23.62531	102.78457
Jing-12-01	N1	23.514267	100.70992
Jing-12-05	N1	23.512033	100.70722
Jing-12-16	N1	23.509333	100.69743
Jing-12-24	N1	23.50885	100.68858
Jing-12-25	N1	23.508417	100.68783
Jing-13-01	P2-3	23.599785	100.72826
Lan-11-01	N2	26.461868	99.448518
Lan-11-02	N2	26.459479	99.446333
Lan-11-04	N2	26.457338	99.434963
Lij-12-01	P2	26.885336	100.24008
Lim-12-05	P2	27.083432	99.576293
Lim-12-26	P2	27.071417	99.557183
Lim-12-42	P3	27.0659	99.546117
Luhe-11-18	N2	25.157047	101.35414
Mek-11-02	Modern	26.485513	99.69906
Midu-11-01	P2-3	25.310403	100.41834
Midu-11-02	P2-3	25.302397	100.39944
Shi-12-01	P2	26.87055	99.748583
Shi-12-02	P2	26.870417	99.700367
Yany-11-07	P2	27.60447	101.55926
Yany-13-02	N2	27.53774	101.52378
Yany-13-03	N2	27.53774	101.52378
Yany-13-04	P2	27.400815	101.53126
Yany-13-08	P2	27.40416	101.52825
Yany-13-11	N2	27.541	101.48976
Yany-13-12	N2	27.54072	101.492
Yany-13-13	N2	27.49935	101.54014

Appendix II: Chapter 2

A.II.1. Grid Search Technique

For samples exceeding 11 possible sources we develop a simple grid search mixing model to determine the optimal mixing proportions of potential contributing sources with no a priori knowledge of which sources to include in the mixture). Each sample is compared to all potential contributing sources using likeness (Satkoski et al., 2013). Sample-to-source likeness values are sorted from highest to lowest. Sources are mixed and these mixtures are compared to the original sample using likeness values. We do not mix sources with likenesses less than 5% as they fall below a reasonable level of identifiable inclusion. We define the optimal mix to be when the maximum likeness value is achieved. We choose likeness to better match the shape of the curves and the proportional sizes of each mode.

In a simple scenario, sample P contains four sources that pass the likeness threshold; S_1, S_2, S_3, and S_4, with likeness values of 0.5, 0.3, 0.2, and 0.1, respectively. S_1 has the highest R^2, therefore in our mixing model is adjusted first in 5% increments starting at $S_1 = 0\%$ for the first mixture. The remaining fraction is split evenly between the other sources $[(100-S_1)/3]$ for source contributions of 0%, 33.3%, 33.3%, and 33.3% for S_1, S_2, S_3, and S_4 respectively. Probability density functions of each source are multiplied by their respective proportions and summed, creating a mixed probability function. This mixture is compared to the original sample using likeness, that value of which is noted (LK_{mix1}).

The proportion for S_1 is varied by 5% for the second mixture, with S_2, S_3, and S_4 taking the remaining fraction, and the mixing process is repeated (5%, 31.67%, 31.67%, 31.67%) and likeness is calculated again (LK_{mix2}). This continues until S_1 reaches 100%. To proceed, we find

the mixture with the highest LK_{mix}, so far. The S_1 value, S_{1f}, for this mixture is held constant for all subsequent mixtures for sample P. S_2 has the second highest R^2 value and is adjusted next in 5% increments between 0% and maximum value of 100% S_{1f}. The model follows the same steps as above. This is repeated until all but one source has been adjusted (i.e. S_{1f}, S_{2f}, and S_{3f} have been found) as the last source, S_4, is adjusted simultaneously with the previous source, or until the fixed values sum to 100%.

A.II.2. Results of the Yangtze River Tributary Dataset.

The Yalong tributary sources primarily Neoproterozoic –Longmenshan zircons, as well as plutonic zircons the Songpan Ganze Terrane (Fig. 7B). For the Yalong, Dadu, Min and Jialing Rivers, which source the eastern flank of the Songpan Ganze Terrane block, as well as the Longmenshan block (Fig. 7), we see high Songpan Ganze Terrane signals in each with the rest remaining zircons derived from Triassic volcanics (i.e. Qiangtang, Yidun, SPGT), Longmenshan, and Jurassic sediments from the Sichuan Basin. The Wu River flows primarily through the Sichuan Basin and the mixing proportions reflect the incorporation of Upper Triassic rather than Jurassic sediments of the Sichuan Basin and Yangtze Cratonic age zircons, along with minor contributions of Neoproterozoic volcanics while seeming to exclude Jurassic sediment. The Han River flows roughly ESE, primarily through the Longmenshan and Qinling-Dabieshan fold belt, which contribute the majority of the Hanjiang's zircons, with some minor contributions from Jurassic Sichuan Basin sediment, which does have an appreciable areal extent within the Hanjiang Catchment. The bedrock of the Yuanjiang catchment appears composed primarily of zircons derived from the South China Block and Sichuan Basin. The drainages of the Xiangjiang and Ganjiang source the Cathaysian block, represented by the North and Oujiang River, as well as Caledonian age and Neoproterozoic age (~830 Ma) plutonic zircons associated with South

China.

Figures
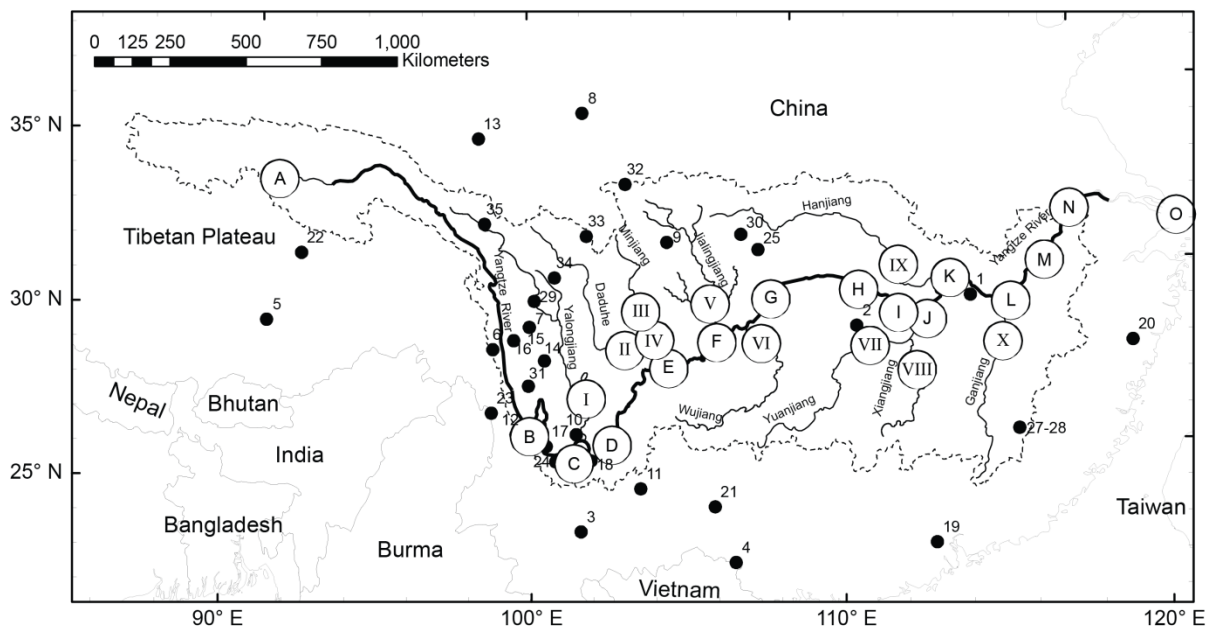
Figure II.1. Drainage of the Yangtze River. Roman Numerals indicate the sampled locations

of the Yangtze River and its major tributaries. Small black dots indicate the approximate

sampling locations of potential source zircon age populations. Source sampling locations may

represent geologically contiguous units. Sources and their references are: **1. Dabie Shan**

Yangtze Block (Clift, Carter, et al., 2006; Hacker et al., 1998); **2. Yangtze Craton Eastern**

(Clift, Carter, et al., 2006; Li, 1999; Zhang et al., 2006a; Zheng et al., 2006; Gao et al., 2011;

Zhang et al., 2006b); **3. Ailao Shan** (Leloup et al., 1993, 1995; Lin et al., 2012; Cao et al., 2011;

Clift, Carter, et al., 2006; Harrison and Leloup, 1996; Wang et al., 1998; Jolivet et al., 1999;

Maluski et al., 2001); **4. Cathaysia** (Li, 2005; Clift, Carter, et al., 2006; Xianhua et al., 1989); **5.**

Gangdese Arc (He et al., 2007; Wen et al., 2008; Ji et al., 2009); **6. Qiangtang Triassic**

Volcanics (Peng et al., 2014a; Zhai et al., 2013); **7. Yidun (K)** (Reid et al., 2007; Peng et al.,

2014b); **8. Laji Shan and West Qinling** (Lease et al., 2007); **9. Longmenshan Neoproterozoic**

Plutons (Pei et al., 2009); **10. Yanbian Terrane Plutons** (Zhou et al., 2006); **11. Luliang** (Zhuo

et al., 2013); **12. Jomda-Weixi Arc** (Yang, Liang, et al., 2014); **13. Kunlunshan** (Chen et al., 2008; Gehrels, Kapp, et al., 2011); **14. Cenozoic Volcanics** (Clift, Carter, et al., 2006; Liu et al., 2013; Yang et al., 2013); **15. Yidun East** (Reid et al., 2007; Peng et al., 2014b); **16. Yidun West** (Reid et al., 2007; Peng et al., 2014b); **17. Emeishan** (Shellnutt, 2014); **18. Yangtze Craton West** (Sun et al., 2009; Greentree and Li, 2008; Wang, Yu, et al., 2012; Wu et al., 2012); **19. North River** (Xu et al., 2007); **20. Oujiang River** (Xu et al., 2007)**; 21. Youjiang Basin** (Yang et al., 2012); **22. Amdo Basement** (Guynn et al., 2006; Zhang et al., 2013); **23. Gaoligong Batholiths** (Xu et al., 2012); **24. Jurassic Yunnan** (Su et al., 2014); **25. Sichuan Basin Triassic** (She et al., 2012); **26. Chizhou Plutons** (Song et al., 2014); **27. Caledonian Plutons** (Wang et al., 2011; Li et al., 2011); **28. South China Protoliths** (Wang et al., 2011; Li et al., 2010); **29. Sichuan Basin Jurassic** (Luo et al., 2014); **30. Xinduqiao** (Weislogel et al., 2010); **31. South Yidun Late Cretaceous** (Wang, Hu, et al., 2014); **32. North Yidun** (Wang et al., 2008) **32-34. Songpan Ganze Terrane** (Weislogel et al., 2010); **35. Qamdo Basin** (Shang et al., 2016)
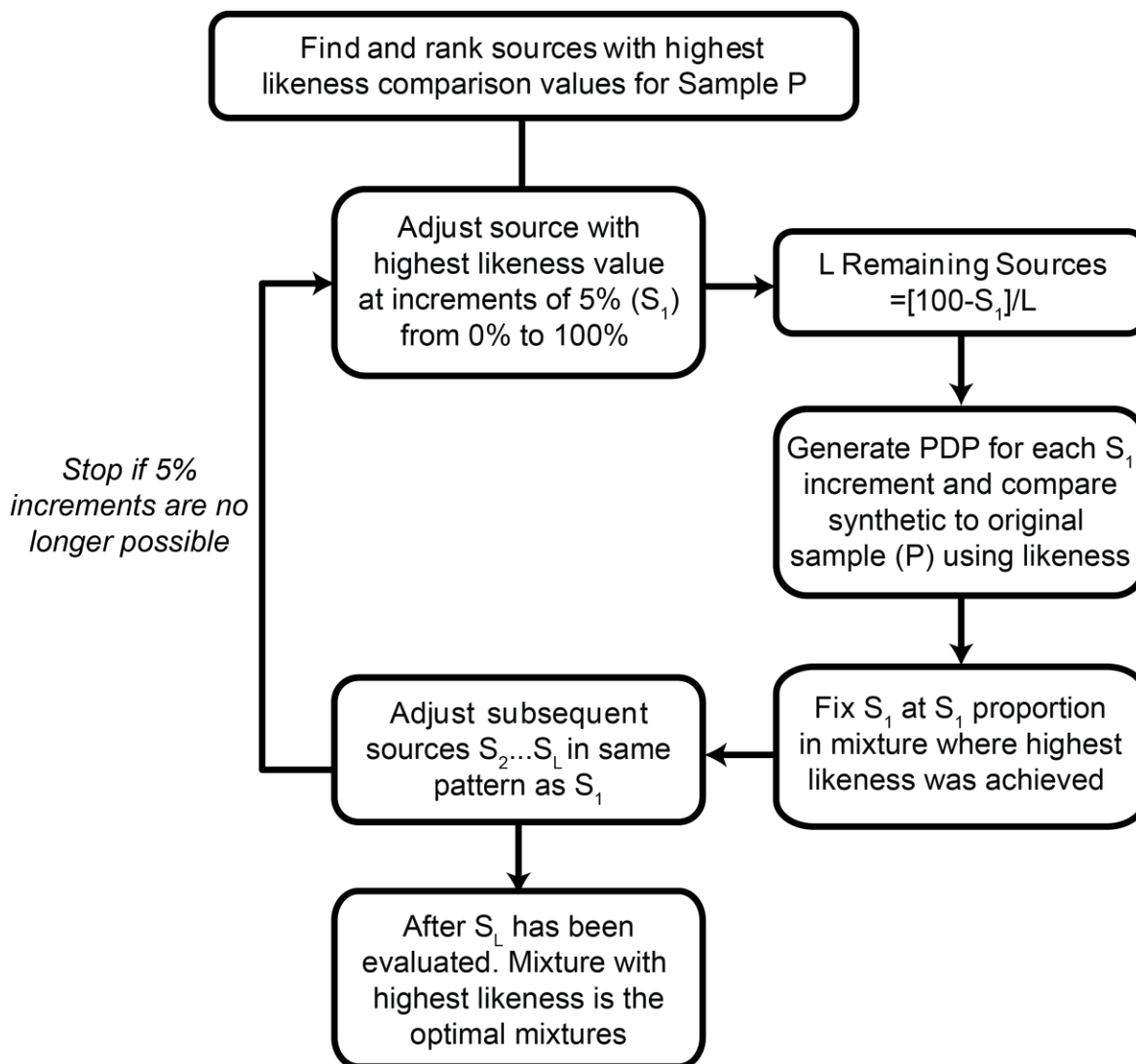
Figure II.2. Flowchart of grid mixing model. The essential steps in determining optimal

mixing proportions of zircon populations
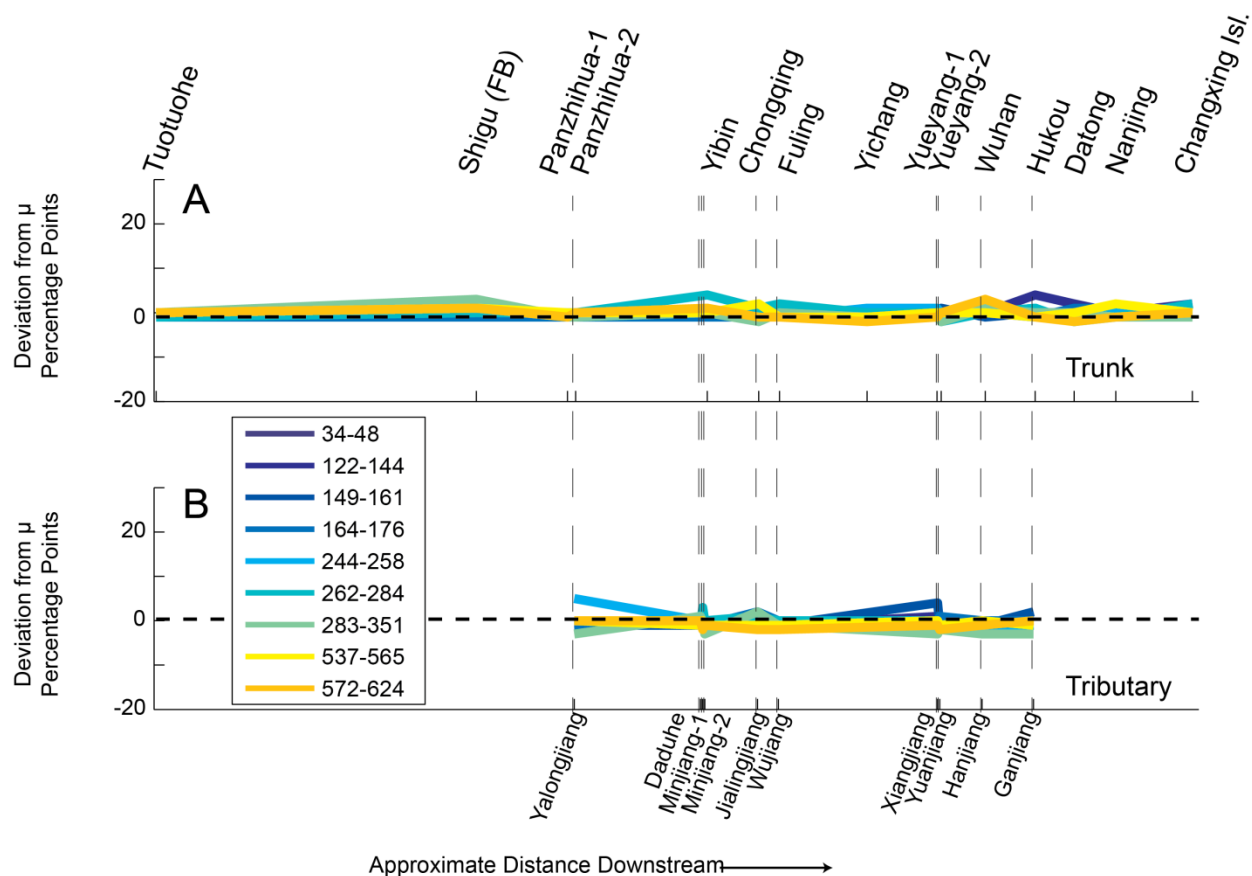
Figure II.3 Gaussian breakdown of the Yangtze River dataset and deviations from means: minor components. A) The black line indicates the summed curve of all trunk stream samples of the Yangtze River. The colored curves are the Gaussian curves which best describe the overall variance of the dataset. The range of each curve at ±2σ from the mean value is given in the legend. B) The deviations (in percentage points) in proportion of the seven components, which account for >75% of the overall variance of the Yangtze River, at each sampling location from the mean value (μ) of that component. μ is given as a percentage in the legend). Top are trunk samples; bottom are tributary samples. Vertical dashed lines indicate the confluence point of the tributaries. Note the Daduhe and Minjiang Tributaries share a confluence point as do the Xiangjiang and Yuanjiang tributaries. C) Model of deviation plot for synthetic unique components with proportions equivalent and color coordination to the seven components in B. Note the similarity in curve shapes to trunk samples of B.**.**

Figure II.4. Bedrock mixing results of the tributaries. The Yangtze catchment outlined with the heavy black line; tributaries are outlined by thin black lines. Model results for mainstream samples are labeled with roman numerals (See Figure 1 and 2 of main text) Pie charts represent optimal mixtures of bedrock probability curves for each sample. Tributaries of the upper reaches show a clear affinity for the Songpan Ganze Terrane. The Sichuan Basin dominates at Wujiang. South China Neoproterozoic zircon are common in Yuanjiang and Ganjiang (pink); the dark red of the Longmenshan can be seen as a relatively consistent signal of the more northern tributaries. Major Geologic Terranes are colored and labeled as follows: QT – Qiangtang Terrane; SPGT – Songpan Ganze Terrane; SB - Sichuan Basin ; TU – Transitional Unit; YC – Yangtze Craton; CA-SC – Cathaysia-South China; QDS – Qinling Dabie Shan Fold Belt; LMS – Longmenshan Fold Belt; Y – Yidun Unit; NYB – Nanyang Basin. Geologic Terranes modified from Burchfiel and Zhiliang, (2013) and Hearn et al., (2000)

Tables

Table II.1. Likeness Results

Table Likeness Values	Tuotuohe	Shigu	Panzhihua-1	Panzhihua-2	Yibin	Chongqing	Fuling	Yichang	Yueyang-1	Yueyang-2	Wuhan	Hukou	Datong	Nanjing	Changxing Is.	Yalongjiang	Daduhe	Minjiang-1	Minjiang-2	Jialingjiang	Wujiang	Xiangjiang	Yuanjiang	Hanjiang	Ganjiang
Tuotuohe	-	49	49	52	37	46	45	40	54	51	50	38	43	46	42	23	35	35	31	46	43	49	40	38	43
Shigu	49	-	53	53	38	46	46	44	56	55	58	44	46	55	52	27	44	43	35	50	40	52	44	44	50
Panzhihua-1	49	53	-	55	47	58	53	58	63	47	61	54	56	49	60	32	44	47	49	54	54	43	51	42	40
Panzhihua-2	52	53	55	-	46	57	54	53	61	50	58	54	54	55	54	30	45	46	45	51	47	48	45	48	44
Yibin	37	38	47	46	-	54	58	54	46	43	52	56	51	44	50	57	52	52	47	44	39	34	51	56	38
Chongqing	46	46	58	57	54	-	59	55	55	46	56	57	53	50	55	37	52	51	48	49	50	43	49	47	46
Fuling	45	46	53	54	58	59	-	54	55	48	58	55	60	52	54	42	52	51	46	52	58	40	53	48	41
Yichang	40	44	58	53	54	55	54	-	52	43	53	59	57	51	54	34	49	52	55	50	51	37	52	46	43
Yueyang-1	54	56	63	61	46	55	55	52	-	54	62	53	52	54	56	32	41	46	43	61	60	48	45	45	42
Yueyang-2	51	55	47	50	43	46	48	43	54	-	55	45	49	58	44	26	37	41	34	43	42	55	42	49	54
Wuhan	50	58	61	58	52	56	58	53	62	55	-	56	59	62	58	37	51	53	47	53	54	46	54	52	45
Hukou	38	44	54	54	56	57	55	59	53	45	56	-	60	52	61	38	55	61	57	44	48	42	45	53	44
Datong	43	46	56	54	51	53	60	57	52	49	59	60	-	53	56	32	48	52	51	50	50	39	56	51	44
Nanjing	46	55	49	55	44	50	52	51	54	58	62	52	53	-	58	32	48	49	45	45	44	49	53	51	49
Changxing Is.	42	52	60	54	50	55	54	54	56	44	58	61	56	58	-	39	54	56	56	53	45	48	50	55	45
Yalongjiang																-	40	42	38	25	24	46	25	27	43
Daduhe																40	-	64	63	37	31	52	36	43	47
Minjiang-1																42	64	-	65	39	37	52	36	38	48
Minjiang-2																38	63	65	-	42	36	53	36	39	48
Jialingjiang																25	37	39	42	-	59	35	40	33	44
Wujiang																24	31	37	36	59	-	29	37	30	43
Xiangjiang																46	52	52	53	35	29	-	41	53	54
Yuanjiang																25	36	36	36	40	37	41	-	54	41
Hanjiang																27	43	38	39	33	30	53	54	-	43
Ganjiang																43	47	48	48	44	43	54	41	43	-

Table II.2 Crossplot R^2 Results

Table Crossplot R2-Values	Tuotuohe	Shigu	Panzhihua-1	Panzhihua-2	Yibin	Chongqing	Fuling	Yichang	Yueyang-1	Yueyang-2	Wuhan	Hukou	Datong	Nanjing	Changxing Is.	Yalongjiang	Daduhe	Minjiang-1	Minjiang-2	Jialingjiang	Wujiang	Xiangjiang	Yuanjiang	Hanjiang	Ganjiang
Tuotuohe	-	2	2	3	2	7	2	1	4	5	2	2	1	2	2	1	0	0	0	2	2	3	1	2	2
Shigu	2	-	22	15	8	13	9	15	15	26	28	17	17	27	19	5	17	15	13	7	2	26	10	21	30
Panzhihua-1	2	22	-	25	27	37	29	49	32	10	37	44	38	23	36	15	28	31	32	18	30	5	27	18	10
Panzhihua-2	3	15	25	-	24	37	26	28	27	13	26	34	25	21	24	16	19	15	16	12	15	11	16	24	17
Yibin	2	8	27	24	-	42	55	36	26	15	37	40	30	24	34	67	19	17	14	23	16	6	42	41	11
Chongqing	7	13	37	37	42	-	46	41	31	16	36	40	31	29	36	30	31	25	24	16	25	9	29	27	19
Fuling	2	9	29	26	55	46	-	30	31	15	35	32	41	23	32	44	16	13	9	27	38	6	33	25	11
Yichang	1	15	49	28	36	41	30	-	31	11	44	50	40	33	35	26	45	42	45	22	25	4	38	29	16
Yueyang-1	4	15	32	27	26	31	31	31	-	21	31	25	20	21	26	19	6	7	7	34	43	11	13	19	7
Yueyang-2	5	26	10	13	15	16	15	11	21	-	20	16	20	35	16	8	4	6	4	6	6	47	16	35	39
Wuhan	2	28	37	26	37	36	35	44	31	20	-	46	40	46	38	27	40	37	33	20	22	9	37	34	17
Hukou	2	17	44	34	40	40	32	50	25	16	46	-	49	41	52	25	55	56	47	12	17	14	31	33	17
Datong	1	17	38	25	30	31	41	40	20	20	40	49	-	41	41	21	33	31	32	19	18	10	47	38	19
Nanjing	2	27	23	21	24	29	23	33	21	35	46	41	41	-	42	19	34	33	32	11	8	19	46	44	30
Changxing Is.	2	19	36	24	34	36	32	35	26	16	38	52	41	42	-	25	38	34	38	21	11	18	35	45	23
Yalongjiang																-	16	11	10	12	8	31	3	8	46
Daduhe																16	-	82	80	4	2	33	3	15	30
Minjiang-1																11	82	-	77	3	29	29	2	13	28
Minjiang-2																10	80	77	-	4	3	35	2	12	30
Jialingjiang																12	4	3	4	-	33	10	3	2	11
Wujiang																8	2	3	3	33	-	3	2	0	7
Xiangjiang																31	33	29	35	10	3	-	19	38	47
Yuanjiang																3	3	2	2	3	2	19	-	34	5
Hanjiang																8	15	13	12	2	0	38	34	-	17
Ganjiang																46	30	28	30	11	7	47	5	17	-

Table II.3 Mixture Model Bedrock Results.

Sample	SPGSE	SPGNE	SPGC	Jurassic Yunnan	Qamdo Basin	Yidun Group	Qiangtang Tr Volcanics	North Yidun	Yidun Tr East (Also SPG)	Jomda-Weixi Arc	Longmenshan	Laji Shan and West Qinling	Dabie Shan Yangtze Block	Oujiang River	Cathaysia	Yanbian Terrane Plutons	Luliang
Tuotuohe	100	0	0	0	0	0	0	0	0	0	0	0	0	0	0	0	0
Yangtze River(a)	25	0	0	0	70	0	0	0	0	5	0	0	0	0	0	0	0
Panzhihua-1	15	0	0	65	5	0	5	0	0	0	0	0	0	0	0	5	0
Panzhihua-2	80	0	0	5	5	10	0	0	0	0	0	0	0	0	0	0	0
Yibin	75	0	0	0	0	10	0	0	0	0	15	0	0	0	0	0	0
Chongqing	70	0	0	5	0	0	0	0	0	0	5	0	5	0	0	0	0
Fuling	95	0	0	0	0	0	0	0	0	0	0	0	0	0	0	0	0
Yichang	0	0	0	45	0	15	5	5	0	0	5	0	0	0	0	10	0
Yueyang-1	80	0	0	20	0	0	0	0	0	0	0	0	0	0	0	0	0
Yueyang-2	15	0	0	0	85	0	0	0	0	0	0	0	0	0	0	0	0
Wuhan	60	0	0	0	15	0	0	0	0	0	5	0	0	0	0	0	0
Hukou	35	0	0	15	0	0	5	0	0	5	10	0	15	0	0	0	0
Datong	50	0	0	15	0	0	5	0	0	0	5	0	0	5	0	0	0
Nanjing	35	0	0	0	15	0	5	0	0	0	0	0	5	0	5	0	5
Changxing Island	45	0	0	20	0	0	0	0	0	0	0	0	15	0	0	0	0
Yalongjiang	35	0	0	0	0	0	0	0	0	0	65	0	0	0	0	0	0
Daduhe	25	0	10	0	0	0	15	0	0	0	20	0	0	0	0	0	0
Minjiang-1	30	5	10	0	0	0	0	0	0	0	15	5	0	0	0	0	0
Minjiang-2	25	0	0	0	0	0	0	0	5	0	5	5	0	0	0	15	0
Jialingjiang	90	5	0	0	0	0	0	0	0	0	0	0	0	0	0	0	0
Wujiang	0	0	0	0	0	0	0	0	0	0	0	0	0	0	0	5	5
Ganjiang	0	0	0	0	0	0	0	0	5	0	0	0	0	0	0	0	0
Xiangjiang	0	0	0	0	0	0	0	0	5	0	0	0	0	0	0	0	0
Hanjiang	0	0	0	0	0	0	0	0	10	0	20	40	10	0	0	0	10
Yuanjiang	0	0	0	0	0	0	0	0	10	0	0	0	0	0	0	0	0

Table II.3 Mixture Model Bedrock Results cont.

Sample	South China Protoliths	Yangtze Craton West	Triassic SS 1 Sichuan Basin	Triassic SS 2 Sichuan Basin	Jurassic S.S. Sichuan Basin	North River	Caledonian Plutons	Chizhou Area	Zheduo-Gonggar massif	Optimal Likeness
Tuotuohe	0	0	0	0	0	0	0	0	0	57
Yangtze River(a)	0	0	0	0	0	0	0	0	0	65
Panzhihua-1	0	0	0	0	0	0	0	0	5	75
Panzhihua-2	0	0	0	0	0	0	0	0	0	61
Yibin	0	0	0	0	0	0	0	0	0	62
Chongqing	0	0	5	0	0	0	0	0	5	67
Fuling	0	0	0	5	0	0	0	0	0	69
Yichang	0	0	0	5	0	0	0	0	5	69
Yueyang-1	0	0	0	0	0	0	0	0	0	70
Yueyang-2	0	0	0	0	0	0	0	0	0	60
Wuhan	15	0	0	0	0	0	0	0	5	73
Hukou	5	0	5	0	0	0	0	0	0	69
Datong	20	0	0	0	0	0	0	0	0	67
Nanjing	10	0	0	0	0	0	5	0	10	65
Changxing Island	5	0	0	5	0	5	0	0	0	67
Yalongjiang	0	0	0	0	0	0	0	0	0	70
Daduhe	0	0	5	5	0	0	0	0	20	68
Minjiang-1	0	0	0	0	0	0	0	0	30	77
Minjiang-2	0	0	15	0	0	0	0	0	30	69
Jialingjiang	0	0	0	0	0	0	0	0	0	59
Wujiang	0	40	45	0	5	0	0	0	0	72
Ganjiang	35	0	0	10	0	25	25	0	0	60
Xiangjiang	0	0	0	25	0	40	25	5	0	60
Hanjiang	0	0	0	0	10	0	0	0	0	65
Yuanjiang	65	0	0	10	15	0	0	0	0	65

Table II.4 Mixture Model Fluvial Results

Sample	Tuotuohe	Yangtze River(a)	Panzhihua01	Panzhihua02	Yibin	Chongqing	Fuling	Yichang	Yueyang01	Yueyang02	Wuhan	Hukou	Datong	Nanjing	Yalongjiang	Daduhe	Jialingjiang	Wujiang	Hanjiang	Xiangjiang	Ganjiang	Yuanjiang	Optimal Likeness
Tuotuohe	100	0	0	0	0	0	0	0	0	0	0	0	0	0	0	0	0	0	0	0	0	0	100
Shigu	100	0	0	0	0	0	0	0	0	0	0	0	0	0	0	0	0	0	0	0	0	0	49
Panzhihua01	45	55	0	0	0	0	0	0	0	0	0	0	0	0	0	0	0	0	0	0	0	0	55
Panzhihua02	30	20	40	0	0	0	0	0	0	0	0	0	0	0	10	0	0	0	0	0	0	0	62
Yibin	0	0	30	15	0	0	0	0	0	0	0	0	0	0	55	0	0	0	0	0	0	0	67
Chongqing	10	0	30	10	30	0	0	0	0	0	0	0	0	0	0	20	0	0	0	0	0	0	67
Fuling	0	0	0	0	20	10	0	0	0	0	0	0	0	0	10	10	10	40	0	0	0	0	71
Yichang	0	0	30	0	20	0	0	0	0	0	0	0	0	0	0	30	0	20	0	0	0	0	68
Yueyang01	0	0	40	35	0	0	0	0	0	0	0	0	0	0	0	0	20	5	0	0	0	0	70
Yueyang02	0	50	0	0	0	0	20	0	0	0	0	0	0	0	0	0	0	0	0	30	0	0	61
Wuhan	0	20	5	0	5	0	10	0	10	5	0	0	0	0	2.5	5	5	10	5	2.5	0	15	73
Hukou	0	0	0	0	20	25	10	30	0	0	5	0	0	0	0	10	0	0	0	0	0	0	68
Datong	0.3	0.3	0.3	0.3	0.3	0.3	35	5	0.3	0.3	25	30	0	0	0.3	0.3	0.3	0.3	0.3	0.3	0.3	0.3	68
Nanjing	0.6	0	0	0	0.6	0	0	5	5	20	30	15	0	0	0.6	0.6	0.6	0.6	5	0.6	0.6	15	68
Changxing Island	0	0	30	0	0	0	0	0	0	0	30	0	25	0	0	0	0	0	15	0	0	0	70

Appendix III: Chapter 3

Figures
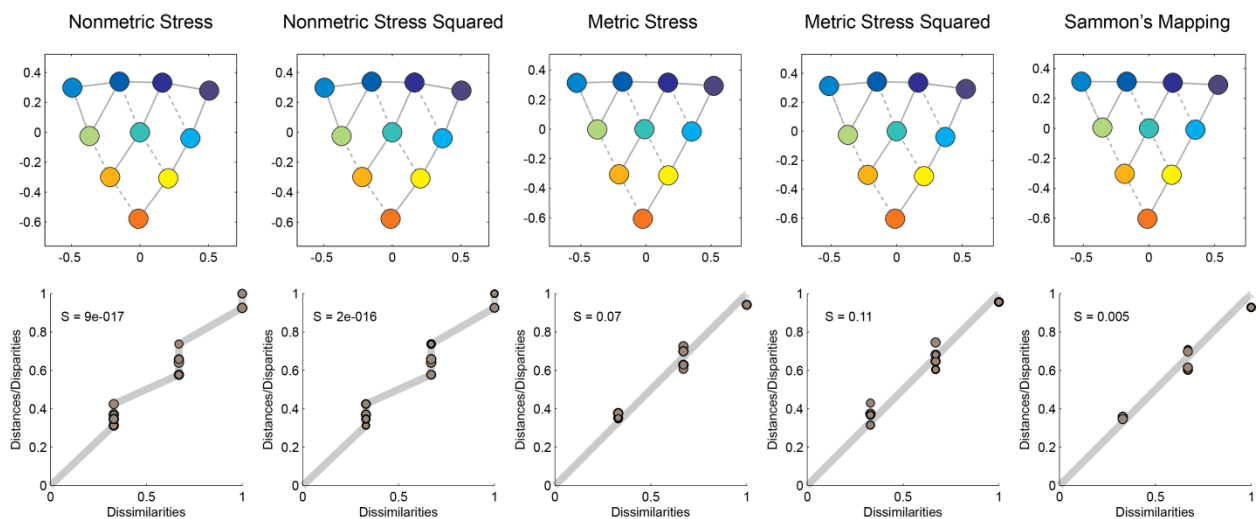
Figure III.1. Multidimensional scaling plots varying methodologies. Plots demonstrate the limited effects of using nonmetric (columns 1 and 2) vs. nonmetric (columns 3-5) MDS and using a variety of goodness of fit criterion. The bottom row is the Shepard plots for each corresponding configuration. Note that nonmetric MDS does result in lower stress values there is little apparent difference in the resulting configuration and spacing.

References

Abendanon, E.C., 1908, Structural Geology of the Middle Yang-Tzïkiang Gorges: The Journal of Geology, v. 16, p. 587–616.

Allen, C.R., Gillespie, a R., Y., Han K.E., S., Zhang, B.C., and Zhu, C.N., 1984, Red River and associated slip faults, Yunnan Province, China: Quaternary geology, slip rates and seismic hazard: Geological Society of America Bulletin, v. 95, p. 687–700.

Allmendinger, R.W., Cardozo, N.C., and Fisher, D., 2013, Structural Geology Algorithms: Vectors & Tensors: Cambridge, England, Cambridge University Press, 289 p.

Amidon, W.H., Burbank, D.W., and Gehrels, G.E., 2005a, Construction of detrital mineral populations: insights from mixing of U-Pb zircon ages in Himalayan rivers: Basin Research, v. 17, p. 463–485, doi: 10.1111/j.1365-2117.2005.00279.x.

Amidon, W.H., Burbank, D.W., and Gehrels, G.E., 2005b, U–Pb zircon ages as a sediment mixing tracer in the Nepal Himalaya: Earth and Planetary Science Letters, v. 235, p. 244–260, doi: 10.1016/j.epsl.2005.03.019.

Andersen, T., 2005, Detrital zircons as tracers of sedimentary provenance : limiting conditions from statistics and numerical simulation: v. 216, p. 249–270, doi: 10.1016/j.chemgeo.2004.11.013.

Andersen, T., 2014, The detrital zircon record: Supercontinents, parallel evolution-Or coincidence? Precambrian Research, v. 244, p. 279–287, doi: 10.1016/j.precamres.2013.10.013.

Andersen, T., Saeed, A., Gabrielsen, R.H., and Olaussen, S., 2011, Provenance characteristics of the Brumunddal sandstone in the Oslo Rift derived from U-Pb, Lu-Hf and trace element analyses of detrital zircons by laser ablation ICMPS: Norsk Geologisk Tidsskrift, v. 91, p.

1–18.

Arboit, F., Collins, A.S., Morley, C.K., King, R., and Amrouch, K., 2016, Detrital zircon analysis of the southwest Indochina terrane, central Thailand: Unravelling the Indosinian orogeny: Geological Society of America Bulletin, p. B31411.1, doi: 10.1130/B31411.1.

Blum, M., and Pecha, M., 2014, Mid-Cretaceous to Paleocene North American drainage reorganization from detrital zircons: Geology (Boulder), v. 42, p. 607–610, doi: 10.1130/G35513.1.

Bonich, M.B., Samson, S.D., and Fedo, C.M., 2016, Incongruity of Detrital Zircon Ages of Granitic Bedrock and its Derived Alluvium: An Example from the Stepladder Mountains, SE California: The Journal of Geology, p. (In Review).

Borg, I., and Groenen, P., 2005, Modern Multidimensional Scaling: theory and applications: New York, Springer-Verlag, 207-212 p.

Botev, Z.I., 2007, Nonparametric Denisty Estimation via Diffusion Mixing:, http://espace.library.uq.edu.au/view/UQ:120006.

Botev, Z.I., Grotowski, J.F., and Kroese, D.P., 2010, Kernel density estimation via diffusion: The Annals of Statistics, v. 38, p. 2916–2957, doi: 10.1214/10-AOS799.

Breiman, L., Meisel, W., and Purcell, E., 1977, Variable kernel estimates of multivariate densities: Technometrics, v. 19, p. 135–144.

Brower, J.C., Millendorf, S.A., and Dyman, T.S., 1978, Methods for the quantification of assemblage zones based on multivariate analysis of weighted and unweighted data: Computers and Geosciences, v. 4, p. 221–227, doi: 10.1016/0098-3004(78)90054-7.

Burchfiel, B.C., and Zhiliang, C., 2013, Tectonics of the Southeastern Tibetan Plateau and Its Adjacent Foreland: Geological Society of America Memoirs, v. 210, p. 1–164, doi:

10.1130/2012.1210(01).

Burrett, C., Meffre, S., Lai, C.K., Khositanont, S., Chaodumrong, P., Udchachon, M., Ekins, S., and Halpin, J., 2014, The configuration of Greater Gondwana—Evidence from LA ICPMS, U–Pb geochronology of detrital zircons from the Palaeozoic and Mesozoic of Southeast Asia and China: Gondwana Research, v. 26, p. 31–51, doi: 10.1016/j.gr.2013.05.020.

Cai, F., Ding, L., Yao, W., Laskowski, A.K., Xu, Q., Zhang, J., and Sein, K., 2015, Provenance and tectonic evolution of Lower Paleozoic–Upper Mesozoic strata from Sibumasu Terrane, Myanmar: Gondwana Research, doi: 10.1016/j.gr.2015.03.005.

Cao, L., Jiang, T., Wang, Z., Zhang, Y., and Sun, H., 2015, Provenance of Upper Miocene sediments in the Yinggehai and Qiongdongnan basins, northwestern South China Sea: Evidence from REE, heavy minerals and zircon U–Pb ages: Marine Geology, v. 361, p. 136–146, doi: 10.1016/j.margeo.2015.01.007.

Cao, S., Liu, J., Leiss, B., Neubauer, F., Genser, J., and Zhao, C., 2011, Oligo-Miocene shearing along the Ailao Shan–Red River shear zone: Constraints from structural analysis and zircon U/Pb geochronology of magmatic rocks in the Diancang Shan massif, SE Tibet, China: Gondwana Research, v. 19, p. 975–993, doi: 10.1016/j.gr.2010.10.006.

Cao, H.W., Zhang, S.T., Lin, J.Z., Zheng, L., Wu, J. De, and Li, D., 2014, Geology, geochemistry and geochronology of the Jiaojiguanliangzi Fe-polymetallic deposit, Tengchong County, Western Yunnan (China): Regional tectonic implications: Journal of Asian Earth Sciences, v. 81, p. 142–152, doi: 10.1016/j.jseaes.2013.11.002.

Cardozo, N., and Allmendinger, R.W., 2013, Spherical projections with OSXStereonet: Computers & Geosciences, v. 51, p. 193–205, doi: 10.1016/j.cageo.2012.07.021.

Carroll, J.D., and Arabie, P., 1980, Multidimensional scaling.: Chapman and Hall/CRC, v. 31,

607-649 p., doi: 10.1146/annurev.ps.31.020180.003135.

Carter, A., and Bristow, C.S., 2003, Linking hinterland evolution and continental basin sedimentation by using detrital zircon thermochronology: A study of the Khorat Plateau Basin, eastern Thailand: Basin Research, v. 15, p. 271–285, doi: 10.1046/j.1365-2117.2003.00201.x.

Carter, A., and Moss, S.J., 1999, Combined detrital-zircon fission-track and U-Pb dating: A new approach to understanding hinterland evolution: Geology, v. 27, p. 235–238, doi: 10.1130/0091-7613(1999)027<0235:CDZFTA>2.3.CO;2.

Carter, A., Roques, D., Bristow, C., and Kinny, P., 2001, Understanding mesozoic accretion in Southeast Asia: Significance of triassic thermotectonism (Indosinian orogeny) in Vietnam: Geology, v. 29, p. 211–214, doi: 10.1130/0091-7613(2001)029<0211:UMAISA>2.0.CO;2.

Chen, X., Chen, Y., Bao, C., Li, G., Yan, J., and Li, D., 2014, U-Pb Dating and Hf Isotopic Composition of Detrtial Zircons in the Sediments from the Lancang Rver and Its Geological Significance: Geochemistry,Ore Deposits and Petrology, v. 28, p. 1170–1182.

Chen, C.H., Hsieh, P.S., Lee, C.Y., and Zhou, H.W., 2011, Two episodes of the Indosinian thermal event on the South China Block: Constraints from LA-ICPMS U-Pb zircon and electron microprobe monazite ages of the Darongshan S-type granitic suite: Gondwana Research, v. 19, p. 1008–1023, doi: 10.1016/j.gr.2010.10.009.

Chen, N., Sun, M., Wang, Q., Zhang, K., Wan, Y., and Chen, H., 2008, U-Pb dating of zircon from the Central Zone of the East Kunlun Orogen and its implications for tectonic evolution: Science in China Series D: Earth Sciences, v. 51, p. 929–938, doi: 10.1007/s11430-008-0072-x.

Chu, M.-F., Chung, S.-L., Song, B., Liu, D., O'Reilly, S.Y., Pearson, N.J., Ji, J., and Wen, D.-J.,

2006, Zircon U-Pb and Hf isotope constraints on the Mesozoic tectonics and crustal evolution of southern Tibet: Geology, v. 34, p. 745, doi: 10.1130/G22725.1.

Chung, S.-L., Lo, C.-H., Lee, T.-Y., Zhang, Y., Xie, Y., Li, X., Wang, K.-L., and Wang, P.-L., 1998, Diachronous uplift of the Tibetan plateau starting 40 Myr ago: Nature, v. 394, p. 769–774.

Clark, M.K., House, M. a., Royden, L.H., Whipple, K.., Burchfiel, B.C., Zhang, X., and Tang, W., 2005, Late Cenozoic uplift of southeastern Tibet: Geology, v. 33, p. 525, doi: 10.1130/G21265.1.

Clark, M.K., and Royden, L.H., 2000, Topographic ooze : Building the eastern margin of Tibet by lower crustal flow: Geology, v. 28, p. 703–706, doi: 10.1130/0091-7613(2000)28<703.

Clark, M.K., Schoenbohm, L.M., Royden, L.H., Whipple, K.X., Burchfiel, B.C., Zhang, X., Tang, W., Wang, E., and Chen, L., 2004, Surface uplift, tectonics, and erosion of eastern Tibet from large-scale drainage patterns: Tectonics, v. 23, p. 1–21, doi: 10.1029/2002TC001402.

Clift, P.D., Blusztajn, J., and Nguyen, A.D., 2006, Large-scale drainage capture and surface uplift in eastern Tibet–SW China before 24 Ma inferred from sediments of the Hanoi Basin, Vietnam: Geophysical Research Letters, v. 33, p. 1–5, doi: 10.1029/2006GL027772.

Clift, P.D., Carter, A., Campbell, I.H., Pringle, M.S., Van Lap, N., Allen, C.M., Hodges, K. V., and Tan, M.T., 2006, Thermochronology of mineral grains in the Red and Mekong Rivers, Vietnam: Provenance and exhumation implications for Southeast Asia: Geochemistry Geophysics Geosystems, v. 7, doi: 10.1029/2006GC001336.

Clift, P.D., and Sun, Z., 2006, The sedimentary and tectonic evolution of the Yinggehai–Song Hong basin and the southern Hainan margin, South China Sea: Implications for Tibetan

uplift and monsoon intensification: Journal of Geophysical Research, v. 111, p. 1–28, doi: 10.1029/2005JB004048.

Cook, K.L., and Royden, L.H., 2008, The role of crustal strength variations in shaping orogenic plateaus, with application to Tibet: Journal of Geophysical Research, v. 113, p. 1–18, doi: 10.1029/2007JB005457.

Cui, X.Z., 2013, The Palaeogene Desert Deposits In The Jianchuan Basin, Eastern Margin Of Tibetan Plateau (SW China), And Its Significance: Chinese Academy of Geological Sciences.

Darby, B.J., and Gehrels, G.E., 2006, Detrital zircon reference for the North China block: Journal of Asian Earth Sciences, v. 26, p. 637–648, doi: 10.1016/j.jseaes.2004.12.005.

Dickinson, W.R., and Gehrels, G.E., 2008, Sediment delivery to the Cordilleran foreland basin: Insights from U-Pb ages of detrital zircons in Upper Jurassic and Cretaceous strata of the Colorado Plateau: American Journal of Science, v. 308, p. 1041–1082, doi: 10.2475/10.2008.01.

Dickinson, W.R., and Gehrels, G.E., 2009, Use of U-Pb ages of detrital zircons to infer maximum depositional ages of strata: A test against a Colorado Plateau Mesozoic database: Earth and Planetary Science Letters, v. 288, p. 115–125, doi: 10.1016/j.epsl.2009.09.013.

Dobson, D.M., Dickens, G.R., and Rea, D.K., 2001, Terrigenous sediment on Ceara Rise: A Cenozoic record of South American orogeny and erosion: Palaeogeography, Palaeoclimatology, Palaeoecology, v. 165, p. 215–229, doi: 10.1016/S0031-0182(00)00161-9.

Dodson, M.H., Compston, W., Williams, I.S., and Wilson, J.F., 1988, A search for ancient detrital zircons in Zimbabwean sediments: Journal of the Geological Society, v. 145, p.

977–983, doi: 10.1144/gsjgs.145.6.0977.

Dong, G., Mo, X., Zhao, Z., Zhu, D., Goodman, R.C., Kong, H., and Wang, S., 2013, Zircon U–Pb dating and the petrological and geochemical constraints on Lincang granite in Western Yunnan, China: Implications for the closure of the Paleo-Tethys Ocean: Journal of Asian Earth Sciences, v. 62, p. 282–294, doi: 10.1016/j.jseaes.2012.10.003.

Doveton, J.H., 1976, Multidimensional Scaling of Sedimentary Rock Descriptors: Elsevier, 143-155 p., doi: 10.1016/B978-0-08-020613-4.50017-3.

Druschke, P., Hanson, A.D., Yan, Q., Wang, Z., Wang, T., The, S., and September, N., 2014, Stratigraphic and U-Pb SHRIMP Detrital Zircon Evidence for a Neoproterozoic Continental Arc , Central China : Rodinia Implications: The Journal of Geology, v. 114, p. 627–636.

Fedo, C.M., George, T., Sircombe, K.N., Rainbird, R.H., and Street, B., 2003, Detrital Zircon Analysis of the Sedimentary Record: Reviews in Mineralogy and Geochemistry, v. 53, p. 277–303, doi: 10.2113/0530277.

Fei, S., Weislogel, A., and Sharma, S., 2013, Evolution of the Mesozoic Qamdo (Changdu) Basin , Eastern Tibet : Linkages between Sedimentation , Climate , and: Search and Discovery, v. 30280.

Feng, J., Mao, J., and Pei, R., 2012, Ages and geochemistry of Laojunshan granites in southeastern Yunnan, China: Implications for W-Sn polymetallic ore deposits: Mineralogy and Petrology, v. 107, p. 573–589, doi: 10.1007/s00710-012-0253-3.

Feng, J., Mao, J., Pei, R., Zhou, Z., and Yang, Z., 2008, SHRIMP zircon U-Pb dating and geochemical characteristics of Laojunshan granite intrusions from the Wazha tugsten deposit, Yunnan Provice and their implications for petrogenesis: Acta Petrolei Sinica, v. 26, p. 845–857, doi: 10.1007/s13398-014-0173-7.2.

Gallen, S.F., Clark, M.K., and Godt, J.W., 2015, Coseismic landslides reveal near-surface rock strength in a highrelief, tectonically active setting: Geology, v. 43, p. 11–14, doi: 10.1130/G36080.1.

Galloway, W.E., Whiteaker, T.L., and Ganey-Curry, P., 2011, History of Cenozoic North American drainage basin evolution, sediment yield, and accumulation in the Gulf of Mexico basin: Geosphere, v. 7, p. 938–973, doi: 10.1130/GES00647.1.

Gao, S., Rudnick, R.L., Yuan, H., Liu, X., Liu, Y., Xu, W., Ling, W., and Ayers, J., 2004, Recycling lower continental crust in the North China craton: v. 432, doi: 10.1038/nature03143.1.

Gao, S., Yang, J., Zhou, L., Li, M., Hu, Z., Guo, J., Yuan, H., Gong, H., Xiao, G., and Wei, J., 2011, Age and growth of the Archean Kongling terrain, South China, with emphasis on 3.3 ga granitoid gneisses: American Journal of Science, v. 311, p. 153–182, doi: 10.2475/02.2011.03.

Gehrels, G.E., 2000, Introduction to detrital zircon studies of Paleozoic and Triassic strata in western Nevada and northern California, *in* Soregham, M.J. and Gehrels, G.E. eds., Paleozoic and Triassic paleogeography and tectonics of western Nevada and northern California, Boulder, Colorado, Geological Society of America, p. 1–17.

Gehrels, G.E., Blakey, R., Karlstrom, K.E., Timmons, J.M., Dickinson, B., and Pecha, M., 2011, Detrital zircon U-Pb geochronology of Paleozoic strata in the Grand Canyon, Arizona: Lithosphere, v. 3, p. 183–200, doi: 10.1130/L121.1.

Gehrels, G.E., Kapp, P., DeCelles, P.G., Pullen, A., Blakey, R., Weislogel, A.L., Ding, L., Guynn, J., Martin, A., Mcquarrie, N., and Yin, A., 2011, Detrital zircon geochronology of pre-Tertiary strata in the Tibetan-Himalayan orogen: Tectonics, v. 30, p. 1–27, doi:

10.1029/2011TC002868.

Gehrels, G.E., Valencia, V.A., and Ruiz, J., 2008, Enhanced precision, accuracy, efficiency, and spatial resolution of U-Pb ages by laser ablation-multicollector-inductively coupled plasma-mass spectrometry: Geochemistry, Geophysics, Geosystems, v. 9, p. n/a–n/a, doi: 10.1029/2007GC001805.

Gehrels, G.E., Yin, A., and Wang, X., 2003, Detrital-zircon geochronology of the northeastern Tibetan plateau Detrital-zircon geochronology of the northeastern Tibetan plateau: Geological Society of America Bulletin, v. 115, p. 881–896, doi: 10.1130/0016-7606(2003)115<0881.

George, B., and George, B., 1936, Physiographic History of the Yangtze: Geographical Journal, v. 87, p. 17–34.

Greentree, M.R., and Li, Z.-X., 2008, The oldest known rocks in south–western China: SHRIMP U–Pb magmatic crystallisation age and detrital provenance analysis of the Paleoproterozoic Dahongshan Group: Journal of Asian Earth Sciences, v. 33, p. 289–302, doi: 10.1016/j.jseaes.2008.01.001.

Gregory, J.W., and Gregory, C.J., 1936, The Geology and Physical Geography of Chinese Tibet, and its Relations to the Mountain System of South-Eastern Asia, from Observations made during the Percy Sladen Expedition, 1922: Philosophical Transactions of the Royal Society of London, v. 213, p. 172–298, doi: 10.1098/rstb.1925.0005.

Guan, H., Sun, M., Wilde, S. a., Zhou, X., and Zhai, M., 2002, SHRIMP U–Pb zircon geochronology of the Fuping Complex: implications for formation and assembly of the North China Craton: Precambrian Research, v. 113, p. 1–18, doi: 10.1016/S0301-9268(01)00197-8.

Guynn, J., and Gehrels, G.E., 2010, Comparison of Detrital Zircon Age Distributions Using the

   K-S Test Visualization and representation of age-distribution data Histograms: , p. 1–16.

Guynn, J.H., Kapp, P., Pullen, A., Heizler, M., Gehrels, G.E., and Ding, L., 2006, Tibetan

   basement rocks near Amdo reveal "missing" Mesozoic tectonism along the Bangong suture,

   central Tibet: Geology, v. 34, p. 505, doi: 10.1130/G22453.1.

Hacker, B.R., Ratschbacher, L., Webb, L., Ireland, T., Walker, D., and Shuwen, D., 1998, U/Pb

   zircon ages constrain the architecture of the ultrahigh-pressure Qinling-Dabie Orogen,

   China: Earth and Planetary Science Letters, v. 161, p. 215–230, doi: 10.1016/S0012-

   821X(98)00152-6.

Hallet, B., and Molnar, P., 2001, Distorted drainage basins as markers of crustal strain east of the

   Himalaya: Journal of Geophysical Research, v. 106, p. 13697–13709.

Harrison, T., and Leloup, P., 1996, Diachronous initiation of transtension along the Ailao Shan-

   Red River shear zone, Yunnan and Vietnam (A. Yin & T. M. Harrison, Eds.): New York,

   Cambridge University Press, 208-226 p., http://www.ipgp.fr/~lacassin/papers/Harrison

   ZipperRRF 1996.pdf.

Hayward, B.W., and Smale, D., 1992, Heavy minerals and the provenance history of Waitemata

   Basin sediments (early Miocene, Northland, New Zealand): New Zealand Journal of

   Geology and Geophysics, v. 35, p. 223–242, doi: 10.1080/00288306.1992.9514516.

He, S., Kapp, P., DeCelles, P.G., Gehrels, G.E., and Heizler, M., 2007, Cretaceous–Tertiary

   geology of the Gangdese Arc in the Linzhou area, southern Tibet: Tectonophysics, v. 433,

   p. 15–37, doi: 10.1016/j.tecto.2007.01.005.

He, M., Zheng, H., Bookhagen, B., and Clift, P.D., 2014, Controls on erosion intensity in the

   Yangtze River basin tracked by U–Pb detrital zircon dating: Earth-Science Reviews, v. 136,

p. 121–140, doi: 10.1016/j.earscirev.2014.05.014.

He, M., Zheng, H., and Clift, P.D., 2013, Zircon U–Pb geochronology and Hf isotope data from the Yangtze River sands: Implications for major magmatic events and crustal evolution in Central China: Chemical Geology, v. 360-361, p. 186–203, doi: 10.1016/j.chemgeo.2013.10.020.

Hearn, P.J., Hare, T., Schruben, P., Sherrill, D., LaMar, C., and Tsushima, P., 2000, GLOBAL GIS DATABASE: Digital Atlas of South Asia:, http://www.agiweb.org/pubs/pubdetail.html?item=624103.

Henck, A.C., Huntington, K.W., Stone, J.O., Montgomery, D.R., and Hallet, B., 2011, Spatial controls on erosion in the Three Rivers Region, southeastern Tibet and southwestern China: Earth and Planetary Science Letters, v. 303, p. 71–83, doi: 10.1016/j.epsl.2010.12.038.

Hennig, D., Lehmann, B., Frei, D., Belyatsky, B., Zhao, X.F., Cabral, a. R., Zeng, P.S., Zhou, M.F., and Schmidt, K., 2009, Early Permian seafloor to continental arc magmatism in the eastern Paleo-Tethys: U–Pb age and Nd–Sr isotope data from the southern Lancangjiang zone, Yunnan, China: Lithos, v. 113, p. 408–422, doi: 10.1016/j.lithos.2009.04.031.

van Hoang, L., Wu, F.-Y., Clift, P.D., Wysocka, A., and Swierczewska, A., 2009, Evaluating the evolution of the Red River system based on in situ U-Pb dating and Hf isotope analysis of zircons: Geochemistry Geophysics Geosystems, v. 10, p. Q11008, doi: 10.1029/2009GC002819.

Hoke, G.D., Liu-Zeng, J., Hren, M.T., Wissink, G.K., and Garzione, C.N., 2014, Stable isotopes reveal high southeast Tibetan Plateau margin since the Paleogene: Earth and Planetary Science Letters, v. 394, p. 270–278, doi: 10.1016/j.epsl.2014.03.007.

Honarkhah, M., and Caers, J., 2010, Stochastic simulation of patterns using distance-based

pattern modeling: Mathematical Geosciences, v. 42, p. 487–517, doi: 10.1007/s11004-010-9276-7.

Hounslow, M.W., and Morton, A.C., 2004, Evaluation of sediment provenance using magnetic mineral inclusions in clastic silicates: Comparison with heavy mineral analysis: Sedimentary Geology, v. 171, p. 13–36, doi: 10.1016/j.sedgeo.2004.05.008.

Hurford, A.J., Fitch, F.J., and Clarke, A., 1984, Resolution of the age structure of the detrital zircon populations of two Lower Cretaceous sandstones from the Weald of England by fission track dating: Geological Magazine, v. 121, p. 269–277, http://search.proquest.com/docview/51446298?accountid=10920\nhttp://uh7qf6fd4h.search. serialssolutions.com/?ctx_ver=Z39.88-2004&ctx_enc=info:ofi/enc:UTF-8&rfr_id=info:sid/ProQ%3Ageorefmodule&rft_val_fmt=info:ofi/fmt:kev:mtx:journal&rft.g enre=article&rft.j.

Ji, W.-Q., Wu, F.-Y., Chung, S.-L., Li, J.-X., and Liu, C.-Z., 2009, Zircon U–Pb geochronology and Hf isotopic constraints on petrogenesis of the Gangdese batholith, southern Tibet: Chemical Geology, v. 262, p. 229–245, doi: 10.1016/j.chemgeo.2009.01.020.

Jiang, T., Cao, L., Xie, X., Wang, Z., Li, X., Zhang, Y., Zhang, D., and Sun, H., 2015, Insights from heavy minerals and zircon U–Pb ages into the middle Miocene–Pliocene provenance evolution of the Yinggehai Basin, northwestern South China Sea: Sedimentary Geology, v. 327, p. 32–42, doi: 10.1016/j.sedgeo.2015.07.011.

Jolivet, L., Maluski, H., Beyssac, O., Goffé, B., Lepvrier, C., Thi, P.T., and Van Vuong, N., 1999, Oligocene-Miocene Bu Khang extensional gneiss dome in Vietnam: Geodynamic implications: Geology, v. 27, p. 67–70, doi: 10.1130/0091-7613(1999)027<0067:OMBKEG>2.3.CO;2.

Kong, P., Granger, D., Wu, F., Caffee, M., Wang, Y., Zhao, X., and Zheng, Y., 2009, Cosmogenic nuclide burial ages and provenance of the Xigeda paleo-lake: Implications for evolution of the Middle Yangtze River: Earth and Planetary Science Letters, v. 278, p. 131–141, doi: 10.1016/j.epsl.2008.12.003.

Kong, P., Zheng, Y., and Caffee, M.W., 2012, Provenance and time constraints on the formation of the first bend of the Yangtze River: Geochemistry, Geophysics, Geosystems, v. 13, doi: 10.1029/2012GC004140.

Koons, P.O., 1995, Modeling the Topographic Evolution of Collisional Belts: Earth and Planetary Science Letters, v. 23, p. 375–408.

Kruskal, J.B., 1964a, Multidimensional scaling by optimizing goodness of fit to a nonmetric hypothesis: Psychometrika, v. 29, p. 1–27.

Kruskal, J.B., 1964b, Nonmetric multidimensional scaling: A numerical method: Psychometrika, v. 29, p. 115–129, doi: 10.1007/BF02289694.

Lang, K. a., Huntington, K.W., and Montgomery, D.R., 2013, Erosion of the tsangpo gorge by megafloods, eastern himalaya: Geology, v. 41, p. 1003–1006, doi: 10.1130/G34693.1.

Lease, R.O., Burbank, D.W., Gehrels, G.E., Wang, Z., and Yuan, D., 2007, Signatures of mountain building: Detrital zircon U/Pb ages from northeastern Tibet: Geology, v. 35, p. 239, doi: 10.1130/G23057A.1.

Lee, C.Y., 1934, The Development of the Upper Yangtze Valley: Bulletin of the Geological Society of China, v. 13, p. 107–118, doi: 10.1111/j.1755-6724.1934.mp13001006.x.

Leier, A.L., Kapp, P., Gehrels, G.E., and DeCelles, P.G., 2007, Detrital zircon geochronology of Carboniferous?Cretaceous strata in the Lhasa terrane, Southern Tibet: Basin Research, v. 19, p. 361–378, doi: 10.1111/j.1365-2117.2007.00330.x.

Leloup, P.H., Amaud, N., Lacassin, R., Kienast, J.R., Harrison, T.M., Phan Trong, T.T., Replumaz, A., and Tapponnier, P., 2006, New constraints on the structure, thermochronology, and timing of the Ailao Shan-Red River shear zone, SE Asia: Journal of Geophysical Research, v. 106, p. 6683–6732.

Leloup, P.H., HARRISON, T.M., RYERSON, F.J., CHEN, W.J., and LI, Q., 1993, Structural, petrological and thermal evolution of a Tertiary ductile strike-slip shear zone, Diancang Shan, Yunnan: Journal of Geophysical Research, v. 98, p. 6715–6743, doi: 10.1029/92JB02791.

Leloup, P.H., Lacassin, R., Tapponnier, P., and Schs, U., 1995, The Ailao Shan-Red River shear zone (Yunnan , China), Tertiary transform boundary of Indochina: v. 251.

Li, R., 2005, The Dabie Orogen as the early Jurassic sedimentary provenance: Constraints from the detrital zircon SHRIMP U-Pb dating: Science in China Series D, v. 48, p. 145, doi: 10.1360/03yd0216.

Li, X.-H., 1999, U–Pb zircon ages of granites from the southern margin of the Yangtze Block: timing of Neoproterozoic Jinning: Orogeny in SE China and implications for Rodinia Assembly: Precambrian Research, v. 97, p. 43–57, doi: 10.1016/S0301-9268(99)00020-0.

Li, D., Chen, Y., Hou, K., Lu, Z., and Cui, D., 2015, Detrital zircon record of Paleozoic and Mesozoic meta-sedimentary strata in the eastern part of the Baoshan block: Implications of their provenance and the tectonic evolution of the southeastern margin of the Tibetan plateau: Lithos, v. 227, p. 194–204, doi: 10.1016/j.lithos.2015.04.009.

Li, S., Currie, B.S., Rowley, D.B., and Ingalls, M., 2015, Cenozoic paleoaltimetry of the SE margin of the Tibetan Plateau: Constraints on the tectonic evolution of the region: Earth and Planetary Science Letters, v. 1, p. 1–10, doi: 10.1016/j.epsl.2015.09.044.

Li, Z.X., Li, X.H., Wartho, J. a., Clark, C., Li, W.X., Zhang, C.L., and Bao, C., 2010, Magmatic and metamorphic events during the early Paleozoic Wuyi-Yunkai orogeny, southeastern South China: New age constraints and pressure-temperature conditions: Geological Society of America Bulletin, v. 122, p. 772–793, doi: 10.1130/B30021.1.

Li, L.M., Sun, M., Wang, Y., Xing, G., Zhao, G., Lin, S., Xia, X., Chan, L., Zhang, F., and Wong, J., 2011, U-Pb and Hf isotopic study of zircons from migmatised amphibolites in the Cathaysia Block: Implications for the early Paleozoic peak tectonothermal event in Southeastern China: Gondwana Research, v. 19, p. 191–201, doi: 10.1016/j.gr.2010.03.009.

Lin, T.-H., Chung, S.-L., Chiu, H.-Y., Wu, F.-Y., Yeh, M.-W., Searle, M.P., and Iizuka, Y., 2012, Zircon U–Pb and Hf isotope constraints from the Ailao Shan–Red River shear zone on the tectonic and crustal evolution of southwestern China: Chemical Geology, v. 291, p. 23–37, doi: 10.1016/j.chemgeo.2011.11.011.

Liu, S., Hu, R., Gao, S., Feng, C., Huang, Z., Lai, S., Yuan, H., Liu, X., Coulson, I.M., Feng, G., Wang, T., and Qi, Y., 2009, U–Pb zircon, geochemical and Sr–Nd–Hf isotopic constraints on the age and origin of Early Palaeozoic I-type granite from the Tengchong–Baoshan Block, Western Yunnan Province, SW China: Journal of Asian Earth Sciences, v. 36, p. 168–182, doi: 10.1016/j.jseaes.2009.05.004.

Liu, F., Wang, F., Liu, P., and Liu, C., 2013, Multiple metamorphic events revealed by zircons from the Diancang Shan − Ailao Shan metamorphic complex , southeastern Tibetan Plateau: Gondwana Research, v. 24, p. 429–450, doi: 10.1016/j.gr.2012.10.016.

Luo, L., Qi, J.-F., Zhang, M.-Z., Wang, K., and Han, Y.-Z., 2014, Detrital zircon U–Pb ages of Late Triassic–Late Jurassic deposits in the western and northern Sichuan Basin margin: constraints on the foreland basin provenance and tectonic implications: International Journal

of Earth Sciences, v. 103, p. 1553–1568, doi: 10.1007/s00531-014-1032-7.

Machado, N., Schrank, A., Noce, C.M., and Gauthier, G., 1996, Ages of detrital zircon from Archean-Paleoproterozoic sequences: Implications for Greenstone Belt setting and evolution of a Transamazonian foreland basin in Quadrilátero Ferrífero, southeast Brazil: Earth and Planetary Science Letters, v. 141, p. 259–276, doi: 10.1016/0012-821X(96)00054-4.

Malusà, M.G., Carter, A., Limoncelli, M., Villa, I.M., and Garzanti, E., 2013, Bias in detrital zircon geochronology and thermochronometry: Chemical Geology, v. 359, p. 90–107, doi: 10.1016/j.chemgeo.2013.09.016.

Malusà, M.G., Resentini, A., and Garzanti, E., 2015, Hydraulic sorting and mineral fertility bias in detrital geochronology: Gondwana Research, doi: 10.1016/j.gr.2015.09.002.

Maluski, H., Lepvrier, C., Jolivet, L., Carter, A., Roques, D., Beyssac, O., Tang, T.T., Thang, N.D., and Avigad, D., 2001, Ar-Ar and fission-track ages in the Song Chay Massif: Early Triassic and Cenozoic tectonics in northern Vietnam: Journal of Asian Earth Sciences, v. 19, p. 233–248, doi: 10.1016/S1367-9120(00)00038-9.

May, S.R., Gray, G.G., Summa, L.L., Stewart, N.R., Gehrels, G.E., and Pecha, M.E., 2013, Detrital zircon geochronology from the Bighorn Basin, Wyoming, USA: Implications for tectonostratigraphic evolution and paleogeography: Geological Society of America Bulletin, v. 125, p. 1403–1422, doi: 10.1130/b30824.1.

McPhillips, D., and Brandon, M.T., 2010, Using tracer thermochronology to measure modern relief change in the Sierra Nevada, California: Earth and Planetary Science Letters, v. 296, p. 373–383, doi: 10.1016/j.epsl.2010.05.022.

McPhillips, D., Hoke, G.D., Liu-zeng, J., Bierman, P.R., Rood, D.H., and Niedermann, S., 2016,

Dating the incision of the Yangtze River gorge at the First Bend using three-nuclide burial ages: Geophysical Research Letters, v. 43, p. 101–110, doi: 10.1002/2015GL066780.

Moecher, D.P., and Samson, S.D., 2006, Differential zircon fertility of source terranes and natural bias in the detrital zircon record: Implications for sedimentary provenance analysis: Earth and Planetary Science Letters, v. 247, p. 252–266, doi: 10.1016/j.epsl.2006.04.035.

Nagy, E.A., Maluski, H., Lepvrier, C., and Scha, U., 2001, Geodynamic Significance of the Kontum Massif in Central Vietnam : Composite 4 0 Ar / 3 9 Ar and U-Pb Ages from Paleozoic to Triassic: The Journal of Geology, v. 109, p. 755–770.

Nie, J., Stevens, T., Rittner, M., Stockli, D., Garzanti, E., Limonta, M., Bird, A., Andò, S., Vermeesch, P., Saylor, J., Lu, H., Breecker, D., Hu, X., Liu, S., et al., 2015, Loess Plateau storage of Northeastern Tibetan Plateau-derived Yellow River sediment: Nature Communications, v. 6, p. 8511, doi: 10.1038/ncomms9511.

Ouimet, W., Whipple, K., Royden, L., Reiners, P., Hodges, K., and Pringle, M., 2010, Regional incision of the eastern margin of the Tibetan Plateau: Lithosphere, v. 2, p. 50–63, doi: 10.1130/L57.1.

Parker, R.N., Densmore, A.L., Rosser, N.J., de Michele, M., Li, Y., Huang, R., Whadcoat, S., and Petley, D.N., 2011, Mass wasting triggered by the 2008 Wenchuan earthquake is greater than orogenic growth: Nature Geoscience, v. 4, p. 449–452, doi: 10.1038/ngeo1154.

Pei, X., Li, Z., Ding, S., Li, R., Feng, J., Sun, Y., Zhang, Y., and Liu, Z., 2009, Neoproterozoic Jiaoziding Peraluminous Granite in the Northwestern Margin of Yangtze Block: Zircon SHRIMP U-Pb Age and Geochemistry and Their Tectonic Significance: Earth Science Frontiers, v. 16, p. 231–249, doi: 10.1016/S1872-5791(08)60096-2.

Peng, T., Zhao, G., Fan, W., Peng, B., and Mao, Y., 2014a, Late Triassic granitic magmatism in

the Eastern Qiangtang, Eastern Tibetan Plateau: Geochronology, petrogenesis and implications for the tectonic evolution of the Paleo-Tethys: Gondwana Research, doi: 10.1016/j.gr.2014.01.009.

Peng, T., Zhao, G., Fan, W., Peng, B., and Mao, Y., 2014b, Zircon geochronology and Hf isotopes of Mesozoic intrusive rocks from the Yidun terrane, Eastern Tibetan Plateau: Petrogenesis and their bearings with Cu mineralization: Journal of Asian Earth Sciences, v. 80, p. 18–33, doi: 10.1016/j.jseaes.2013.10.028.

Prentice, I.C., 1980, Multidimensional scaling as a research tool in quaternary palynology: A review of theory and methods: Review of Palaeobotany and Palynology, v. 31, p. 71–104, doi: 10.1016/0034-6667(80)90023-8.

Press, W., Teukolsky, S., Vetterling, W., and Flannery, B., 1987, Numerical Recipes: The Art of Scientific Computing: v. 29, 501 p., doi: 10.2307/1269484.

Press, W., Teukolsky, S., Vetterling, W., and Flannery, B., 1988, Numerical Recipes: The Art of Scientific Computing: Cambridge, Cambridge University Press, v. 29, 623-649 p., doi: 10.2307/1269484.

Pullen, A., Ibáñez-Mejía, M., Gehrels, G.E., Ibáñez-Mejía, J.C., and Pecha, M., 2014, What happens when n= 1000? Creating large-n geochronological datasets with LA-ICP-MS for geologic investigations: Journal of Analytical Atomic Spectrometry, v. 29, p. 971, doi: 10.1039/c4ja00024b.

Qi, X., Zhu, L., Grimmer, J.C., and Hu, Z., 2015, Tracing the Transhimalayan magmatic belt and the Lhasa block southward using zircon U–Pb, Lu–Hf isotopic and geochemical data: Cretaceous – Cenozoic granitoids in the Tengchong block, Yunnan, China: Journal of Asian Earth Sciences, v. 110, p. 170–188, doi: 10.1016/j.jseaes.2014.07.019.

Reid, A.J., Fowler, A.P., Phillips, D., and Wilson, C.J.L., 2005, Thermochronology of the Yidun
Arc, central eastern Tibetan Plateau: constraints from 40Ar/39Ar K-feldspar and apatite
fission track data: Journal of Asian Earth Sciences, v. 25, p. 915–935, doi:
10.1016/j.jseaes.2004.09.002.

Reid, A., Wilson, C.J.L., Shun, L., Pearson, N., and Belousova, E., 2007, Mesozoic plutons of
the Yidun Arc , SW China : U / Pb geochronology and Hf isotopic signature: v. 31, p. 88–
106, doi: 10.1016/j.oregeorev.2004.11.003.

Reiners, P.W., 2005, Past, Present, and Future of Thermochronology: Reviews in Mineralogy
and Geochemistry, v. 58, p. 1–18, doi: 10.2138/rmg.2005.58.1.

Reiners, P.W., Campbell, I.H., Nicolescu, S., Allen, C.M., Hourigan, J.K., Garver, J.I.,
Mattinson, J.M., and Cowan, D.S., 2005, (U-Th)/(He-Pb) Double Dating of Detrital
Zircons: American Journal of Science, v. 305, p. 259–311.

Richardson, N.J., Densmore, a. L., Seward, D., Fowler, a., Wipf, M., Ellis, M. a., Yong, L., and
Zhang, Y., 2008, Extraordinary denudation in the Sichuan Basin: Insights from low-
temperature thermochronology adjacent to the eastern margin of the Tibetan Plateau:
Journal of Geophysical Research, v. 113, p. B04409, doi: 10.1029/2006JB004739.

Richardson, N.J., Densmore, a. L., Seward, D., Wipf, M., and Yong, L., 2010, Did incision of the
Three Gorges begin in the Eocene? Geology, v. 38, p. 551–554, doi: 10.1130/G30527.1.

Robinson, R. a. J., Brezina, C. a., Parrish, R.R., Horstwood, M.S. a., Bird, M.I., Walters, A.S.,
and Oliver, G.J.H., 2014, Large rivers and orogens: The evolution of the Yarlung Tsangpo–
Irrawaddy system and the eastern Himalayan syntaxis: Gondwana Research, v. 26, p. 112–
121, doi: 10.1016/j.gr.2013.07.002.

Royden, L.H., Burchfiel, B.C., King, R.W., Wang, E., Chen, Z., Shen, F., and Liu, Y., 1997,

Surface Deformation and Lower Crustal Flow in Eastern Tibet: Science, v. 276, p. 788–790, doi: 10.1126/science.276.5313.788.

Sambridge, M.S., and Compston, W., 1994, Mixture modeling of multi-component data sets with application to ion-probe zircon ages: Earth and Planetary Science Letters, v. 128, p. 373–390.

Sammon, J.W., 1969, A Nonlinear Mapping for Data Structure Analysis: IEEE Transactions on Computers, v. 18, p. 401–409, doi: 10.1109/t-c.1969.222678.

Satkoski, A.M., Wilkinson, B.H., Hieptas, J., and Samson, S.D., 2013, Likeness among detrital zircon populations--An approach to the comparison of age frequency data in time and space: Geological Society of America Bulletin, v. 125, p. 1783–1799, doi: 10.1130/B30888.1.

Saylor, J.E., Knowles, J.N., Horton, B.K., Nie, J., and Mora, A., 2013, Mixing of Source Populations Recorded in Detrital Zircon U-Pb Age Spectra of Modern River Sands: The Journal of Geology, v. 121, p. 17–33, doi: 10.1086/668683.

Schoenbohm, L.M., Burchfi, B.C., and Liangzhong, C., 2006, Miocene to present activity along the Red River fault , China , in the context of continental extrusion , upper-crustal rotation , and lower-crustal fl ow: GSA Bulletin, v. 118, p. 672–688, doi: 10.1130/B25816.1.

Schoene, B., Schaltegger, U., Brack, P., Latkoczy, C., Stracke, A., and Günther, D., 2012, Rates of magma differentiation and emplacement in a ballooning pluton recorded by U-Pb TIMS-TEA, Adamello batholith, Italy: Earth and Planetary Science Letters, v. 355-356, p. 162–173, doi: 10.1016/j.epsl.2012.08.019.

Shang, F., Weislogel, A.L., Robinson, D.M., and Jackson, W.T., 2016, Detrital zircon geochronology from the Mesozoic Qamdo (Changdu) basin, southeastern Tibet:

Implications for the Paleo- and Meso-Tethys evolution: , p. (In Review).

She, Z., Ma, C., Wan, Y., Zhang, J., Li, M., Chen, L., Xu, W., Li, Y., Ye, L., and Gao, J., 2012, An Early Mesozoic transcontinental palaeoriver in South China: evidence from detrital zircon U-Pb geochronology and Hf isotopes: Journal of the Geological Society, v. 169, p. 353–362, doi: 10.1144/0016-76492011-097.

Shellnutt, J.G., 2014, The Emeishan large igneous province: A synthesis: Geoscience Frontiers, v. 5, p. 369–394, doi: 10.1016/j.gsf.2013.07.003.

Shi, G.R., 1993, Multivariate data analysis in palaeoecology and palaeobiogeography -- a review: Palaeogeography, Palaeoclimatology, Palaeoecology, v. 105, p. 199–234, doi: 10.1016/0031-0182(93)90084-V.

Sircombe, K.N., 2000, Quantitative comparison of large sets of geochronological data using multivariate analysis: A provenance study example from Australia: Geochimica et Cosmochimica Acta, v. 64, p. 1593–1616, doi: 10.1016/S0016-7037(99)00388-9.

Sircombe, K.N., and Hazelton, M.L., 2004, Comparison of detrital zircon age distributions by kernel functional estimation: Sedimentary Geology, v. 171, p. 91–111, doi: 10.1016/j.sedgeo.2004.05.012.

Smosna, R., Bruner, K.R., and Burns, A., 1999, Numerical analysis of sandstone composition, provenance, and paleogeography: Journal of Sedimentary Research, v. 69, p. 1063–1070, doi: 10.2110/jsr.69.1063.

Song, G., Qin, K., Li, G., Evans, N.J., and Li, X., 2014, Mesozoic magmatism and metallogeny in the Chizhou area, Middle–Lower Yangtze Valley, SE China: Constrained by petrochemistry, geochemistry and geochronology: Journal of Asian Earth Sciences, v. 91, p. 137–153, doi: 10.1016/j.jseaes.2014.04.025.

Spencer, C.J., and Kirkland, C.L., 2015, Visualizing the sedimentary response through the orogenic cycle: A multidimensional scaling approach: Lithosphere, p. 1–9, doi: 10.1130/L479.1.

Su, J., Dong, S., Zhang, Y., Li, Y., Chen, X., and Cui, J., 2014, Detrital zircon geochronology of pre-Cretaceous strata: tectonic implications for the Jiangnan Orogen, South China: Geological Magazine, p. 1–21, doi: 10.1017/S0016756813001003.

Sun, W.-H., Zhou, M.-F., Gao, J.-F., Yang, Y.-H., Zhao, X.-F., and Zhao, J.-H., 2009, Detrital zircon U–Pb geochronological and Lu–Hf isotopic constraints on the Precambrian magmatic and crustal evolution of the western Yangtze Block, SW China: Precambrian Research, v. 172, p. 99–126, doi: 10.1016/j.precamres.2009.03.010.

Sunila, R., and Kollo, K., 2007, A comparison of geostatistics and fuzzy application for digital elevation model: The International Archives of the Photogrammetry, Remote Sensing and Spatial Information Science, v. 34, http://www.isprs.org/proceedings/XXXVI/2-C43/Session2/paper_Sunila_Kollo.pdf.

Tapponnier, P., Peltzer, G., and Armijo, R., 1986, On the mechanics of the collision between India and Asia: Geological Society, London, Special Publications , v. 19 , p. 113–157, doi: 10.1144/GSL.SP.1986.019.01.07.

Torgerson, W.S., 1952, Multidimensional scaling: I. Theory and method: Psychometrika, v. 17, p. 401–419, doi: 10.1007/BF02288916.

Vermeesch, P., 2004, How many grains are needed for a provenance study? Earth and Planetary Science Letters, v. 224, p. 441–451, doi: 10.1016/j.epsl.2004.05.037.

Vermeesch, P., 2013, Multi-sample comparison of detrital age distributions: Chemical Geology, v. 341, p. 140–146, doi: 10.1016/j.chemgeo.2013.01.010.

Vermeesch, P., 2012, On the visualisation of detrital age distributions: Chemical Geology, v. 312-313, p. 190–194, doi: 10.1016/j.chemgeo.2012.04.021.

Vermeesch, P., and Garzanti, E., 2015, Making geological sense of "Big Data" in sedimentary provenance analysis: Chemical Geology, v. 409, p. 20–27, doi: 10.1016/j.chemgeo.2015.05.004.

Vezzoli, G., Garzanti, E., Limonta, M., Andò, S., and Yang, S., 2016, Erosion patterns in the Changjiang (Yangtze River) catchment revealed by bulk-sample versus single-mineral provenance budgets: Geomorphology, v. 261, p. 177–192, doi: 10.1016/j.geomorph.2016.02.031.

Wang, L.-J., Griffin, W.L., Yu, J.-H., and O'Reilly, S.Y., 2010, Precambrian crustal evolution of the Yangtze Block tracked by detrital zircons from Neoproterozoic sedimentary rocks: Precambrian Research, v. 177, p. 131–144, doi: 10.1016/j.precamres.2009.11.008.

Wang, L.-J., Griffin, W.L., Yu, J.-H., and O'Reilly, S.Y., 2013, U–Pb and Lu–Hf isotopes in detrital zircon from Neoproterozoic sedimentary rocks in the northern Yangtze Block: Implications for Precambrian crustal evolution: Gondwana Research, v. 23, p. 1261–1272, doi: 10.1016/j.gr.2012.04.013.

Wang, X.-S., Hu, R.-Z., Bi, X.-W., Leng, C.-B., Pan, L.-C., Zhu, J.-J., and Chen, Y.-W., 2014, Petrogenesis of Late Cretaceous I-type granites in the southern Yidun Terrane: New constraints on the Late Mesozoic tectonic evolution of the eastern Tibetan Plateau: Lithos, v. 208-209, p. 202–219, doi: 10.1016/j.lithos.2014.08.016.

Wang, E., Kirby, E., Furlong, K.P., van Soest, M., Xu, G., Shi, X., Kamp, P.J.J., and Hodges, K. V., 2012, Two-phase growth of high topography in eastern Tibet during the Cenozoic: Nature Geoscience, v. 5, p. 640–645, doi: 10.1038/ngeo1538.

Wang, C., Liang, X., Xie, Y., Tong, C., Pei, J., Zhou, Y., Jiang, Y., Fu, J., Dong, C., and Liu, P., 2014, Provenance of Upper Miocene to Quaternary sediments in the Yinggehai-Song Hong Basin, South China Sea: Evidence from detrital zircon U-Pb ages: Marine Geology, v. 355, p. 202–217, doi: 10.1016/j.margeo.2014.06.004.

Wang, C., Liang, X., Zhou, Y., Fu, J., Jiang, Y., Dong, C., Xie, Y., Tong, C., and Pei, J., 2015, Detrital zircon record of sediments from six modern rivers: geochronology and its implications, Western Hainan, China: Earth Science Frontiers,.

Wang, L., Liu, C., Fei, M., Shen, L., Zhang, H., and Zhao, Y., 2015, First SHRIMP U–Pb zircon ages of the potash-bearing Mengyejing Formation, Simao Basin, southwestern Yunnan, China: Cretaceous Research, v. 52, p. 238–250, doi: 10.1016/j.cretres.2014.09.008.

Wang, L., Liu, C., Gao, X., and Zhang, H., 2014a, Provenance and paleogeography of the Late Cretaceous Mengyejing Formation, Simao Basin, southeastern Tibetan Plateau: Whole-rock geochemistry, U-Pb geochronology, and Hf isotopic constraints: Sedimentary Geology, v. 304, p. 44–58, doi: 10.1016/j.sedgeo.2014.02.003.

Wang, L., Liu, C., Gao, X., and Zhang, H., 2014b, Provenance and paleogeography of the Late Cretaceous Mengyejing Formation, Simao Basin, southeastern Tibetan Plateau: Whole-rock geochemistry, U–Pb geochronology, and Hf isotopic constraints: Sedimentary Geology, v. 304, p. 44–58, doi: 10.1016/j.sedgeo.2014.02.003.

Wang, P.L., Lo, C.H., Lee, T.Y., Chung, S.L., Lan, C.Y., and Yem, N.T., 1998, Thermochronological evidence for the movement of the Ailao Shan-Red River shear zone: A perspective from Vietnam: Geology, v. 26, p. 887–890, doi: 10.1130/0091-7613(1998)026<0887:TEFTMO>2.3.CO;2.

Wang, X., Metcalfe, I., Jian, P., He, L., and Wang, C., 2000, The Jinshajiang-Ailaoshan Suture

Zone, China: Tectonostratigraphy, age and evolution: Journal of Asian Earth Sciences, v. 18, p. 675–690, doi: 10.1016/S1367-9120(00)00039-0.

Wang, Q.W., Wang, K.M., Han, Z.Z., Fu, X.F., Liang, B., Yao, Z.D., Dai, Z.M., Luo, S.L., Zhong, C.H., and Wei, Y.F., 2008, The Granite in West Sichuan and its Metallogenic Series: Geological Publishing House, Beijing, doi: 10.1016/j.lithos.2014.08.016.

Wang, B., Wang, W., and Zhou, M., 2013, Geoscience Frontiers Provenance and tectonic setting of the Triassic Yidun Group , the Yidun Terrane , Tibet: Geoscience Frontiers, v. 4, p. 765–777, doi: 10.1016/j.gsf.2013.02.007.

Wang, J.H., Yin, A., Harrison, T.M., Grove, M., Zhang, Y.Q., and Xie, G.H., 2001, A tectonic model for Cenozoic igneous activities in the eastern Indo-Asian collision zone: Earth and Planetary Science Letters, v. 188, p. 123–133, doi: 10.1016/S0012-821X(01)00315-6.

Wang, L.-J., Yu, J.-H., Griffin, W.L., and O'Reilly, S.Y., 2012, Early crustal evolution in the western Yangtze Block: Evidence from U–Pb and Lu–Hf isotopes on detrital zircons from sedimentary rocks: Precambrian Research, v. 222-223, p. 368–385, doi: 10.1016/j.precamres.2011.08.001.

Wang, Y., Zhang, A., Fan, W., Zhao, G., Zhang, G., Zhang, Y., Zhang, F., and Li, S., 2011, Kwangsian crustal anatexis within the eastern South China Block: Geochemical, zircon U–Pb geochronological and Hf isotopic fingerprints from the gneissoid granites of Wugong and Wuyi–Yunkai Domains: Lithos, v. 127, p. 239–260, doi: 10.1016/j.lithos.2011.07.027.

Wei, H.-H., Wang, E., Wu, G.-L., and Meng, K., 2015, No sedimentary records indicating southerly flow of the paleo-Upper Yangtze River from the First Bend in southeastern Tibet: Gondwana Research, doi: 10.1016/j.gr.2015.02.006.

Weislogel, A.L., Graham, S.A., Chang, E.Z., Wooden, J.L., and Gehrels, G.E., 2010, Detrital

zircon provenance from three turbidite depocenters of the Middle-Upper Triassic Songpan-Ganzi complex, central China: Record of collisional tectonics, erosional exhumation, and sediment production: Geological Society of America Bulletin, v. 122, p. 2041–2062, doi: 10.1130/B26606.1.

Weislogel, A.L., and Robinson, D.M., 2010, The Impact of Mesozoic Tectonism on Eastern Tibet Plateau Crustal Infrastructure : Implications for Plateau Evolution: , p. 1–2, doi: 10.1029/2001TC001332.Kapp.

Wen, D., Liu, D., Chung, S., Chu, M., Ji, J., Zhang, Q., Song, B., Lee, T., Yeh, M., and Lo, C., 2008, Zircon SHRIMP U–Pb ages of the Gangdese Batholith and implications for Neotethyan subduction in southern Tibet: Chemical Geology, v. 252, p. 191–201, doi: 10.1016/j.chemgeo.2008.03.003.

Whipple, K.X., and Tucker, 1999, Dynamics of the stream-power river incision model: Implications for height limits of mountain ranges, landscape response timescales, and research needs: Journal of Geophysical Research, v. 104, p. 661–674, doi: 10.1029/1999JB900120.

Wilk, M.B., and Gnanadesikan, R., 1968, Probability plotting methods for the analysis of data.: Biometrika, v. 55, p. 1–17, doi: 10.1093/biomet/55.1.1.

Wilkinson, B.H., and McElroy, B.J., 2007, The impact of humans on continental erosion and sedimentation: Bulletin of the Geological Society of America, v. 119, p. 140–156, doi: 10.1130/B25899.1.

Wittmann, H., von Blanckenburg, F., Maurice, L., Guyot, J.L., Filizola, N., and Kubik, P.W., 2011, Sediment production and delivery in the Amazon River basin quantified by in situ-produced cosmogenic nuclides and recent river loads: Bulletin of the Geological Society of

America, v. 123, p. 934–950, doi: 10.1130/B30317.1.

Wu, Y., Gao, S., Zhang, H., Zheng, J., Liu, X., Wang, H., Gong, H., Zhou, L., and Yuan, H., 2012, Geochemistry and zircon U–Pb geochronology of Paleoproterozoic arc related granitoid in the Northwestern Yangtze Block and its geological implications: Precambrian Research, v. 200-203, p. 26–37, doi: 10.1016/j.precamres.2011.12.015.

Xianhua, L., Tatsumoto, M., Premo, W.R., and Xuntang, G., 1989, Age and origin of the Tanghu Granite, southeast China: Results from U-Pb single zircon and Nd isotopes: Geology , v. 17 , p. 395–399, doi: 10.1130/0091-7613(1989)017<0395:AAOOTT>2.3.CO;2.

Xu, X., O'Reilly, S.Y., Griffin, W.L., Wang, X., Pearson, N.J., and He, Z., 2007, The crust of Cathaysia: Age, assembly and reworking of two terranes: Precambrian Research, v. 158, p. 51–78, doi: 10.1016/j.precamres.2007.04.010.

Xu, Y., Sun, Q., Cai, G., Yin, X., and Chen, J., 2014, The U–Pb ages and Hf isotopes of detrital zircons from Hainan Island, South China: implications for sediment provenance and the crustal evolution: Environmental Earth Sciences, v. 71, p. 1619–1628, doi: 10.1007/s12665-013-2566-x.

Xu, Y., Sun, Q., Yi, L., Yin, X., Wang, A., Li, Y., and Chen, J., 2014, Detrital Zircons U-Pb Age and Hf Isotope from the Western Side of the Taiwan Strait: Implications for Sediment Provenance and Crustal Evolution of the Northeast Cathaysia Block: Terrestrial, Atmospheric and Oceanic Sciences, v. 25, p. 505, doi: 10.3319/TAO.2014.02.18.01(TT).

Xu, Y., Yang, Q., Lan, J., Luo, Z., Huang, X., and Shi, Y., 2012, Journal of Asian Earth Sciences Temporal – spatial distribution and tectonic implications of the batholiths in the Gaoligong – Tengliang – Yingjiang area , western Yunnan : Constraints from zircon U – Pb ages and Hf isotopes: Journal of Asian Earth Sciences, v. 53, p. 151–175, doi:

10.1016/j.jseaes.2011.06.018.

Yan, Y., Carter, A., Huang, C.-Y., Chan, L.-S., Hu, X.-Q., and Lan, Q., 2012, Constraints on Cenozoic regional drainage evolution of SW China from the provenance of the Jianchuan Basin: Geochemistry Geophysics Geosystems, v. 13, p. 1–12, doi: 10.1029/2011GC003803.

Yan, Y., Carter, A., Palk, C., Brichau, S., and Hu, X., 2011, Understanding sedimentation in the Song Hong-Yinggehai Basin, South China Sea: Geochemistry, Geophysics, Geosystems, v. 12, doi: 10.1029/2011GC003533.

Yang, J., Cawood, P. a., Du, Y., Huang, H., and Hu, L., 2012, Detrital record of Indosinian mountain building in SW China: Provenance of the Middle Triassic turbidites in the Youjiang Basin: Tectonophysics, v. 574-575, p. 105–117, doi: 10.1016/j.tecto.2012.08.027.

Yang, T.N., Ding, Y., Zhang, H.R., Fan, J.W., Liang, M.J., and Wang, X.H., 2014, Two-phase subduction and subsequent collision defines the Paleotethyan tectonics of the southeastern Tibetan Plateau: Evidence from zircon U-Pb dating, geochemistry, and structural geology of the Sanjiang orogenic belt, southwest China: Geological Society of America Bulletin, p. 1654–1682, doi: 10.1130/b30921.1.

Yang, W., Jolivet, M., Dupont-Nivet, G., and Guo, Z., 2013, Mesozoic – Cenozoic tectonic evolution of southwestern Tian Shan: Evidence from detrital zircon U/Pb and apatite fission track ages of the Ulugqat area, Northwest China: Gondwana Research, doi: 10.1016/j.gr.2013.07.020.

Yang, T.N., Liang, M.J., Fan, J.W., Shi, P.L., Zhang, H.R., and Hou, Z.H., 2014, Paleogene sedimentation, volcanism, and deformation in eastern Tibet: Evidence from structures, geochemistry, and zircon U–Pb dating in the Jianchuan Basin, SW China: Gondwana Research, v. 26, p. 521–535, doi: 10.1016/j.gr.2013.07.014.

Yang, R., Willett, S.D., and Goren, L., 2015, In situ low-relief landscape formation as a result of river network disruption: Nature, v. 520, p. 526–529, doi: 10.1038/nature14354.

Zhai, Q., Jahn, B., Su, L., Wang, J., Mo, X.-X., Lee, H., Wang, K., and Tang, S., 2013, Triassic arc magmatism in the Qiangtang area, northern Tibet: Zircon U–Pb ages, geochemical and Sr–Nd–Hf isotopic characteristics, and tectonic implications: Journal of Asian Earth Sciences, v. 63, p. 162–178, doi: 10.1016/j.jseaes.2012.08.025.

Zhang, X., Shi, R., Huang, Q., Liu, D., Gong, X., Chen, S., Wu, K., Yi, G., Sun, Y., and Ding, L., 2013, Early Jurassic high-pressure metamorphism of the Amdo terrane, Tibet: Constraints from zircon U–Pb geochronology of mafic granulites: Gondwana Research, doi: 10.1016/j.gr.2013.08.003.

Zhang, Z., Tyrrell, S., Li, C., Daly, J.S., Sun, X., and Li, Q., 2014, Pb isotope compositions of detrital K-feldspar grains in the upper-middle Yangtze River system: Implications for sediment provenance and drainage evolution.: Geochemistry Geophysics Geosystems, v. 15, p. 2765–2779, doi: 10.1002/2014GC005391.Received.

Zhang, S.-B., Zheng, Y.-F., Wu, Y.-B., Zhao, Z.-F., Gao, S., and Wu, F.-Y., 2006a, Zircon isotope evidence for ≥3.5Ga continental crust in the Yangtze craton of China: Precambrian Research, v. 146, p. 16–34, doi: 10.1016/j.precamres.2006.01.002.

Zhang, S.-B., Zheng, Y.-F., Wu, Y.-B., Zhao, Z.-F., Gao, S., and Wu, F.-Y., 2006b, Zircon U-Pb age and Hf-O isotope evidence for Paleoproterozoic metamorphic event in South China: Precambrian Research, v. 151, p. 265–288, doi: 10.1016/j.precamres.2006.08.009.

Zhao, M., Shao, L., Liang, J., and Li, Q., 2015, No Red River capture since the late Oligocene: Geochemical evidence from the Northwestern South China Sea: Deep Sea Research Part II: Topical Studies in Oceanography, p. 1–10, doi: 10.1016/j.dsr2.2015.02.029.

Zhao, X.-F., Zhou, M.-F., Li, J.-W., Sun, M., Gao, J.-F., Sun, W.-H., and Yang, J.-H., 2010, Late Paleoproterozoic to early Mesoproterozoic Dongchuan Group in Yunnan, SW China: Implications for tectonic evolution of the Yangtze Block: Precambrian Research, v. 182, p. 57–69, doi: 10.1016/j.precamres.2010.06.021.

Zheng, H., Clift, P.D., Wang, P., Tada, R., Jia, J., He, M., and Jourdan, F., 2013, Pre-Miocene birth of the Yangtze River: PNAS, v. 110, p. 7556–7561, doi: 10.1073/pnas.1216241110/-/DCSupplemental.www.pnas.org/cgi/doi/10.1073/pnas.1216241110.

Zheng, J., Griffin, W.L., Reilly, S.Y.O., Zhang, M., Pearson, N., and Pan, Y., 2006, Widespread Archean basement beneath the Yangtze craton:, doi: 10.1130/G22282.1.

Zhou, M., Ma, Y., Yan, D., Xia, X., Zhao, J., and Sun, M., 2006, The Yanbian Terrane (Southern Sichuan Province, SW China): A Neoproterozoic arc assemblage in the western margin of the Yangtze Block: Precambrian Research, v. 144, p. 19–38, doi: 10.1016/j.precamres.2005.11.002.

Zhou, J.-C., Wang, X.-L., and Qiu, J.-S., 2009, Geochronology of Neoproterozoic mafic rocks and sandstones from northeastern Guizhou, South China: Coeval arc magmatism and sedimentation: Precambrian Research, v. 170, p. 27–42, doi: http://dx.doi.org/10.1016/j.precamres.2008.11.002.

Zhuo, J., Jiang, X., Wang, J., Cui, X., Xiong, G., Lu, J., Liu, J., and Ma, M., 2013, Opening time and filling pattern of the Neoproterozoic Kangdian Rift Basin, western Yangtze Continent, South China: Science China Earth Sciences, v. 56, p. 1664–1676, doi: 10.1007/s11430-013-4694-2.

Biographical Data

Name of Author: Gregory Karl Wissink

Place of Birth: Ithaca, New York USA

Date of Birth: February 28, 1989

Undergraduate School Attended:

Boston University, Boston, Massachusetts

Degrees Awarded:

Bachelor of Arts, 2011, Earth Sciences, *cum laude*

Professional Experience:

Teaching and research assistant, Department of Earth Sciences, Syracuse University, 2011-2016

Science Tutor, Stevenson Tutoring Center, Syracuse University, 2016

Laboratory and field assistant and technician, Department of Earth Sciences, Boston University, 2008-2011